Holographic Sensors for the Detection of Liquid Phase Analytes

Sabad-e Gul
Technological University Dublin

Holographic sensors for the detection of liquid phase analytes

A thesis submitted in partial fulfilment of the requirement for the degree of Doctor of Philosophy

by

Sabad-e-Gul (M.Phil)

Supervisors: Prof. Izabela Naydenova

Prof. John Cassidy

Centre for Industrial Engineering and Optics

School of Physics & Clinical & Optometric Sciences

Dublin Institute of Technology

Date of submission: 07 December 2018

Abstract

The aim of this project is to design, fabricate and study experimentally photonic structures created by holographic lithography for application in sensing. The aim is to modify the photonic structures with analyte sensitive materials and view of their application in environmental and biomedical sensing. Two types of photonic structures were investigated in these studies: modified surface relief holographic gratings and volume holographic gratings.

The initial phase of this work involved development of a protocol and a skill to produce surface relief holograms with consistent properties- high diffraction efficiency (35 %± 5) and high surface amplitude (400 nm). This was achieved by recording holographic gratings with spatial frequency (300 lines/mm) in a photopolymer layers. Initially combined volume and surface relief structures were created. The maximum diffraction efficiency achieved was 50%-60% for the combined photopolymer photonic structure. After thermal treatment the diffraction efficiency was found to be decrease to (35%) and predominantly due to the periodic surface relief structures.

Zeolite nanoparticles are characterised by well-defined pore sizes capable of recognising dications and it is possible to create nanozeolite-functionalised photonic structures that change their optical properties in the presence of the analyte. The next step was to use zeolites nanoparticles in photonic structures and fabricate a portable sensor which can detect heavy metals in fresh water and particularly the research interest was on divalent metal ions. The reported sensor in this research work was modified by LTL-zeolites nanoparticles in a sol-gel and that sensor is sensitive to copper, lead ions and divalent cations. The limit of detection of this sensor is 63 ppm for copper and lead. Little sensitivity was detected to monovalent ions, such as copper chloride, sodium and potassium.

Then the surface structures were functionalised with dibenzo-18-crown-6 (DC) and Tetraethyl 4-tert-butylcalix[4]arene (TBC). Crown ethers have different binding strengths and selectivity for metal cations. Whereas TBC is well known for sodium complexation. Both ionophores have great potential in the fabrication of highly sensitive and selective biosensors. In this case, the application of the sensor is metal ion detection particularly K^+ and Na^+ ions. The second types of sensors were modified with a chelating compound DC and TBC in a plasticised Polyvinyl chloride or Sol gel matrix. The DC sensor gives a selective response for potassium ions and the TBC sensor gives selective response for sodium ions. The sensor responds within the physiological ranges.

Another main objective is to develop a new photopolymer formulation which will be stable in water. A novel formulation was developed based on cellulose acetate and polyethylene glycol binder. Volume holographic gratings (VGH) were recorded successfully. A maximum diffraction efficiency 50-55% was achieved. The holograms are able to work in water environment. Preliminary results showed that the VGH have a potential to work as a sensor for sodium.

The research work demonstrated the feasibility to use holographic diffraction gratings (SRG and VHG) as disposable sensors which can detect analyte in water environment.

This thesis is dedicated to my parents

Zulfiqar Hussain, Gulshan Ijaz
and my late grandfather
Ijaz ur Rehman

Declaration

I hereby declare that this thesis is entirely my own original work. All other sources of information presented which are not part of my work have been properly cited.

This thesis was prepared according to the regulations for postgraduate studies by research of the Dublin Institute of Technology and has not been submitted for any of my degree at any other Institute or University.

This work reported on this thesis conforms to the principle and requirements of the Dublin Institute of Technology's guidelines for ethics in research.

The Institute has permission to keep, or lend or to copy this thesis in whole or in part, on condition that use the material or thesis be duly acknowledged.

Signature ———————————————— Date ————————————————

Acknowledgements

List of abbreviations and symbols

PVA	Polyvinylalchol
AA	Acrylamide
BAA	N,N'Methylenebisacrylamide
TEA	Triethanolamine
EB	Erthrosine B dye
DOPT	Dioctyl terephthalate plasticizer
TBC	Tetraethyl 4-tert-butylcalix[4]arene
DC	Dibenzo-18-crown-6
CA	Cellulsoe acetate
PEG	Polyethylene glycol
NPG	N-phenylglycine
d	Grating thickness
Δd	Grating thickness change
$\Delta \lambda$	Wavelength shift
Δn	Refractive index modulation
$\Delta \eta$	Diffraction efficiency variation
θ_B	Bragg angle
I_t	Intensity of the transmitted beam
I_d	Intensity of the diffracted beam
I_0	Intensity of the incident beam
λ	Wavelength of light
Λ	Fringe spacing of a holographic grating

n₀	Average refractive index of the medium
η	Diffraction efficiency of a holographic grating
DI	Deionised water
POCT	Point-of-care testing
LOD	Limit of detection
γ	Activity coefficient

Table of Contents

Chapter 6 – Development of novel cellulose acetate based volume photonic structures 168

Chapter 7 – Conclusions and Future work 203

List of Figures

List of Tables

Chapter 1 – Introduction

1.1. The demand for environmental monitoring

Recently, environmental monitoring has become even more important as the human populations increases, adding a strain on the environment. Harmful environmental changes result from population increases and concentrated human activities. For example, in the United States, the industrial and agricultural revolutions of the last 100 years have produced large amounts of waste by-products that, until the late 1960s, were released into the environment without regard to consequences [1]. In many parts of the developing world, waste is still being disposed of without treatment. Through environmental monitoring we know that most surface soils, bodies of waters, and even ice caps contain trace and ultratrace levels of synthetic chemicals (e.g., dioxins) and nuclear-fallout components (e.g., radioactive cesium). Also, many surface waters, including rivers and lakes, contain trace concentrations of pesticides because of agricultural runoff and rainfall tainted with atmospheric pollutants. The indirect effects of released chemicals into the environment are also a cause of concern. Carbon dioxide gas from automobiles and power plants and Freon (refrigerant gas) released into the atmosphere may be involved in climatic changes as outlined in Figure 1.1. Continuous environmental monitoring is essential to protect the environment [2] from toxic contaminants and pathogens that can be released into air, soil and water, which may cause serious health problems [3].
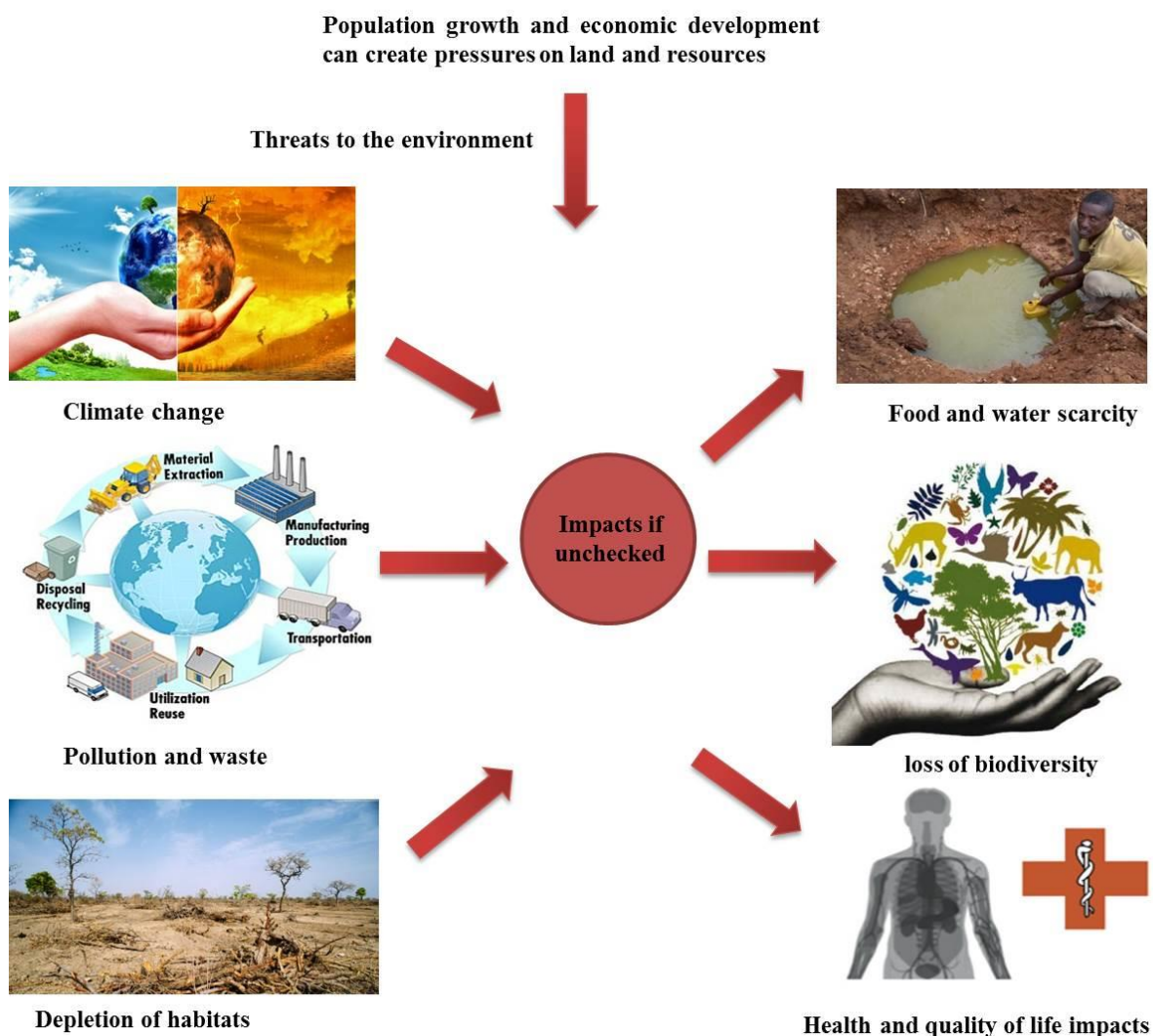
Figure 1. 1. Threats to the natural environment

1.1.1. Water pollution influence on health

Water is progressively becoming more polluted in our environment due to discharge of large amounts of metal ion-contaminated wastewater by industry [4] directly into the water supply. Several heavy metals are particularly of interest such as zinc, copper, nickel, mercury, cadmium, lead and chromium [5] which can be found in wastewater. These metal ion contaminants need to be removed before recycling or discharging directly into the surface water in order to prevent toxic conditions and serious health problems as a result of exposure [6]. Interestingly, small amounts of some elements are common in our environment and diet and are necessary for good health [7].

However, in excessive amounts of heavy metals are toxic; short term exposure results in damaged or reduced central nervous functions, lower energy levels, damaged lungs, kidneys, liver and other vital organs. Long term exposure may result in slowly progressing physical, muscular and neurological degenerative processes that mimic cancer [6]. Therefore, it is important to be aware of heavy metal toxicity and to take protective measures against excessive exposure. Water pollution problems have been becoming more complex, and threaten the quality of potable drinking water [8] prepared from these sources requiring complicated continuous on-line monitoring and multi-stage treatment processes [9-10]. The Earth contains 1.48×10^9 km^3 of water and it covers almost 70% of planet area [11]. Of the total global water, 3.5% is fresh water. Figure.1.2 shows that some water is locked up as ground water and ice [12]. The world faces a large range of environmental and human health crises related to the improper management of clean fresh water [13]. Worldwide deficiency and desertification are predicted to sharpen this burning issue. According to the World Watch Institute, in 2025 approximately two-third of the world's population will be affected by water shortages.
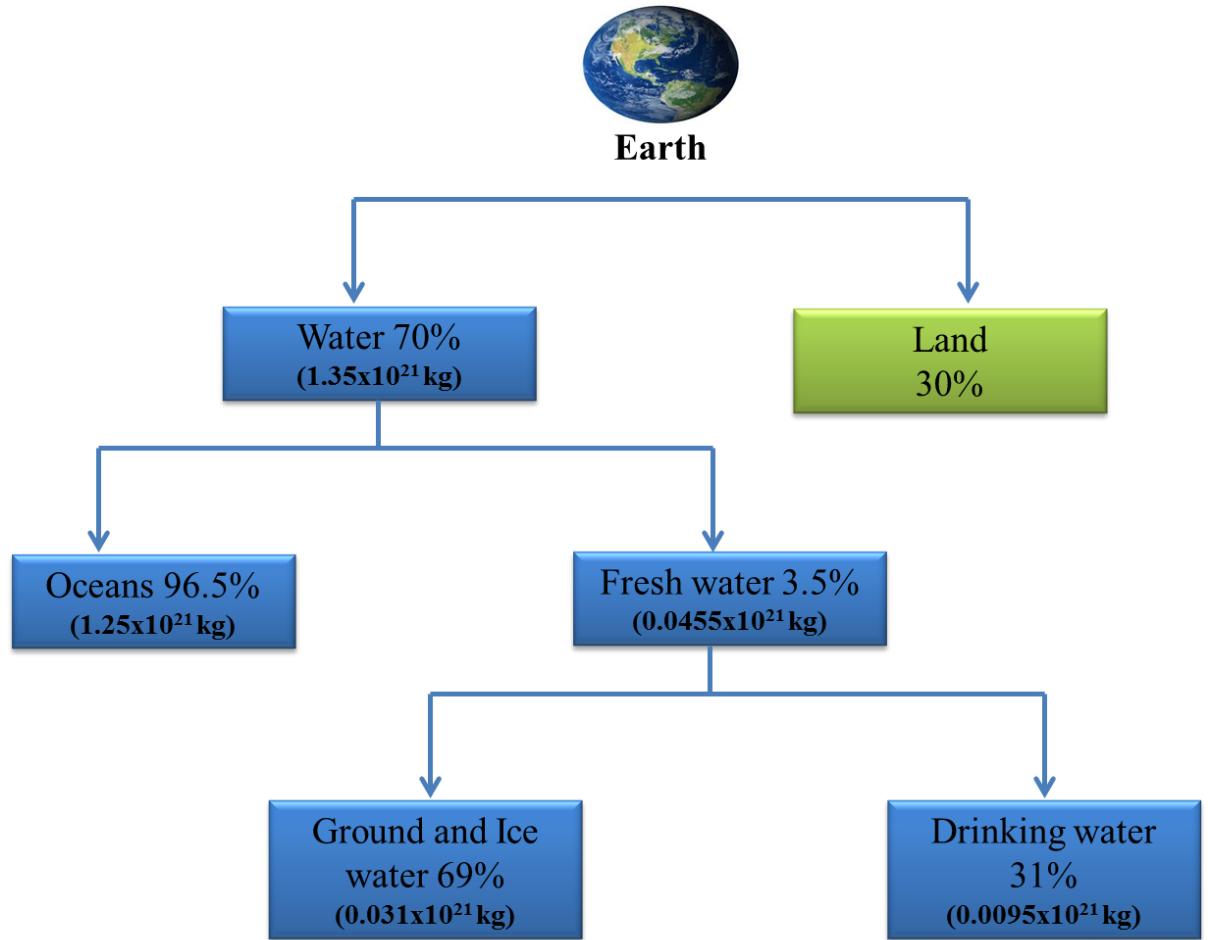
Figure 1. 2.Distribution of earth's water

Recently the development of sensors to determine pollutants in water is one of the approaches for the implementation of more sustainable use of fresh water. Water resources take up a unique position amongst other natural resources [14]. Water is the origin of existence of life on earth and one of the main components of environment. For sustaining high quality of life, social and economic development, water is essential.

1.1.2. Optical environmental sensors

The field of optical chemical sensors has been a growing research area over the last three decades. With the increase of urbanization of our society and climate change, there is an increase in the numbers of chemicals that are produced and used, which may

eventually reach environment through air or water systems. Optical chemical sensors have generated a great interest in the determination of various pollutants [15]. These devices offer online detection, miniaturization enabling at-site measurements and minimal waste production, which contributes to a better quality of life. There is a need for low cost, accurate, fast and long term monitoring of environmental contaminants using sensors that can be operated on site. For each contaminant a portable sensor is sought that can provide rapid response, ease of operation for field use and an appropriate detection limit. To meet market requirements [16], manufacturers have created novel devices including a remote sensor for environmental monitoring. Thus all countries should try to develop new technologies to overcome this problem [17]. Techniques have been developed to detect volatile organic compounds and pesticides in water. Smart sensors have been validated by the U.S. Environmental Protection Agency (EPA) to aid in spotting carcinogens in groundwater [18].

1.2. Technology advancement of point care testing

Current medical diagnostics monitoring of many diseases by conventional analysis in laboratory and hospital is perceived as invasive, time consuming and expensive. Point-of-care testing (POCT), also known as near-patient testing, refers to any analytical test performed outside the laboratory and may be located either within a hospital as an adjunct to the main laboratory or for primary healthcare outside the hospital setting. The users of this service are often nonlaboratory staff. Public awareness of the availability of POCT has increased dramatically, and access to this technology has never been greater.

Point-of-care testing beyond the laboratory

POCT beyond the laboratory is increasingly popular in some countries and it is particularly useful when patients live a distance away from a hospital laboratory [19]. The popularity of such devices is due to technological advances in the usability and reliability of these devices. Instrument manufacturers are producing devices that are simple to use, are autocalibrated and require minimum maintenance. POCT devices can be used to measure various blood physiological parameters, such as metabolites, blood gases and ions [20].

POCT testing is a simple medical test performed close to the patient where the results are available more quickly than for samples sent to a laboratory. Examples include the use of dipstick monitors, based on Immunoassays (IA) technology, which are thin plastic strips with several squares of different colors attached along the strip. Each square is used to measure a different component of the sample, usually urine. The entire test strip is dipped into the sample for the stated period and the color changes noted after stated time. Color change reference data is usually portrayed on the side of the container for the test sticks. The chemistry involved in the process leading to the color change is sophisticated and in general is proprietary to the manufacturer. An example of this sophistication is the detection of glucose for diabetes monitoring. Here glucose oxidase liberates hydrogen peroxide from the glucose and this reacts with a potassium iodide chromogen under the action of peroxidase to give a color change from green to brown [21]. The use of dipsticks for screening for drugs or their metabolites is common in many areas, for example, athlete screening, emergency medical care, consulting rooms, and drug detoxification programs. Tests can detect the commonly used

recreations drugs: cocaine, amphetamines, methamphetamines, marijuana, phencyclidine, barbiturates, benzodiazipines, and opiates [22].

The main advantages of dipsticks are the convenience, the ease of use, the low cost, and that an assessment of up to 17 drugs can be available within 5–8 minutes depending on the supplier. They can be used in the consulting room or in the home. There are however some limitations to these tests. They are generally not quantitative and the results may vary for different drugs from the same group, for example, the benzodiazipines. There is an insufficient level of specificity toward many of the pain management drugs and IA-based tests in this application are used for screening purposes only.

Point-of-care (POCT) technology for testing and monitoring of biomedical markers is a promising approach to: (i) decrease cost, save time and reduce complexity of analysis; (ii) enable close-to-home patient testing in medical centres and (iii) enable delivery of home healthcare services. However, even when highly accurate, many current clinical methods/techniques for biomarkers analyses have some limitations in terms of cost, size and integration into portable point-of-care medical devices. For instance electrochemical detection systems can offer high sensitivity, low-cost, good miniaturization potential and easy integration in compact analytical devices. Emerging POCT devices with miniaturized sensors based on different electrochemical techniques (e.g., potentiometric, amperometric) have the potential to supply real time information for the diagnosis and management of several diseases via self-analysis of physiological fluids such as blood, urine and sweat. Electrochemical biosensors are inexpensive, mass-produced disposable devices. Miniaturisation and use of only one drop of a few microliters of body sample is another factor that enables their use to be moved to the POCT setting [23].

1.3. Importance of human health monitoring

The presence of pathogens in environmental matrices mainly in water can cause a serious danger for human health [24]. In most countries chronic diseases lead to high health care costs and reduced productivity of people in society. The current global healthcare expenditure has grown into an economic sector exceeding 5-trillion-dollars [19]. Healthcare organizations want real-time, reliable, and accurate diagnostic results provided by devices that can be monitored remotely, whether the patient is in a hospital, clinic, or at home.

In recent years, heart disease has been a major widespread public health problem in most countries. Heart disease is costly for healthcare systems in many countries [25]. Diabetes is another common chronic disease in nearly all countries. There are an estimated 285 billion adults with diabetes in 2010 [26]; this number will continue to increase globally due to an aging population, growth of population size, urbanization and high occurrence of obesity and sedentary lifestyle [26].

In chronic disease patients, if monitoring of their health situation is carried out with high quality in coordination with nutrition program and physician orders, the quality of their health will improve dramatically. Modern technology tools should be used to the best advantage to reduce costs of health sector, increase the empowerment of people, improve the monitoring of patients through continuous assessment of symptoms and signs of disease and checking compliance with self-management programs and prevention of chronic diseases [27]. Telemedicine is a main tool for remote health care delivery and home care [19]. Some of the advantages of this technology in the health domain are fast and timely access to health information, reduced medical errors, and increased coordination among health care professionals and reduced travelling and the necessity for the physical presence of patients in urban health centres. One of the

innovations in the field of information technology in healthcare applications is mobile health systems. The application of remote medical diagnosis and monitoring system based on mobile health systems provides doctors and health care professionals access to central database and patient information. Mobile health could be a solution to overcome barriers of the requirement of the presence of health service personnel and timely access to health information related to patient especially in emergency situations. In addition it prevents test duplication and delays and errors in suitable treatment to patient.

Despite the potential advantage for mobile health programs, many challenges exist for developing and implementing these tools. Accordingly effective use of mobile devices in health systems requires extensive research and investigation of different aspects. Work on the development of mobile devices will benefit the general healthcare system.

Biosensors

The future of point-of-care diagnostics depends on the development of low cost, noncomplex, and easily integrated systems to examine biological samples such as blood and urine obtained directly from the patient. Some biosensors were recently proposed for biological ions detection [28-29]. Concentrations of biologically relevant ions are very important characteristics associated with state of health for diseases prediction. The detection of potassium and sodium ions is important for biomedical application research. The changes in potassium ions in human serum may be due to acute cardiac arrhythmia and the changes in sodium ion concentration in human blood may be due to kidney failure [30]. Ion Sensitive Field-Effect Transistors (ISFETs) fabricated with semiconductor technology [31] are very promising devices for the detecting of ion activity in human body. In the detection of clinically relevant ions, selectivity, accuracy, sensitivity and linearity are the important parameters [32].

1.4. Levels of water quality assessment

Monitoring activities must be appropriate to the socio-economic, technical and scientific development of the countries [33]. For instance, some water quality variables (e.g. organic micropollutants and trace elements) require highly trained technicians and costly laboratory facilities. Basically it is possible to distinguish three levels with increasingly sophisticated equipment as mentioned below.

➢ Simple monitoring based on a limited number of samples, simple analyses or observations, and data treatment which can be performed by pocket calculator.

➢ Intermediate-level monitoring requiring some specific laboratory facilities and more financial support to increase the number of stations, samples, analytical variables, etc. Personal computers (PCs) are recommended for processing data.

➢ Advanced-level monitoring involving sophisticated techniques and highly trained technicians and engineers. The analytical facilities can perform any pollutant determination required, with an increasing number of variables per sample, and of samples taken. Large computer data storage and handling facilities, such as a mainframe computer, are required for data treatment.

All elements of assessment, from objective setting to data interpretation, will be related to these three levels. The ultimate aim is to promote monitoring operations from the basic level to the more elaborate ones, in accordance with increasing complexity of water quality problems.

1.5. Chemical sensors components

The chemical sensors area (detectors/transducers) covers a wide category of devices used to monitor, measure, test, analyse data as generated due to changes in a measured

norm (usually concentration for chemical sensors) into an analytically electrical signal. The chemical information may originate from a chemical reaction by a biomaterial, chemical compound, or a combination of both attached onto the surface of a physical transducer toward the analyte. The chemical sensor area is an emerging discipline formed by the multidisciplinary study of chemistry, biology, optics, mechanics, acoustics, semiconductor technology, microelectronics technology, and membrane technology. Although the history of chemical sensors dates back not too long ago, it has gained increasing attraction for applications in environmental monitoring, industrial process monitoring, medicine, gas composition analysis etc [34].

The overall sensor quality is dependent on the total sensor system components, which are the sensitive layer (immobilization techniques), transduction mechanism (optical, electrochemical, calorimetric etc.), data-acquisition electronics and evaluation software. Moreover, chemical sensor mainly depends on sensitive layer and transducer shown in Figure1.3. [35].
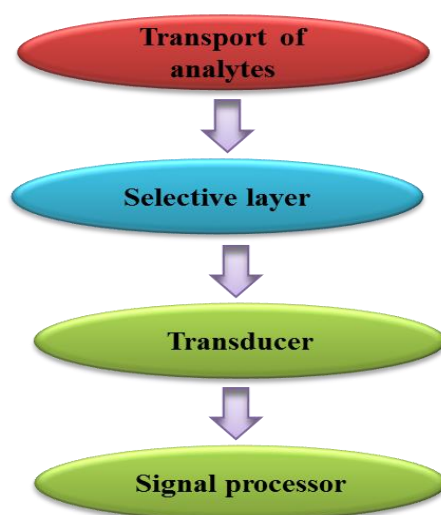
Figure 1. 3.Generalized schematic representation of chemical sensor

The analyte sensitive layer represents the main part of the sensor. Many materials such as organic, inorganic or hybrid organic-inorganic polymers can be used as active layers, providing that pollutants can diffuse into the matrix and be trapped, thus modifying the physical or/and chemical properties of the material. The active layer can also be doped with specific probe-molecules able to react selectively with the targeted pollutants, thus enhance the selectivity of the sensor [36].

1.6. Performance Factors

With respect to the development of new chemical sensors the following requirements must be addressed: sensitivity, accuracy, repeatability, reproducibility, stability, reversibility, low maintenance and plausibility of data. As analyses may be carried out in remote locations, they require more rugged but reliable instrumentation than laboratory installations [37]. Performance of a chemical sensor depends on the mentioned factors below:

I.   **Selectivity:** This is the most important characteristics of sensors. This part is responsible to discriminate between different substances.

II. **Limit of detection/Sensitivity:** This usually needs to be sub-millimolar, but in special cases can go down to the femtomolar (10^{-15} M) range

III. **Accuracy:** this needs to be better than $\pm$ 5%

IV. **Nature of solution:** Conditions such as pH, temperature, liquid/solid/gas environment

V.   **Response time:** This is usually much longer (30s or more) with a biosensor than with chemical sensor

VI. **Recovery time (reversibility):** Recovery time indicates the elapses before the sensor is ready to analyse the next sample, it must not be more than a few minutes

VII. **Stability:** This can vary from sensor to sensor: it can range from a few days to few months.

VIII. **Linearity:** Maximum linear value of the sensor calibration curve. Linearity of the sensor must be high for the detection of high substrate concentration.

IX. **Signal to noise ratio:** Ideally this should be high in order to determine the analyte accurately

X. **Repeatability:** The ability of a sensor to repeat a measurement in the same environment conditions

XI. **Reproducibility:** The ability of a sensor is to repeat the study (n) duplicate or triplicate.

1.7. Optical techniques for detection of analytes

An optical chemical sensor is a device that transforms chemical information, ranging from the concentration of a specific sample component to total composition analysis, into an analytically useful signal. Optical techniques are a popular and effective way of transducing sensor interactions into readable signals [38]. These include collection and analysis of absorption spectra, reflectance spectra, surface plasmon resonance data, luminescence intensity and evanescent waves data. Optical chemical sensors have enabled the determination of various pollutants in the environment, which can be toxic and may cause serious health problems [15]. In order to yield a response, optical methods rely on physical changes in the components materials. Such changes include

photon emission or transfer, change in reflectivity, refractive index, scatter coefficient and dielectric constant. Changes can be caused by the interactions with the analytes. Optical techniques are typically preferred over others because of their ability for remote sensing. However each technique has its own limitations and new challenges: large scale manufacturing and stability hurdles have yet to be overcome.

The principal function of optical sensors is to recognize the analyte in the samples and to translate this recognition into optical property changes. The effectiveness of an optical chemical sensor depends on the proper choice of indicators and the sensing platforms are chosen to determine the analyte [15]. The chemical information can originate from a chemical reaction of the analyte or from a physical property of the investigated system [39].

Typically optical chemical sensors contain some basic functional units:

- ❖ Receptor part (sensing element)
- ❖ Transducer part

In the receptor part of a sensor the chemical information is transformed into a form of energy which may be measured by the transducer. The receptor part defines a parameter e.g, the concentration of the given compound and provides an optical signal. In some cases a membrane is used to impart selectivity. The transducer part is a device capable of transforming the energy carrying the chemical information about the sample into a useful analytical signal shown in Figure 1.4. the transducer role is to convert the variation of a physical property e.g. refraction index, dimensions due to chemical/physico-chemical interaction (H-bond formation, chemical reaction) and measure the optical signal which is proportional to the pollutant concentration. Optical

methods of transduction based on absorption or fluorescence measurements provide the fast response of the sensor [36] but typically require an electronic read-out.
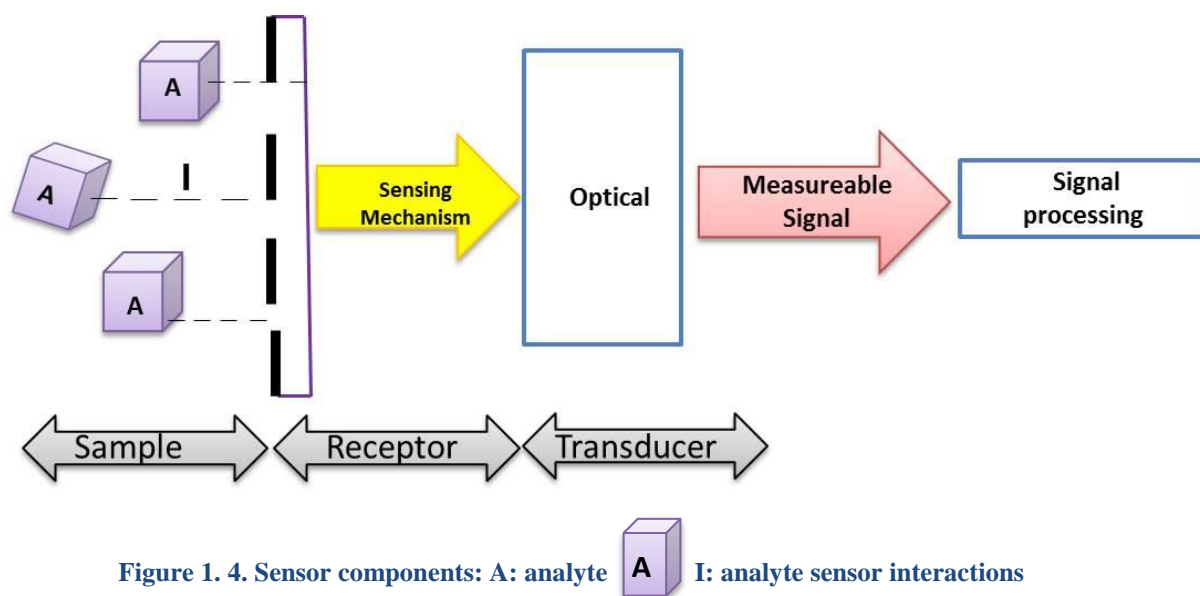
Figure 1. 4. Sensor components: A: analyte **A** **I: analyte sensor interactions**

The recognition component (Receptor) and the transducer are shown in Figure 1.4. The analyte interacts with the sensor at the recognition component and generates a change. The nature of this change is known as the sensing mechanism and it is governed by the analyte sensor interactions and in combination, the change is interpreted by the transducer generating a measurable signal. Understanding these fundamental elements is important for developing new/different sensors. Once an analyte is known to interact with a recognition component, the sensing platform can be designed. Therefore, designing new sensors relies mostly on understanding the sensing mode, the analyte interactions with the recognition component, and the change observed in the sensing mechanism. Since that is the scope of this work, particular attention will be paid to these factors and to the physical properties of the analytes and materials used in the sensor components.

1.8. Metal ion sensors

1.8.1. Introduction

The chemical sensor market has been projected to grow to worldwide within the next 10 years [15]. Some of the primary motivations to develop nanostructured chemical sensors are monitoring and control of environmental pollution; improved diagnostics for point of care medical applications; reductions in measurement time, sensor size and power consumption; improvement of precision and accuracy; process and quality control of industrial applications. Various types of metal ion sensors have been developed for detection and monitoring of metals in solutions.

The miniaturisation of analytical instruments using microfluidics is one strategy to move this concept forward. Microfluidics refers to a set of technologies which deals with precise control and manipulation of fluids in micro and picolitre scales that are geometrically constrained in microfluidic devices with internal sizes ranging from approximately 1 to 1000 μm [40]. Soft lithography using polydimethylsiloxane (PDMS) allows one to fabricate complex channels in microfluidic devices easily and at low cost. A PDMS drawback is it swells in the presence of many organic solvents significantly degrading the performance of the device. However, this holds great potential for scale-up and the high volume production of inexpensive devices capable of performing sophisticated functions [41]. The possibility of manipulating smaller amounts of sample volume combined with the need for faster response times has placed great demands on the corresponding detection systems. The advancement in Light emitting diode (LED) sources and photodetector technologies provide a solution to these issues as they are compact, low power and low cost detectors for incorporating colorimetric analytical methods into remotely deployable devices.

LEDs have been widely used in consumer electronic devices, and in more specialist applications such the illumination source for fibre optic sensors and reflectometers [42]. LED sources and photodetector technologies are compact, low power and low cost detectors for incorporating colorimetric analytical methods into remotely deployable devices [43]. LEDs have the ability to be coupled (for example, with waveguides or optical fibers) to a wide variety of detectors such as, photodiode-arrays.

Thin film materials can lead to unique new chemical sensor platforms. The sol-gel technique is getting the worldwide attention of researchers in the field of material science, due to its versatility in synthesising inorganic ceramic materials at mild conditions. High purity, homogeneity, controlled porosity and nanoscale structuring are the most remarkable features offered by this method for generating highly sensitive and selective matrices to incorporate analyte molecules [44]. The crafting of sol-gel sensors through molecular imprinting has allowed the development of innovative chemical sensors [45].

Sections 1.82, 1.8.3 and 1.8.4 provide an overview of most promising recent technologies including LED interrogated sensors, microfludic sensors and sol gel sensors.

1.8.2. LED interrogated chemical sensors

Light emitting diode (LED) based chemical sensors are popular due to their non-invasive, increased lifetime, low cost, flexible configurations. They also have reduced power consumption, enhanced spectral purity, small size due to the commercial availability of 247 nm-1550 nm spectral band LEDS. They can be utilised to monitor environmental hazards which are the source of health risk and can also be employed as

a chemical sensor to monitor nitrate/nitrite, ammonia, phosphorus, cations/metals and anions [43].

Carducci et al. developed cost-effective, linear and highly sensitive portable optical sensors designed to detect very low chlorophyll concentration and low level turbidity using an optical method. The presented model was integrated on a board where two LED sources emitting red and blue light were used to measure both chlorophyll-a and turbidity. The system had a chlorophyll sensitivity of 1 mV/2.5 µg/l [46].

C.L.M de Moris et al. present work on novel microcontrolled photometer based on light-emitting-diodes (LEDs) for detection of Pb^{2+} using gold nanoparticles (AuNPs). The photometer makes use of a single LED as a light source, a sensor and electronic card as an acquisition system. On the sensor, the light from the three closely adjoined red, green, and blue LEDs composing the "white" light source LED is contact-coupled to the map-illumination pointed toward the detection cell. To maintain a constant light intensity, a common white-color LED (emitting a 450–620 nm continuous spectrum) was employed as a controllable light source. Pb^{2+} measurements are based on the color change of AuNPs due to their aggregation provoked by Pb^{2+}. The method showed excellent selectivity for Pb^{2+} compared to other metal ions ($Ag+, Ba^{2+}, Ca^{2+} Cd^{2+} Co^{2+}, Cr^{3+}, Cu^{2+}, Fe^{2+}, Hg^+, K^+, Li^+, Mg^{2+}, Ni^{2+}, Sn^{2+}, Sr^{2+}$, and Zn^{2+}). Pb^{2+} was detected with the photometer and also monitored via UV-Vis. Solutions containing Pb^{2+} in the concentration range from 0.6 to 10 mmol L^{-1} were employed to construct the analytical curves, proving a limit of detection (LOD) of 0.89 mmol L^{-1}. The sensitivity was compared to that obtained with a UV-Vis spectrophotometer at 520 nm. A repeatability of 4.11% (expressed as the relative standard deviation of 10

measurements) was obtained. The proposed method was successfully applied to detect Pb^{2+} in polluted water samples [47].

1.8.3. Microfluidic Sensors

The history of microfluidic sensors is relatively short. With microfluidic/nanofluidic technology it is possible to control the flow of liquids on microscale or nanoscale level (liquids for controlling or sensing purposes) [48]. The microfluidic system, which is base on a fluidic platform, possesses many advantages owing to the miniaturization of the devices. These merits include reduced consumption of reagents and analytes, improved time efficiency in the analysis, shrinkage in the size and weight of the systems, increased portability, reduced amount of harmful by-products, and potentially low cost in fabrication. Consequently, microfluidic systems have found a wide range of applications. Three clear fields utilizing the advantages of micromechanics and system design have materialised. The application fields are ink jet printer heads with nozzle arrays, micro dosing systems and micro chemical analysis systems.

Zhihong Nie et al. fabricated microfluidic paper-based electrochemical (mPED) sensing devices. The mPEDs comprise paper-based microfluidic channels patterned by photolithography or wax printing, and electrodes screen-printed from conducting inks (carbon or Ag/AgCl). mPEDs are capable of quantifying the concentrations of various analytes (e.g., heavy metal ions and glucose) in aqueous solutions. The measurements of heavy metal ions in the mPEDs have high sensitivity and low limit of detection of 1.0 ppb. This sensor is low-cost uses, small sample volumes has a quick response and applicability to a wide range of analytes [49].

Lafleur et al. reported a microfluidic sensor for the rapid detection of two important classes of environmental contaminants such as heavy metals and pesticides, using gold nanoparticles. The detection limits as low as 0.6 µg L^{-1} and 16 µg L^{-1} could be obtained for the heavy metal mercury and the dithiocarbamate (DTC) pesticide ziram, respectively. These results revealed that the sensor offers an attractive detection of environmental contaminants, such as Hg and ziram, on portable microfluidic devices. The simple microfluidic system presented allows mixing of all the necessary standards and reagents directly on the disposable chip. They also reported a novel detection scheme for DTC pesticides with a detection range extending from 0.61µg L^{-1} for Hg and 16µg L^{-1} to 150 µg L^{-1} for ziram. The low detection limits achieved with fluorescence quenching determined as blank and wide linear ranges suggest that these devices could be used in conjunction with small, portable detection equipment, such as cameras readily found in consumer electronics for direct sensing at remote locations. Optical properties of gold nanoparticle probes are combined with the inherent qualities of microfluidic platforms to offer simple, portable and sensitive sensors for environmental monitoring [50].

1.8.4. Sol-gel based sensors

An important aspect of the sol gel technology is the possibility to control the mechanism and kinetics of the chemical reactions, thus defining the final structure (particle size, porosity, thin layer thickness) of the materials. A low processing temperature is required for the synthesis of porous matrices for entrapping organic and inorganic compounds for optical and electrochemical sensors. Sol-gel technology performs new analytical tasks that are unattainable by other technologies. However, the simplicity and versatility of the sol-gel process allows it to be used more efficiently for sensing applications than other matrices that are currently produced. [44].

Samadi et al. presented a highly selective optical sensor for Fe (II) ions based on entrapment of a sensitive reagent, 2,4,6-tri(2-pyridyl)-s-triazine (TPTZ), in a silica sol–gel thin film coated on a glass substrate. The proposed sensor is able to determine iron even in the presence of other metal ions that can exist in natural waters with detection limit of 1.68 ng mL^{-1}. The fabricated sensor has a high performance in number of key parameters such as reproducibility, reversibility, stability, fast response time and long-term stability in comparison to the sensors which were previously reported [51].

A Zn(II) optical sensor was developed by incorporating 4-(2-pyridylazo)resorcinol in a sol–gel thin film. The sensor was coupled to a multicommutated flow system and applied to the direct determination of Zn(II) in injectable insulins. Optical transduction was based on the use of a dual-color LED and a photodiode. The sensor showed optimum response at pH 5.5 with maximum absorbance at 500 nm. A linear response was obtained for Zn(II) concentration range of 5.0–25.0 µg L^{-1}, with detection limit of 2.0 µg L^{-1} and sampling frequency of 16 samples h^{-1}. The results obtained on real samples analyzed were in good agreement with those obtained by a standard method, with relative standard deviation errors less than to 1.2% [52].

1.9. Molecular Recognition Components

1.9.1. Zeolites

Sensors made of nanomaterials have the potential for offering new generation of sensing devices that are smaller, inexpensive, with less power consumption and having a higher performance than conventional sensors. Zeolites are microporous crystalline solids with well-defined framework structures with regular and uniform pores of molecular dimensions [53]. One of the possible solutions in the development of effective

environmental sensors could be zeolite crystalline nanoparticles which can be used in the design and fabrication of analyte selective structures. These are sensitive to their environment and can be used to detect the presence of a particular environmental stressor such as water pollutants [54]. Zeolites have several unique features which make them suitable for the fabrication of metal ion sensors in water. Zeolites are characterised by a porous structure with a pore size similar to the size of many industrially important molecules. Their main application is in catalysis and membrane design. There are many reports on trapping of a variety of chemicals in zeolites[55-61]. Due to the large variety of zeolite nanoparticles structure and chemical composition, the flexibility in their synthesis and the possibility to functionalise them, these nanoparticles are ideal candidates for incorporation in the design of sensors.

1.9.2. Ionophores

1.9.2.1. Crown ethers

Another possible approach for the development of effective sensors is the use of crown ethers. They have a remarkable capacity to form stable complexes with certain cations, particularly with alkali and alkaine earth cations which feature in blood monitoring (i.e., Na^+, K^+ and Ca^{2+}). Complexation of metal ions with chelating agents is employed in separation, removal of specific species, ion-selective electrodes, biological mimics and reaction catalysts. Commonly used species of complexation agents are crown ethers and calixarenes, which consist of cyclic compounds that comprise ether groups. Crown ethers have different binding strengths and selectivities for metal cations. They have great potential in the fabrication of highly sensitive and selective metal ion sensors [62].

1.9.2.2. Calixarenes

An Ionophore is a ligand able to form complexes with ions or neutral molecules and to transport them within a membrane [63]. Tetraethyl p-tert-butylcalix[4]arene tetraacetate (also called sodium ionophore) is the sensing element material in PVC-based membrane sensors. It was previously reported that sodium ionophores had a very good selectivity over common alkali, alkaline earth and heavy metal ions [64].

1.9.3. Phenylboronic acid

Recently, there is an increasing interest in boronic acid compounds. Boronic acid compounds are important because their usage in the synthesis of biologically active compounds. Binding diols with high affinity through reversible ester formation with the boronic group is one of the important characteristics [65]. Phenylboronic acid and its derivatives show fluorescence which can be decreased on binding sugars resulting in the development of glucose sensor. Such a system can be composed from one or several components and can be characterized by the increase or decrease of fluorescence emission intensity [66].

1.9.3. Cellulose Acetate

Cellulose Acetate is an amorphous, colorless, transparent, and moderately hard thermoplastic with good optical properties. Cellulose is an abundant and renewable resource found in most parts of the world, which makes it a cheap raw material for various applications. It has been studied extensively in the past two decades for possible application in mopping up toxic heavy metals from the water [67]. The material has some special properties, such as good environmental stability, light weight, flexible and is easy to fabricate [68]. Cellulose acetate has a property of salt rejection. Furthermore

the membrane can be modified by adding a pore former Polyethylene glycol (PEG) in order to get a porous structure. Moreover the layers possess moderate UV stability. Owing to its high moisture absorption the normal difficulties of dimensional changes arise since it is easily swollen.

1.9.4. Molecular imprinted polymers

Molecular imprinting is a very powerful synthetic method for preparation of robust materials with pre-designed molecular selectivity [69]. Molecular imprinted polymers (MIPs) are cross linked polymers, containing cavities. Molecular imprinting technology offers a means of preparing materials with cavities that are able to recognise a certain molecule in terms of shape, size and chemical functionality. The cavities are prepared in the presence of a template molecule and can exhibit high affinity and selectivity for target molecules. These templates are created by copolymerisation of cross linking monomers and functional monomers along with an imprinted molecule or template. MIPs are attractive candidates for determining antibodies in many analytical and bioanalytical [70] applications, e.g. for development of biosensors and for drug assays. In addition to selective molecular binding, new functions are being added to MIPs to make the synthetic materials responsive to different environmental conditions, making it possible to modulate the binding and release of different molecular targets and to simplify affinity separation [71].

1.10. Target analytes and their detection

The applications of chemical sensors for detection of analytes in liquids and to identity the relevant ions is focused in the present research work. The analysis of metal ions is important in the modern world. Specifically there are two direct situations where rapid metal analysis can have an important effect in public health. The first is water pollution

where toxic metals (copper, lead, nickel, cadmium, etc) enter the water supply and can have a severe toxic effect on the population unless identified immediately [72]. Health risk associated with polluted water includes different diseases such as respiratory disease, kidney, diarrheal disease, skin, neurological disorder and cardiovascular disease [73]. The second is rapid physiological measurements to monitor the levels of primary ions such as sodium, potassium and calcium; such monitoring allows the physician to identify whether the health of the patient is deteriorating. The present research work focuses on the detection of five important metal ions analytes. Therefore, it is important to be aware of heavy metal toxicity and to take protective measures against excessive exposures.

1.10.1. Copper (Cu^{2+})

Essential metals are vital elements for human biology; at low levels copper is one of the essential micronutrient for life [74]. In the human body, copper appears in both oxidation states: Cu(I) and Cu(II). Copper absorbed from the diet (food, supplements and water) is mainly Cu(II), but in order for it to be absorbed in the intestine by the enterocyte's membrane it has to be reduced to Cu(I) via reductases [75]. The excessive ingestion of copper brings about serious toxicological concerns, such as vomiting, cramps, convulsions, or even death.

 Copper levels at the tap is regulated under the Environmental Protection Agency's (EPA's) copper and lead Rule at an action level of 1.3 mg/L [76], and as a result, many drinking water utilities practice corrosion control (e.g., phosphate addition, pH adjustment). In drinking water systems, oxygen and disinfectants are used to destroy microorganisms and control biofilms such as free chlorine, monochloramine and chlorine-dioxide. These decay as they interact with bulk water constituents, drive

copper corrosion and react with other materials on the pipe wall including biofilm. The challenge is to provide good drinking water quality, both biologically and chemically.

1.10.2. Lead (Pb2+)

Lead is a metal that is known to be neurotoxic to humans, and to have many other harmful health effects at high levels of exposure. At lower exposure levels, children appear to be particularly vulnerable to environmental lead effects, with an association with intellectual and cognitive outcomes observed at blood lead levels below $10\,\mu g/L$. Lead can cause central nervous system damage, damage the kidney, liver and reproductive system, basic cellular processes and brain functions. The toxic symptoms are anemia, insomnia, headache, dizziness, irritability, weakness of muscles, hallucination and renal damages [77]. Humans are exposed to lead through ingestion and inhalation. The main sources of lead for humans are leaded paint, water contacting lead bearing plumbing, diet, soil, dust and dirt. Although the potential routes for lead entering into the body are relatively well documented, there is still much to understand about the factors determining uptake, particularly around how interactions and genetic factors influence lead absorption [78]. Lead is found in drinking water when it dissolves from lead pipework, mains connections and plumbing fittings. The upper limit for lead in drinking water is $10\,\mu g/L$ [79].

1.10.3. Calcium (Ca2+)

Drinking water also provides small daily doses of calcium and other essential minerals, and may be an important source throughout the entire lifespan [80]. Hard water does not appear to have a deleterious effect on animals, but it often is reported as part of water quality analysis. Hardness is a measure of the calcium and magnesium ions present in

the drinking water. Water with high total dissolved solids or salinity may or may not be hard water. Water is classified according to calcium and magnesium salt content as follows: soft water ranges from 0 to 60 ppm $CaCO_3$, hard water varies from 120 to 180 ppm and very hard water is greater than 180 ppm $CaCO_3$ [81].

1.10.4. Potassium (K+)

Potassium is the most abundant cation in the body and is widely spread in tissues of animals and plants. Potassium ions play key roles in biological systems, including blood pressure regulation, maintenance of muscular strength and extracellular osmolality, transmission of nerve impulses, proper digestion, protein synthesis and enzyme activation [82]. Potassium ion concentration in blood and other biological fluids is typically determined in clinical analysis [83]. Serum concentrations are low, its normal range being between 3.5 and 5 mmol/l [84]. This implies that small variations in serum potassium concentrations may represent a significant decrease in intracellular or extracellular potassium. It is known that variations in its concentration, both hypokalaemia and hyperkalaemia, are associated with mortality. Hyperkalemia is characterized by a serum potassium level > 5.5 mmol/L. Although there is some variability among laboratories in the definition of the normal range of values for potassium, urgent treatment is usually considered when the potassium level is higher than 6.0 mmol/L. Hypokalemia is defined as a serum K^+ level <3.5 mmol/L and is one of the most common electrolyte disorders. It can be associated with either decreased or normal total body potassium content. Abnormal K^+ concentration is a symptom of several diseases, including kidney diseases, alcoholism, anorexia, heart disease and diabetes. Thus, selective and sensitive K^+ sensors are important for the detection of physiological potassium ions level to facilitate diagnosis and treatment [85].

1.10.5. Sodium (Na+)

Sodium is not only the predominant ion of seawater but one of the most ample salt in the earth's crust, often found in mineral waters [86]. The detrimental effects of a high salt diet on human health high dietary salt intake can be reason to cause cardiovascular diseases [87]. Sodium intake may be linked to healthy or unhealthy food that may exaggerate the effect of sodium intake.

Serum sodium concentration is considered an important regulatory factor for extracellular volume status and blood pressure [88]. Excess dietary sodium has been linked to elevations in blood pressure. High dietary sodium can adversely affect multiple target organs and tissues, including the vasculature, heart, kidneys, and areas of the brain that control autonomic outflow. Physiological requirements for sodium are <500 mg/day in most healthy individuals [89]. Normal levels of sodium in serum are 135-145 mmol/L [21]. Abnormal levels are very common electrolyte disturbance in hospitalised patients. Hyponatremia and hypernatremia are associated with adverse outcomes in patients admitted to intensive care units. Hyponatremia is generally defined as a serum levels of < 135mmol/L. Hypernatremia, defined as sodium levels higher than 145 mmol/L.

By choosing appropriate sensing layers one can demonstrate that the optical platform can be used as a valuable tool in the detection of analytes described above to benefit public healthcare.

1.11. Overview of Holographic sensors

A hologram is a three dimensional image made with a laser beam. Holograms produced in polymer hydrogels, such as acrylate, acrylamide and vinyl alcohol, have been used for holographic sensing of glucose, lactate, alcohol, toluene, pH and different types of ions by introducing extra functional groups. Polymers in general have been explored as potential sensor components due to their flexibility. Including functional groups in the polymers is a way of enhancing the chemical and physical interactions with the analytes, thereby conferring improved sensitivity and selectivity. The physiochemical interaction will vary depending on the analyte-sensor types.

Holography allows the fabrication of disposable sensors that are lightweight for miniaturization and multiplexing purposes [62]. A hologram integrates all the components which are required for a sensor to function. Holograms can be modified to detect and quantify environmental changes, such as changing temperature or humidity, and also the presence of certain substances such as harmful gases and metals. The sensing mechanism is based on a change in the holographic gratings properties due to dimensional change or change in in the optical properties of the layer. In Figure 1.5 elements similar to those in Figure 1.4 in a holographic sensor are wavelength λ or diffraction efficiency η as a signal. The periodic structure as the transducer; changes in (fringe spacing) Λ or refractive index (n) as the sensing mechanisms; and the film or particles as the recognition components. The principle of operation of holographic sensors is straightforward. The operating principle of a holographic sensor is based on detection of the scattering of the light wave propagating through a 3D periodic structure that changes its properties under exposure to the analyte. The interaction with the

analyte produces changes in optical properties of the sensitive film and in the holographic grating geometry.
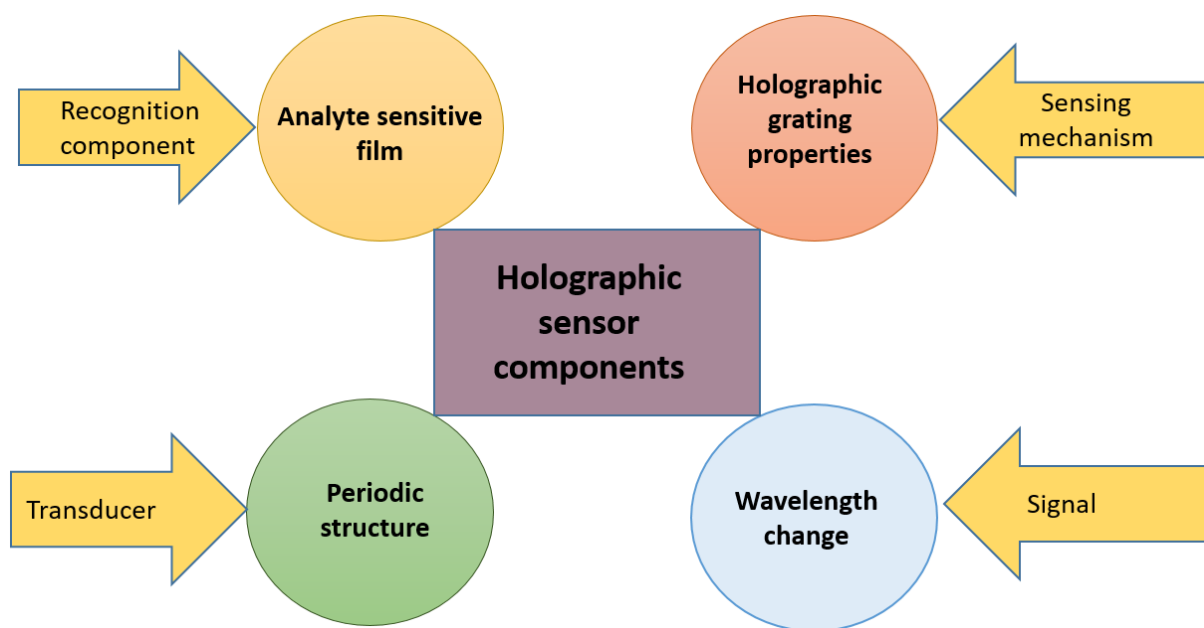
Figure 1. 5. Components of Holographic sensors

These changes ultimately cause alterations in the direction of the diffracted light and the diffraction efficiency due to dimensional changes or change in average refractive index/ modulation of the refractive index occurring in the photopolymer layer, when it is exposed to an analyte.

Laboratory based instrumental technologies involve the use of sophisticated, electronic and expensive signal processing equipment. In most of the cases a high degree of operator expertise and knowledge is required. Holographic sensors are analytical devices that systematically diffract narrowband light in the ultraviolet to near-infrared range for application in the detection and quantification of analytes and/or physical parameters. Photopolymers have become popular as a medium for recording holograms in recent years, due to their self-developing property when exposed to light [90]. The main advantage in using photonic holograms created in photopolymerisable

nanocomposites, for sensing, is the possibility for visual indication of the outcome of the detection process and easily interpretation by a non-specialist [3].

1.11. Aims of the project

The work described in this dissertation aims to address how the properties of different analyte sensitive materials can be used to fabricate disposable sensors by modifying the surface the with different analyte sensitive materials including

- ❖ LTL-Zeolites
- ❖ 18-Crown ethers-6
- ❖ Ionophores
- The aim is to produce holographic sensors for liquid phase analytes preferably, for copper [91], lead, and calcium. Detection of potassium and sodium because of their physiological relevance and mostly monitored in laboratory. Holographic surface gratings (SRG: periodically variation on the surface of the layer) will be modified and used as transducers of chemical interactions between hologram materials and liquid phase analytes. The resulting changes will provide a change in diffraction efficiency signal due to change in refractive index.
- SRG Holograms will be fabricated in self-processing acrylamide based photopolymer system, by incorporating LTL-zeolites nanoparticles, Dibenzo18-crown-6 chelating agents and calixarenes ionophores in surface relief holograms [92] will be investigated to develop chemical sensors for application in environmental monitoring and biomedical sensing in the liquid phase.

- A new formulation for volume holograms based on cellulose acetate will be developed. The material will be optimised in order to achieve maximum diffraction efficiency.

1.12. Chapter Summary

Chapter 2: Provides the basic theory of Holography optical elements (HOE) .This chapter also gives a brief introduction about the principle of operation of diffraction gratings, along with volume and surface holographic gratings. Also the chapter presents a literature review of the different holographic sensors technology

Chapter 3: This chapter describes in detail the results of fabrication and modification surface relief holograms (SRG's). This chapter also explains the underlying principle change in diffraction efficiency after exposure to an analyte.

Chapter 4: Describes the fabrication of copper, lead and calcium sensors by incorporation of LTL-zeolites nanoparticles. The structures were functionalised by modifying the surface with an over layer of sol gel including LTL. This chapter provides detailed description of the characterization techniques used in order to interpret the results of LTL-zeolites nanoparticles and surface relief holograms.

Chapter 5: Describes the sensor fabrication of sensors for metal ions detection in liquid phase sample. The structures were functionalized by incorporation of chelating agent dibenzo-18-crown-6 and tetraethyl 4-tert-butylcalix[4]arene (TBC) in plasticised polyvinyl chloride and in a sol gel matrix, providing results and discussion of the obtained results. The performance of the sensors for detection of K^+ and Na^+ was investigated.

Chapter 6: Development of new material to fabricate volume holographic gratings. These are diffractive elements consisting of a periodic refractive index variation throughout the entire volume of the element. This chapter provides information on optimisation of the cellulose acetate based diffraction grating and its response to the water environment. Preliminary results are presented for these holograms with functionalised with Tetraethyl p-tert-butylcalix[4]arene (TBC).

Chapter 7: This chapter consists of the main conclusions from the PhD research, and discusses some potential areas for future work. The outputs resulting from the dissemination of the research are also presented in this chapter.

References

[1]   David A. Sonnenfeld, "Maxico's '"Green Revolution,"' 1940-1980: Towards an Enviromenatl History," in *Enviromental History Review*, New York: Cambridge University Press, 1992, pp. 28–52.

[2]   R. K. Singh, "Environment Protection : Factors and Affecting Actions," *International Journal of Research -Granthaalayah*, vol. 3, pp. 2–4, 2015.

[3]   C. K. Ho, A. Robinson, D. R. Miller, and M. J. Davis, "Overview of Sensors and Needs for Environmental Monitoring," *Sensors*, vol. 5, no. 1, pp. 4–37, 2005.

[4]   M. Sa'idi, "Experimental studies on effect of Heavy Metals presence in Industrial Wastewater on Biological Treatment," *International Journal of Environmental Sciences*, vol. 1, no. 4, pp. 666–676, 2010.

[5]   P. A. Turhanen, J. J. Vepsalainen, and S. Peraniemi, "Advanced material and approach for metal ions removal from aqueous solutions," *Scientific Reports*, vol. 5, pp. 1–8, 2015.

[6]   F. Fu and Q. Wang, "Removal of heavy metal ions from wastewaters: A review," *Journal of Environmental Management*, vol. 92, no. 3, pp. 407–418, 2011.

[7]   F. S. Al-Fartusie and S. N. Mohssan, "Essential Trace Elements and Their Vital Roles in Human Body," *Indian Journal of Advances in Chemical Science*, vol. 5, no. 3, pp. 127–136, 2017.

[8]   B. Ochoo, J. Valcour, and A. Sarkar, "Association between perceptions of public drinking water quality and actual drinking water quality: A community-based exploratory study in Newfoundland (Canada)," *Environmental Research*, vol.

159, no. August, pp. 435–443, 2017.

[9]   S. Zhuiykov, "Solid-state sensors monitoring parameters of water quality for the next generation of wireless sensor networks," *Sensors and Actuators, B: Chemical*, vol. 161, no. 1, pp. 1–20, 2012.

[10]   E. Eltzov, R. S. Marks, S. Voost, B. a. Wullings, and M. B. Heringa, "Flow-through real time bacterial biosensor for toxic compounds in water," *Sensors and Actuators, B: Chemical*, vol. 142, no. 1, pp. 11–18, 2009.

[11]   I. Shiklomanov, "World fresh water resources," *Water in crisis a guide to the world's fresh water resources*. Oxford University Press, New York, pp. 13–24, 1993.

[12]   A. Oren, "Saline lakes around the world: Unique systems with unique values , 10th ISSLR conference and 2008 FRIENDS of Great Salt Lake forum , May 11-16 , 2008 , University of Utah , Salt Lake CIty," *Natural Resources and Environmental Issues*, vol. 15, 2009.

[13]   I. C. Karagiannis and P. G. Soldatos, "Water desalination cost literature: review and assessment," *Desalination*, vol. 223, no. 1–3, pp. 448–456, 2008.

[14]   M. F. Chaplin, "Water: Its importance to life," *Biochemistry and Molecular Biology Education*, vol. 29, no. 2, pp. 54–59, 2001.

[15]   H. Qazi, a Mohammad, and M. Akram, "Recent Progress in Optical Chemical Sensors," *Sensors*, vol. 12, no. 12, pp. 16522–16556, 2012.

[16]   K. Gainer, "Environmental Sensing and Monitoring Technologies: Global Markets," Wellesley, MA, 2014.

[17] P. H. Gleick, "Water in crisis: Paths to sustainable water use," *Ecological Applications*, vol. 8, no. 3, pp. 571–579, 1998.

[18] S. Neethirajan, D. S. Jayas, and S. Sadistap, "Carbon dioxide (CO 2) sensors for the agri-food industry-A review," *Food and Bioprocess Technology*, vol. 2, no. 2. University of Manitoba, Winnipeg, Canada, pp. 115–121, 2009.

[19] J. Barjis, G. Kolfschoten, and J. Maritz, "A sustainable and affordable support system for rural healthcare delivery," *Decision Support Systems*, vol. 56, no. 1, pp. 223–233, 2013.

[20] L. J. Stoot, N. A. Cairns, F. Cull, J. J. Taylor, J. D. Jeffrey, F. Morin, J. W. Mandelman, T. D. Clark, and S. J. Cooke, "Use of portable blood physiology point-of-care devices for basic and applied research on vertebrates: A review," *Conservation Physiology*, vol. 2, no. 1, pp. 1–21, 2014.

[21] B. F. Thomas, *Analytical Chemistry for Assessing Medication Adherence Emerging Issues in Analytical Chemistry Series Editor*. Cambridge, MA, USA: Elsevier Inc., 2016.

[22] https://www.sciencedaily.com/releases/2006/11/061113175828.htm [accessed 06-10-2018].

[23] A. Tricoli and G. Neri, "Miniaturized bio-and chemical-sensors for point-of-care monitoring of chronic kidney diseases," *Sensors (Switzerland)*, vol. 18, no. 4, pp. 1–18, 2018.

[24] C. Justino, A. Duarte, and T. Rocha-Santos, "Recent Progress in Biosensors for Environmental Monitoring: A Review," *Sensors*, vol. 17, no. 12, p. 2918, 2017.

[25] N. Mohammadzadeh, R. Safdari, and A. Rahimi, "Multi-agent system as a new approach to effective chronic heart failure management: key considerations," *Healthcare Informmatics Research*, vol. 19, no. 3, pp. 162–166, 2013.

[26] P. Zhang, X. Zhang, J. Brown, D. Vistisen, R. Sicree, J. Shaw, and G. Nichols, "Global healthcare expenditure on diabetes for 2010 and 2030," *Diabetes Research and Clinical Practice*, vol. 87, no. 3, pp. 293–301, 2010.

[27] G. Pare, K. Moqadem, G. Pineau, and C. St-Hilaire, "Clinical effects of home telemonitoring in the context of diabetes, asthma, heart failure and hypertension: A systematic review," *Journal of Medical Internet Research*, vol. 12, no. 2, 2010.

[28] S. Gayathri, N. Rajkumar, and V. Vinothkumar, "Human Health Monitoring System Using Wearable Sensors," *International Research Journal of Engineering and Technology*, vol. 2, no. 8, pp. 2395–56, 2015.

[29] S. Kabilan, A. J. Marshall, F. K. Sartain, M. C. Lee, A. Hussain, X. Yang, J. Blyth, N. Karangu, K. James, J. Zeng, D. Smith, A. Domschke, and C. R. Lowe, "Holographic glucose sensors," *Biosensors and Bioelectronics*, vol. 20, no. 8 SPEC. ISS., pp. 1602–1610, 2005.

[30] K. I. Ho, T. F. Lu, C. P. Chang, C. S. Lai, and C. M. Yang, "Sodium and potassium ion sensing properties of EIS and ISFET structures with fluorinated hafnium oxide sensing film," *Proceedings of IEEE Sensors*, pp. 1128–1131, 2009.

[31] Y. Guo, K. Seki, K. I. Miyamoto, T. Wagner, M. J. Schöning, and T. Yoshinobu, "Device simulation of the light-addressable potentiometric sensor with a novel photoexcitation method for a higher spatial resolution," *Procedia Engineering*,

vol. 87, pp. 456–459, 2014.

[32] C. S. Lee, S. Kyu Kim, and M. Kim, "Ion-sensitive field-effect transistor for biological sensing," *Sensors*, vol. 9, no. 9, pp. 7111–7131, 2009.

[33] C. A. Sierra, M. Mahecha, G. Poveda, E. Álvarez-Dávila, V. H. Gutierrez-Velez, B. Reu, H. Feilhauer, J. Anáya, D. Armenteras, A. M. Benavides, C. Buendia, Á. Duque, L. M. Estupiñan-Suarez, C. González, S. Gonzalez-Caro, R. Jimenez, G. Kraemer, M. C. Londoño, S. A. Orrego, J. M. Posada, D. Ruiz-Carrascal, and S. Skowronek, "Monitoring ecological change during rapid socio-economic and political transitions: Colombian ecosystems in the post-conflict era," *Environmental Science and Policy*, vol. 76, no. June, pp. 40–49, 2017.

[34] W. Wang, "Introductory Chapter: What is Chemical Sensor," in *Progresses in Chemical Sensor*, London, Uk: Intech, 2016, pp. 3–8.

[35] W. Z. and Y. Z. Shengbo Sang, "Review on the Design Art of Biosensors," *State of the Art in Biosensors - General Aspects*, pp. 89–110, 2013.

[36] S. G. and F. I. Adam Hulanicki, "Commission on General Aspects of Analytical Chemistry, Chemical Sensors," *International Union of Pure and Applied Chemistry*, vol. 63, no. 9, pp. 1247–1250, 1991.

[37] Frank M., Butterworth, R. Villalobos-Pietrini, and M. E. Gonsebatt, "Introduction," *Biomonitors and biomarkers as indicators of environmental change 2: a handbook*, pp. 1–9, 2001.

[38] J. R. Askim, M. Mahmoudi, and K. S. Suslick, "Optical sensor arrays for chemical sensing: the optoelectronic nose," *Chemical Society Reviews*, vol. 42, no. 22, p. 8649, 2013.

[39] E. Sorsak, J. V. Valh, S. K. Urek, and A. Lobnik, "Application of PAMAM dendrimers in optical sensing," *Analyst*, vol. 140, no. 4, pp. 976–989, 2015.

[40] S. Halldorsson, E. Lucumi, R. Gómez-Sjöberg, and R. M. T. Fleming, "Advantages and challenges of microfluidic cell culture in polydimethylsiloxane devices," *Biosensors and Bioelectronics*, vol. 63, pp. 218–231, 2015.

[41] A. R. Abate, D. Lee, T. Do, C. Holtze, and D. A. Weitz, "Glass coating for PDMS microfluidic channels by sol-gel methods," *Lab on a Chip*, vol. 8, no. 4, pp. 516–518, 2008.

[42] K. Lau, S. Baldwin, M. O. Toole, R. Shepherd, and W. J. Yerazunis, "A Low-cost Optical Sensing Device Based on Paired Emitter-detector Light Emitting Diodes," *Anal. Chim. Acta*, 2005.

[43] M. O'Toole and D. Diamond, "Absorbance based light emitting diode optical sensors and sensing devices," *Sensors*, vol. 8, no. 4, pp. 2453–2479, 2008.

[44] J. G. O.Lev, M.Tsionsky, L. Rabinovich, V.Glezer, S. Sampath, I.Pankratov, "Sol-Gel Sensors," *Analytical Chemistry*, vol. 67, no. 1, 1995.

[45] A. Mujahid, P. A. Lieberzeit, and F. L. Dickert, "Chemical sensors based on molecularly imprinted sol-gel materials," *Materials*, vol. 3, no. 4, pp. 2196–2217, 2010.

[46] F. Attivissimo, C. Guarnieri, C. Carducci, A. Maria, L. Lanzolla, A. Massaro, and M. R. Vadrucci, "Sea Quality Monitoring," vol. 15, no. 1, pp. 146–153, 2015.

[47] C. de L. M. de Morais, J. C. Carvalho, C. Sant'Anna, M. Eugênio, L. H. S.

Gasparotto, and K. M. G. Lima, "A low-cost microcontrolled photometer with one color recognition sensor for selective detection of Pb^{2+} using gold nanoparticles," *Anal. Methods*, vol. 7, no. 18, pp. 7917–7922, 2015.

[48] J. Wu and M. Gu, "Microfluidic sensing: state of the art fabrication and detection techniques.," *Journal of biomedical optics*, vol. 16, no. 8, p. 080901, 2011.

[49] Z. Nie, C. A. Nijhuis, J. Gong, X. Chen, A. Kumachev, A. W. Martinez, M. Narovlyansky, and G. M. Whitesides, "Electrochemical sensing in paper-based microfluidic devices.," *Lab on a Chip*, vol. 10, no. 4, pp. 477–83, 2010.

[50] J. P. Lafleur, S. Senkbeil, T. G. Jensen, and J. P. Kutter, "Gold nanoparticle-based optical microfluidic sensors for analysis of environmental pollutants," *Lab on a Chip*, vol. 12, no. 22, p. 4651, 2012.

[51] A. Samadi-Maybodi, V. Rezaei, and S. Rastegarzadeh, "Sol-gel based optical sensor for determination of Fe (II): A novel probe for iron speciation," *Spectrochimica Acta - Part A: Molecular and Biomolecular Spectroscopy*, vol. 136, no. PB, pp. 832–837, 2015.

[52] P. C. A. Jerónimo, A. N. Araújo, and M. C. B. S. M. Montenegro, "Development of a sol-gel optical sensor for analysis of zinc in pharmaceuticals," *Sensors and Actuators, B: Chemical*, vol. 103, no. 1–2, pp. 169–177, 2004.

[53] E. M. Flanigen, R. W. Broach, and S. T. Wilson, "Zeolites in Industrial Separations and Catalysis," *Zeolites in Industrial Separation and Catalysis*, pp. 1–26, 2010.

[54] M. A. Barakat, "New trends in removing heavy metals from industrial wastewater," *Arabian Journal of Chemistry*, vol. 4, no. 4, pp. 361–377, 2011.

[55]   S. C. Byun, Y. J. Jeong, J. W. Park, S. D. Kim, H. Y. Ha, and W. J. Kim, "Effect of solvent and crystal size on the selectivity of ZSM-5/Nafion composite membranes fabricated by solution-casting method," *Solid State Ionics*, vol. 177, no. 37–38, pp. 3233–3243, 2006.

[56]   A. Ates, "Characteristics of Fe-exchanged natural zeolites for the decomposition of N2O and its selective catalytic reduction with NH3," *Applied Catalysis B: Environmental*, vol. 76, no. 3–4, pp. 282–290, 2007.

[57]   V. Valtchev and S. Mintova, *Ordered Porous Solids recent advances and prospects*, 1 edition. Elsevier B.V, 2009.

[58]   H. Awala, J.-P. Gilson, R. Retoux, P. Boullay, J.-M. Goupil, V. Valtchev, and S. Mintova, "Template-free nanosized faujasite-type zeolites," *Nat Mater*, vol. 14, no. 4, pp. 447–451, 2015.

[59]   J. Yang, J. Y. Yang, Y. Zhou, F. Wei, W. G. Lin, and J. H. Zhu, "Hierarchical functionalized MCM-22 zeolite for trapping tobacco specific nitrosamines (TSNAs) in solution," *Journal of Hazardous Materials*, vol. 179, no. 1–3, pp. 1031–1036, 2010.

[60]   R. Krishna, J. M. van Baten, E. Garcia-Perez, and S. Calero, "Diffusion of CH4 and CO2 in MFI, CHA and DDR zeolites," *Chemical Physics Letters*, vol. 429, no. 1–3, pp. 219–224, 2006.

[61]   Y. Cao, Z. Y. Yun, J. Yang, X. Dong, C. F. Zhou, T. T. Zhuang, Q. Yu, H. D. Liu, and J. H. Zhu, "Removal of carcinogens in environment: Adsorption and degradation of N′-nitrosonornicotine (NNN) in zeolites," *Microporous and Mesoporous Materials*, vol. 103, no. 1–3, pp. 352–362, 2007.

[62] A. K. Yetisen, I. Naydenova, F. Da Cruz Vasconcellos, J. Blyth, and C. R. Lowe, "Holographic sensors: Three-dimensional analyte-sensitive nanostructures and their applications," *Chemical Reviews*, vol. 114, no. 20, pp. 10654–10696, Oct. 2014.

[63] A. Lisowska-Oleksiak, U. Lesińska, A. P. Nowak, and M. Bocheńska, "Ionophores in polymeric membranes for selective ion recognition; Impedance studies," *Electrochimica Acta*, vol. 51, no. 11, pp. 2120–2128, 2006.

[64] W. Al Zoubi and N. Al Mohanna, "Membrane sensors based on Schiff bases as chelating ionophores - A review," *Spectrochimica Acta - Part A: Molecular and Biomolecular Spectroscopy*, vol. 132, pp. 854–870, 2014.

[65] W. Yang, X. Gao, and B. Wang, "Boronic acid compounds as potential pharmaceutical agents," *Medicinal Research Reviews*, vol. 23, no. 3, pp. 346–368, 2003.

[66] K. Kur-kowalska, M. Przybyt, and E. Miller, "The study of phenylboronic acid optical properties towards creation of a glucose sensor," *Biotechnology and Food sciences*, vol. 78, no. 2, pp. 101–110, 2014.

[67] S. Waheed, A. Ahmad, S. M. Khan, M. Hussain, T. Jamil, and M. Zuber, "Synthesis, characterization and permeation performance of cellulose acetate/polyethylene glycol-600 membranes loaded with silver particles for ultra low pressure reverse osmosis," *Journal of the Taiwan Institute of Chemical Engineers*, vol. 57, pp. 129–138, 2015.

[68] K. Wang, L. Guo, L. Zhou, and J. Zhu, "Imaging mechanism of the holographic recording material dichromated cellulose triacetate.," *Applied optics*, vol. 35, no.

32, pp. 6369–74, 1996.

[69]   L. Ye, "Molecularly imprinted polymers with multi-functionality," *Analytical and Bioanalytical Chemistry*, vol. 408, no. 7, pp. 1727–1733, 2016.

[70]   Y. Fuchs, O. Soppera, and K. Haupt, "Photopolymerization and photostructuring of molecularly imprinted polymers for sensor applications-A review," *Analytica Chimica Acta*, vol. 717, pp. 7–20, 2012.

[71]   P. Spégel, L. Schweitz, and S. Nilsson, "Molecularly imprinted polymers," *Analytical and Bioanalytical Chemistry*, vol. 372, no. 1, pp. 37–38, 2002.

[72]   M. Haseena, M. F. Malik, A. Javed, S. Arshad, N. Asif, SharonZulfiqar, and J. Hanif, "Water pollution and human health.," *Environmental Risk Assessment and Remediation*, vol. 1, no. 3, pp. 16–19, 2017.

[73]   S. Ganguly, *Environment and human health*, vol. 110, no. 6. Copenhagen, Denmark, 2012.

[74]   National Research Council (US) Committe on Copper in Drinking Water, *Copper in Drinking Water*. National Academy Press, Washington, D.C., 2000.

[75]   M. Siotto and R. Squitti, "Copper imbalance in Alzheimer's disease: Overview of the exchangeable copper component in plasma and the intriguing role albumin plays," *Coordination Chemistry Reviews*, vol. 371, pp. 86–95, 2018.

[76]   D. A. Lytle and J. Liggett, "Impact of water quality on chlorine demand of corroding copper," *Water Research*, vol. 92, pp. 11–21, 2016.

[77]   F. Fu and Q. Wang, "Removal of heavy metal ions from wastewaters: A review," *Journal of Environmental Management*, vol. 92, no. 3, pp. 407–418, 2011.

[78] P. Jarvis, K. Quy, J. Macadam, M. Edwards, and M. Smith, "Intake of lead (Pb) from tap water of homes with leaded and low lead plumbing systems," *Science of the Total Environment*, vol. 644, pp. 1346–1356, 2018.

[79] E. Cooney, C. Ni Eidhin, D. Page, P. Gillard, C. Doyle, N. Dunne, and R. Barrington, "Drinking Water Report for Public Water Supplies," *Enviromental Protection Agency*, pp. 1–44, 2017.

[80] C. Dahl, A. J. Sogaard, G. S. Tell, L. Forsén, T. P. Flaten, D. Hongve, T. K. Omsland, K. Holvik, H. E. Meyer, and G. Aamodt, "Population data on calcium in drinking water and hip fracture: An association may depend on other minerals in water. A NOREPOS study," *Bone*, vol. 81, pp. 292–299, 2015.

[81] M. P. Carlson, *Water Quality and Contaminants*. Hopkinsville, KY, United States: Elsevier Inc., 2018.

[82] C. Day, S. Søpstad, H. Ma, C. Jiang, A. Nathan, S. R. Elliott, F. E. Karet Frankl, and T. Hutter, "Impedance-based sensor for potassium ions," *Analytica Chimica Acta*, pp. 1–7, 2018.

[83] K. Thajee, L. Wang, K. Grudpan, and E. Bakker, "Colorimetric ionophore-based coextraction titrimetry of potassium ions," *Analytica Chimica Acta*, vol. 1029, pp. 37–43, 2018.

[84] M. Heras and M. J. Fernández-Reyes, "Serum potassium concentrations: Importance of normokalaemia," *Medicina Clinica*, vol. 148, no. 12, pp. 562–565, 2017.

[85] H. Su, W. Ruan, S. Ye, Y. Liu, H. Sui, Z. Li, X. Sun, C. He, and B. Zhao, "Detection of physiological potassium ions level in human serum by Raman

scattering spectroscopy," *Talanta*, vol. 161, no. September, pp. 743–747, 2016.

[86] C. Biochemistry, *The Management of Hypertension The Clinical Biology of Sodium The Physiology and Pathophysiology of*. 1992.

[87] S. Haase, N. Wilck, M. Kleinewietfeld, D. N. Muller, and R. A. Linker, "Sodium chloride triggers Th17 mediated autoimmunity," *Journal of Neuroimmunology*, no. June, pp. 0–1, 2018.

[88] B. Rutkowski, P. Tam, F. M. Van Der Sande, A. Vychytil, V. Schwenger, R. Himmele, and A. Gauly, "Low-Sodium Versus Standard-Sodium Peritoneal Dialysis Solution in Hypertensive Patients: A Randomized Controlled Trial," *American Journal of Kidney Diseases*, vol. 67, no. 5, pp. 753–761, 2016.

[89] W. B. Farquhar, D. G. Edwards, C. T. Jurkovitz, and W. S. Weintraub, "Dietary sodium and health: More than just blood pressure," *Journal of the American College of Cardiology*, vol. 65, no. 10, pp. 1042–1050, 2015.

[90] D. Cody, E. Mihaylova, L. O'Neill, and I. Naydenova, "Determination of the polymerisation rate of a low-toxicity diacetone acrylamide-based holographic photopolymer using Raman spectroscopy," *Optical Materials*, vol. 48, pp. 12–17, 2015.

[91] J. Kecht, Z. Tahri, V. De Waele, M. Mostafavi, S. Mintova, and T. Bein, "Colloidal Zeolites as Host Matrix for Copper Nanoclusters," *Chemistry of Materials*, vol. 18, no. 8, pp. 3373–3380, 2006.

[92] K. Trainer, K. Wearen, D. Nazarova, I. Naydenova, and V. Toal, "Optimization of an acrylamide-based photopolymer system for holographic inscription of surface patterns with sub-micron resolution," *Journal of Optics*, vol. 124012, pp.

1–7, 2010.

Chapter 2–Review of Holography and Holographic Sensors

2.1 Short history of Holography

Holography has been known since 1947 as a method for recording electromagnetic wave wavefront. Dennis Gabor developed the theory of holography while working on increased resolution of the electron microscope. He described a new method to obtain the image of an object from the diffraction pattern produced by the object. His method is also known as in-line holography [1]. His invention and development of the holographic method earned him the 1971 Nobel Prize in Physics. Prior to his work, holographic imaging can be traced back to work by Wofke and Bragg in X-ray crystallography, which led to the development of the "Bragg X-ray microscope"[2]. However, the technique of holography was not practically realised until the invention of the laser in the 1960's, which provided the first truly coherent source of light. In 1962 Emmett Leith and Juris Upatnieks recorded the first 3-D transmission holograms of real objects. Since then, the field of holography has expanded dramatically.

By definition, Holography is a technique by which a wavefront can be recorded and thereafter reconstructed in the absence of the original wavefront. A hologram is formed when a light sensitive material is exposed by the interference pattern created by an object and reference beam. In conventional recording techniques such as photography, a two dimensional image of a three-dimensional scene is recorded on a light-sensitive surface. In photography the intensity distribution of the light from the original object is recorded. In other words, the recording is merely the light intensity distribution scattered by the original scene. As a result, all information about the relative phases of the light waves from different points or, in other words, information about the relative

optical paths to different parts of the object is lost. Whereas in holography the complete phase information of the light scattered by an object and its intensity distribution are recorded [3].

2.2. Holographic Recording

A photosensitive medium is one which responds to incident light via change in its physical properties. The phase information of an object can be converted to variations in intensity by creating an interference pattern between the light scattered from the object beam and reference beam.

2.3. Geometry of holographic recording

One of the primary factors used to distinguish between holograms is the geometry used for recording. The holographic gratings can be classified into two types depending on the geometry of holographic recording. The two main classifications of holograms distinguishable in this way are transmission and reflection holograms.

2.3.1. Transmission Hologram

In transmission mode recording, both the reference and object wavefronts are incident on the recording medium from the same side as shown in Figure 2.1(a). When both the reference and object beams consist of coherent plane waves incident at the same angle, this will create fringes perpendicular to the photosensitive medium surface; this recording is known as an unslanted recording. These fringes will be spaced equidistantly throughout the photosensitive medium. Whereas in slanted recording the two beams are incident at different angles with respect to the layer's surface. As a result the interference fringes are not perpendicular (parallel in reflection mode) to the surface

48

of the recording medium. The spacing of the formed fringes Λ can be calculated using the Bragg equation [5- 6]:

$$\lambda = 2\ \Lambda\ Sin\theta \qquad \textbf{(2.1)}$$

where, λ recording wavelength in air, Λ is the fringe spacing inside the photosensitive material, θ is angle between the two beams in the air. The fringe spacing is depends on the angle between the two beams. Transmission holograms are usually reconstructed by blocking the object beam and illuminating with only the reference beam as shown in Figure.2.1 (b).
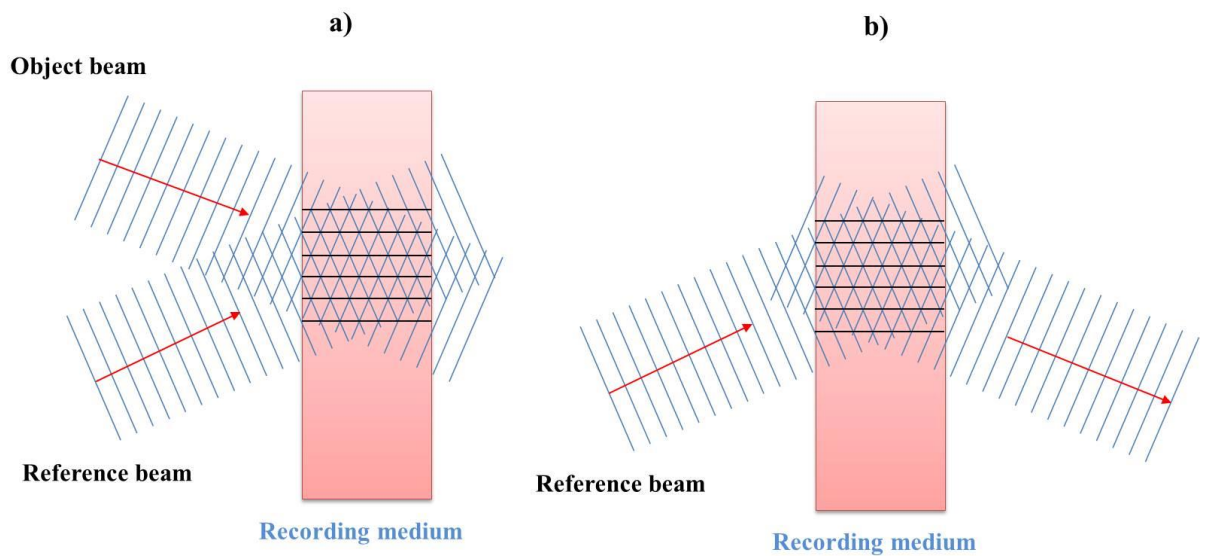
Figure 2. 1. (a) Recording and (b) Reconstruction of transmission hologram

2.3.2. Reflection hologram

In a reflection mode of recording the object beam and reference wavefronts are incident on the photosensitive medium from opposite sides as shown in Figure.2.2 (a). Reconstruction occurs in a similar fashion as for transmission mode; the reflection grating reflects the reference beam to reconstruct the second recording beam as shown in Figure 2.2 (b). This geometry allows for much higher spatial frequencies to be

possible, restriction will depend on spatial frequency limitation of the recording material, refractive index of the recording material and wavelength. Reflection mode holograms can reconstruct with a white light source, which is one of the main advantages of this recording geometry.

$$\frac{\lambda}{n} = 2\,\Lambda\,\mathrm{Sin}\theta \qquad \textbf{(2.2)}$$

where, $\frac{\lambda}{n}$ wavelength inside the medium, Λ is the fringe spacing inside the medium, θ is angle between the two beams inside the medium.
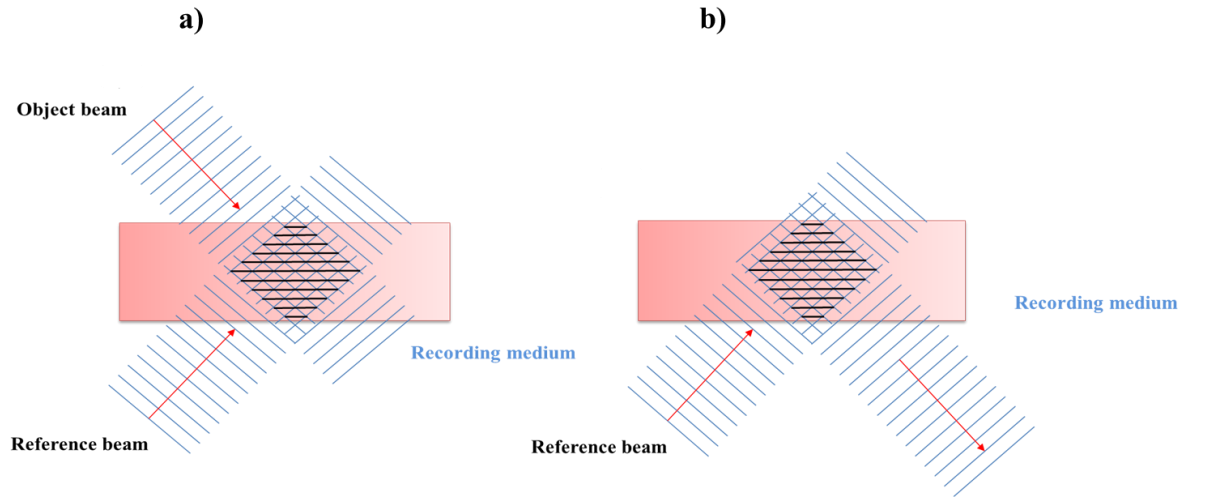
Figure 2. 2. (a) Recording and (b) Reconstruction of reflection hologram

Reflection holograms are also known as white light holograms because the image can be observed after illumination with white light. A popular geometry for reflection mode recording is the Denisyuk type setup [6]. In this method, a single beam first passes through the recording medium. Part of the transmitted light is then reflected back from

50

the object; the hologram can then be mounted on a reflective backing for viewing with white light as shown in Figure 2.3.
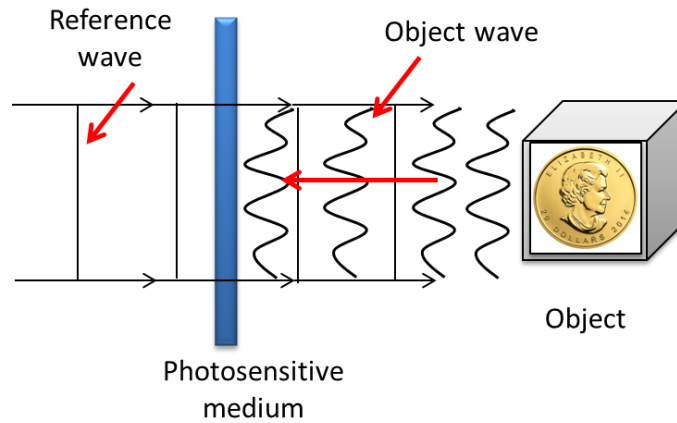
Figure 2. 3.Recording of Denisyuk reflection hologram

The main characteristics of transmission and reflection gratings are outlined in table 2.1.

Table 2. 1. Characteristics of transmission and reflection gratings

	Transmission (T)	**Reflection (R)**
Recording geometry	Beams illuminate sample from same side	Beams illuminate sample from opposite sides
Spatial Resolution	Approximately max. 3000 l/mm	Approximately > 4000 l/mm
Stability Requirements	Less sensitive to stability issues	Requires excellent stability of optical system
Hologram Reconstruction	monochromatic (laser) light	White light, monochromatic light
Applications	Sensors, Holographic optical elements, Holographic data storage, Security	Display Holography, Holographic optical element, Sensors, Security

2.4. Types of holograms

A hologram is classified as either an amplitude or phase hologram depending on which parameter is modulated during the recording.

2.4.1. Phase and amplitude holograms

A hologram is classified as a phase hologram if the phase of the probe wave is modified on propagation through the medium. This is due to the spatial variation of the thickness or refractive index of the medium which occurs during the recording process. The extent of the variation is determines to the intensity of the recording light pattern. An amplitude hologram is one in which the absorbance of the photosensitive medium is altered on exposure to light. A common example of an amplitude-type recording medium is a standard photographic emulsion. Both amplitude and phase holograms can be recorded using either transmission or reflection mode geometries. In this work the holograms utilised to develop sensors are phase and amplitude holograms.

2.4.2. Thick and thin holograms

Depending on the thickness and spatial frequency of the photosensitive medium, the recorded holographic gratings can be classified as thin (plain) or thick (volume). Common characteristics of thick and thin holograms described in Table 2.2.

Table 2. 2. Characteristics of Thin vs Thick holograms

Thin Holograms	Thick Holograms
Multiple orders of diffraction	One order of diffraction
Low angular selectivity, Diffraction orders are produces practically for every incident angle	Observed only when incident beam is at Bragg/near Bragg angle
Describe by Raman- Nath Theory	Usually describe by Kogelnik's theory

An important parameter for the classification is the ratio of the fringe spacing (Λ) and the thickness of the photosensitive layer (d). The holographic gratings are considered thin if the thickness of the recording medium is small compared to the average fringe spacing. In order to have a more quantitative method for determining whether holograms are thick or thin, the Q parameter is used to classify holographic gratings. According to [7] the Q parameter is defined by the relation[7]:

$$Q = \frac{2\pi\lambda_0 d}{n_0 \Lambda^2} \qquad (2.3)$$

Where λ_0 is the vacuum wavelength of the recording light, d is the thickness of the photosensitive medium, n_0 is the average refractive index of the recording material and Λ is the fringe spacing to distinguish between two diffraction regimes. Holographic gratings with values $Q<1$ are considered as thin gratings (were believed to give Raman-Nath operation) whereas those with $Q>10$ are thick gratings (were believed to give Bragg regime operation). The holograms characterised by $1<Q<10$ are intermediate type with mixed properties. It also good to consider another parameter called ρ to conclude weather the gratings is thick or thin. Parameter is ρ defined [8] in equation 2.4.

$$\boldsymbol{\rho} = \frac{\lambda_0^2}{\Lambda^2 n_0 \Delta n} \qquad \textbf{(2.4)}$$

(where Δn is the modulation of the refractive index and λ_0, Λ, and n_0 are as defined before) can be reliably used to predict whether one is in the Raman-Nath regime or in the Bragg regime. Raman-Nath defined parameter ρ first; he conceded the case of normal incidence. Also pointed out that, if ρ is very large, the diffraction effect will not be prominent, as is otherwise the case where ρ is nearly zero. Table 2.3 shows how Q and ρ are closely related.

Table 2. 3. Relationship between the two criteria: Q = Δφ. ρ

	Q	ρ
Thick Holograms	> 10	> 10
Thin Holograms	≤ 1	≤ 1

The advantage of thick holograms is that they can have high diffraction efficiency theoretically reaching 100% but also they have a narrow angular bandwidth and a narrow spectral bandwidth. Whereas in thin holograms they have limited diffraction efficiency (up to 33% for phase surface holograms) with a large angular bandwidth and spectral bandwidth and they can be used in some applications with broader angular bandwidth [4- 2]. The characteristics of volume and surface holograms will be outlined in chapter 3.

2.5. Recording materials for holographic sensing

Holographic diffraction gratings may be used as a platform to fabricate optical sensors for the detection of certain analytes. These gratings may be functionalized with polymers or inorganic (sol gel) matrices which allow indirect optical measurements of physical or chemical stimuli [5]. There are two main requirements that the photonic material must fulfil to be used in holographic sensing typically: (1) it should be suitable for holographic recording and (2) the presence of stimuli must cause a change in the optical properties of the sensing material. Holographic sensing materials can be divided into three groups based on their fabrication: (1) photopolymers, (2) silver halides-based materials and (3) hybrid materials.

2.5.1. Photopolymer Materials

Photopolymers are characterized by a relatively high sensitivity, large dynamic range, self-processing nature, and relatively low cost, which makes them an attractive holographic recording material. A number of organic materials are known to be activated through a photosensitizer to exhibit thickness and refractive index changes due to photopolymerization or cross-linking. Thick layers can be made to yield volume phase holograms with high diffraction efficiency and high angular selectivity, which can be viewed immediately after exposure. After the exposure a continuing dark reaction due to diffusion of the monomer into the zones of polymerization increases the refractive index modulation. Photopolymer systems for recording holograms typically comprise one or more monomers, a photoinitiaton system and an inactive component often referred as a binder. The resulting composition is typically a viscous fluid or a solid with a low glass transition temperature, which is prepared for exposure either by

coating onto a solid or flexible substrate, or by confining it between two transparent solid substrates [9].

In photopolymers, a refractive index grating is formed as a result of localized photopolymerization during holographic recording; the polymer formed bears receptor units sensitive to a specific stimulus. This section aims to detail the nature of the different components used in the photopolymer composition. Polymerization is defined as the process in which many small molecules (monomers) are linked up together to form a large molecule (polymer). A large majority of the investigated water-soluble holographic photopolymers are acrylamide (AA) based due to their ability to readily record high diffraction efficiency holograms. A drawback of these materials is the carcinogenic and toxic nature of AA in its monomer form. The fabrication of the holographic sensor in the acrylamide derivative based photopolymer includes two steps. Firstly, the photopolymer layers are prepared by mixing photopolymer components (detail of the process is mentioned in section 2.5) followed by coating the solution on a substrate and drying at ambient temperature and low relative humidity. Secondly, the photonic structure is created by holographic patterning of the photopolymer layer as show in Figure 2.4. Details of the photopolymer components are present in the following sections.
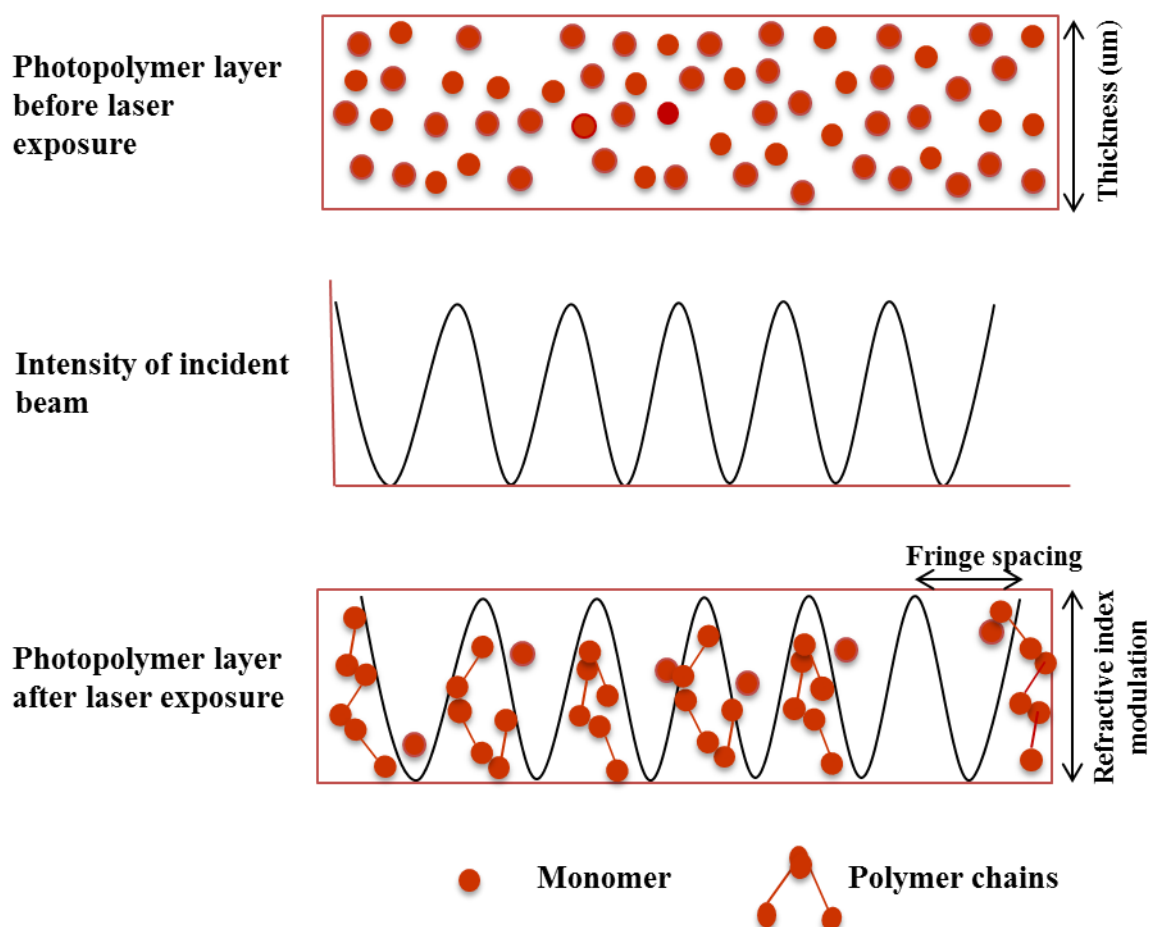
Figure 2. 4. Schematic of a holographic grating formation through photopolymer layer

2.5.1.1 Binder

The function of the binder matrix is to hold all of the photopolymer components together in the composition and to facilitate the formation of a solid layer. 80 % hydrolysed Polyvinyl Alcohol (PVA) solution in water (10% wt/vol) was used in all experiments for recording surface holograms fabrication. The chemical structure of PVA is shown in Figure 2.5. Different percentages of hydrolysation of PVA in the standard acrylamide based formulation have been investigated previously by researchers

in IEO [10]. A hydrolysation percentage of PVA of 80% was found to be optimum for holographic recording.
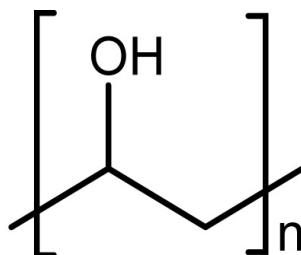
Figure 2. 5. Chemical structure of Polyvinyl Alcohol

2.5.1.2. Monomer

Acrylamide (AA) shown in in Figure 2.6 was used as a monomer in the experiment. The sensitivity of the medium is strongly dependant on the concentration of acrylamide in the layer. An increased concentration on the monomer will increase the reaction rates, making the diffraction efficiency increase more rapidly during exposure.
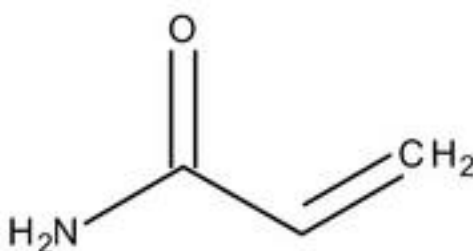
Figure 2. 6. Chemical structure of Acrylamide

2.5.1.3. Cross-linking monomer

N,N-methylene bisacrylamide (BA) is a well-known crosslinker for AA; a polyacrylamide gel formed from a combination of AA and BA is commonly used in

biology as an electrophoresis matrix for the separation of proteins and nucleic acids [11]. The use of BA as a cross linker in AA based holographic formulation is well established[12][10][13]. The chemical structure of BA is shown in Figure 2.7 and the mechanism for the crosslinking of AA polymer chains by BA is shown in Figure 2.8. The function of BA crosslinker in the photopolymer composition is to bind the polymer chains together during the photoinduced photopolymerization reaction. This restricts the diffusion of the polymer chains out of the illuminated regions, thus maximising the refractive index modulation of the recorded hologram. The presence of the crosslinker also prohibits post recording decay of holograms recorded in the photopolymer.
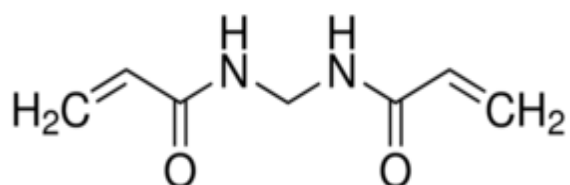
Figure 2. 7. Chemical structure of N, N-methylene bisacrylamide
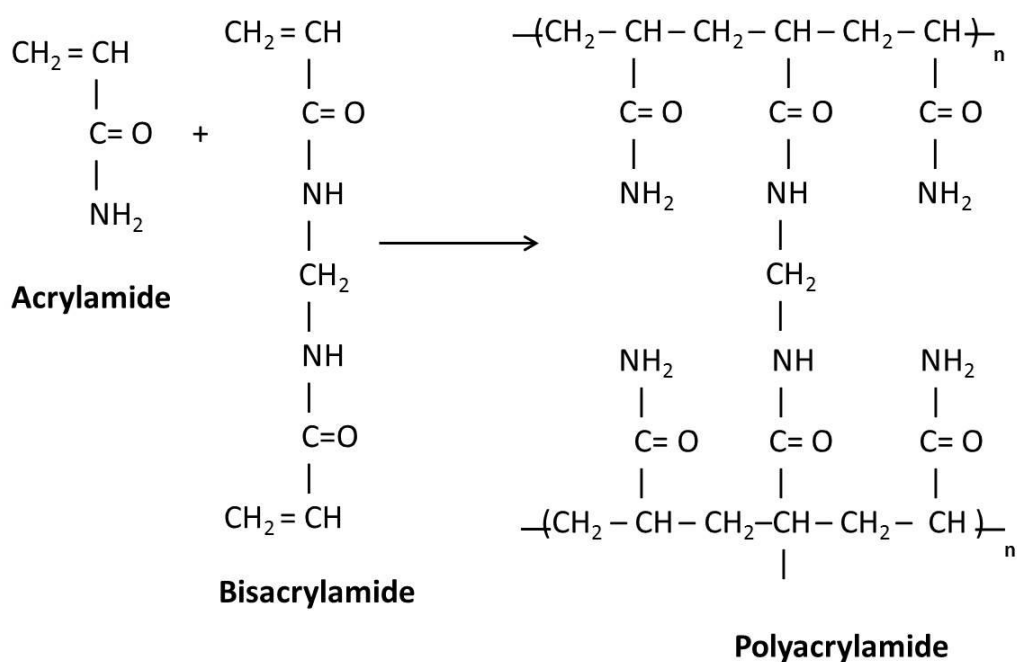
Figure 2. 8. Crosslinking reaction between AA and BA to produce crosslinked polyamide

2.5.1.4. Electron Donor

Triethanolamine (TEA) is used as an electron donor in the photopolymer composition. Its function is to create free radicals upon illumination in order to facilitate the photo polymerisation reaction; it is also act as a plasticizer; which improves layer stability by preventing crystallisation of the solid components out of the photopolymer layers. The chemical structure of TEA is shown in Figure 2.9.
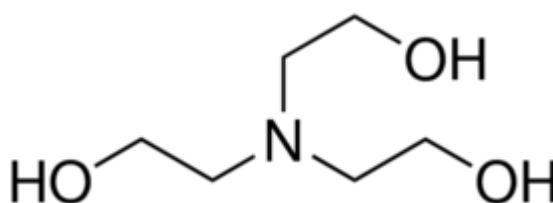
Figure 2. 9. Chemical structure of triethanolamine

2.5.1.5. Photosensitive dye

Erythrosine B (EB) was used as the sensitizing dye in all experiments described. It is sensitive to wavelengths of light between 400 and 550 nm. When selecting a photosensitive dye for a photopolymer system, it is important that the dye meets certain criteria. Strong absorption of the dye at the illumination wavelength is required for more effective excitation of the dye molecules. It is also important that the photosensitising system i.e. the dye and electron donor is efficient in producing free radicals. The chemical structure of EB dye is shown in Figure 2.10.
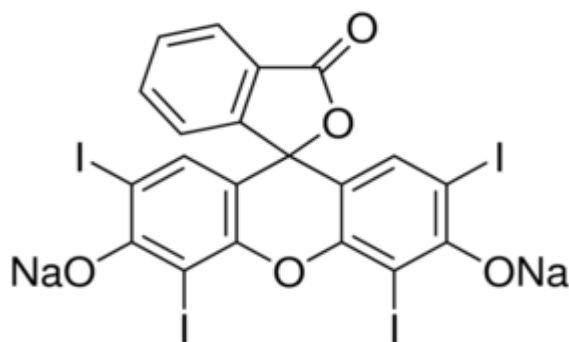
Figure 2. 10. Chemical structure of Erthysoine B

2.5.1.6. Photopolymerisation

Holograms are recorded in photopolymers via a radical chain photopolymerization mechanism. A typical holographic photopolymer [15-16] consists of a monomer, a cross-linker, an electron donor, a photosensitizing dye, and a polymer binder, which holds all of the components together. These photopolymer components are then spatially redistributed during holographic recording, when photopolymerization takes place. The recording material used in this research is self-processing acrylamide-based photopolymer which have been developed at the IEO centre [12][17-19].

This process consists of three steps: initiation, propagation and termination. In this reaction upon illumination to laser, the dye molecules absorb photons of light of a particular wavelength, and are promoted to excited singlet energy states.

$DYE + hv$ ⟶ DYE_1 *   (Excited Singlet state)

The energy of the molecule in an excited singlet state can be released by returning quickly back to the ground state and emitting light of a longer wavelength via

fluorescence process, or by energy transfer to another molecule (electron donor such as, TEA), this process called fluorescence quenching.

$$DYE^*_1 \longrightarrow DYE + hv \qquad\qquad \text{(Fluorescence)}$$

$$DYE^*_1 + TEA \longrightarrow DYE + TEA \qquad\qquad \text{(Fluorescence quenching)}$$

The exited dye molecule can be converted to a more stable triplet state dye molecule through inter system crossing.

$$DYE^*_1 \longrightarrow DYE^*_3 \qquad\qquad \text{(Inter-system crossing)}$$

The produced triplet state dye molecule can reacts with the electron donor (TEA) to produce a free radical.

$$DYE^*_3 + TEA \longrightarrow DYE^\bullet + TEA^\bullet \qquad\qquad \text{(Free radical production)}$$

These radicals can react with the monomers (M) to initiate the polymerisation process.

$$TEA^\bullet + M \longrightarrow TEA\text{-}M^\bullet \qquad\qquad \text{(Initiating step)}$$

The growing chain continues via propagation when this radical monomer reacts with another monomer molecule.

$$M + TEA\text{-}M^\bullet \longrightarrow TEA(M)_2{}^\bullet \qquad\qquad \text{(Propagation step)}$$

This propagation step will continue until one of two termination reactions occurs, namely combination or disproportionation.

$$TEA\text{-}M_n{}^\bullet + TEA\text{-}M_m{}^\bullet \longrightarrow TEA\text{-}(M)_{nm}\text{-}TEA \qquad\qquad \text{(Combination)}$$

$$TEA\text{-}M_n{}^\bullet + TEA\text{-}M_m{}^\bullet \longrightarrow TEA\text{-}(M)_n + TEA\text{-}(M)_m \qquad\qquad \text{(Disproportionation)}$$
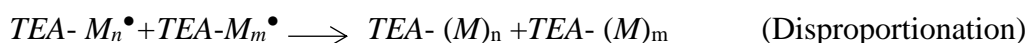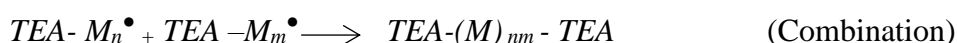
Areas in the material where polymerisation takes place undergo a change in refractive index. The relative difference in refractive index between illuminated and non-illuminated areas of the photopolymer is what constitutes the phase hologram. There is also evidence to show that mass transport of the monomer from the dark to bright fringe regions during polymerisation further increases the refractive index modulation[17].

2.5.1.6. Advantages of photopolymer for applications in sensing

I.   Photopolymers can spontaneously develop and thus there is no need of post-exposure processing. This real-time recording characteristic excludes the need for complicated development procedures and makes them promising candidates for sensor applications.

II. Thick photopolymer layers can be fabricated which gives high diffraction efficiency and good angular selectivity, which makes photopolymers suitable for applications such as holographic sensors [4].

III. Photopolymers are considered a good recording medium because of the properties they possess including high sensitivity, high diffraction efficiency, large dynamic range, real-time imaging abilities, easy fabrication steps, low scattering loss and low cost.

2.5.16.2. Disadvantages of photopolymer

I.   Photopolymerisation is not a reversible process and therefore photopolymer holograms cannot be erased and reused.

II. Volume shrinkage that occurs during photopolymerisation remains a major hurdle to the practical application of photopolymers [18]. Shrinking [19] of the photopolymer layers results in a change in the fringe spacing [20].

Holography allows fabrication of disposable sensors. The potential applications of holographic sensors are mentioned in Figure 2.11 [5]. Holographic sensors offer many other advantages such as low cost fabrication, which make them ideal for disposable devices. Moreover for a reflection type of holographic sensor, there is no need for an additional readout panel or power supply for their operation. All these characteristics make them candidates for portable applications. Further applications of holographic sensors are yet to come with the advances in holographic materials, as well as with their combination with other enabling technologies such as microfluidics, which is possible due to another advantage of holographic devices their capability for miniaturization.
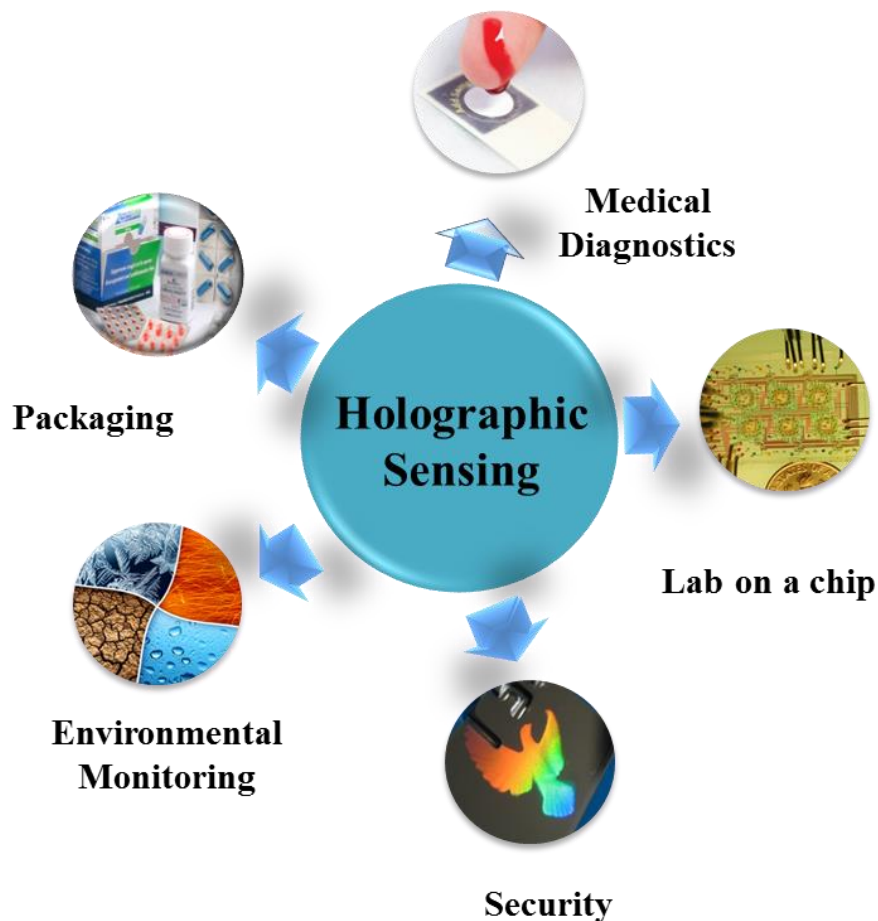
Figure 2. 11. Potential applications of holographic sensors

2.5.2. Silver halide based materials

The second class of holographic recording materials used in sensing is a silver halide based material which has higher light sensitivity than photopolymers [21][22]. Silver halide emulsions[23] consist of silver halide with a light sensitive dye dispersed in a functionalised polymer matrix. Silver bromide is the most commonly used silver halide. The polymer matrix can be composed of gelatine, poly(2- hydroxyethylmethacrylate) and polyacrylamide /or polyvinylalcohol. Utilisation of different synthetic dyes allows holographic recording at different wavelengths. In contrast to photopolymer materials, the development of the sensor based on silver halide materials is a time consuming process and consists of many steps [22]. The creation of the holographic sensor through silver halide chemistry includes 1) making the analyte-sensitive polymer matrix, 2) diffusion of silver ions into the matrix and formation of silver halides, 3) holographic patterning of the material to produce multilayer photonic structure and 4) developing and post-processing steps to fix the hologram and improve the diffraction efficiency. A volume phase grating developed by silver halide photochemistry represents a periodic variation of the refractive index produced by periodic distribution of silver nanoparticles in the functionalised polymer matrix. The sensitivity of the hologram to a target analyte originates from the ability of functionalised polymer matrix to alter its properties on exposure to the analyte. A variety of holographic sensors have been developed with silver halides [5] [22][24].

2.5.3. Hybrid materials

The third class are photopolymers which are doped with nanosized zeolites [25]. Zeolites are crystalline materials with a very regular pore structure of molecular dimensions [26]. There is a large variety of nanosized zeolites depending on their

framework type, pore dimensions and Si/Al or Al/P ratios [27]. The incorporation of zeolites having various shapes and structures into a photopolymer medium [28][19] can improve the dynamic range of the material [29], decrease its shrinkage [30] and create selectivity of the material toward a specific analyte [31]. Doping the photopolymer solution with the nanoparticle suspension can be done during the mixing photopolymer components Figure 2.12. In case of surface holograms it can be functionalised after recording fabrication method of modification of surface is described in chapter 4.
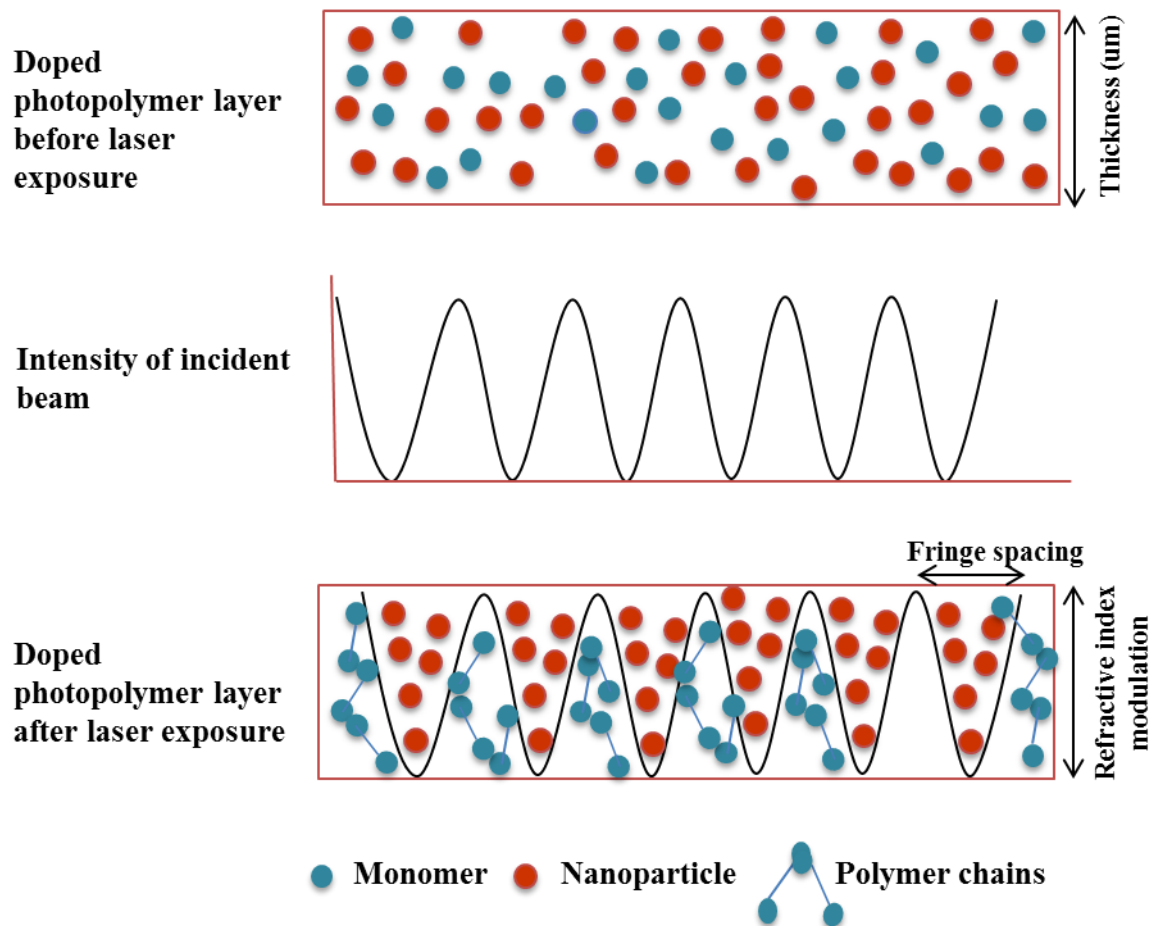
Figure 2. 12. Schematic of grating formation in a photopolymer doped with nanoparticles

2.6. Diffractive optical elements for sensing application

''Diffractive optical elements can be used for optical-pattern generation, especially for applications in which the laser spots or pattern elements must be created at precisely defined positions''. DOEs are micro or nanostructures which are designed to modify the spatial distribution of a light beam to generate any desired pattern. There is an ever-increasing demand for miniaturizing optical systems to achieve high resolution, speed, and portability [32]. Diffractive Optical Elements (DOEs) are progressively being used for a broad range of applications [33] for instance computer generated holograms [34]. Optical diffraction is a physical phenomenon which occurs when a light beam encounters an obstacle and propagates in many different directions. The smaller the obstacle, the larger the diffraction angle and the stronger the diffraction effects become [35].

Sensors based on Diffractive optical elements (DOEs) can be quick to build and cheaper. Fast progress of holographic optics design methodology and manufacturing techniques is evident. Diffractive optical elements (DOEs) and computer-generated holograms (CGHs) have become an integral part of many advanced optical systems [36]. DOEs shape and split laser beams in an energy efficient manner and provide wide range of applications with minimal light loss. Microfabrication technology can meet the demand for DOE production, permitting size reduction and mass production and providing for a flexible assembly of optical components. Diffractive optical elements (DOEs) are key components in the miniaturization of optical systems because of their planar structure and extreme thinness. DOE's can be divided into four different types categorise according to their function as shown in Figure 2.13.
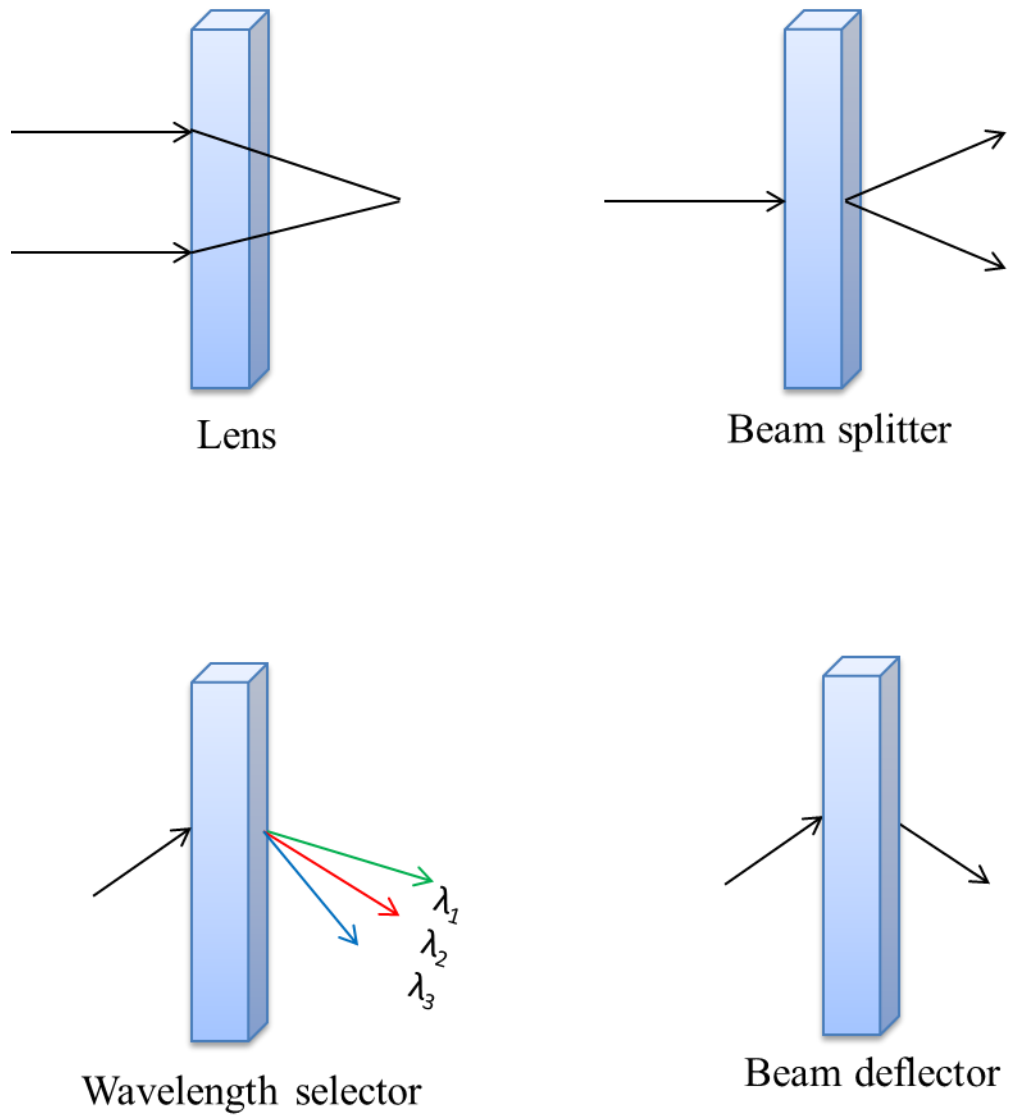
Figure 2. 13.Examples of diffractive optical elements (DOE) examples

Holographic Optical Element for sensing application

Holographic Optical Elements (HOEs) are a class of DOE's. HOE's are widely used as the incident beam is transformed by a hologram; the hologram is made up of an array of apertures that diffract the light. This array of apertures is created by the interference of two wavefronts to produce a patterned layer that will be used to act as an optical component. DOE's have diffractive structures and can also be made by using

nonholographic method such as direct lithography, moulding and stamping processes. Although the production processes are different, the principle of operation is identical, the diffractive element changes the path of the incident light through diffraction at the sub-micron structures and these structures have been designed to produce a particular output such as focused, deflected or patterned light.

The schematic of a typical holographic optical system, which uses a DOE (e.g: beam splitter) to convert a laser beam to generate patterns or structure illumination into a desired intensity distribution at special diffraction angle or propagation distance. A number of holographic structures created by DOE's [5] can be used as a sensor platforms. In general, diffraction-based sensors operate by shining light on a grating and characterizing the resulting diffraction. The intensity of the diffracted light depends on the structure (e.g., height and periodicity, both of which are optimized at a fixed wavelength, and the refractive indices of the grating and the environment. Z. Zhou and co-workers demonstrated a proof-of-principle of sensing application based on bioactive diffractive optical elements (DOE's) microfabricated by using functionalized silk fibroin films. The authors reported that Silk material based on DOEs, have tremendous optical qualities while retaining the activity of embedded bioactive dopants (e.g., enzymes, vaccines, cells, etc.) used as sensitizing agents. Silk-DOEs are permeable to water and gases, unlike glass, which increases the effective refractive index due to the presence of the analytes [37].

The sensor reported in the current research work is created by holographic used to create SRG in a self-processing photopolymer material, which is particularly useful when a flexible design of the sensing structures is required. A variety of spatial frequencies can be achieved by simply changing the angle between the two recording beams. More complex surface patterns can be achieved by using more than two beams

or by multiplexing more than one optical pattern in the same location. The surface relief amplitudes can be easily tuned by varying the exposure time or photopolymer chemical composition. It has been previously demonstrated that the initial surface relief modulation is very important for the performance of the sensor as it determines the starting diffraction efficiency and the dynamic range of the sensor [38]. Interrogation of these structures by light allows indirect measurements of chemical analytes' concentration in real time. A particular advantage of the sensor based on low spatial frequency SRG is that the diffraction efficiency is not dependent on the polarisation of the probe beam, which is a significant issue in surface plasmon resonance sensors.

A holographic optical element (such as a lens, filter, beam splitter or diffraction grating) can be produced by using a holographic imaging process. The key characteristic is that they are able to implement several features in a single flat device which also which has a high diffraction efficiency and a narrow-band frequency characteristic. They are in general wavelength dependent i.e. they operate typically at the wavelength used to record them. It is possible to create HOEs with very large aperture size, and they can be recorded in lightweight materials. One of the benefits of flat diffraction elements with a surface phase relief is the possibility of combining a number of functions in a single element (e.g. beamsplitter, diffraction grating and aberration corrector) and simple methods of copying (e.g. using polymer materials). HOE's are used for many applications including in data storage, holographic concentrators, security and holographic sensors.

2.7. Progress in holographic Sensors

The project is focused on the application of holographic gratings for the development of holographic sensors and the following section describes the fundamentals of

holographic sensors and progress in holographic sensors. Holographic sensors are another advancing field of holography which has stimulated some of the world's most fascinating and profound theoretical and experimental work in materials science and engineering optics. Holograms can be modified to detect and monitor [5] biological liquids [39][40], heavy metals in liquids[31][41], metabolites[42-44] physical parameters such as humidity and temperature[43][44] and the presence of certain substances in gases [47-48].

The spatial variation in light intensity or state of polarization is recorded in the material as a variation in refractive index, absorption or thickness. In the most general case the recorded pattern is a diffraction grating that produces diffracted light when illuminated with light of appropriate spectral or polarization characteristics and in the appropriate direction. The properties of the diffracted light – intensity, wavelength, phase or state of polarization depend on the properties of the recorded diffraction pattern and are useful for the design of holographic sensors [47]. The availability of a large variety of holograms and holographic materials makes the design of holographic sensors a very flexible process.

 Dimensional and other changes in the hologram occur in response to some external influence. For example, a change in the refractive index of the hologram due to a physical/chemical interaction between a hologram constituent and some analyte would allow for the detection of the analyte. Alternatively a change in the spacing of a recorded fringe pattern due to shrinkage or swelling of the material results in a change in the angular position of the Bragg peak for transmission holograms, or a change in the spectral position of the Bragg peak in reflection holograms. The IEO has previously developed diffractive grating structures (Figure 2.13) for humidity and temperature sensors [48][20].

2.7.1. Sensors based on transmission holographic gratings

There are two types of holographic sensors depending on the recording geometry of the holographic grating utilised. The first type is a sensor based on a transmission diffraction grating. This sensor relies on the alteration of the diffraction efficiency and the Bragg angle shift when interaction with a target analyte occurs. The sensor requires both a light source of a specific wavelength for its illumination and a photodetector to monitor a change in a signal level, such as diffraction efficiency alteration or variation of the diffracted light direction. For thick holographic transmission gratings, diffraction efficiency (η) is defined by Kogelnik's coupled wave theory [49],[50]:

$$\eta = \sin^2\left(\frac{\pi \, \Delta n d}{\lambda r \cos \theta_B}\right) \qquad (2.5)$$

Where Δn is the refractive index modulation (the difference between exposed and unexposed areas), λ_r is the wavelength of the reconstructing beam, θ_B is the Bragg angle inside the photosensitive material and d is the thickness of the grating. Changes in the diffraction efficiency occur due to the variation of the refractive index or thickness of the grating. Thickness changes arise through swelling and shrinkage of the bulk material leading to the changes in the spacing, causing Bragg angles shift. Figure 2.14 Illustrates the sensing principle of a holographic sensor based on a transmission grating. Consider the case of a volume transmission grating with the following parameters: the thickness d_1, the refractive index modulation Δn_1, the spatial period Λ_1 and the Bragg angle outside the layer θ_1. Upon illumination, the grating diffracts the light and the diffraction efficiency of the grating is a function of d_1, Δn_1, Λ_1 and θ_1. The interaction with the analyte produces changes in optical properties of the sensitive film and in holographic grating geometry. These changes ultimately cause alterations in the direction of the

diffracted light and the diffraction efficiency which is now a function of new parameters: d_2, Δn_2, Λ_2 and θ_2.
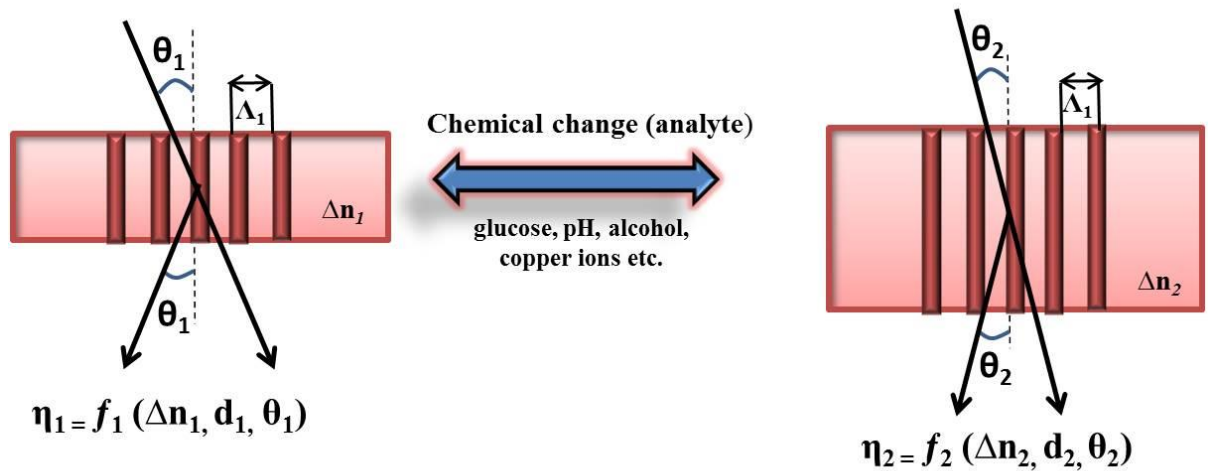
Figure 2. 14. Working Principle of holographic sensors on transmission based gratings

Diffraction efficiency alterations ($\Delta\eta$) can be caused by the effect of the two physical parameters of the hologram that are influenced by the presence of the analyte are the Δn and the d of the hologram. The other two parameters wavelength and angle can be controlled externally and they depend on the design of the interrogation system [4]:

2.7.2. Reflection holographic sensors

This type of the holographic sensor is a sensor based on a reflection grating. The sensor operates via changes in the wavelength (colour) of the diffracted light under exposure to an analyte. These sensors are the focus of the most of the research as they can be used as visual indicators which don't need an additional readout device to interpret the response. The direction of the maximum intensity of the light diffracted from the periodic photonic structure created in reflection mode is determined by Bragg's law.

When illuminated with a light with a broad spectral range, a reflection hologram will selectively diffract a specific wavelength range and the maximum diffraction efficiency will occur at a wavelength determined by equation 2.6 [4].

$$\lambda = 2n_0 \Lambda \sin\theta_B \qquad (2.6)$$

Where θ_B is the Bragg angle, λ is the wavelength of the reconstructing light, n_0 is the average refractive index of the recording medium and Λ is the grating period. Depending on the properties of the sensitive medium, the fringe spacing variation and the change in the overall refractive index of the sensitive medium will have impact on the spectral response of the sensor [5]. The operation principle of a holographic reflection grating sensor is shown in Figure 2.15:
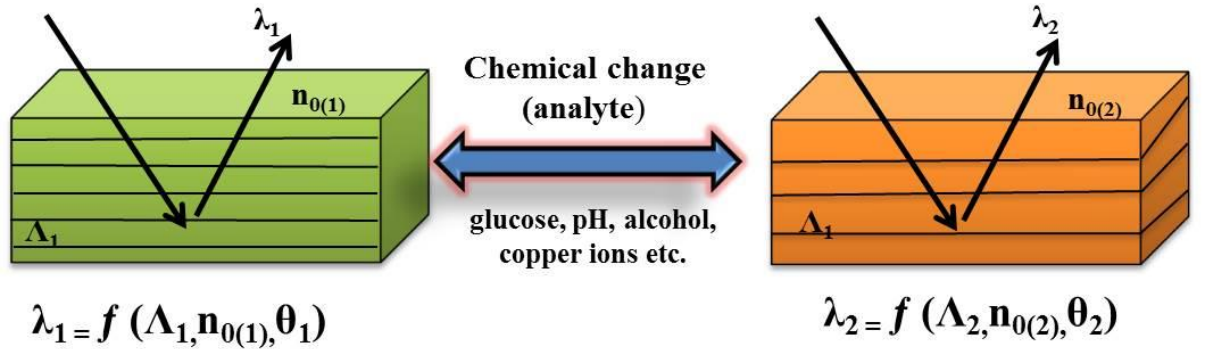
Figure 2. 15.Working Principle of holographic sensors on reflection based grating

The colour of the observed light strongly depends on the fringe spacing and average refractive index. The interaction with the analyte causes the dimensional changes of the sensitive medium due to its shrinkage or swelling. This leads to the variation in fringe spacing and, hence, the wavelength of the diffracted light alters. Thus, if the sensing material swells, the wavelength of the diffracted light will shift to longer wavelengths.

Moreover, the interaction with the analyte can have effect on the effective refractive index of the sensitive medium. The effective refractive index can be changed because of the physicochemical modification of the holographic material during exposure to the analyte. These changes ultimately cause a change in the optical path length between holographic fringes leading to the wavelength shift. An observable change in the wavelength of the diffracted light due to refractive index variation can be obtained in the case of a significant change of the refractive index. The physicochemical properties of a holographic recording material are a key factor for the development of the holographic sensor. Holographic materials with selective sensitivity to a specific analyte are needed for the applications in holographic sensor production. Holographic recording materials available for holographic sensing applications are discussed in the following section.

2.8. A short review on holographic sensors

Holographic structures can be used to fabricate sensors which can be sensitive to a wide range of applications by functionalisation with different analyte sensitive materials. Holographic sensors fabricated using different photonic materials are summarised in this section. A short review provides an overview of holographic sensors platform which can be used to monitor chemical, biological, and physical stimuli such pressure, humidity and temperature.

2.8.1. Holographic sensors for biochemical analytes

The use of holographic elements as biochemical sensors device for monitoring protease activity was reported [51]. A reflection phase hologram was recorded under buffer at room temperature by exposure of the pre-swollen film to a beam of He-Ne laser light at

with wavelength of 633 nm. The authors outlined the possibility of creating a family of specific, reagent less, low cost holographic sensors with direct visual output. A quantitative optical response of a holographic element constructed in gelatin is demonstrated for a range of trypsin concentrations down to 25 nM with a response time within 20 min. These data demonstrate the principle for a general protease sensor which has particular relevance to the measurement of trypsin activity below normal physiological duodenal fluids levels. The holographic devices respond with a change in wavelength (color) and/or a change in brightness [51].

A sensor for glucose detection recorded on a Denisyuk hologram and after contact with the analyte, the matrix changed its configuration, and the distance between layers of silver in the hologram changed. As a result, the wavelength of the reflected light also changes. Swelling or contraction of hydrogel matrices was determined by changes in the total degree of ionization of the polymer molecules. The sensor responded to glucose at different pH and ionic strengths [52].

A low cost holographic sensor was reported for potassium ions (K^+) detection. The sensors have been fabricated from crown ethers incorporated into polymeric hydrogels. The volume holograms recorded using frequency doubled Nd:YAG laser. The resulting holographic reflection spectrum was used to characterize the shrinkage and swelling behaviour. The 18-crown-6 holographic film was to be able to quantitate K^+ concentrations over the physiologically relevant range. It was almost unaffected by variations for the sodium (Na^+) ion concentration within the normal physiological variation (0.13- 0.15 M) and the proposed sensor showed great potential as a K^+ sensor for medical applications [53].

A novel glucose sensor based on a physically patterned glucose responsive hydrogel was fabricated. The hydrogel was based on polyacrylamide, N,N

methylenebisacrylamide polymerized with a phenylboronic acid. The patterning was carried out by microimprinting of a hexagonal structure from PDMS mirror-replica of a 2.5D honeycomb grating. Sensing was carried out by optical diffraction measurements from the patterned hydrogel surface in the presence of different glucose concentrations. Glucose binding with phenylboronic acid resulted in physical swelling of the hydrogel, which led to the expansion of the sensor's surface imprinted with micro-patterns. This change in the Bragg diffraction was measured in a far-field transmission configuration. A clear modulation of the 1st-order interspace against varying glucose concentration was recorded. Direct observation of glucose-induced swelling of the hydrogel was carried under an optical microscope. A linear relationship between the surface and volume expansions was established. A minimum glucose concentration of 1 mM was successfully recorded suggesting the sensor's usability in physiological conditions. The proposed sensor is quick and cost-effective as compared to its conventional counterparts, and it is suitable for mass production [54].

Recently optical glucose sensor based on diffuser architecture in a contact lens was reported. The diffuser structure was initially mirror-replicated onto a glucose-sensitive hydrogel. The structure of the diffuser was based on microengineered lens arrays that exhibited a focal length modulation in response to the overall size modification of the hydrogel upon exposure to different glucose concentrations. Consequently, the changing focal lengths changed the diffused light profile being transmitted or reflected from the surface of the sensor, thereby changing the light intensity of the diffused spot within a given transmission area. This change was measured as a function the glucose concentration in the range of 0 to 100 mM. The sensor was sensitive to glucose well within the physiological conditions. More importantly, this optical sensor can be

adapted as a minimally invasive real time measurement method as important when finger prick blood sampling in glucose measurements at point-of-care settings is associated with low patient compliance. The developed sensor was also reversible and reusable and exhibited no signal drift and hysteresis over multiple cycles or glucose concentration increase and depletion. The proposed technology can be used to monitor type 1 diabetics, where continuous glucose monitoring is an important necessity for blood glucose management at point-of- care settings [55].

2.8.2. Holographic sensors for chemical analytes

The holographic sensor technique introduced has the ability of measuring water contents in hydrocarbon solvents [24]. The Denisyuk reflection hologram was recorded in a gelatin based holographic plate using a HeNe laser. A visual color change was observed when the hologram was immersed in a wet hydrophobic liquid for instance when the water content in xylene was increased from 47 to 120 ppm and 0–1% (w/w) ethanol in water was monitored visual changes were observed. This study showed a proof of concept of low cost and simple holographic water sensor for hydrophobic liquids.

A simple liquid phase alcohol sensor based on a reflection hologram distributed throughout the volume of a crosslinked poly (hydroxyethyl methacrylate) film was developed [56]. The sensor was interrogated optically through the back of the film, by measuring the peak wavelength of the narrowband reflection spectrum when the hologram was illuminated with white light. The sensor was able to measure the thickness changes in the film with great accuracy. When the sensor was exposed to alcohol the polymer film swelled directly proportional to concentration and of alcohol content determined by measurement of the wavelength of the reflected spectral peak.

The sensor was relatively insensitive to pH in the range 3-6.5 and was highly stable, both in use and in storage. The performance of the sensor was demonstrated by measuring the alcohol contents of a wide range of alcoholic beverages such as wines and beers, with no sample pre-treatment. Alcohol concentrations were determined to be within approximately 0.3 vol % of their stated values [56].

G. Bianco et al. developed a holographic sensor for heavy metal detection in bath water. Volume hologram gratings (VGHs) were recorded and the novel approach in this sensor was that sol gel was used as a recording material. An interferometric set up was used with a laser source at 532nm to record VHGs for 1000 lines/m. A change in thickness swelling, shrinkage cross-linking density of the polymer can be caused by the hologram interaction with an analyte. Variations of the first order diffraction angle shifts (2°-3°) were observed before and after the exposure of the holographic gratings by a lead solution. Also shifts were found reversible when the gratings are washed with water. The preliminary results showed response when exposed to lead dissolved in water, opening the possibility to utilize VHG as a real-time optical sensor for heavy metals in bathing water [41].

2.8.3. Holographic sensors for physical parameters

An acrylamide monomer based pressure sensor was presented in [57]. An emulsion consisting of acrylamide:methacrylamide (2:1 v/v) and a crosslinker methylenebisacrylamide (5 mol. %) was deposited on a substrate to create a film, which was then polymerised via a free radical polymerisation reaction. A hologram was recorded while the substrate was soaking in a water bath using a frequency doubled Nd:YAG laser. The resulting hologram was sandwiched using another transparent substrate and pressure was applied onto the holograms using a pair of G-clamps. The

pressure of the clamps on the hologram resulted in a contraction in the volume of the hologram, thus causing the λ to blue-shift by a total of 3 nm. While this work demonstrated the principle of operation of a pressure sensitive hologram, a shift of 3 nm in λ is not large enough to produce a change in the colour of the reconstructed hologram visible to the human eye, and implies that the sensitivity of the reported material to pressure is not large enough for pressure sensing applications.

A pressure sensor was developed based on diacetone acrylamide monomer and recording in reflection mode. The photopolymer material used in this research was elastic and can be compressed by applying pressure with a thumb or touch. The pressure changes the original colour or image of the hologram. The photopolymer solution was deposited on a microscopic glass slide and after drying for 24 hours it was laminated with 50μm thick melinex polyester film to protect the grating during the application of pressure [58] .

A humidity sensor was reported based on acrylamide monomer photopolymer [48]. A reflection hologram recorded which is sensitive to humidity sensitive and changed its colour on exposure to humidity, mainly due to swelling or shrinkage of the photopolymer medium. The proposed sensor is reversible and fast response time [48]. Another study based on volume phase transmission gratings found that on exposure to humidity changes the diffraction efficiency and Bragg angle of gratings, the effects are fully reversible if the temperatures are kept low. When gratings were exposed to relative humidity of 80 % and 90 % at a temperature of 8 °C the observed changes were reversible, if the temperature during the humidity exposure was higher than 16°C irreversible changes were observed[59].

As described in above section, a range of holographic sensors has been developed for different analytes. However, only few surface hologram platforms have been developed for sensors applications in liquid phase analytes. A substantial part of this project is focused on the development of surface holographic sensors and modified those holograms for different analyte sensitive materials and views their application in environmental and biomedical sensing. Chapter 5 and 6 present experimental results obtained during the research.

2.9. Conclusions

In this chapter a brief overview of the field of holography has been given. The principles behind holographic recording, the different classifications of holograms, several holographic recording media and holographic applications, focused on holographic sensor technology. A description of the different components of the photopolymer composition and their individual roles has been given. The mechanism of holographic recording in photopolymers has been outlined in detail. Significant part of the present work was focused on surface holograms and the process of surface holograms fabrication will be discussed in detail in chapter 4.

References

[1]   D. Gabor, "A New Microscopic Principle," *Nature*, vol. 161, no. 4098. Nature Publishing Group, p. 777, 1948.

[2]   M. P. Givens, *Introduction to holography*, vol. 35, no. 11. Boca Raton, FL: Taylor & Francis Group, 1967.

[3]   P.Hariharam, *Context-aware user-driven news recommendation*, vol. 1542. University of Sydney, Australia: Cambridge University Press, 2015.

[4]   I. Naydenova, J. Raghavendra, S. Martin, and V. Toal, *Holographic Humidity Sensors, In Humidity Sensors*. Nova Science Publishers, 2011.

[5]   A. K. Yetisen, I. Naydenova, F. Da Cruz Vasconcellos, J. Blyth, and C. R. Lowe, "Holographic sensors: Three-dimensional analyte-sensitive nanostructures and their applications," *Chemical Reviews*, vol. 114, no. 20, pp. 10654–10696, Oct. 2014.

[6]   H. Bjelkhagen, J. Chang, and K. Moneke, "High-resolution contact Denisyuk holography," *Applied optics*, vol. 31, no. September 1990, pp. 1041–1047, 1992.

[7]   W. R. Klein and B. D. Cook, "Unified Approach to Ultrasonic Light Diffraction," *IEEE Transactions on Sonics and Ultrasonics*, vol. 14, no. 3, pp. 123–134, 1967.

[8]   M. G. Moharam and L. Young, "Criterion for Bragg and Raman-Nath diffraction regimes," *Applied Optics*, vol. 17, no. 11, p. 1757, 1978.

[9]   E. Donth, *Springer Series in Springer-Verlag Berlin Heidelberg GmbH Physics and Astronomy Springer Series in*. 2001.

[10]   R. Jallapuram, I. Naydenova, V. Toal, S. Martin, and R. Howard, "Spatial Frequency Response of Acrylamide Based Holographic Photopolymer Spatial frequency response of Acrylamide based holographic photopolymer," *Laser Application and Optical Metrology*, pp. 275–279, 2003.

[11]   I. M. Rosenberg, *Pro tein Analysis and Purification, Benchtop Techniques*. Boston, MA, 1996.

[12]   S. Martin, P. E. Leclere, V. Total, and Y. F. Lion, "Characterization of an acrylamide-based dry photopolymer holographic recording material," *Optical Engineering*, vol. 33, no. 12, p. 3942, 1994.

[13]   M. Ortuno, S. Gallego, C. Garcia, I. Pascual, C. Neipp, and A. Belendez, "Holographic characteristics of an acrylamide/bisacrylamide photopolymer in 40-1000 um thick layers," *Physica Scripta T*, vol. T118, pp. 65–68, 2005.

[14]   E. Fernández, A. Márquez, S. Gallego, R. Fuentes, C. García, and I. Pascual, "Hybrid ternary modulation applied to multiplexing holograms in photopolymers for data page storage," *Journal of Lightwave Technology*, vol. 28, no. 5, pp. 776–783, 2010.

[15]   J. Rosen, *Holography, Research and Technologies*. Rijeka, Croatia: InTech, 2011.

[16]   S. Martin, C. A. Feely, and V. Toal, "Holographic recording characteristics of an acrylamide-based photopolymer.," *Applied optics*, vol. 36, no. 23, pp. 5757–68, 1997.

[17]   I. Naydenova, R. Jallapuram, R. Howard, S. Martin, and V. Toal, "Investigation of the diffusion processes in a self-processing acrylamide-based photopolymer

system.," *Applied optics*, vol. 43, no. 14, pp. 2900–2905, 2004.

[18]   I. Naydenova, E. Mihaylova, S. Martin, and V. Toal, "Holographic patterning of acrylamide-based photopolymer surface.," *Optics express*, vol. 13, no. 13, pp. 4878–4889, 2005.

[19]   D. Yu, H. Liu, D. Mao, Y. Geng, W. Wang, L. Sun, and J. Lv, "Enhancement of spectrum strength in holographic sensing in nanozeolites dispersed acrylamide photopolymer," *Optics Express*, vol. 23, no. 22, pp. 29113–29126, 2015.

[20]   I. Naydenova, R. Jallapuram, V. Toal, and S. Martin, "Characterisation of the humidity and temperature responses of a reflection hologram recorded in acrylamide-based photopolymer," *Sensors and Actuators, B: Chemical*, vol. 139, no. 1, pp. 35–38, 2009.

[21]   Y. Gentet and P. Gentet, "Ultimate emulsion and its applications: A laboratory-made silver halide emulsion of optimized quality for monochromatic pulsed and full color holography," *Holography 2000*, vol. 4149, no. October 2000, pp. 56–62, 2000.

[22]   A. K. Yetisen, *Holographic Sensors*. Springer International Publishing AG Switzerland, 2015.

[23]   Y. Gentet and P. Gentet, "'Ultimate' emulsion and its applications: A laboratory-made silver halide emulsion of optimized quality for monochromatic pulsed and full color holography," *Holography 2000*, vol. 4149, no. 33, pp. 56–62, 2000.

[24]   J. Blyth, R. B. Millington, A. G. Mayes, E. R. Frears, and C. R. Lowe, "Holographic sensor for water in solvents.," *Analytical chemistry*, vol. 68, no. 7, pp. 1089–94, 1996.

[25] I. Naydenova, S. Mintova, S. Martin, and V. Toal, "Nanocomposites for novel holographic applications," *SPIE Newsroom*, pp. 2–4.

[26] E. M. Flanigen, R. W. Broach, and S. T. Wilson, "Zeolites in Industrial Separations and Catalysis," *Zeolites in Industrial Separation and Catalysis*, pp. 1–26, 2010.

[27] H. Awala, J.-P. Gilson, R. Retoux, P. Boullay, J.-M. Goupil, V. Valtchev, and S. Mintova, "Template-free nanosized faujasite-type zeolites," *Nature Materials*, vol. 14, no. 4, pp. 447–451, 2015.

[28] I. Naydenova, H. Sherif, S. Mintova, S. Martin, and V. Toal, "Holographic recording in nanoparticle-doped photopolymer," in *International Conference on Holography, Optical Recording, and Processing of Information*, 2006, vol. 625206, no. June 2006, pp. 625206-625206–6.

[29] E. Leite, I. Naydenova, S. Mintova, L. Leclercq, and V. Toal, *PhD thesis*, vol. 49, no. 19. 2010.

[30] M. Moothanchery, I. Naydenova, S. Mintova, and V. Toal, "Nanozeolites doped photopolymer layers with reduced shrinkage," *Optics Express*, vol. 19, no. 25, p. 25786, 2011.

[31] S. e. Gul, D. Cody, A. Kharchenko, S. Martin, S. Mintova, J. Cassidy, and I. Naydenova, "LTL type nanozeolites utilized in surface photonics structures for environmental sensors," *Microporous and Mesoporous Materials*, vol. 261, no. May 2017, pp. 268–274, 2018.

[32] G. S. Spagnolo and D. Ambrosini, "Diffractive optical element based sensor for roughness measurement," *Sensors and Actuators, A: Physical*, vol. 100, no. 2–3,

pp. 180–186, 2002.

[33]   M. Roeder, P. Schilling, D. Hera, T. Guenther, and A. Zimmermann, "Influences on the Fabrication of Diffractive Optical Elements by Injection Compression Molding," *Journal of Manufacturing and Materials Processing*, vol. 2, no. 1, p. 5, 2018.

[34]   G. A. Cirino, D. B. Mazulquim, R. Barcellos, and L. G. Neto, "Diffractive Optics An Overview for Industrial Applications," in *Latin America Optics and Photonics Conference*, 2010, no. August 2016, pp. 1–4.

[35]   P. Kress, B. C. and Meyrueis, *Digital Holographic Optics, in Applied Digital Optics, Micro-Optics to Nanophotonics*. UK,Chichester: John Wiley & Sons, Ltd, 2009.

[36]   A. L. Mikaelian, A. N. Palagushkin, and S. A. Prokopenko, *International Trends in Optics and Photonics. Springer Series in Optical Sciences*, vol. 74, no. 44. Berlin, Heidelberg: Springer, Berlin, Heidelberg, 1999.

[37]   Z. Zhou, Z. Shi, X. Cai, S. Zhang, S. G. Corder, X. Li, Y. Zhang, G. Zhang, L. Chen, M. Liu, D. L. Kaplan, F. G. Omenetto, Y. Mao, Z. Tao, and T. H. Tao, "The Use of Functionalized Silk Fibroin Films as a Platform for Optical Diffraction-Based Sensing Applications," *Advanced Materials*, vol. 201605471, pp. 1–7, 2017.

[38]   D. Cody and I. Naydenova, "Theoretical modeling and design of photonic structures in zeolite nanocomposites for gas sensing Part I: surface relief gratings," *Journal of the Optical Society of America A*, vol. 34, no. 12, p. 2110, 2017.

[39] B. Madrigal González, G. Christie, C. A. B. Davidson, J. Blyth, and C. R. Lowe, "Divalent metal ion-sensitive holographic sensors," *Analytica Chimica Acta*, vol. 528, no. 2, pp. 219–228, 2005.

[40] S. e. Gul, S. Martin, J. Cassidy, and I. Naydenova, "Development of sensitive holographic devices for physiological metal ion detection," *Proceedings of SPIE - The International Society for Optical Engineering*, vol. 10354, 2017.

[41] G. Bianco, M. A. Ferrara, F. Borbone, F. Zuppardi, A. Roviello, V. Striano, and G. Coppola, "Volume holographic gratings as optical sensor for heavy metal in bathing waters," *SPIE Optical Sensors*, vol. 9506, p. 95062B, 2015.

[42] A. J. Marshall, D. S. Young, J. Blyth, S. Kabilan, and C. R. Lowe, "Metabolite-Sensitive Holographic Biosensors," *Analytical Chemistry*, vol. 76, no. 5, pp. 1518–1523, 2004.

[43] T. Mikulchyk, S. Martin, and I. Naydenova, "N-isopropylacrylamide-based photopolymer for holographic recording of thermosensitive transmission and reflection gratings," *Applied Optics*, vol. 56, no. 22, p. 6348, 2017.

[44] T. Mikulchyk, J. Walshe, D. Cody, S. Martin, and I. Naydenova, "Humidity and temperature induced changes in the diffraction efficiency and the Bragg angle of slanted photopolymer-based holographic gratings," *Sensors and Actuators, B: Chemical*, vol. 239, pp. 776–785, 2017.

[45] J. L. Martı´nez-Hurtado, C. A. B. Davidson, J. Blyth, and C. R. Lowe, "Holographic Detection of Hydrocarbon Gases and Other Volatile Organic Compounds," *Langmuir : ACS*, vol. 26, pp. 15694–15699, 2010.

[46] M. Zawadzka, T. Mikulchyk, D. Cody, S. Martin, A. K. Yetisen, H. B. Juan

Leonardo Martinez-Hurtado, E. Mihaylova, H. Awala, S. Mintova, S. H. Yun, and I. Naydenova, *Photonic Materials for Sensing, Biosensing and Display Devices*, vol. 229. 2016.

[47] V. A. Postnikov, A. V Kraiskii, and V. I. Sergienko, "Holographic Sensors for Detection of Components in Water Solutions," *Basic Principles and Contemporary Applications*, 2013.

[48] I. Naydenova, R. Jallapuram, V. Toal, and S. Martin, "A visual indication of environmental humidity using a color changing hologram recorded in a self-developing photopolymer," *Applied Physics Letters*, vol. 92, no. 3, pp. 0–12, 2008.

[49] H. Kogelnik, "Coupled Wave Theory for Thick Hologram Gratings," *Bell System Technical Journal*, vol. 48, no. 9, pp. 2909–2947, 1969.

[50] P.Hariharan, *Context-aware user-driven news recommendation*, vol. 1542, no. 9. University of Sydney, Australia: Cambridge University Press, 2015.

[51] R. B. Millington, A. G. Mayes, J. Blyth, and C. R. Lowe, "A Holographic Sensor for Proteases," *Analytical Chemistry*, vol. 67, no. 23, pp. 4229–4233, 1995.

[52] V. A. Postnikov, A. V. Kraiski, and M. A. Shevchenko, "The change response of holographic glucose sensors when changing pH of the solution," *Proceedings of the International Conference on Advanced Optoelectronics and Lasers, CAOL*, vol. 6661, pp. 418–419, 2013.

[53] Andrew G. Mayes, Jeff Blyth, and Roger B. Millington, and C. R. Lowe, "Divalent metal ion-sensitive holographic sensors," *Analytica Chimica Acta*, vol. 74, pp. 3649–3657, 2002.

[54] M. Bajgrowicz-Cieslak, Y. Alqurashi, M. I. Elshereif, A. K. Yetisen, M. U. Hassan, and H. Butt, "Optical glucose sensors based on hexagonally-packed 2.5-dimensional photonic concavities imprinted in phenylboronic acid functionalized hydrogel films," *RSC Advances*, vol. 7, no. 85, pp. 53916–53924, 2017.

[55] M. Elsherif, M. U. Hassan, A. K. Yetisen, and H. Butt, "Glucose Sensing with Phenylboronic Acid Functionalized Hydrogel-Based Optical Diffusers," *ACS Nano*, vol. 12, no. 3, pp. 2283–2291, 2018.

[56] A. G. Mayes, J. Blyth, M. Kyröläinen-Reay, R. B. Millington, and C. R. Lowe, "A holographic alcohol sensor," *Analytical Chemistry*, vol. 71, no. 16, pp. 3390–3396, 1999.

[57] C. R. Lowe, J. Blyth, A. Peter, and W. James, "Patent Application Publica," *US 20080094635 A1*, 2008.

[58] D. Cody, S. Gribbin, E. Mihaylova, and I. Naydenova, "Low-Toxicity Photopolymer for Reflection Holography," *ACS Applied Materials & Interfaces*, vol. 8, no. 28, pp. 18481–18487, 2016.

[59] T. Mikulchyk, S. Martin, and I. Naydenova, "Humidity and temperature effect on properties of transmission gratings recorded in PVA/AA-based photopolymer layers," *Journal of Optics*, vol. 15, p. 105301, 2013.

Chapter 3 – Description of the Sensing platform based on surface relief structures

Introduction

The aim of this study is to fabricate, functionalise and modify surface relief holograms (SRG's) and to explain in detail the principle of SRG fabrication and to discuss the mechanism underlying the change in the refractive index, when holographic gratings are exposed to a target analyte. The main challenges with the formulation of photopolymers that had been used are that they are water soluble. Recently it was found that surface relief diffraction gratings made from the standard formulation were stable in water for up to 15-20 minutes if they have been cured at 220℃ [1] after that the layer starts peeling off from the glass substrate.

This chapter demonstrates a sample platform for sensors fabrication used in the current research. These structures can easily be modified with porous over layers or sensitive analyte materials, which increase the available surface area and increase the sensitivity. The fabrication method of surface relief holograms is described. The results from the optimisation of the material in order to achieve maximum surface relief modulation are presented in this chapter. The main factors in this research are mentioned below:

- Mode of formation of Surface relief diffraction gratings (SRG) with high modulation

- Functionalisation/modification the SRG's in order to detect an analyte in liquid

- Evaluation of the surface modification, sensitivity, selectivity, limits of detection and reversibility the device which will be discuss in chapter 5 and 6.

3.1. Background SRG formation in acrylamide based photopolymers

In the present research, surface relief holograms have been recorded using low a spatial frequency of 300l/mm. The recording material consists of a photopolymer layer including a polyvinyl alcohol binder, two monomers acrylamide and *N,N*-methylenebisacrylamide, triethanolamine as an initiator and erythrosin B as a photosensitive dye. The layer thickness typically averaged about $30\mu m \pm 3\mu m$. Optimization of an acrylamide based photopolymer system for holographic application using different spatial frequency has been investigated previously [2].

To record a holographic diffraction grating, laser light is split into two beams that are then redirected to overlap and interfere on the surface and throughout the volume of the photopolymer layer. Because the monomer only begins to polymerize in bright regions of the interference pattern, a concentration gradient is created and a diffusion process begins. Unpolymerized acrylamide in the dark regions begins to diffuse into the bright regions, where it is subsequently polymerized. Previous studies of the process of SRG formation reveal that mainly the monomer mass transport is responsible for the formation of surface relief peaks[1-2]. This was supported by observation of the locations of the surface relief peaks with respect to the interference pattern. The various parameters such as the intensity of the irradiance, the temperature, the chemical nature of the components controlling the characteristics of the relief generated, were examined. When a holographic transmission diffraction grating is recorded in an acrylamide-based photopolymer, a surface relief grating can be formed in addition to the volume holographic grating [1-2]. The simultaneous formation of volume and surface relief gratings is due to a polymerization driven diffusion of photopolymer components. The mechanism of the reaction has been discussed in detail in chapter 3.

Spatial frequency limitation

The intensity of the recording light has a strong influence on the amplitude of the relief created just after the illumination. The surface relief modulation is observed only at low spatial frequencies. Photo polymerisation was found to continue after the end of irradiation. The purpose of a subsequent UV exposure is to ensure any residual monomer is polymerised. Samples were prepared by using the optimized conditions (chemical compositions, exposure condition and spatial frequency).

To identify the spatial frequency limit holographic diffraction gratings were recorded at various spatial frequencies in the range from 500 to 1600 lines∕mm. It was found that recording at lower spatial frequency leads to formation of higher surface amplitude. The results showed that the decrease of the TEA concentration and the increase of monomer concentration both contribute to lead to higher SRG amplitudes (Figure 3.1). But the effect which contributes most to an increase in the amplitude is by exposing the gratings to an elevated temperature. The samples were placed in the oven set to 120℃ to be thermally treated. Every 10 minutes the oven temperature was increased by 10°C until the oven reached 220℃ [2].
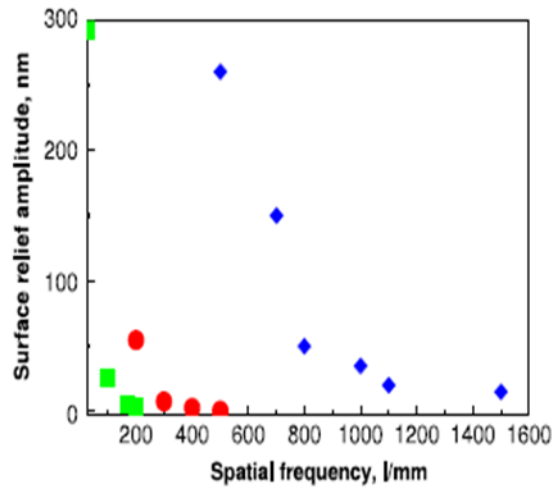
Figure 3. 1. Spatial frequency dependence of the SRG amplitudes: (■) after optimisation of recording conditions, (●) after optimisation of photopolymer conditions, after exposure to elevated temperatures (◆) [2]

3.2. Surface holograms formation

The following section aims to explain the fabrication of surface relief holograms. When a photopolymer recording material is illuminated with an interference pattern of light, polymerization takes place in the bright region as shown in Figure. 3.2. On polymerization, each double bond is replaced by two single bonds. This results in depletion of monomer in bright regions and a concentration gradient of the monomer resulting in the diffusion of monomer from the dark unexposed regions to the bright exposed regions.

The overall refractive index is higher in the polymerized region than in the unpolymerized region due to the increased density. Holograms recorded by this mechanism are known as phase holograms. It has been previously observed that in addition to the volume holographic structure, a surface relief structure with amplitude strongly depending on the spatial frequency of the recorded grating is developed. The amplitude of the surface structure can be additionally increased by exposure to elevated

93

temperature [1]. The diffraction efficiency of the hologram depends on the difference in refractive index Δn, between the polymer and the gap in the valley.

This approach was used in the present study. In order to obtain surface relief structures with high amplitude, the samples were placed in an oven (Lennox laboratory supplies Ltd) set at 120℃ to be thermally treated. The oven temperature was increased by 10℃ every 10 minutes upto a temperature of 220℃. It was found that the gradual exposure to elevated temperature is crucial for the formation of a stable SRG. Instant exposure to elevated temperature above 160℃ leads to the complete destruction of the recorded gratings, both for volume and surface gratings. The contribution of the two gratings to the diffraction efficiency of the recorded structure was analysed before and after exposure to elevated temperature.

Interference Pattern

Uniform monomer distribution before light illumination

Pohotpolymerisation after light illumination and thermal treatment 120°C to 220°C

n_{air} n_{bright}

After modification with receptor material

Expose to the analyte solution
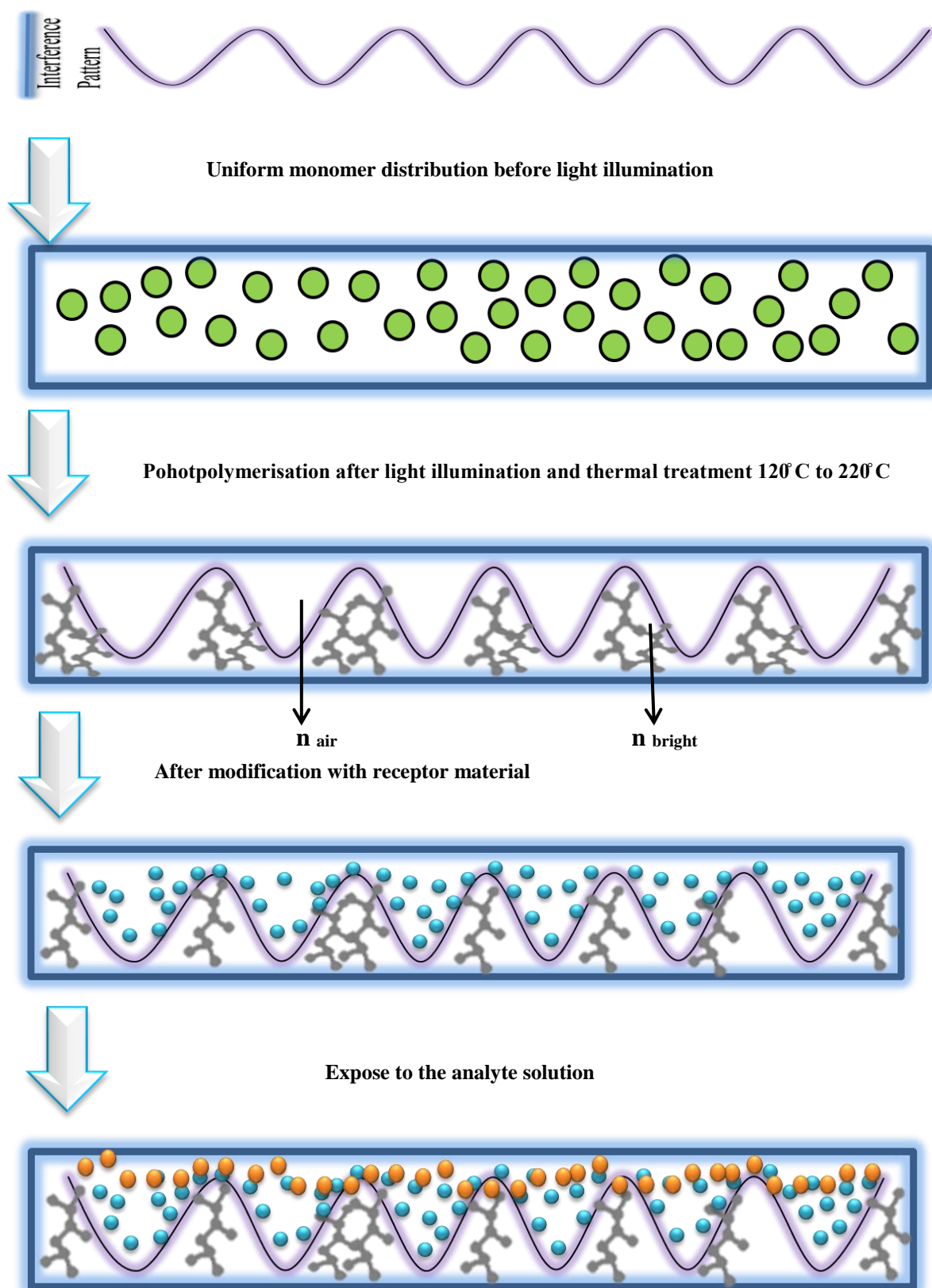
Figure 3. 2. Distribution of constituents of photopolymerisable nanocomposites (monomer molecules, polymer chain, modified receptor material and after exposure to analyte) during the holographic exposure

In a multi-component system, the exact mechanism of the change of the refractive index modulation is quite complex and depends on many physical and chemical factors and the composition of the photopolymer system itself.

3.3. Process of fabrication characterisation of holographic surface relief photonic structures

The fabrication process of surface relief grating is described in Figure 3.3. The photopolymer solution was prepared and cast on a microscope slide. Next the layers were characterised by White Light Interferometry or an atomic force microscope and by measurement of the Bragg angle before and after thermal treatment. After this, they were modified with the analyte sensitive material.
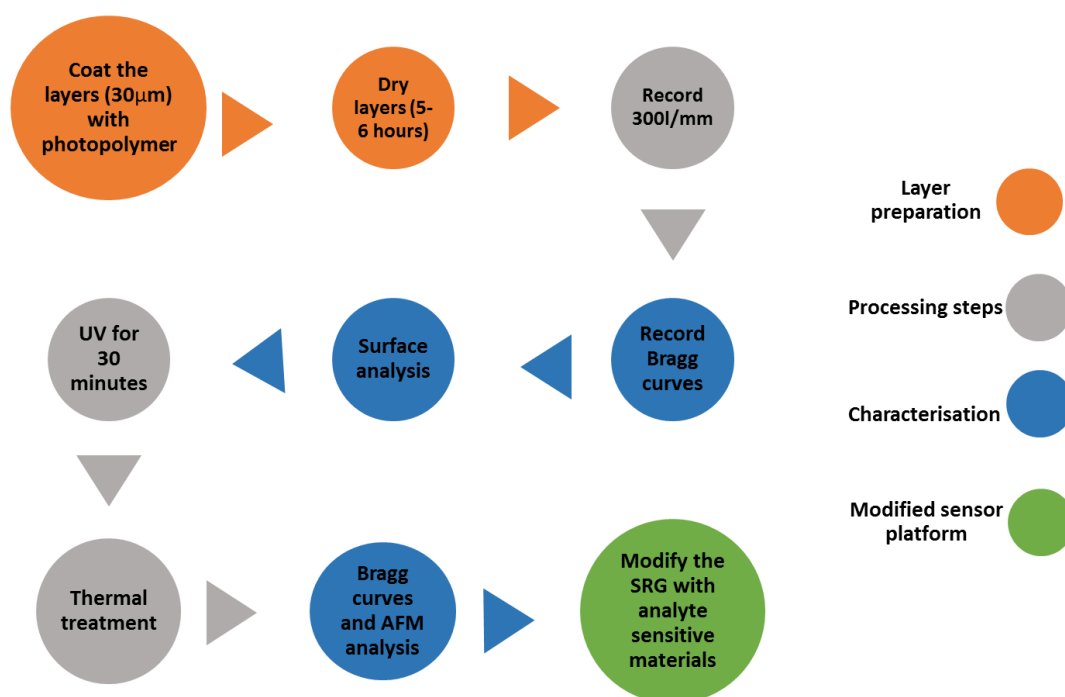
Figure 3. 3. Fabrication process of surface relief gratings (SRG)

The surface relief profile of the gratings used in this thesis was studied by White light interferometry (WLI) and an atomic force microscope (AFM). It was determined that the amplitude of the recorded grating was < 10nm Figure 3.4(a) and after thermal treatment it increased up to 350-400 nm as shown in Figure.3.4 (b and c) as shown by both WLI and AFM.
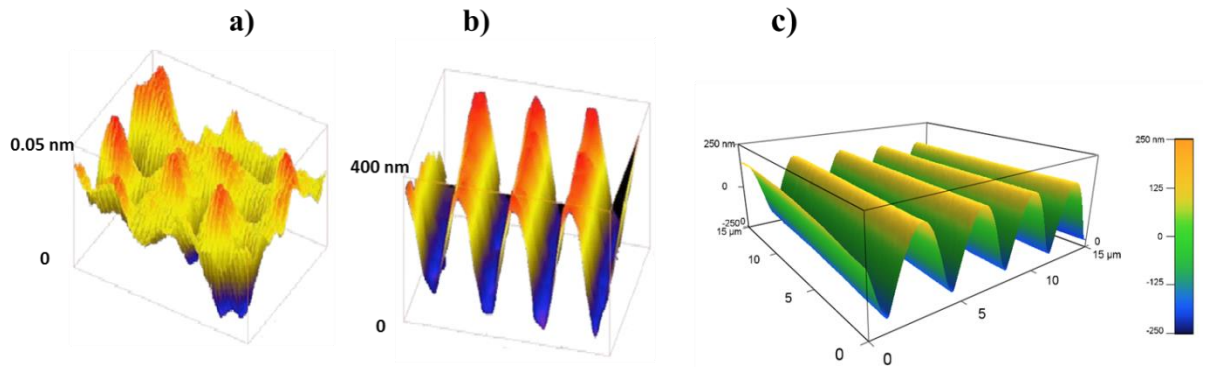
Figure 3. 4. WLI and AFM images of the SRG (a) before thermal treatment, (b) after thermal treatment and (c) AFM image of the SRG

3.4. Principle of operation a surface relief sensors

The SRG acts as a support structure for the receptor material (as shown in Figure 3.5). The interaction between the ion selective layer and the underlying SRG is primarily a physical inclusion where the layer fills the valleys of the SRG. The sensitive material Where, Δn is defined as the difference between the refractive index of the support structure (i.e. photopolymer n_p) and the analyte sensitive material (n_R). On exposure to an analyte, the analyte molecules change its properties, resulting in a change in Δn, which in turn produces a measurable change in the η of the sensor as a function of analyte concentration. The initial refractive index Δn of the surface grating is calculated from the difference between the refractive index of the photopolymer material n_p and receptor n_R. Any change in the value of Δn of the grating will vary the phase difference

(φ) between the beams propagating in directions along the zero (I_t) and the higher

orders (I_d) of diffraction from the grating when illuminated with a probe beam (I_o).

This causes a measurable change in the grating diffraction efficiency η, defined here as

the ratio of I_d to I_0. Whereas working with volume gratings is more challenging since

analyte solutions have to permeate through the volume of the layer, SRGs have the

potential to give a faster response time [3].

$$\eta = \frac{I_d}{I_0} * 100$$
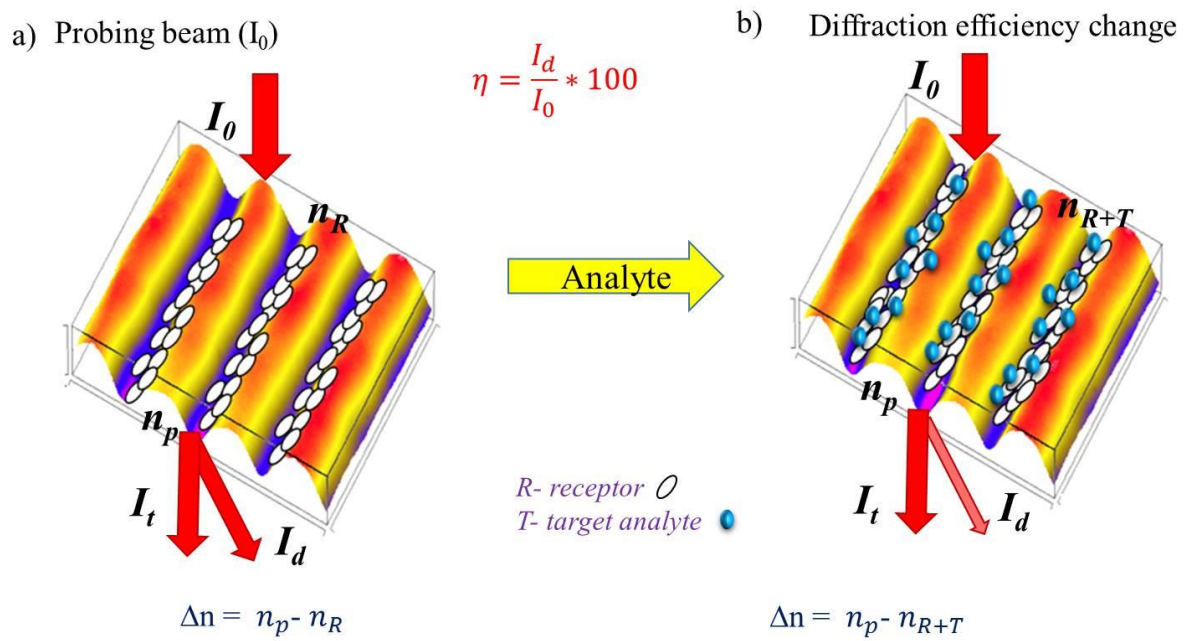
Figure 3. 5. Modified SRG (a) before (b) after analyte exposure

SRG's are promising for many applications such as sensors. Fabrication and

modification of SRG provide versatile solutions for sensing different analytes and they

can be used as diffraction grating sensors for different purposes [4-5]. The

characteristics of volume and surface holograms are outlined in table 3.1. Surface relief

structures feature across a range of optical sensor platforms including surface plasmon

resonance-based sensors for detection of chemical and biological molecules [6] and

optical fibre Bragg grating-based sensors for volatile organic compounds (VOC)

detection [7-8] and temperature monitoring [9]. The inscription of molecularly-imprinted polymers via interference photolithography has facilitated the production of testosterone sensors [10]. Aztec holograms which are essentially a combination of the surface structure and Bragg reflector geometries, were originally proposed in [11] and have recently been functionalized for humidity sensing via coating with hydrophilic materials such as polyvinyl alcohol and glycerol[12].

Table 3.1. Characteristics of volume and surface holograms in the context of sensors development

Structure	Advantages	Disadvantages
Volume $Q>10$	Large dynamic range (large range of changes of the parameters, theoretically diffraction efficiency 100 % is possible), in reflection mode holograms – a single colour is detected (colorimetric sensors)-	Slower response, more challenging to synthesise a material that is both – capable of recording a hologram and sensitive to the analyte
Surface $Q<1$	Faster response time, more flexible- one photonic structure can be easily functionalised for different analytes by variation of the coating	Limited dynamic range (maximum diffraction efficiency -33% for sinusoidal profiles), colorimetric sensors are not easily achieved with this configuration

Here, a sensor based on a surface relief grating inscribed holographically in a photopolymer layer is proposed. The period and surface relief amplitude of the grating are controlled via variation of the holographic recording conditions. Depending on these parameters, the surface relief grating may be defined as either thin or thick, in accordance with the Klein-Cook Q parameter [13]:

$$Q = \frac{2\pi\lambda_r d}{n_0 \Lambda^2} \qquad (3.1)$$

where n_0 is the recording medium refractive index and λ_r is the reconstruction wavelength. Q values larger than 10 correspond to thick gratings which may be described using Kogelnik's Coupled Wave Theory [14], whereas gratings with a Q value of less than 1 are considered in the thin regime, and may be described using Raman-Nath Theory [15]. Surface relief gratings fabricated in photopolymer media are typically in the thin regime, as the surface relief amplitudes required to be classified as thick are very difficult to achieve at the necessary grating spatial frequencies. In the present research, surface relief structures were utilized with a spatial frequency of 300 l/mm (3.3 µm) with thickness of 400 nm. According to Equation (3.1), these parameters correspond to Q factor of about 9.5×10^{-3}.

The output of the surface relief grating-based sensor as a function of analyte concentration is measured via change in grating diffraction efficiency, η. For thin phase gratings in the Raman-Nath regime, η is defined as:

$$\eta = J_m^2 \left(\frac{\pi \Delta n d}{\lambda_r} \right) \qquad (3.2)$$

Where J_m is the Bessel function of the order m. The incident beam is diffracted into a number of orders, with the diffracted amplitude in the mth order proportional to the

value of the Bessel function more explanation for Bessel function provided in appendix A.

3.5. Theoretical curve showing the response of the sensor for 400nm height and change in refractive index of the modified surface film

The blue line in Figure 3.6 represents the theoretical data from equation 3.2 and the coloured points correspond to the experimentally measured diffraction efficiency ($m =1$) values for a 400 nm surface relief grating initially uncoated $\eta = (0.35)$ after coating $\eta = (0.20)$, and after 3 minutes exposure to analyte $\eta = (0.03)$ solution. Theoretically, the maximum achievable diffraction efficiency of the sinusoidal surface structure is 33 % [15]. The refractive index of the photopolymer material is 1.5 and refractive index of air is 1 and $d = 400$ nm. The probe wavelength is 633 nm, thus the diffraction efficiency of the structure is estimated to be 0.33. This implies that the contribution of the volume structure has been significantly suppressed. By analysing the experimental data it was concluded that the main contributor to the response of the fabricated sensor is the surface relief photonic structure. The overall value of Δn for the SRG will increase or decrease. It is assumed the case consider in Figure 3.6 the overall value of Δn for the SRG will decrease. Therefore, for this theoretical study the sensor is operating in a regime based on the left hand side of the theoretical Bessel curve. The diffraction efficiency of the surface relief photonic structures after modification with receptor further decreased (Figure 3.6). This is due to the fact that now air is replaced by a material with a refractive index higher than 1, and thus the Δn decreases. This could be explained by the fact that when analyte is adsorbed in the receptor (which is a porous material), the refractive index modulation further decreases. A detailed study of the variation of the diffraction efficiency change of the modified structures upon exposure to analyte solutions results will be described in chapter 4 and 5.
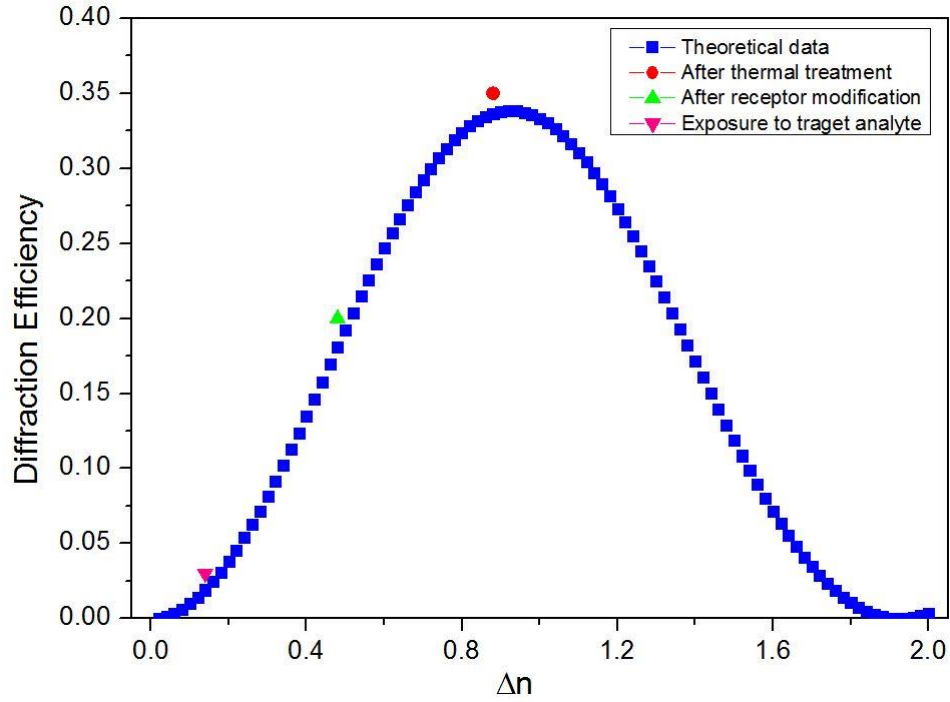
Figure 3. 6. Diffraction efficiency vs. change in refractive index Δn. Blue line represents theoretical data and coloured points represents experimental data (d = 400nm and λ$_r$ = 633nm)

3.6. Surface relief structures and their application in sensing

The primary advantage of surface relief grating structures for sensing is that the target analyte is not required to shorter diffusion into the structure as is the case for volume grating holographic sensors; interaction of the target analyte with the surface structure can result in a measurable change in the sensor output. This can potentially enhance the device sensitivity and facilitate faster response times [16]. A limitation of surface relief structure sensors is that the sensitivity of the device is governed by the aspect ratio of the surface relief grating [3]. The aspect ratio is defined as the maximum achievable surface relief amplitude divided by of grating period (d/Λ). Sensors based on modified surface relief gratings with higher aspect ratios will produce a greater sensor response as a function of analyte concentration. However, the ability to achieve large d at high spatial frequency is governed by the properties of the holographic recording medium.

Fabrication and modification of SRG provide versatile solutions for sensing different analytes and they can be used as diffraction grating sensors for different purposes [4-5].

The development of sensor technology platform based on surface relief gratings has been attracting significant attention recently. A surface sensor platform was developed for biosensing based on the aminopropyltriethoxysilane modified with nanoporous polymeric gratings. Modification with aminopropyltriethoxysilane helps biomolecules be easily immobilised onto the polymeric surface grating. The authors reported detection of several biomolecules including biotin, streptavidin, biotinylated anti-rabbit IgG, and rabbit-IgG [5]. A novel sensing method based on diffraction gratings reported by using poly (acrylic acid) hydrogel modified with glucose oxidase. The sensor was developed for quantitative glucose detection [4].

Holographic molecularly imprinted polymers (MIP) for chemical sensing were developed. A rapid, inexpensive and reproducible approach was described in which MIP thin films were developed by using photopatterning interference photolithography. The authors reported that holographic microstructures are capable of specifically binding the steroid testosterone [17].

3.7. Characteristics of the surface relief grating

> Grating period: Greater diffraction efficiency can be obtained by increasing the aspect ratio (d/Λ) for a sinusoidal surface-relief grating. The diffraction efficiency η of the surface relief grating was calculated using equation 3.3 [15]:

$$\eta = J_m^2(\Delta\varphi) \qquad\qquad (3.3)$$

where $\Delta\varphi$ is the change in phase, and m is the diffraction order. J_m is the Bessel function of the order m. The incident beam is diffracted into a number of orders,

with the diffracted amplitude in the mth order proportional to the value of the Bessel function. The influence of initial phase $\Delta\boldsymbol{\varphi}$ between the probe and diffracted beams introduced by the grating depends on the initial properties of the grating and is defined as:

$$\Delta\boldsymbol{\varphi} = \frac{2\pi\,\Delta nd}{\lambda_r} \qquad (3.4)$$

where Δn is the refractive index modulation, d is the surface relief amplitude, and λ_r is the reconstruction wavelength.

➢ Aspect ratio: The value of the diffraction efficiency changes with the grating amplitude (d/Λ).

➢ Diffraction efficiency: The maximum diffraction efficiency of a sinusoidal surface relief grating is 33% and maximum diffraction efficiency of a volume grating is 100% [18].

3.8. Conclusion

The process of SRG platform fabrication discussed. During the fabrication of SRG holograms it was observed that the efficient surface relief formation in this material depends on the intensity of recording beams, UV exposure after recording and proper thermal treatment. Characteristics of SRG were discussed. The SRG platform is promising for sensors applications. Modified SRGs are possible sensors when the sensing layer contributes to the refractive index in the grooves of the SRG.

References

[1] K. Trainer, K. Wearen, D. Nazarova, I. Naydenova, and V. Toal, "Optimization of an acrylamide-based photopolymer system for holographic inscription of surface patterns with sub-micron resolution," *Journal of Optics*, vol. 124012, pp. 1–7, 2010.

[2] K. Pavani, I. Naydenova, S. Martin, and V. Toal, "Photoinduced surface relief studies in an acrylamide-based photopolymer," *Journal of Optics A: Pure and Applied Optics*, vol. 9, no. 1, pp. 43–48, 2006.

[3] D. Cody and I. Naydenova, "Theoretical modeling and design of photonic structures in zeolite nanocomposites for gas sensing Part I: surface relief gratings," *Journal of the Optical Society of America A*, vol. 34, no. 12, p. 2110, 2017.

[4] G. Ye, X. Li, and X. Wang, "Diffraction grating of hydrogel functionalized with glucose oxidase for glucose detection," *ChemComm*, vol. 2, pp. 3872–3874, 2010.

[5] V. K. S. Hsiao, J. R. Waldeisen, Y. Zheng, P. F. Lloyd, J. Bunning, and T. J. Huang, "Aminopropyltriethoxysilane（APTES）-functionalized nanoporous polymeric gratings：fabrication and application in biosensing," *Journal of Materials Chemistry*, vol. 17, pp. 4896–4901, 2007.

[6] W. Chien, M. Zeeshan, X. Dai, and A. G. Kirk, "Chemical Monolithically integrated surface plasmon resonance sensor based on focusing diffractive optic element for optofluidic platforms," *Sensors and Actuators B :*, vol. 138, pp. 441–445, 2009.

[7] A. K. Yetisen, I. Naydenova, F. Da Cruz Vasconcellos, J. Blyth, and C. R. Lowe, "Holographic sensors: Three-dimensional analyte-sensitive nanostructures and their applications," *Chemical Reviews*, vol. 114, no. 20, pp. 10654–10696, Oct. 2014.

[8] T. L. Lowder, J. D. Gordon, S. M. Schultz, and R. H. Selfridge, "Volatile organic compound sensing using a surface-relief D-shaped fiber Bragg grating and a polydimethylsiloxane layer.," *Optics letters*, vol. 32, no. 17, pp. 2523–2525, 2007.

[9] T. L. Lowder, K. H. Smith, B. L. Ipson, A. R. Hawkins, R. H. Selfridge, and S. M. Schultz, "High-temperature sensing using surface relief fiber Bragg gratings," *IEEE Photonics Technology Letters*, vol. 17, no. 9, pp. 1926–1928, 2005.

[10] Y. Fuchs, S. Kunath, O. Soppera, K. Haupt, and A. G. Mayes, "Molecularly imprinted silver-halide reflection holograms for label-free opto-chemical sensing," *Advanced Functional Materials*, vol. 24, no. 5, pp. 688–694, 2014.

[11] J. J. Cowan, "Aztec surface-relief volume diffractive structure," *Journal of the Optical Society of America A*, vol. 7, no. 8, p. 1529, 1990.

[12] A. K. Yetisen, H. Butt, T. Mikulchyk, R. Ahmed, Y. Montelongo, M. Humar, N. Jiang, S. Martin, I. Naydenova, and S. H. Yun, "Color-Selective 2.5D Holograms on Large-Area Flexible Substrates for Sensing and Multilevel Security," *Advanced Optical Materials*, vol. 4, no. 10, pp. 1589–1600, 2016.

[13] W. R. Klein and B. D. Cook, "Unified Approach to Ultrasonic Light Diffraction," *IEEE Transactions on Sonics and Ultrasonics*, vol. 14, no. 3, pp. 123–134, 1967.

[14] H. Kogelnik, "Coupled Wave Theory for Thick Hologram Gratings," *Bell System Technical Journal*, vol. 48, no. 9, pp. 2909–2947, 1969.

[15] C. V. Raman and N. S. N. Nath, "The diffraction of light by high frequency sound waves: Part III," *Proceedings of the Indian Academy of Sciences - Section A*, vol. 84, 1936.

[16] S. e. Gul, D. Cody, A. Kharchenko, S. Martin, S. Mintova, J. Cassidy, and I. Naydenova, "LTL type nanozeolites utilized in surface photonics structures for environmental sensors," *Microporous and Mesoporous Materials*, vol. 261, no. May 2017, pp. 268–274, 2018.

[17] Y. Fuchs, O. Soppera, A. G. Mayes, and K. Haupt, "Holographic molecularly imprinted polymers for label-free chemical sensing," *Advanced Materials*, vol. 25, no. 4, pp. 566–570, 2013.

[18] K. Yokomori, "Dielectric surface-relief gratings with high diffraction efficiency," *Appl. Opt.*, vol. 23, no. 14, pp. 2303–2310, 1984.

Chapter 4 – Development of novel holographic sensors for the detection copper ions in fresh water by incorporation of LTL-type zeolites nanoparticles

4.1. Introduction

In this chapter, the sensors are created by holographic recording of surface relief gratings (SRG) in a self-processing photopolymer material as described in chapter 4. Interrogation of these structures by light allows indirect measurements of ion concentration in real time. The SRG structures are modified by coating with porous LTL-nanoparticles (nanosized zeolites) which selectively adsorb divalent cations. The suitability of the sensors for detection of copper (II), calcium (II) and Lead (II) present in water at concentration levels 1–4 mM is reported. Information regarding the synthesis of LTL- zeolite nanoparticles from colloidal solution and the preparation of the sensing structure is provided. LTL-zeolites nanoparticles were provided and synthesised by the group of Prof. Mintova, University of Caen, France.

In this work we introduced a new approach for sensors fabricated in photonic structures to target liquid phase analytes which are low cost, disposable and easy to fabricate. The proposed holographic sensors were tested to detect Cu^{2+}, Pb^{2+} and Ca^{2+} [1] the performance of the sensors will be discussed in this chapter. Zeolite frameworks consist of crystalline hydrated aluminosilicates, containing pores [2]. They have the ability for cation-exchange binding, heavy metal incorporation and have molecular sieve properties. Applications of zeolites for chemical and wastewater treatment have proved that they are a promising technique in environmental cleaning processes. The development of sensing systems is the main application of nanomaterials [3], since they can enhance the analytical performance of sensor devices.

Zeolites

Zeolites are defined as crystalline alumina silicate materials consisting of framework structures with regular and uniform pores of molecular dimensions [4]. Structurally, alumina silicalites zeolites are inorganic materials based on connected framework of SiO_4 and AlO_4 tetrahedra that are linked to each other by shared oxygen atoms. Each AlO_4 tetrahedron in the framework bears a net negative charge that is balanced by an extra framework cation [2]. The general empirical formula is [4]:

$$M_{x/m} Al_x Si_{2-x} O_4 . n H_2O$$
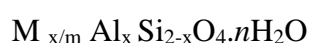
where *m* is the valence of cations *M*, *n* the water content.

On the other hand, microporous aluminophosphates are a new class of inorganic materials often called zeo type materials. The basis for the synthesis of these materials is the crystal chemical similarity between Si and P and SiO_2 and $AlPO_4$ in particular [4]. Their framework consists of alternating Al^{3+} and P^{5+} sites and the overall framework is electrically neutral since the positive charge of inorganic cations is balanced by the simultaneous occlusion of OH- groups [5]. The general formula aluminophospahate molecular sieve product composition expressed in terms of oxide ratios is:

$$[(AlO_2)_x (PO_4)_x].yH_2O$$

The properties of zeolites are dependent on the topology of its framework, the size, shape and accessibility of its free channels, the charge location and size of the cations within the framework. The feature that is common in zeolite materials is that they all have a 3-dimensional, 4-connected framework structure constructed from corner-sharing TO_4 tetrahedra (basic building unit), where T is any tetrahedrally coordinated

cation (T is an aluminium or silicon atom in aluminosilicalites or phosphorus in aluminophosphates) [6-7].

Zeolites materials are classified according to their framework type. This framework structure is relatively open and characterized by the presence of channels and cavities of tetrahedral atoms. An important structural parameter is the size of the pore opening through which molecules diffuse into the channels and cages of zeolites[8-9]. The pore size is related to ring size defined as the number of tetrahedral atoms forming the pore [8].

Depending on the structural type, the pore sizes range from 0.3 to 1 nm [8]. Among the zeolites, there are materials with small pore openings such as LTA (4.1 Å) with 8 atoms rings, with medium pore openings, i.e. MFI- and MEL (5.5 Å) with 10 atom rings and with large pore openings such as FAU-, LTL-, and BEA- molecular sieves (>7.0 Å) with 12 atom ring. The pore volume of a zeolite is related to the framework density defined as the number of tetrahedral atoms per 1000 Å [5]. The tetrahedra are linked together to form cages connected by pore openings of defined size. LTL-zeolites (used in this study) framework can be seen in Figure 4.1 [8].

View along b*-axis   View along c-axis   View along a*-axis
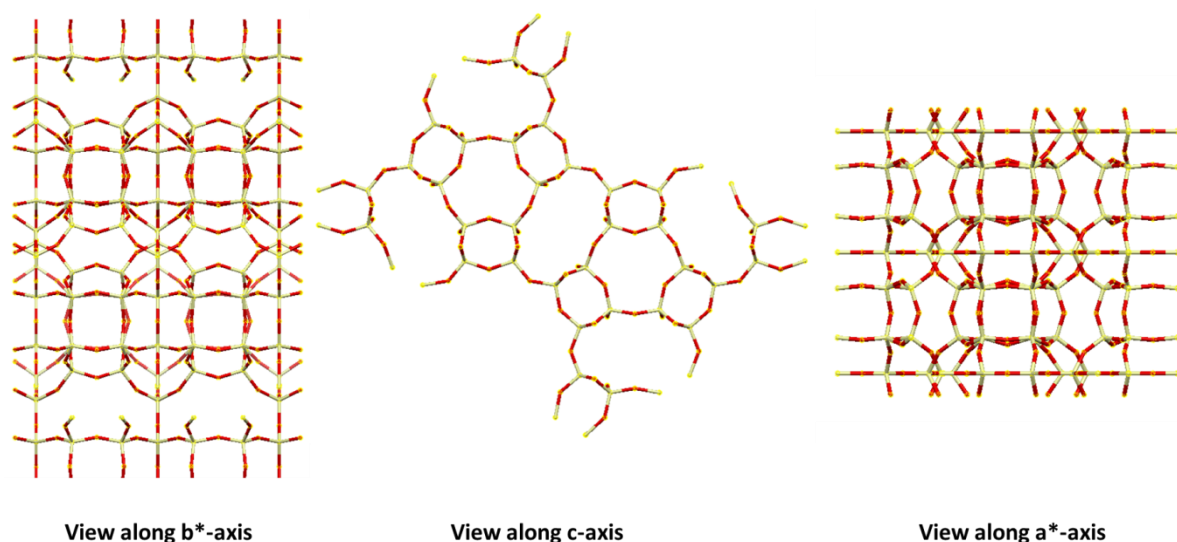
Figure 4. 1. LTL-zeolite framework used in the present work.

In order to modify or functionalise holographic sensors, zeolite nanoparticles are good candidates because of the ability to ion exchange. This research section describes sensors based on surface relief grating (SRG) structures created by holographic recording in photopolymers. These holographic structures constitute a flexible platform (as described in chapter 4) for fabrication of sensor devices since they can be modified with the help of different materials and thus make them selective to a specific analyte. The response to pollutants such as copper, lead and calcium ions in water is presented in this chapter.

4.2. Experimental

4.2.1. Materials and Methods

The acrylamide based photopolymer was prepared as described in Table 4.1. The components were well mixed in water by using a magnetic stirrer. All the materials used in this work were of analytical grade purchased from Sigma Aldrich without any purification.

Components	Amount (g)	Amount (% w/w) in dry layer	$n=\frac{m}{Mw}$ $(moles)$
Acrylamide (AA)	1.0	24.5	1.4×10^{-2}
N,N'Methylenbisacrylamide(BAA)	0.2	4.9	1.29×10^{-3}
Polyvinyl alcohol (10% wt/wt) (PVA)	1. 75	43.0	1.75×10^{-4}
Triethanolamine (TEA)	1. 12	27.5	7.50×10^{-3}
Erthrosine B dye (0.01% wt/wt) (EB)	0. 0044	0.1	5.26×10^{-6}
Total weight	4.07		

4.2.2. Preparation of Photopolymer films

All the samples were prepared under ambient laboratory conditions - temperature 16-22° C; relative humidity 40 – 60% as follows. In order to obtain a stock solution of 10 % w/w. Polyvinyl alcohol (PVA) was dissolved in deionised water while heated at 70° C. Erythrosine B (EB) was dissolved in water without any heating in order to get a dye stock solution of 0.11 % w/w. Next Triethanolamine initiator was added into the PVA solution. Next, acrylamide(AA) and N,N'Methylenebisacrylamide (BAA) were added as the two monomers, along with the dye solution. Finally, all the components were mixed for 1 hour [10] at room temperature. 300µl of photopolymer solution was spread evenly on a glass substrate. The coated glass substrate was placed on a levelled surface and allowed to dry in the dark for typically 5-6 hours. The thickness of the dry sample

was 30 ± 3μm [11]. Information on the synthesis and characterisation of zeolites can be found in appendix (B).

4.2.3. Recording of the surface relief gratings (SRG)

The set up used for recording the holographic gratings, as shown in Figure 4.2, is a bi-beam holographic lithography arrangement. The angle is set to 9.16˚ between the two beams to get an interference pattern with a spatial frequency of 300 lines/mm ±10 lines/mm. The recording light source Nd: YVO4 laser emitting at 532 nm (green light source) (Supplied by Coherent, Model Verdi 5w) is used in order to obtain a transmission holographic grating. The intensity of the light source is set to 10 mWcm^{-2} and an exposure time of 100 seconds used. Details of the optimisation process were reported previously [12]. In order to achieve the selectivity curve of a recorded grating, an s- polarized Helium-Neon laser (He-Ne) (supplied by Uniphase mellon Avenue, Model No 106-1) of wavelength 633 nm was used as a probe beam incident at Bragg angle to the grating as shown in Figure 4.2.

1. Nd: YAG laser @ 532nm
2. Shutter
3. Half Wave Plate
4. Polariser
5. Spatial filter
6. Collimating lens
7. Aperture
8. Beam Splitter
9. Mirror
10. Neutral density filter
11. Photopolymer
12. He-Ne laser @ 633 nm
13. Detector
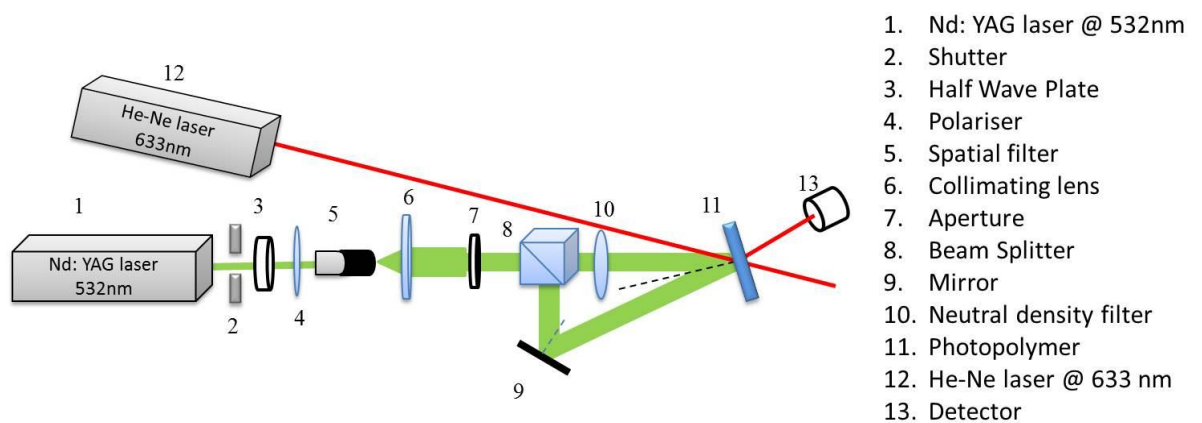
Figure 4. 2. Experimental set-up for recording transmission holograms

The intensity of the diffracted beam was measured by using an optical power meter (Newport 1830-C). The grating was placed on the rotational stage in order to measure the diffracted beam intensity as a function of the incident angle of the probe beam. (The accuracy of this measurement was 1×10^{-3} deg). An optical power meter was used in order to measure the 1st order diffracted beam intensity of the recorded gratings. The diffraction efficiency is purely determined by the volume diffraction grating before exposure to elevated temperature. The surface relief amplitude is (d= < 1nm). The diffraction efficiency after exposure to elevated temperature is mainly determined by the surface relief structure (d= 400nm). Whereas the diffraction efficiency η was recorded at the Bragg angle, which is the ratio of the two intensities the first diffraction order beam intensity I_d and the incident beam intensity I_0 of the probe beam as follows:

$$\eta = \frac{I_d}{I_0} \times 100 \qquad\qquad (4.1)$$

After holographic recording the SRGs were exposed to UV cured for 15 minutes with the exposure of 2.5mW/cm^2 using a UV Exposure unit (Mega Electronics, model LV 202E-) in order to polymerise all residual monomers. Figure 4.3 is a schematic of the grating formation; details of the process are explained in chapter 3.
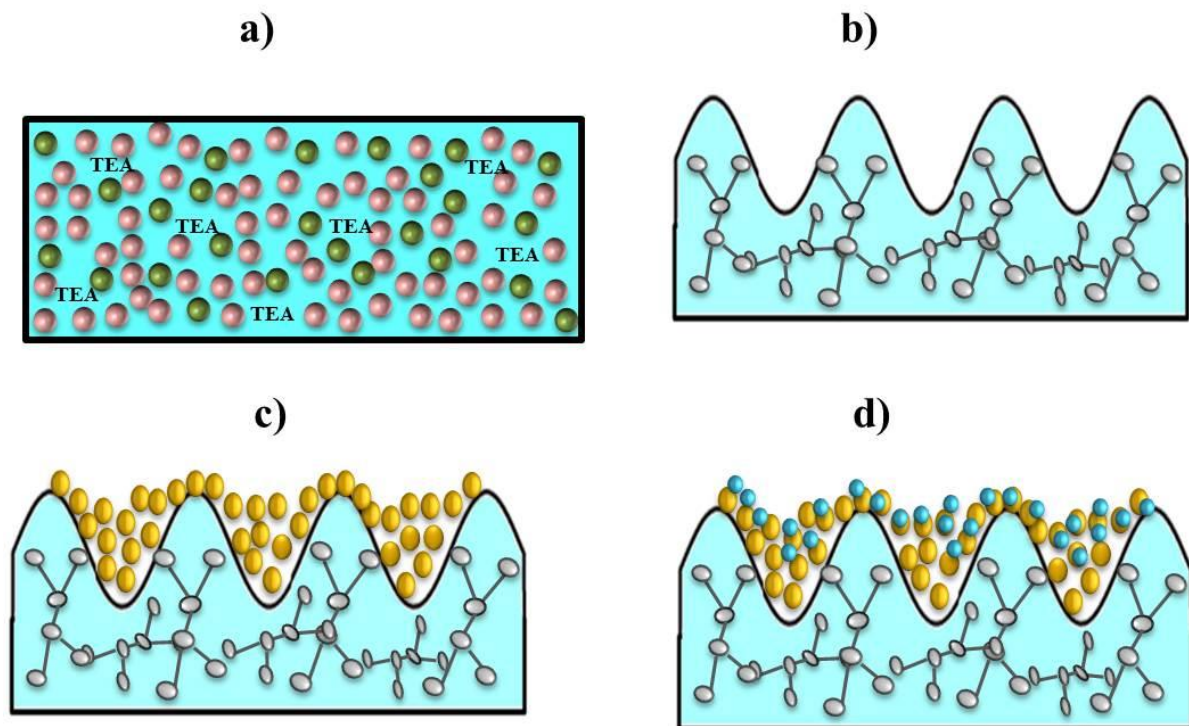
Figure 4. 3.Distribution of constituents of photopolymerisable nanocomposites: a) acrylamide (AA) ,bisacrylamide (BAA) monomer molecules and initiator Triethanolamine (TEA), b) after polymerization, c) after coating with LTL-zeolite nanoparticles and d) exposure to analyte.

The photopolymer surface was studied using a white light interferometry (WLI) surface profiler MicroXAM S/N 8038 and AFM using an Asylum MFP-3D AC microscope. Here, the SRG acts as a support structure for the zeolites, and Δn is defined as the difference between the refractive index of the support structure (i.e. photopolymer) and the sol gel layer containing zeolite nanoparticles. On exposure to an analyte, the analyte molecules exchange into the zeolite nanoparticles that fill the valley (Figure 4.3 d), resulting in a change in Δn, which in turn produces a measurable change in the η of the sensor as a function of analyte concentration (Figure 4.3 d). More information about refractive index change due to exposure to the analyte can be found in the appendix C.

4.3. Photonic structures coated with LTL-zeolite nanoparticles

Initially layers were coated with LTL-zeolites nanoparticles dispersed in ethanol. When the coated layers were studied under WLI, the results revealed that after exposure to copper solution nanoparticles were washed away from the surface as shown in Figure.4.4
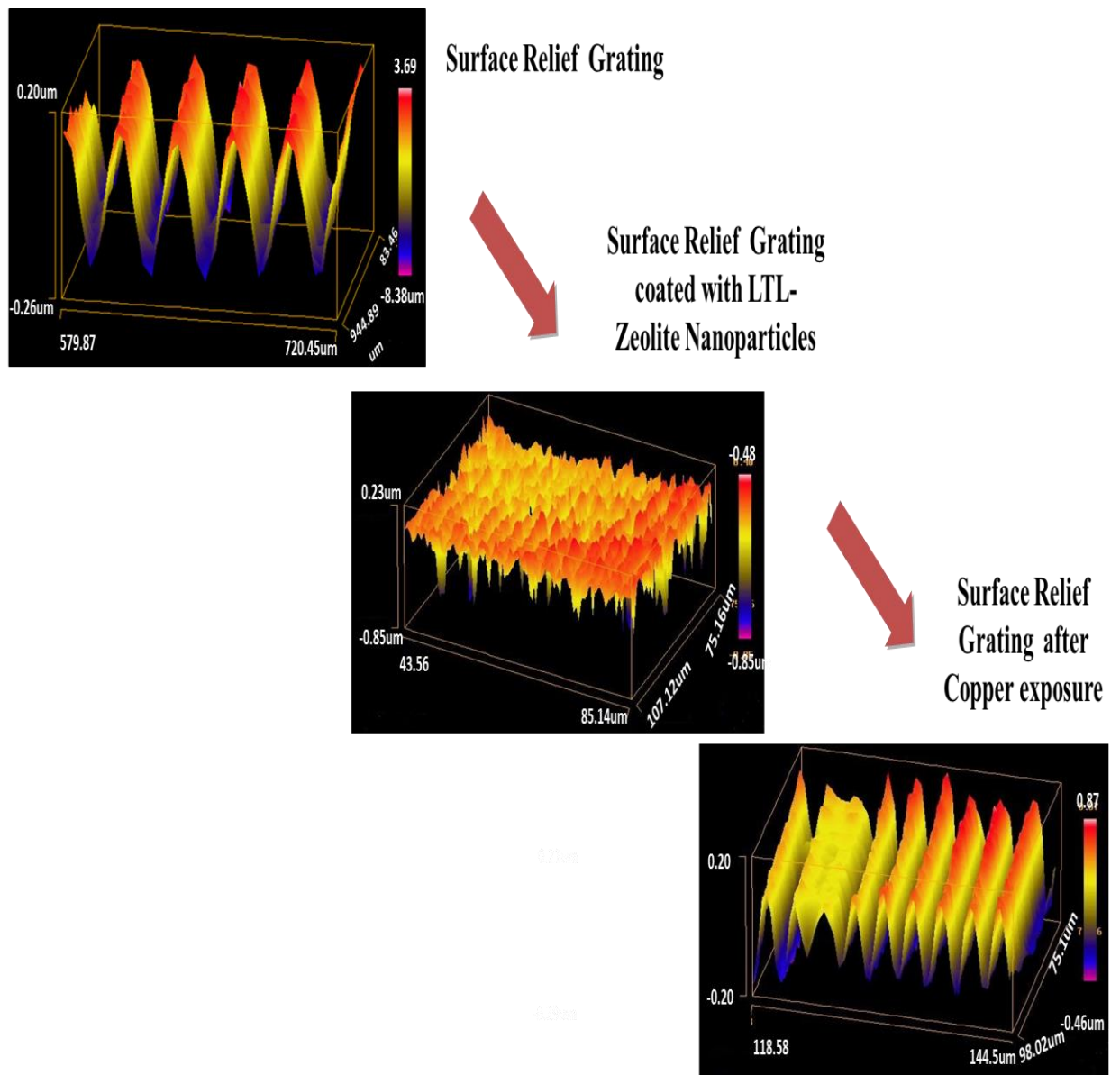
Figure 4. 4.WLI images of surface relief gratings (a) SRG, (b) SRG with LTL-zeolites nanoparticles and (c) SRG after copper exposure

Initially surface modulation 450nm observed in the in the surface structure and after coating it decrease to 23nm and after exposure to copper again it observed 400nm which is a clear indication the nanoparticles washed away from the surface. After literature review [13] it was found that the nanoparticles can be incorporated in sol –gel in order to ensure that the nanoparticles will remain incorporated in the surface structure after exposure to the liquid. Figure 4.4 indicated that coatings without sol gel did not work in order to work in a liquid environment.

Modified SRG

In order to facilitate absorption of the target analyte molecules and enhance sensor function, the surface relief grating is modified through coating with zeolite nanoparticles. The layer was prepared by a sol gel process. The Bragg angle measurements were taken of before and after modification of the surface. A typical composition consisted of tetraethyl orthosilicate TEOS (24 mL), ethanol (18 mL), 1.5 % w/w LTL-zeolite nanoparticle suspension (12 mL) and 0.04 M nitric acid (3 mL)[13]. The added amount of LTL-zeolites % w/w was varied between 2.1×10^{-3} and 3.15×10^{-3} and 3.9×10^{-3}. 3.15×10^{-3} was found optimum because a layer cannot accommodate more nanoparticles in it. The use of the TEOS was necessary in order to stabilise (improve mechanical stability) the layer of nanoparticles in water environment. The porous matrix allow pollutants (in this case di-cations such as Cu (II)) to diffuse easily into the functionalized layer and to interact with the zeolite nanoparticles. The optimisation involved finding the maximum amount of zeolite nanoparticles that can be incorporated in a functionalising layer while still preserving a good optical quality. The solution was stirred for 24 hours at room temperature and then spin coated at 500 rpm on the thermally treated SRG structures.

The samples were left for 24 hours at room temperature before further studies. Next the gratings were exposed to the different copper solution for pre-determined time intervals and their diffraction efficiency was measured. The layers were studied under white light interferometer and atomic force microscope. The diffraction efficiency change was measured at different stages of experiment. The optical bench set up is as shown in Figure 4.5.
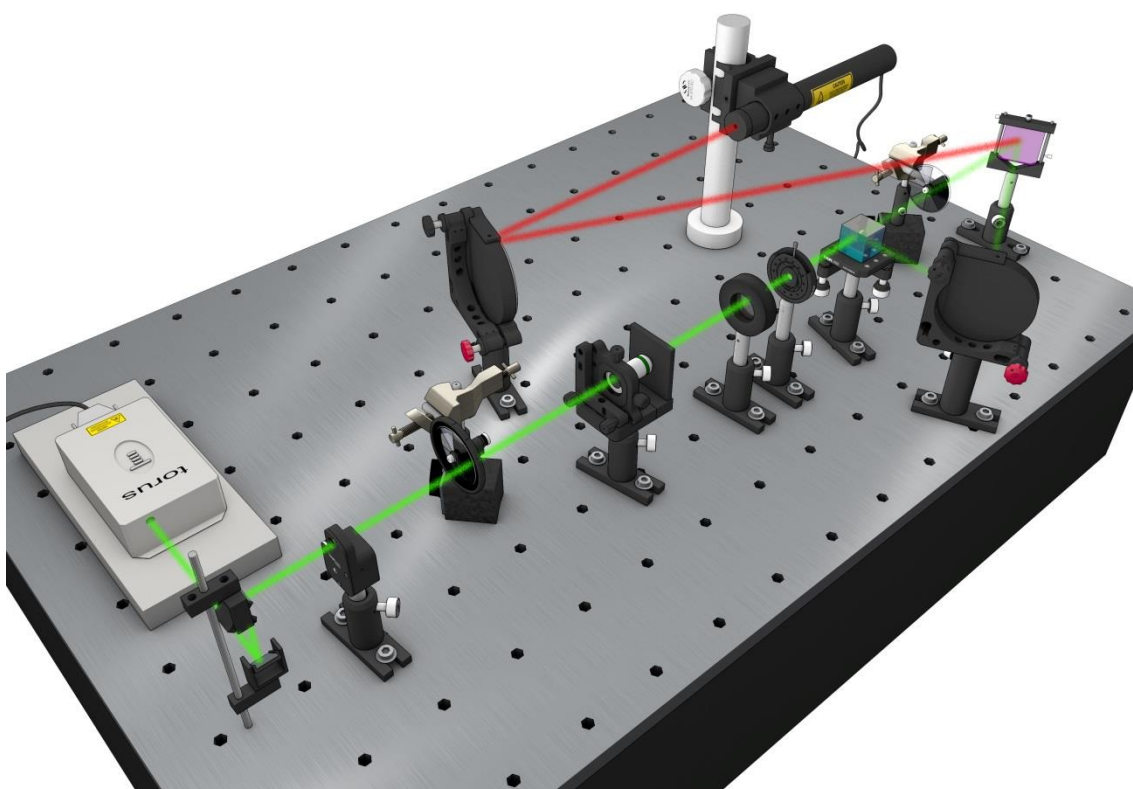
Figure 4. 5. Optical bench with set up (detector is not included in the figure)

4.4. Characterization of LTL-zeolites nanoparticles and Photonic structures

4.4.1. Dynamic Light Scattering (DLS)

The particle size distribution of LTL zeolites and degree of agglomeration in the crystalline product was investigated by using DLS Malvern Instruments zeta sizer (laser wavelength of 632.8 nm).

4.4.2. Scanning Electron Microscope (SEM)

The morphology of the nanoparticles on SRG was studied by electron microscope (SEM). Hitachi SU 6600 Fe-SEM instrument (Hitachi high Technologies Europe GMBH Whitebrook Park Lower Cookham Road Maidenhead SL6 8YA UK) was used in this study. Calibration of SEM was performed with Au on carbon standard provided by Agar Scientific (Essex, UK).

4.4.3. Atomic Force Microscope (AFM)

The morphology of the surface gratings and sol-gel coated surfaces were assessed by AFM using an Asylum MFP-3D AC microscope, fitted with an aluminium coated silicon tip at a scan rate of 0.7 Hz. Damage to the tip and sample surface was minimised by running the experiment in tapping mode. The surface amplitude values are calculated with inbuilt AFM software using root mean square values of surface height measurements. The spatial frequency of the grating used in this study was 300 lines/mm.

4.5. Results and discussions

4.5.1. Characterisation of holographic Surface Relief Structures

4.5.1.1. AFM

Profiles of surface relief structures measured by AFM are presented in Figure 4.6. The spatial frequency of the structure was determined to be 300l/mm from 3.3 μm ± 3μm line spacing observed in the AFM results. Previous studies revealed that peaks and troughs of the surface relief structure correspond respectively to the bright and dark regions in the pattern confirming that mass transport from dark to bright regions is the main mechanism of photoinduced surface relief formation. [12]. The amplitude of the troughs observed by these images was in the range 350 nm- 400 nm. Figure 4.6(a) shows 3D surface topography of the grating after thermal treatment, and after spin coating with the modified LTL-zeolite layer. After spin coating with the LTL-zeolite layer, the surface relief amplitude has decreased from 350 nm to approximately 20 nm indicating that the sol gel has filled in the troughs (Figure 4.6 b). The diffraction efficiency and the surface profile of the SRG structures were measured at each stage of the experiment.

a). Surface Relief Grating(SRG)

b). SRG spin coated with LTL-Zeolite Nanoparticles

c). SRG after Copper exposure
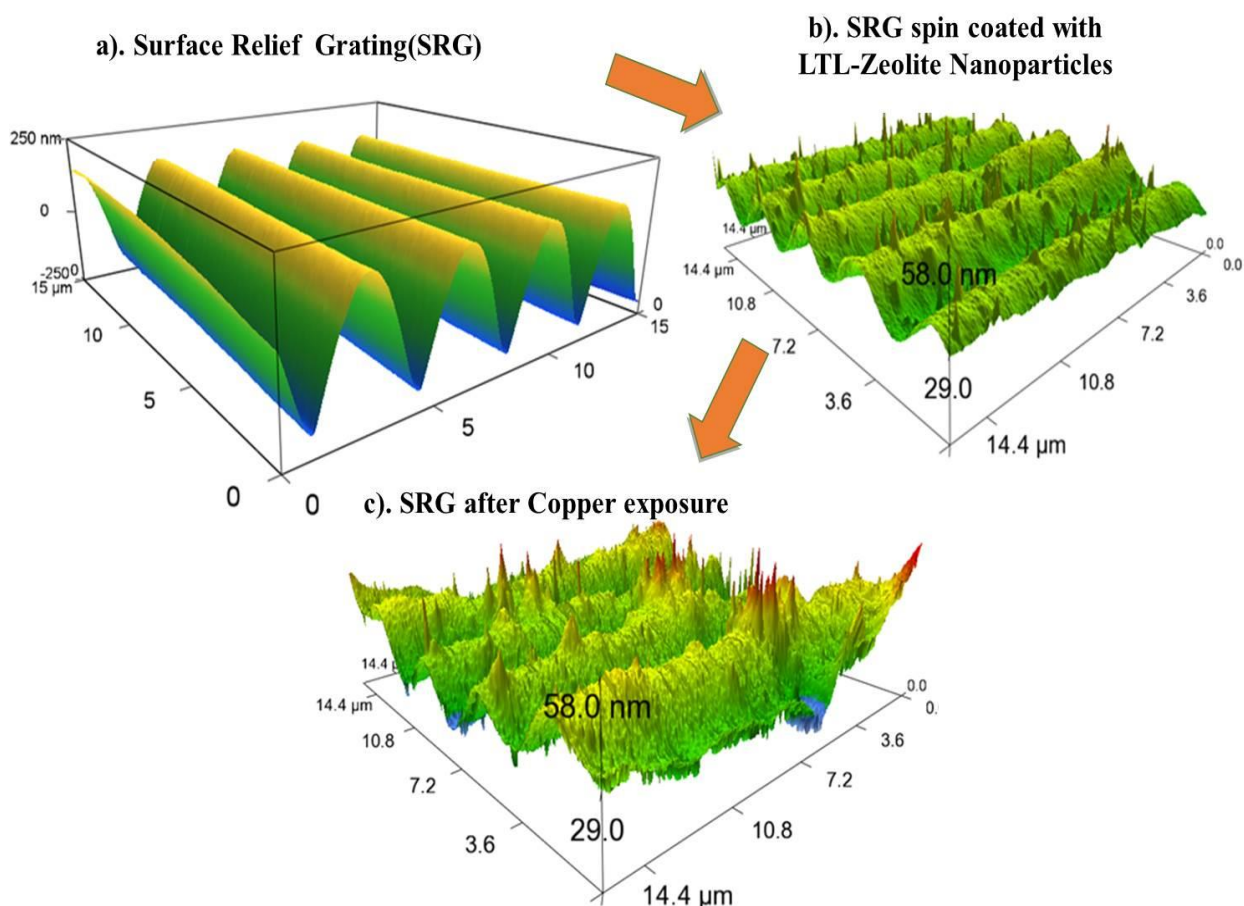
Figure 4. 6. AFM images (3 dimensional view) of (a) SRG, (b) SRG modified with LTL-zeolite nanoparticles and (c) SRG after copper exposure. AFM scan of the SRG of spatial frequency 300 lines/mm.

After exposure to analyte solution the amplitude increased to 30nm. This is possibly due to swelling of the sol gel layers. AFM results confirmed that the zeolite nanoparticles are still present in the layer after exposure to water and copper solutions, which facilitate sensor to increase to work better on exposure with analyte solutions.

4.5.1.2. Diffraction efficiency and angular selectivity studies

Figure 4.7 shows the diffraction efficiency as a function of angle of rotation for the photonic gratings at different stages of the experiment i.e. before thermal treatment, after thermal treatment, after coating with LTL dispersed in the sol-gel, and after exposure to copper ions. A maximum diffraction efficiency of the photopolymer layers of 60% was achieved immediately after holographic recording as outlined in table 4.2. This value is due to the volume diffraction grating since at this stage the surface relief grating has negligible amplitude (<1nm).
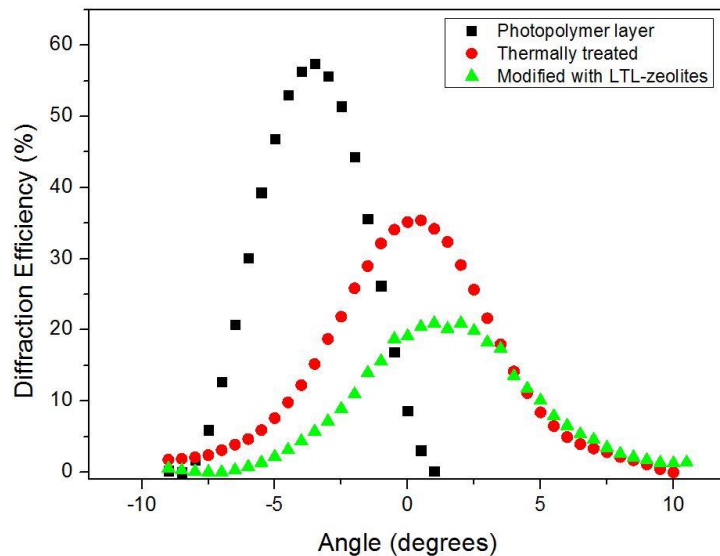
Figure 4. 7. Bragg curves with spatial frequency centered at 300 l/mm recorded in layers with thickness of 30 µm on a glass slide taken for the photopolymer before ■ and after thermal treatment ● and after spin coating with LTL-zeolites ▲

The maximum diffraction efficiency of the photopolymer layer is 60%. The shift observed in thermally treated structures is most probably due to an increase in the effective refractive index of the photopolymer layer, as the density of the layer is increased after thermal treatment. After thermal treatment the diffraction efficiency decreased to ˷35% due to combined effects of enhancement of the surface relief grating

and the nearly complete erasure of the volume grating. The diffraction efficiency of the volume grating after index matching was measured to be 2.5 %, therefore, after thermal treatment the diffraction efficiency is mainly due to the SRG. A shift in the Bragg angle was observed as it can be seen in the Figure 4.7. Taking into account the height of the surface relief amplitude - 400 nm and the diffraction efficiency of the structure, the refractive index difference Δn, is estimated to be 0.9. Other possible causes of the shift are shrinkage of the layer and a change of the spatial frequency of the structure. The Bragg angle measurement was then taken for layers modified with sol-gel dispersed zeolites nanoparticles. A further decrease in the diffraction efficiency was seen at this point due to substitution of the air in the troughs with material with higher refractive index.

Table 4. 2.Change in DE (%), height and thickness of SRG

Photonic structure	Diffraction Efficiency (DE %)	Surface modulation (nm)
Photopolymer layer (volume grating)	60% ±5	<1
Post thermal treatment (surface grating)	35% ±3	400
Sol- gel/zeolite coated grating (modified surface grating)	20% ±2	20
Sol- gel/ zeolite coated grating exposed to Cu^{+2} for 3 mins	3% ±1	30

Assuming that the sol-gel/LTL nanoparticles fully cover the surface relief structure, based on the measured diffraction efficiency after coating (20%) one can estimate the refractive index of the coating layer to be 1.4, which is a reasonable value taking into account the porosity of the material. A further decrease of the diffraction efficiency was observed under exposure of the sample to the analyte. A summary of the relevant

parameters from Figure 4.7 is presented in table 4.2. A detailed dependence of this decrease on the analyte concentration is presented in section 4.6.

4.5.2. SEM of surface relief gratings

The LTL-zeolites nanoparticles incorporated in sol–gel surface was also studied in SEM images shown in Figure.4.8. Before exposure to the copper solution the size of nanoparticles was confirmed 80nm which was also confirmed by DLS studies.
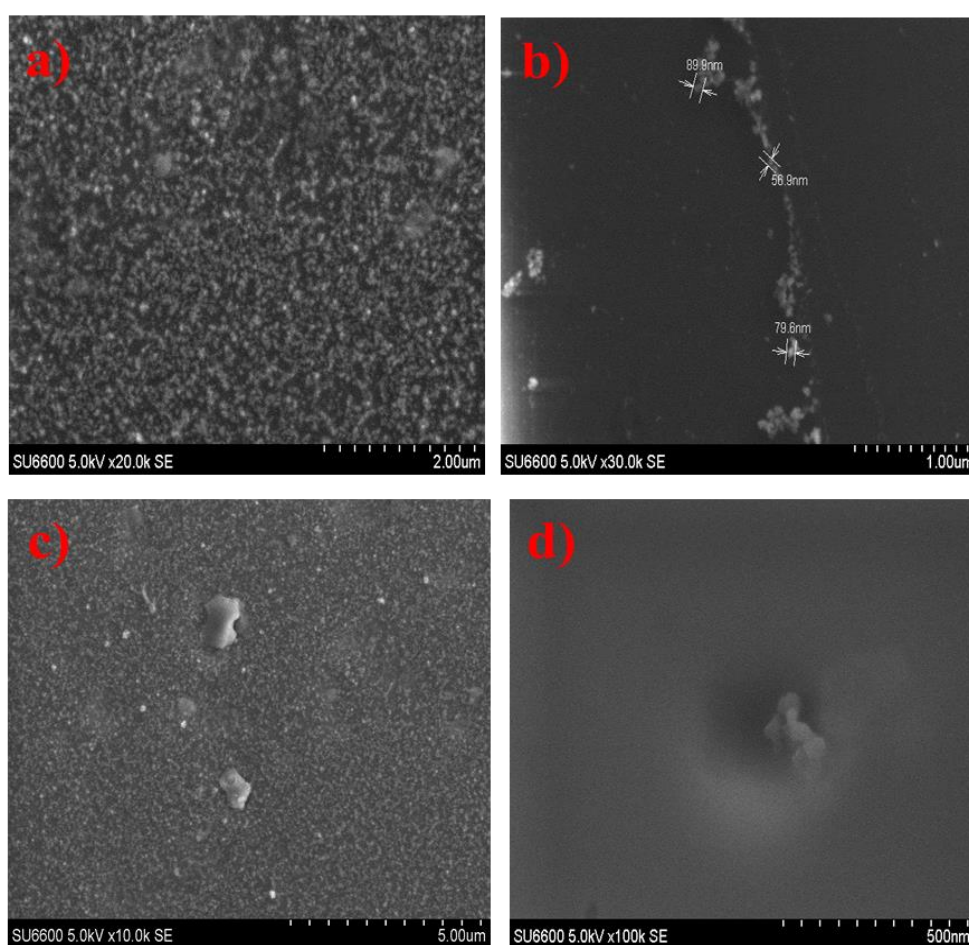
Figure 4. 8.(a,b) LTL-zeolites incorporated sol-gel (c,b) exposure to Cu^{+2}

After exposure to copper solutions, it appears that the LTL- zeolites nanoparticles were released from the LTL-incorporated sol-gel or the increase in the AFM amplitude

suggest that it could be from swelling of the sol gel layer. Some agglomeration was observed after exposure to copper as shown in Figure.4.8(c) and (d).

4.5.3. DLS

It was observed in the DLS studies that the mean particle diameter is centred at 80 nm. It is worth noticing, that the width of the particle size distribution curve for the LTL sample is relatively narrow, starting from 40 to 105 nm Figure. 4.9. Polydispersity (PDI) 0.09 value indicated that the distribution of nanoparticles in the sample is monodisperse [14] .
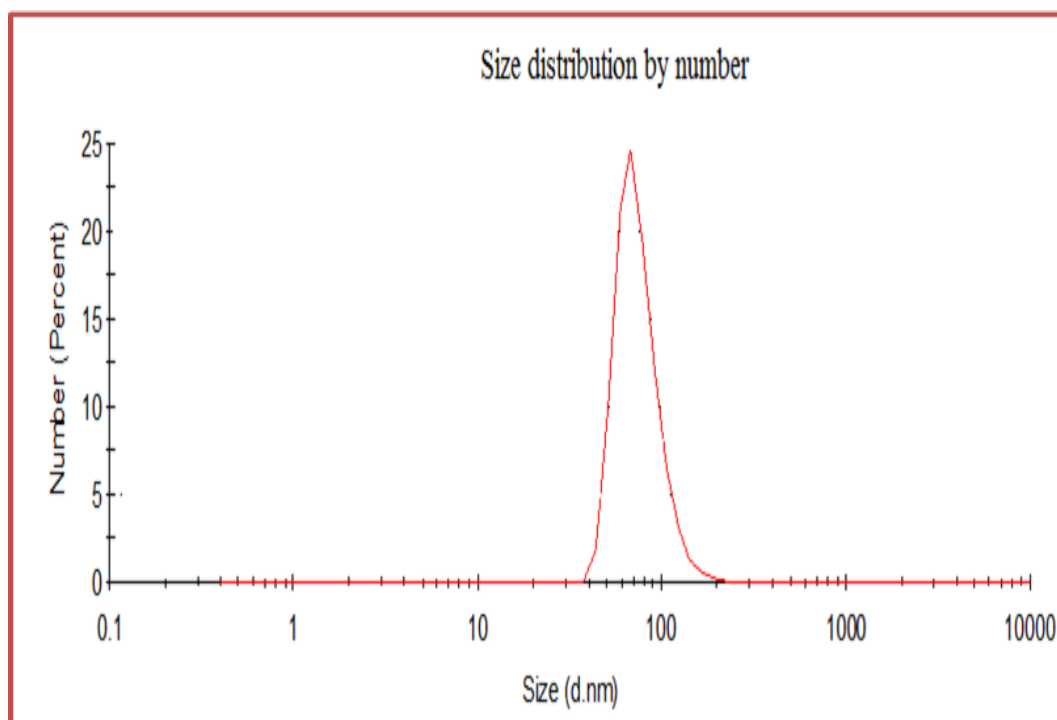
Figure 4. 9. DLS data of LTL-zeolites nanoparticles of the colloidal suspension

4.6. Exposure to the target analytes

Each SRG were characterized by measuring its diffraction efficiency. In order to determine the applicability of the proposed holographic sensor for the detection of analytes, the zeolite coated SRG was exposed to monovalent and divalent cations with different molar concentrations. The procedure of the experiment is outlined in Figure 4.10. All the molar concentrations were prepared in deionised water. A new grating was used for each experiment. Also the fabrications of gratings are very reproducible typically initial diffraction efficiency (η) $\approx 20\% \pm 2\%$ (range determined on the order of 50 diffraction graphs based on sol gel modification containing LTL-nanoparticles).
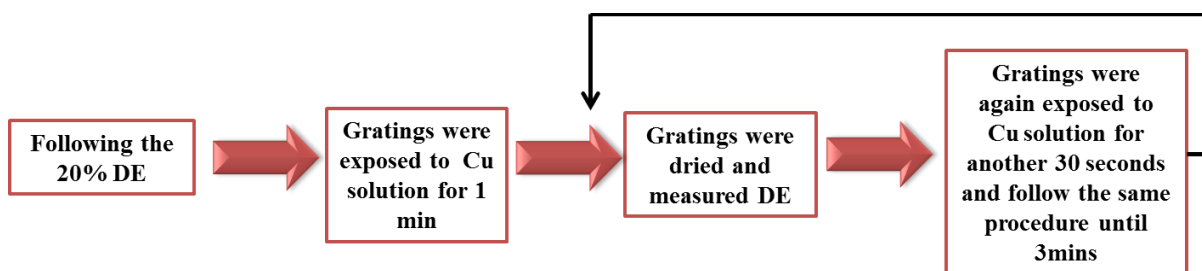
Figure 4. 10. Flow chart of experiment

As it was described in section 4.3 that the sensor was modified with LTL-zeolites nanoparticles incorporated into the sol gel. In Figure.4.11 the modified sensors were exposed to fresh water (tap water) and DI water in to order to get the reference readings. As it can be seen that in deionised water normalised DE drops down from 1 to 0.75 whereas for fresh water it drops down from 1 to 0.6. It shows that the sensors have a greater response for fresh water. It is obvious that the drinking water contains certain levels of minerals and for that reason the curve corresponding to the fresh water reveals

a large change in diffraction efficiency [15]. (In figures captions n represents number of times experiment repeated)
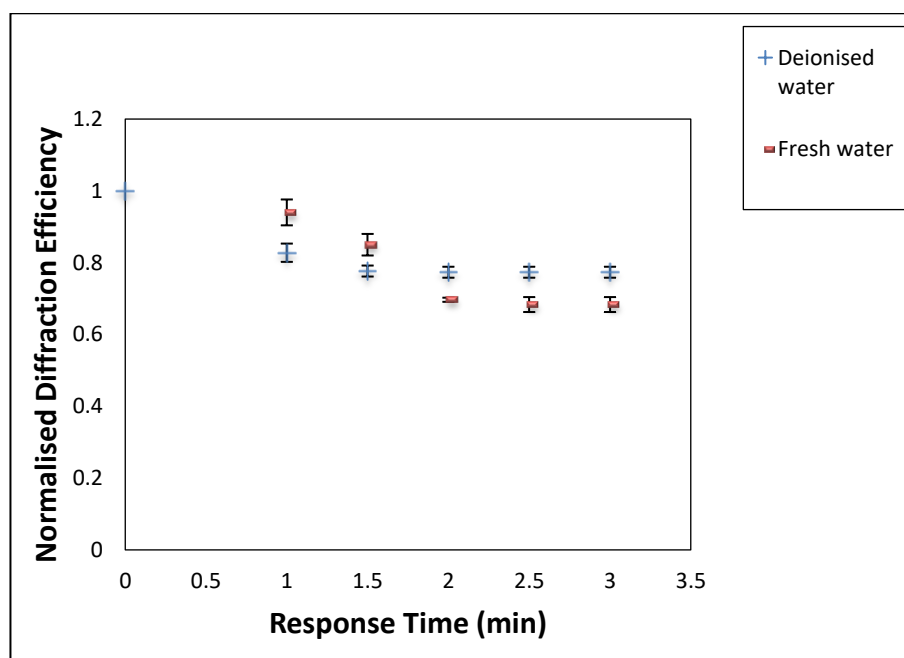
Figure 4. 11. Comparison of the sensor's response to fresh water and deionised water (n=3)

4.6.1. Selectivity

The selectivity of the proposed sensor is determined by the selectivity of LTL nanoparticles. The SRG sensor for determination of analyte, solutions of CuCl, $Cu^{+2}Cl_2$ and $Cu^{+2}SO_4.5H_2O$ were prepared. The sensor was exposed to solutions with different molar concentrations of copper (CuCl, $Cu^{+2}Cl_2$ and $Cu^{+2}SO_4.5H_2O$). All the molar concentrations were prepared in deionised (DI) water. The first set of experiment shows the results from testing the SRG structures when exposed to solutions with 10-40mM concentration of CuCl, $Cu^{+2}Cl_2$ and $Cu^{+2}SO_4.5H_2O$ in Figure.4.12. As it is indicated in 40mM the normalised diffraction efficiency decreases as the exposure time increases and molar concentration increases. The normalised diffraction efficiency drops down 1

to 0.7 in CuCl whereas in $Cu^{+2}Cl_2$ it drops down from 1 to 0.4 and there is a greater response for $Cu^{+2}SO_4.5H_2O$ as the normalised diffraction efficiency drops down from 1 to 0.2. Sol gel containing LTL nanoparticles are more responsive to it because it is dication whereas in CuCl and $Cu^{+2}Cl_2$ and $Cu^{+2}SO_4$ complexes possibly have different behaviour in terms of dissociation in the solution. The greater sensitivity to $Cu^{+2}SO_4$ possibly due to complete dissociation while the CuCl and $Cu^{+2}Cl_2$ may not be fully dissociated or less dissociated in the solution [16].

Comparison with CuCl, $Cu^{+2}Cl_2$ and $Cu^{+2}SO_4.5H_2O$
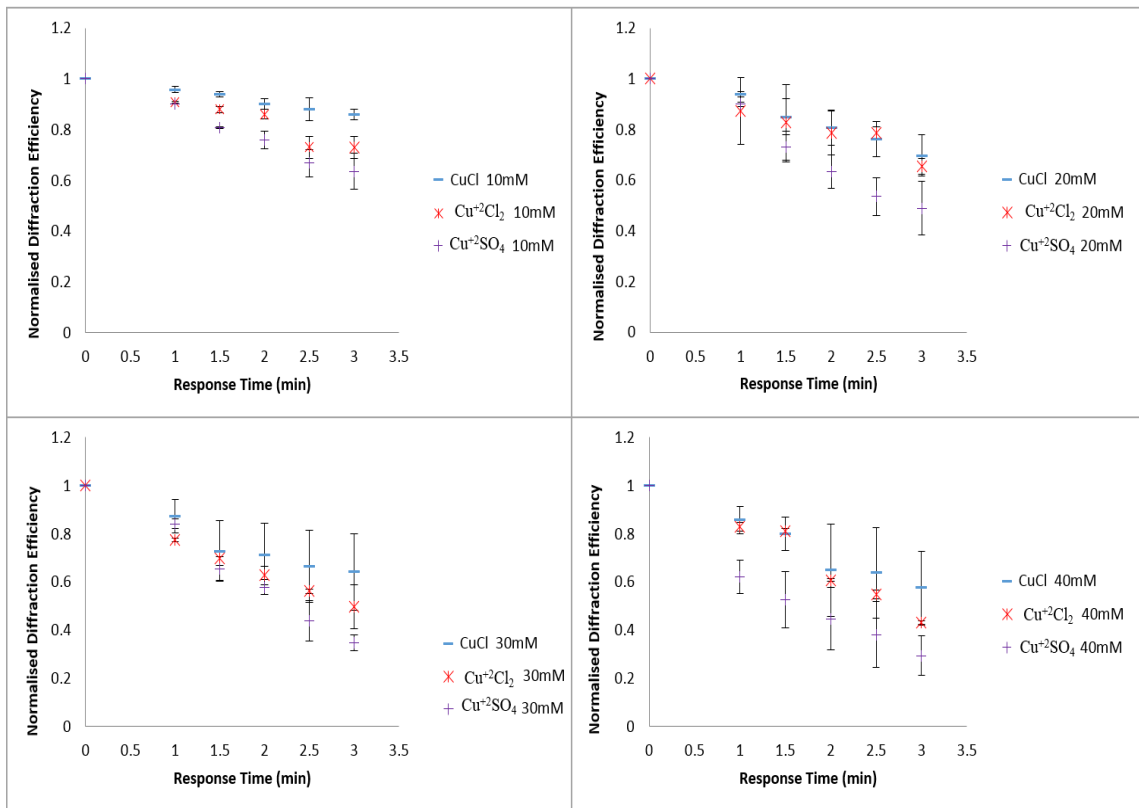
Figure 4. 12..Comparison of relative response of CuCl, $Cu^{+2}Cl_2$ and Cu^{+2} $SO_4.5H_2O$ photonic structures coated with LTL-nanoparticles (loading 8 ml) 10-40 mM concentrations (n=2)

In order to understand the behaviour of ionic activity in the solution Debye-Huckel theory was used to calculate the ionic activity coefficient, $\gamma\pm$ of the CuCl, in $Cu^{+2}Cl_2$ and $Cu^{+2}SO_4.5H_2O$ in aqueous solution at room temperature by using equation 4.2 [17].

$$-\log Y_i = 0.5\ Z\ i^2\ \sqrt{\mu} \qquad \textbf{(4.2)}$$

Whereas, μ is used for both ionic strength $Z\ i^2$ represents positive or negative integer.

Calculated ion activity coefficients are mentioned in below table 4.3.

Table 4. 3. Activity coefficient

Concentration (mM)	CuCl	Y	$Cu^{+2}Cl_2$	Y	$Cu^{+2}SO_4$	Y
10	0.0089	0.89	0.0082	0.82	0.0079	0.79
20	0.016	0.849	0.015	0.75	0.0144	0.72
30	0.0246	0.82	0.0215	0.701	0.0201	0.67
40	0.031	0.794	0.0270	0.676	0.0252	0.63
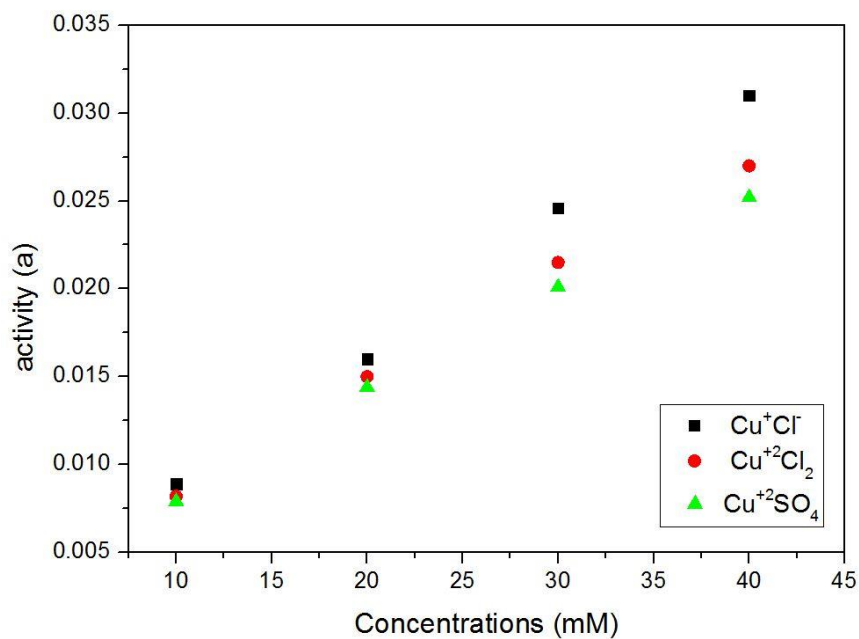
Figure 4. 13. A plot of activity vs concentration 10-40 mM

A plot of activity vs concentration shows in Figure 4.13 that there is clear difference between the ionic strength of the dissociated ion of Cu^+Cl^-, $Cu^{+2}Cl_2$ and $Cu^{+2}SO_4.5H_2O$ in aqueous solution which is more prominent in 30 mM and 40 mM concentrations. Figure 4.13 is a clear indication that the Cu^+Cl^- and $Cu^{+2}Cl_2$ the chloride complexes more dissociated in aqueous solution as compared to $Cu^{+2}SO_4.5H_2O$ but the reason for

more selectivity towards $Cu^{+2}SO_4$ (Figure 4.12) is probably due to +2 oxidation state because LTL-zeolites have strong chelate effect with dications.

4.6.1.1. Copper (II)

The second set of data presented in this is the study of $Cu^{+2}SO_4.5H_2O$ in lower molar concentration and this proposed photonic structure sensor sensitive and able to detect copper ions 1-4 mM. In Figure 4.14, the normalised diffraction efficiency vs exposure time is shown for the LTL zeolite coated SRGS exposed to deionised water (DI) and 1-4 mM copper solutions. The normalised diffraction efficiency and observed to decrease in all cases with increasing exposure time and a clear dependence on the concentration of copper is observed. However, it was also observed that on exposure to the control solution, deionised water, the normalised DE drops down from 1 to 0.8, whereas it can be seen there is greater decrease when exposed to copper normalised diffraction efficiency drops from 1 to 0.2 at 4mM.
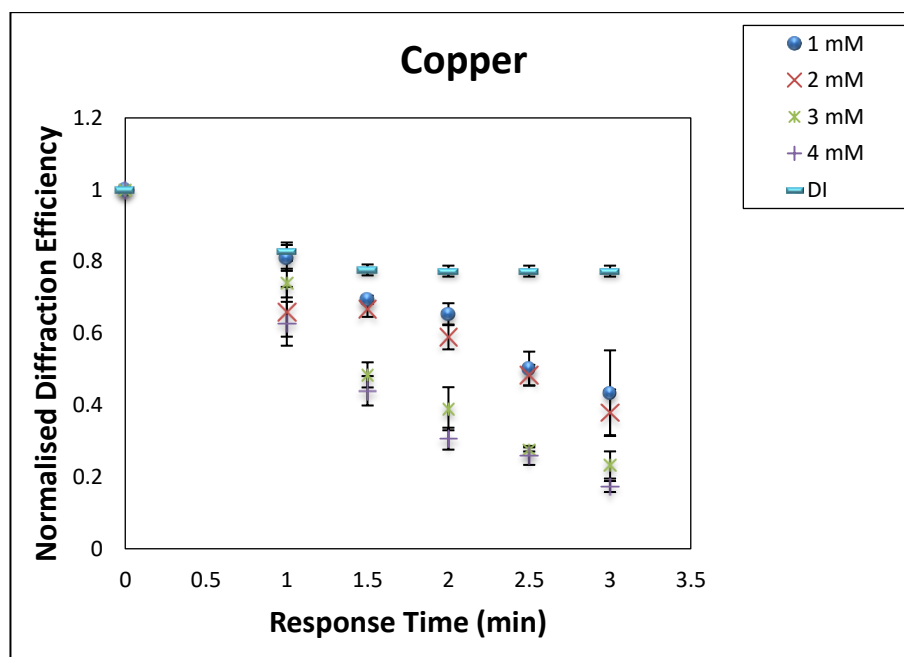
Figure 4. 14. Copper (II) exposure (1-4mM) response in terms of normalised diffraction efficiency change of LTL-zeolites nanoparticles (loading 12 ml) photonic structures (n=3)

In order to check whether the sensor response is due to the sol-gel or due to the presence of LTL-zeolites nanoparticles, the SRG grating was also coated with sol-gel containing no nanoparticles as a reference. Figure. 4.15 shows the diffraction efficiency versus exposure time for SRG coated with sol-gel only and sol-gel containing zeolites to a (4 mM) copper(II) solution. A significant improvement in the sensor response to copper is observed due to the inclusion of LTL zeolites. The normalised diffraction efficiency drops down 1 to 0.2 sol gel containing nanoparticles, whereas in sol gel only coated sample normalised diffraction efficiency drops down only 1 to 0.88.
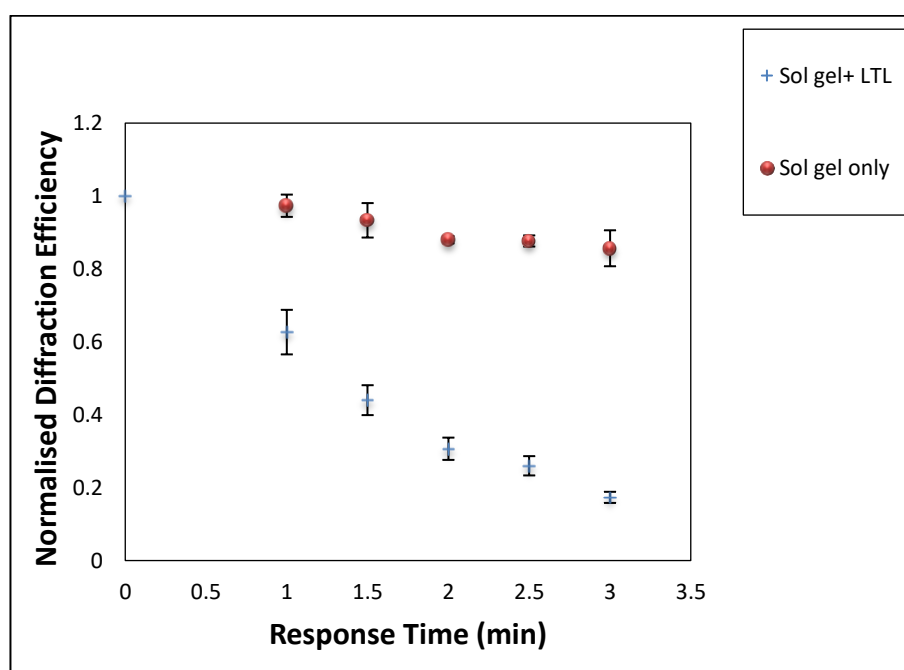
Figure 4. 15. Comparison sol gel coated with LTL-zeolites and sol gel incorporated LTL-zeolites nanoparticles in 4 mM Cu (II)

4.6.1.2. Calcium (II)

In the third set of data the sensor is also able to detect hardness (Ca^{+2}) of water. The sensor was exposed to solutions with different molar concentrations of calcium and it is possible to determine Ca^{+2} down to 1mM. The normalised diffraction efficiencies are

plotted in Figure. 4.16. Hard water is a common quality of water which contains dissolved compounds of calcium and magnesium and sometimes, other divalent and trivalent metallic elements. The degree of hardness standard as established by the American Society of Agricultural Engineers and the Water Quality Association (WQA) is: <17.0 ppm $CaCO_3$ is soft water and 120-180 ppm hard water. 1mM Ca^{2+} corresponds to 100 ppm $CaCO_3.$
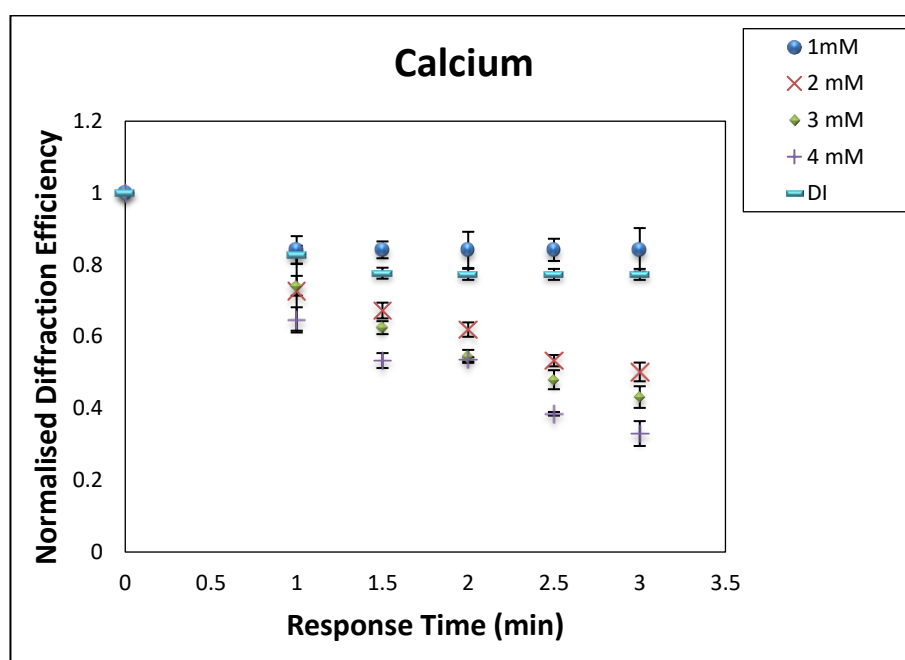
Figure 4. 16. Calcium (II) exposure (1-4mM) response in terms of normalised diffraction efficiency change of LTL-nanoparticles (loading 12 ml) photonic structures (n=3)

4.6.1.3. Lead (II)

The fourth set of experiments was the study of Pb^{+2} analyte. The LTL-coated zeolite SRG was exposed to lead solutions (1-4mM) concentrations and DI water. The sensor response was observed due to the presence of Pb^{+2}. In Figure 4.17 the normalised diffraction efficiency vs. exposure time is shown. Although at shorter exposure times the response is not linear, after 3 min exposure to the analyte the diffraction efficiency change depends linearly on the concentration of the analyte.
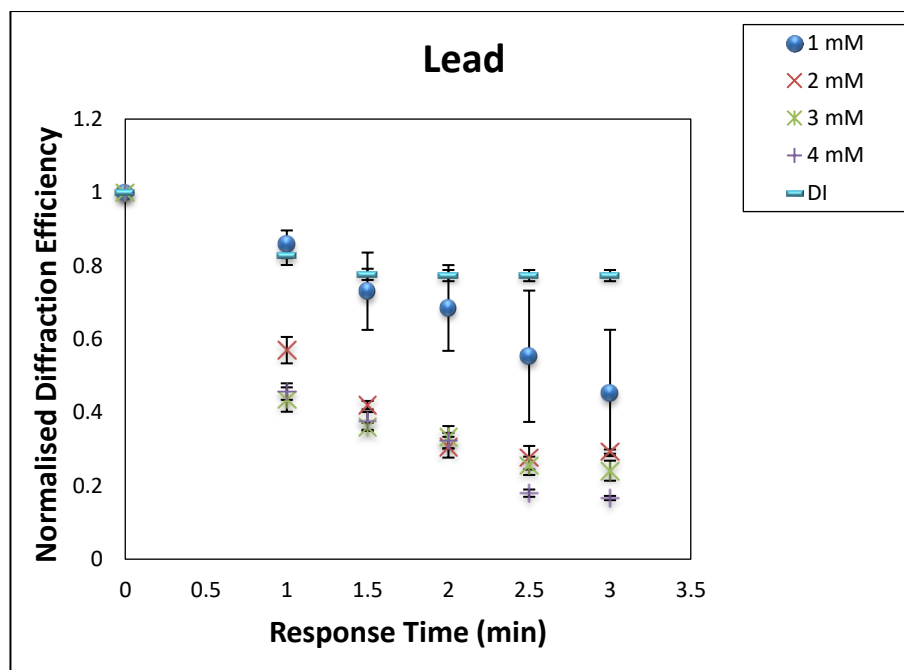
Figure 4. 17. Lead (II) exposure (1-4mM) response in terms of normalised diffraction efficiency change of LTL-zeolites nanoparticles (loading 12 ml) photonic structures (n=3)

4.6.1.4. Sodium and Potassium

Next the photonic sensor was exposed to Sodium (Na^+) and Potassium (K^+) cations as shown in Figure 4.18. This study is performed in order to investigate the behaviour of the sensor towards monovalent cation. At a shorter exposure time for instance at 2 min almost no change in normalised diffraction efficiency was observed in comparison to the divalent ions Ca^{2+}, Pb^{2+} and Cu^{2+}.
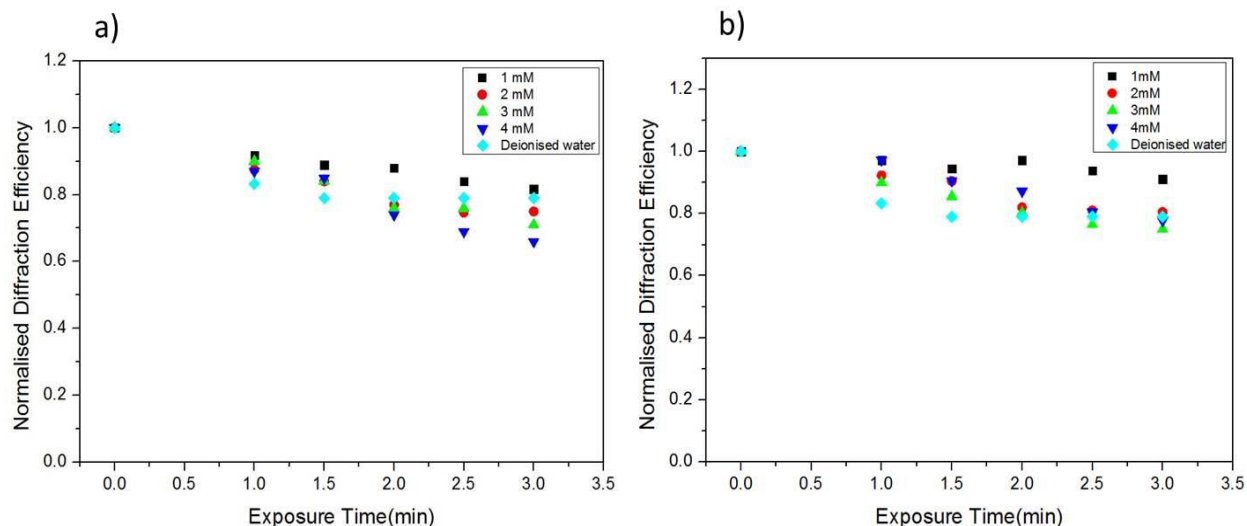
Figure 4. 18.(a) Sodium (b) Potassium exposure to (1-4mM) response in terms of normalised diffraction efficiency change of LTL-zeolites nanoparticles (loading 12 ml) photonic structures

When compared with other metal ions, it can be seen that the sensor is more sensitive to dications as can be seen in Figure 4.19. It is clear that the sensor is less responsive to sodium and potassium as compared to calcium, copper, and lead. The selectivity of the response to dications can be attributed to the LTL-nanoparticles, since they have diverse responses for different oxidation states [8]; it was observed that they were more responsive to +2 oxidation states, as compared to the other oxidation states as shown in Figure 4.19.
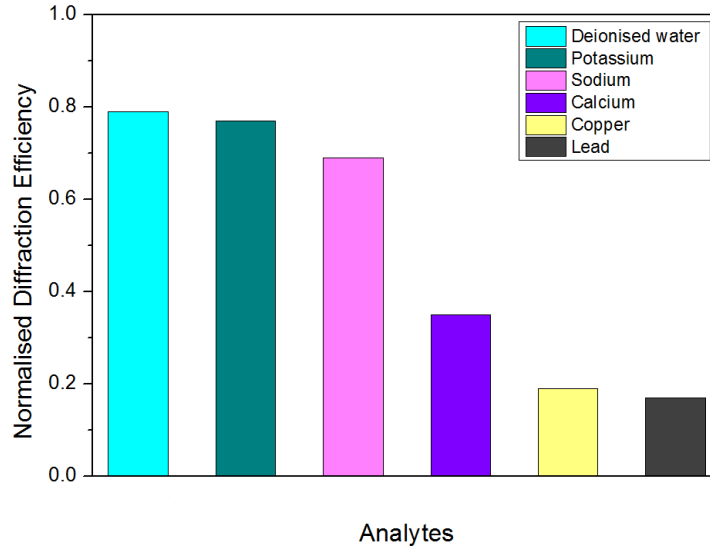
Figure 4. 19. Comparison of change in normalised diffraction efficiency to different analytes at 4mM exposure 3mins

4.6.1. Sensitivity

The DE change depends linearly on the concentration of the analyte, as shown in Figure 4.20. Sensitivity at 3 min exposure to calcium analyte (DE/mM) of 8.85 %/ mM , lead analyte (DE/mM) of 4.56%/ mM and for the copper analyte (DE/mM) of 13.6 %/ mM was calculated for the sensors Figure 4.20(a-c). The changes in diffraction efficiency were calculated here with respect to the reference values of diffraction efficiency of devices exposed to water in order to ensure that only the change due to the presence of the specific analyte is taken into account.
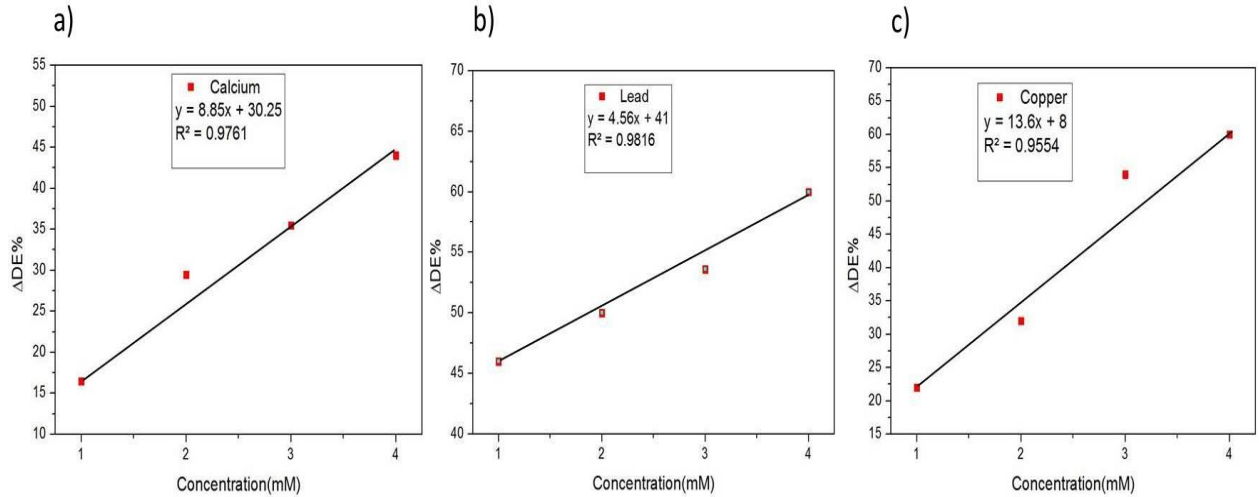
Figure 4. 20. Sensitivity of the response at 3 min for calcium, copper and lead (from figure 4.14, 4.16 and 4.17)

The limit of detection (LOD) is an important parameter used to estimate the device sensing capability (lowest detectable concentration). LOD's may also be calculated based on the standard deviation of the response (S_y) of the curve and the slope of the calibration curve (S). The S_y values were obtained by using STEYX function in excel. The limit of detection can be expressed as [18]:

$$LOD = 3.3 \left(\frac{S_y}{S} \right) \qquad \textbf{(4.3)}$$

Table 4. 4. Calculation of LOD

Steyx	R2	LOD
0.334021	0.9554	Cu^{2+}:1.153727
0.244268	0.9761	Ca^{2+} :0.825819
0.214645073	0.9816	Pb^{2+} :0.721606

LOD estimated based on equation 4.3. Linear responses were obtained of the proposed sensors with the limit of detection Cu^{2+} 1.15 mM, Ca^{2+} 0.82 mM and for Pb^{2+} 0.72 mM, respectively.

4.6.2. Reversibility

The sensor reversibility was also examined as indicated in Figure 4.21(a). The sensor which was already exposed to Cu^{2+} $SO_4.5H_2O$ washed with deionised water when it was dried. Then further the sensor was exposed to NaCl solution in order to check that sensor shows any reversible behaviour. After exposing to NaCl solution the diffraction efficiency increased 3% to 6% but it was not fully reversible as it can be seen in Figure 4.21(b). The results indicated that sensor is irreversible.
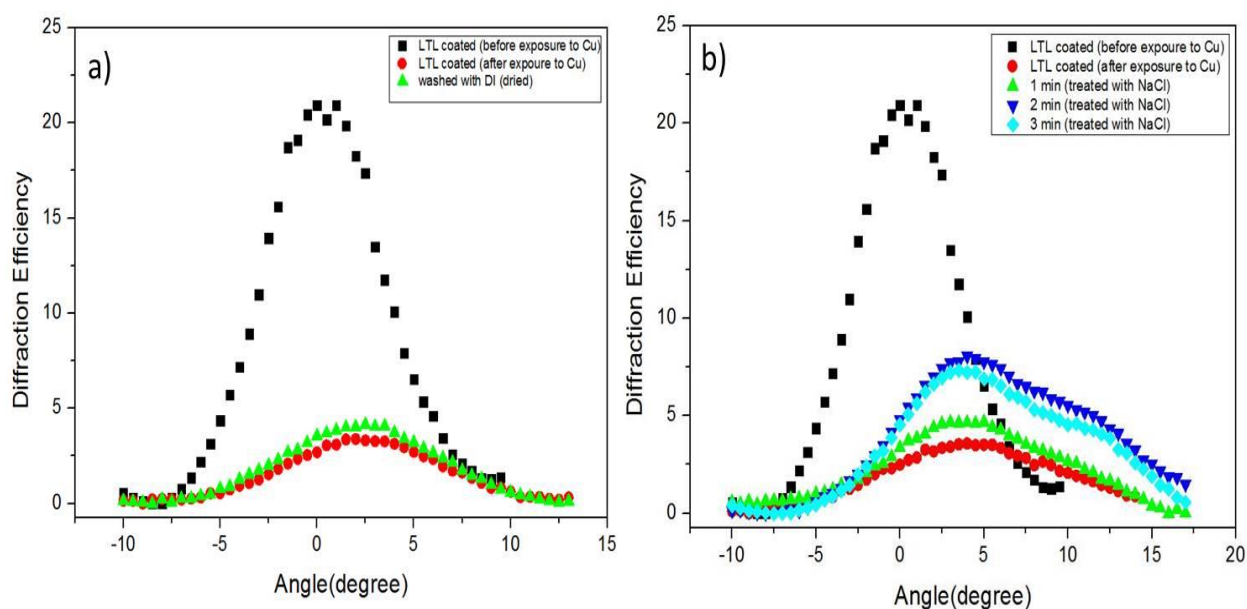
Figure 4. 21. Bragg curves showing irreversibility of the sensor (a) exposed to copper and (b) exposed to NaCl (50mM)

4.6.3. Temperature dependence of the sensor response

The temperature dependence studies was also carried out as this effect is important in producing response signals and play a significant role to activate the diffusion process. It was found that sensor response rate increases with temperature. Possibly with the increment of temperature the rate of diffusion and adsorption increases. The temperature

range which was investigated here is 25℃ to 40℃. The grating containing LTL zeolites nanoparticles in sol gel was exposed to 4mM copper solution. The grating was exposed to copper solution for 1min, then the sample was dried, the temperature of the grating was increased from 25℃ to 40℃ and the diffraction efficiency was measured. The sensor was further exposed to copper solution for different intervals as mentioned in Figure 4.9 and the response of the sensor observed. Figure 4.22(a) shows normalised diffraction efficiency versus exposure temperature. The same data plotted for better understanding in a different presentation in Figure 4.22(b) shows normalised diffraction efficiency versus exposure time including DI water response. A significant decrease in normalised diffraction efficiency was observed due to inclusion of LTL-zeolite nanoparticles also normalised diffraction efficiency drops down 1 to 0.12 after 2.5 minutes. Whereas the samples without temperature exposure normalised diffraction efficiency drops down from 1 to 0.2 after 3 minutes.
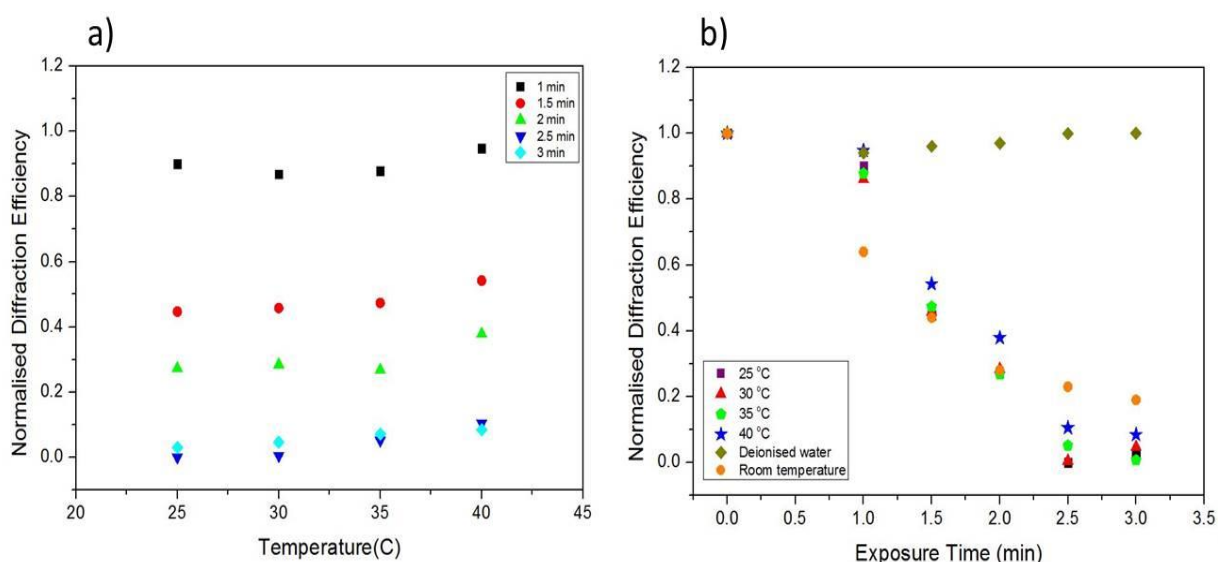
Figure 4.22. Temperature dependence studies copper exposure (4 mM) response in terms of normalised diffraction efficiency change of LTL-zeolites nanoparticles photonic structure (a) normalised diffraction efficiency vs. exposure temperature and (b) normalised diffraction efficiency vs. exposure time

4.7. Microfluidics Platform

The microfluidic system, which is based on a microfluidic chamber Figure 4.23 (a) (provided by senior research scientist Giuseppe Coppola from Italian National Research Council) based on Polydimethylsiloxane, was combined with a SRG grating Figure 4.23 (b) and response of DI, 10 and 20 milli molar concentrations of $Cu^{2+}SO_4.5H_2O$ were investigated. One end of the micro-tube delivering liquid to the microfluidics chamber was immersed into the analyte solution. A second micro-tube connected to the chamber was connected to a syringe Figure 4.23(c). The solution was introduced to the microfluidic chamber by pulling out the air with the syringe. The change in the diffraction efficiency was observed in real time using Helium-Neon laser (He-Ne) of wavelength 658 nm was used as a probe beam incident at the grating as shown in Figure 4.23 (c). The grating was placed on the rotational stage in order to measure the diffracted beam. The intensity of the 1st diffracted beam was measured by using an optical power meter. Whereas the diffraction efficiency η was recorded was calculated with equation 4.1. The results explained with modified SRG gratings are the platform which can be functionalised for analyte sensitive materials as previous sections described that the present functionalisation is capable for sensing dications including copper. In the current section we demonstrated how microfluidics can be combine together with functionalised SRG in order to continuous sample delivery for real time monitoring.
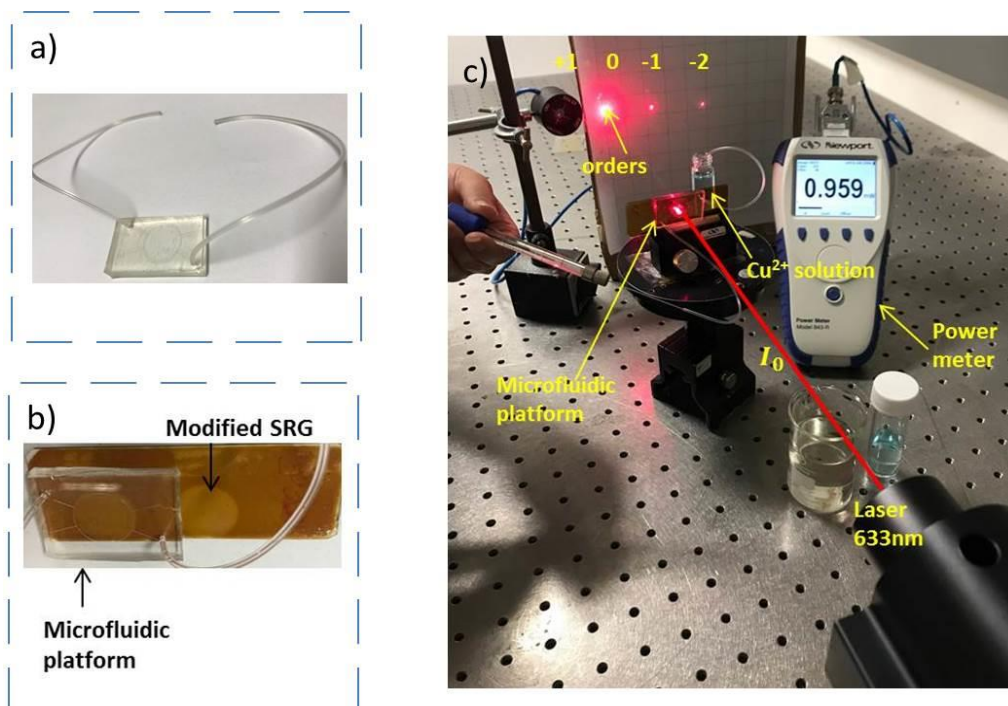
Figure 4. 23. (a) Microfluidic chamber, (b) SRG embedded with microfluidics platform and (c) diffraction efficiency measurement set up

The deionised water (DI) was pumped past into of the sensing device (Figure 4.23 b) until diffraction efficiency start stabilisied. The response of the sensor on exposure to DI and copper solutions of different molar concentrations (10mM and 20mM) was observed during the experiment. One end of the microfluidic (tube) system was immersed into deionised water (DI) and the solution was pumped past the sensor. Initially there was an immediate change in normalised diffraction efficiency (η) was observed to increase from 1.0 to 1.3 Figure 4.24 and then normalised diffraction efficiency reached a stable value of 1.3. This discrepancy of results may be explained by the fact that the TEOS matrix swells upon exposure to the DI water and analyte solutions change of refractive index due to the swelling of the matrix. The refractive index of air is 1 and for water it is approximately 1.33. However, the measurements indicated that the pores filled with water and the refractive index varied in the structure on exposure to water. Then one end of the microfluidic (tube) system was immersed

140

into a copper solution (10mM) and the solution was pumped past the sensor. The normalised η decreased down 1.3 to 0.85 after 16minutes in this case. Next a higher concentration of copper solution (20mM) passed the sensor and the normalised η again increased from 0.85 to 0.96 and then it went back again to 0.79. The measurement was taken again when the SRG was dried and the normalised diffraction efficiency calculated to be 0.07.
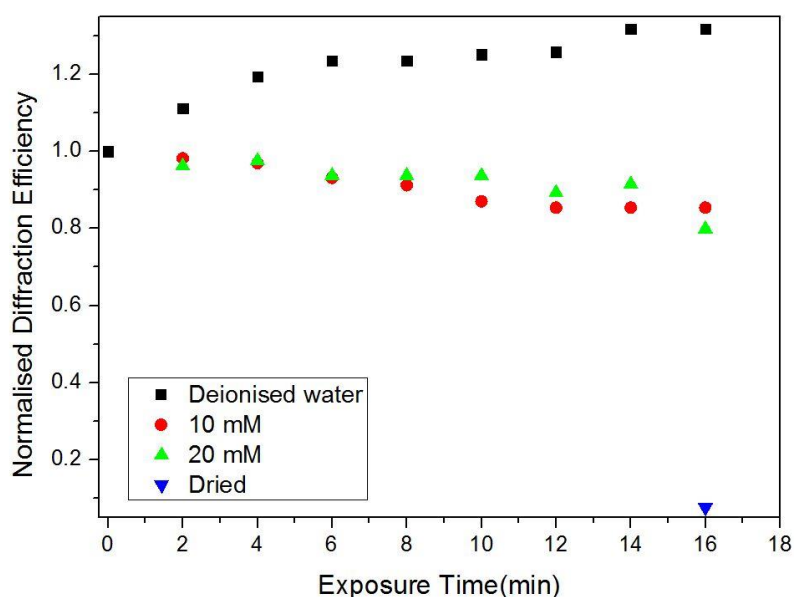
Figure 4. 24. Microfluidics device response to copper (II) 10-20 mM and Deionised water in terms of normalised diffraction efficiency change of LTL-zeolites nanoparticles photonic structure

It appears that the diffraction efficiency decreases on exposure to Cu^{2+} relative to water. Previously the layer was found not to be reversible. Initial results showed that this new platform of sensor suitable for fabrication of a sensor device which can measure the response in real time. However more work required in future to fully understand the behaviour of a sensing device process.

4.8. Conclusions

The sensors are created by holographic recording of surface relief structures in a self-processing photopolymer material and functionalised by spin coating LTL-zeolites in a sol-gel. The sensor is able to differentiate between dications and monocations. LTL-nanoparticles have a different response for different oxidation states; it was observed that they were more responsive to $^{+2}$ oxidation state as compared to the other oxidation sates. The sensor provides a selective response to divalent ions it has good reproducibility (n= 3 for Cu^{2+}, Pb^{2+} and Ca^{2+}) and the preparation is straightforward. The loadings of LTL-zeolites were tailored in order to detect 1-4 mM Cu^{2+} and Pb^{2+} also the sensor is able to detect hardness (Ca^{2+}) of water. Further work required in order to detect lower molar concentrations. The sensor has linearity sensitivity at 3 min exposure was calculated for Ca^{2+} (DE /mM) of 8.85 %/ mM, Pb^{2+} (DE /mM) of 4.56%/ mM and for the Cu^{2+} (DE /mM) of 13.6 %/mM. SEM images proved that the nanoparticle distribution is uniform throughout the layer and the particle size also agrees with the DLS studies. To the best of the author's knowledge, this is the first use of surface relief structures in a self-processing photopolymer coated with a sensing layer for metal ions detection. The advantage of disposable holographic sensor also has a relatively fast response time, low cost, and allows for real time monitoring of environmental water quality. A novel and attractive microfluidic platform is proposed and applied for the detection of Cu^{2+} model samples in water. The advantage of this approach can open the way to much more reliable, low cost, portable and simple to use devices. Further research required in order to detect lower molar concentration.

References

[1]   M. Bhargavi, S. Sethuraman, U. Maheswari, and J. B. B. Rayappan, "Sensors and Actuators B : Chemical A review on detection of heavy metal ions in water – An electrochemical approach," *Sensors & Actuators: B. Chemical*, vol. 213, pp. 515–533, 2015.

[2]   J. Kecht, Z. Tahri, V. De Waele, M. Mostafavi, S. Mintova, and T. Bein, "Colloidal Zeolites as Host Matrix for Copper Nanoclusters," *Chemistry of Materials*, vol. 18, no. 8, pp. 3373–3380, 2006.

[3]   C. I. L. Justino, T. A. P. Rocha-Santos, S. Cardoso, and A. C. Duarte, "Strategies for enhancing the analytical performance of nanomaterial-based sensors," *Trends in Analytical Chemistry*, vol. 47, pp. 27–36, 2013.

[4]   P. Yang, *The chemistry of nanostructured materials*. Singapore: World Scientific Publishing Co. Pte. Ltd., 2003.

[5]   J. Cejka, H. Van Bekkum, A. Corma, and F. Schüth, *Studies in Surface Science and Catalysis 168: Introduction to Zeolite science and practice*, vol. 168. Oxford, UK: Elsevier, 2007.

[6]   E. Leite, I. Naydenova, S. Mintova, L. Leclercq, and V. Toal, "Photopolymerizable Nanocomposites for Holographic Recording and Sensor Application," *Condensed Matter Physics Commons*, pp. 0–28, 2010.

[7]   P. Vanelderen, J. Vancauwenbergh, B. F. Sels, and R. A. Schoonheydt, "Coordination chemistry and reactivity of copper in zeolites," *Coordination Chemistry Reviews*, vol. 257, no. 2, pp. 483–494, 2013.

[8]   A. Kharchenko, O. I. Lebedev, V. Zholobenko, V. de Waele, and S. Mintova, "Formation of Copper Nanoparticles in LTL Nanosized Zeolite: Kinetics Study," *The Journal of Physical Chemistry C*, vol. 120, p. 26300−26308, 2016.

[9]   S. C. Byun, Y. J. Jeong, J. W. Park, S. D. Kim, H. Y. Ha, and W. J. Kim, "Effect of solvent and crystal size on the selectivity of ZSM-5/Nafion composite membranes fabricated by solution-casting method," *Solid State Ionics*, vol. 177, no. 37–38, pp. 3233–3243, 2006.

[10]   I. Naydenova, E. Mihaylova, S. Martin, and V. Toal, "Holographic patterning of acrylamide-based photopolymer surface.," *Optics express*, vol. 13, no. 13, pp. 4878–4889, 2005.

[11]   R. Jallapuram, I. Naydenova, V. Toal, S. Martin, and R. Howard, "Spatial Frequency Response of Acrylamide Based Holographic Photopolymer Spatial frequency response of Acrylamide based holographic photopolymer," *Laser Application and Optical Metrology*, pp. 275–279, 2003.

[12]   K. Trainer, K. Wearen, D. Nazarova, I. Naydenova, and V. Toal, "Optimization of an acrylamide-based photopolymer system for holographic inscription of surface patterns with sub-micron resolution," *Journal of Optics*, vol. 124012, pp. 1–7, 2010.

[13]   S. Jaiswal, P. McHale, and B. Duffy, "Preparation and rapid analysis of antibacterial silver, copper and zinc doped sol-gel surfaces," *Colloids and Surfaces B: Biointerfaces*, vol. 94, pp. 170–176, 2012.

[14]   M. Hflzl, S. Mintova, and T. Bein, "Colloidal LTL zeolite synthesized under microwave irradiation," *Studies in Surface Science and Catalysis*, vol. 158, pp.

11–18, 2005.

[15]   F. Kozisek, "Health Risks From Drinking Demineralised Water," in *Nutrients in Drinking Water*, Czech Republic: National Institute of Public Health, 2005, pp. 148–163.

[16]   M. and Ohlson and N. Vannerberg, "copper stability," *Acta Chemia Scandinavica*, vol. 28, pp. 1021–1035, 1974.

[17]   D. Harvey, *Modern Analytical Chemistry*, 1st ed. Boston, USA: The McGraw-Hill Higher Education, 1976.

[18]   Alankar Shrivastava and V. B. Gupta, "Methods for the determination of limit of detection and limit of quantitation of the analytical methods Abstract," *Chronicles of Young Scientists*, vol. 2, no. 1, pp. 21–25, 2011.

Chapter 5 – Modified Surface Relief layer created by holographic lithography: Application to Sodium and Potassium Sensing

5.1. Introduction

In this chapter the research aim is to develop a holographic biosensor platform, which will allow an increase in sensitivity and selectivity, lower operating costs and facilitate the development of portable devices. The point-of-care diagnostics will rely upon the development of low cost, noncomplex, and easily integrated systems in order to examine biological samples such as blood and urine obtained from the patient. The development of selective metal ion sensors is a focus of significant interest because of their clinical relevance. In future biosensors will become an essential part of modern healthcare because the demand for personalised medicine is increasing[1]. Moreover point-of care devices are cheaper diagnostic tools, therefore it is expected that biosensors will become essential tools in the future [2]. Biosensor development is prompted by the development of new materials that can be used as functionalising materials [3].

The levels of blood electrolytes, particularly H^+, K^+, Na^+ and Cl^- , are widely used to monitor aberrant physiologies related to pulmonary emphysema, acute and chronic renal failure, heart failure and diabetes [4]. Particularly the Potassium (K^+) ion analysis is challenging due to interference from high concentrations of Sodium (Na^+) in blood. It has been previously found that crown ethers have a remarkable capacity to form stable complexes [5] with certain cations, mainly with alkali and alkaline earth ions.

The holographic gratings reported in this chapter were modified by the incorporation of either dibenzo-18-crown-6 (DC) or tetraethyl 4-tert-butylcalix[4]arene (TBC) (structures

146

shown in Figure 5.1) as a chelating agent in a plasticised polyvinyl chloride binder or in a sol-gel matrix for the detection of potassium and sodium [6-7]. Interrogation of these structures by light allows indirect measurements of the analytes concentration. The influence of polymer matrices with different porosities, plasticised polyvinyl chloride (PVC) and a sol gel matrix, on the performance of the sensors for detection of K^+ and Na^+ is investigated. Here the proof of concept demonstrates that by using a matrix with higher porosity one can increase the sensitivity of the sensor. It was observed that the DC sensing layer provides a selective response to K^+ over Na^+ and the TBC modified grating is more responsive to Na^+ over K^+. These sensors respond to Na^+ and K^+ within the physiological concentration ranges. The holographic recording method of surface relief gratings in a self-processing photopolymer material was already discussed in detail in chapter 3 and 4.
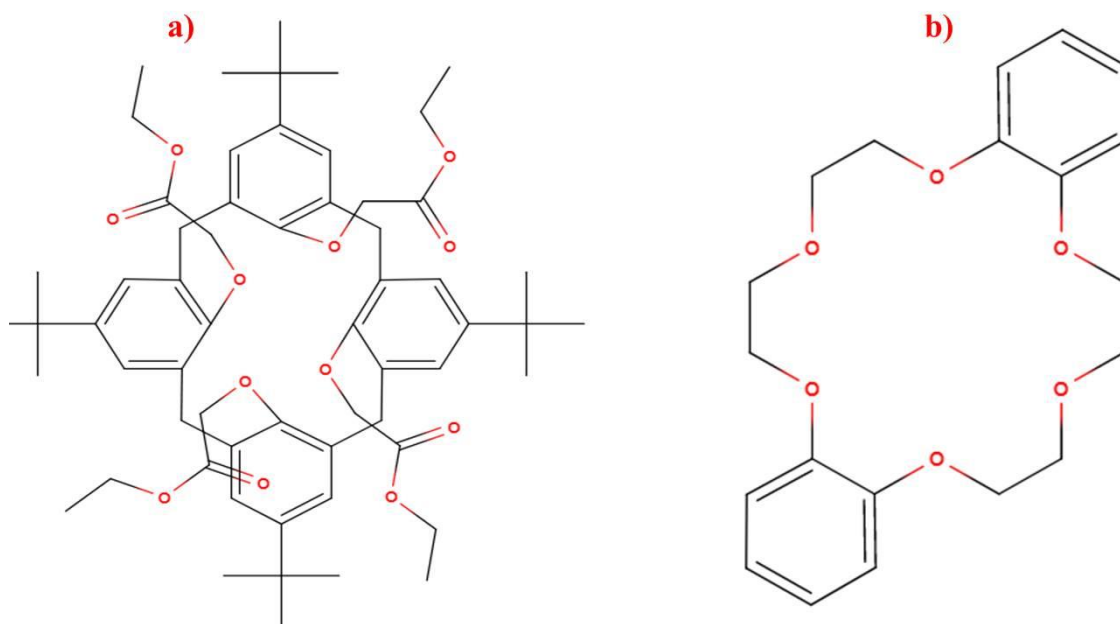
Figure 5. 1.Structures of (a) tetraethyl 4-tert-butylcalix[4]arene (TBC) and (b) dibenzo-18-crown-6 (DC)

5.1.1 Crown ethers

Crown ethers are generally defined as macrocyclic polyethers consisting of repeating (-O-CH_2-CH_2-) $_n$ units (i.e., 4, 5, 6 or more). The term "crown" refers to the similarity of the molecular models of the compounds to a regal crown and to the ability of these compounds to "crown" cations by complexation. Charles Pedersen discovered the first synthetic neutral compounds, the crown ethers, [8] which formed stable complexes with metal cations [9]. He reported that crown ethers complex alkali and alkaline earth and transition metals. He proposed that the cation in the complex is held in the center of the cyclic molecule of the crown ether by the electrostatic attraction between the positive charge of the cation and the negative dipolar charge on the oxygen atoms symmetrically arranged in the polyether ring [10]. This theory suggested that the binding occurs when the size of the hole in the center of a crown ether molecule and the cation diameter are the same.

The target ions to be detected are potassium and sodium. Potassium and sodium ions are most commonly analysed by clinical laboratories. The cavity size of the 18-crown-6 is the right fit for potassium ions. They are selective to potassium ions, also provides ion−dipole interaction with potassium ions shown in schematic in Figure 5.2 [11].
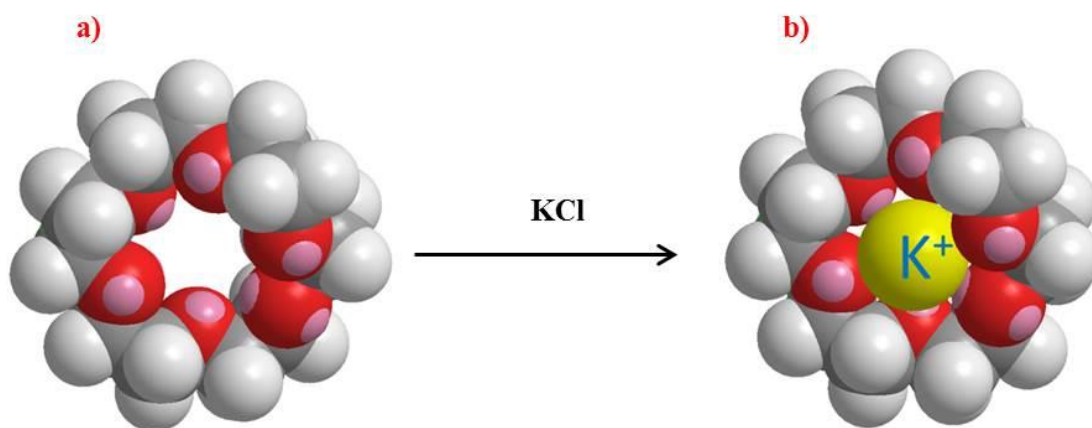
Figure 5. 2. (a) 18-crown-6 ether (b) 18-crown-6 ether after exposure to KCl solution

The cavity in the center of the crown ether molecule is lined with oxygen atoms and is large enough to be occupied by a cation, such as K^+. The cation is stabilized by interacting with lone pairs of electrons on the surrounding oxygen atoms. It can be clearly seen that the K^+ cation is nestled within the central cavity of the molecule and interacts with lone pairs of electrons on the oxygen atoms Figure 5.2 (b).

5.1.2. Calixarenes

A relatively new class of ionophores, calixarenes, was introduced after 1990s [12]. Tetraethyl 4-tert-butylcalix[4]arene (TBC) are well-known as good sodium ionophores. Calixarenes comprise the phenolic oxygens, which provide for a scaffold on which various functional groups can be attached, giving an optimum cavity for the complexation of Na^+ [13]. Applications of calix[n]arenes in the field of chemical sensors are based on potentiometric detection using polyvinyl chloride (PVC) membranes for the assay of alkali metal cations, alkaline earth elements and heavy metals [14]. The membranes were prepared by dissolution of the calixarenes ionophore, PVC, plasticizer and a lipophilic anion salt as tetraphenylborate in an organic solvent. The presence of the lipophilic anion salt is crucial as without this salt, the membrane will lose its perm selectivity

5.2. Experimental

The composition of the material in order to create photonic surface relief structures, recording light conditions such as intensity and time of exposure and layer preparation were similar to those listed in chapter 4, section 4.2. Modification of the biosensor is different and is described in section 5.2.1.

5.2.1. Preparation of sensing layer

5.2.1.1. DC or TBC in PVC matrix

The surface holograms were modified with sensing layer with Calixarene ionophores (TBC) immobilised in the PVC plasticised matrix [15-16] or dibenzo-18-crown-6 (DC) [17-18]. The composition of chemicals that were studied during this experiment are presented in the table 5.1 below.

Table 5.1. Composition of the coating layer

Components	Amounts(g)	Amount (% w/w) in dry TBC layer	Amount (% w/w) in dry DC layer
Polyvinyl Chloride (PVC)	0.3	28.571	28.571
Dioctyl terephthalate plasticizer (DOTP)	0.6	57.143	57.143
Dibenzo-18-crown-6 (DC)	0.1	-	9.524
tetraethyl 4-tert-butylcalix[4]arene Ionophore (TBC)	0.1	9.524	-
Sodium tetraphenylborate	0.05	4.762	4.762

All the components were stirred for 2 hours in 20ml of tetrahydrofuran (THF) at 60 ℃ until all the chemicals completely dissolved in the mixture. Then this solution was spin coated on the SRG at 1000rpm and the solvent allowed to evaporate to form a bilayer. Next the gratings were exposed to the K^+ and Na^+ to check the response of the sensors for different time intervals and the performance of the sensors for detection of K^+ and Na^+ was investigated.

The SRG were coated with tetraethyl orthosilicates (TEOS, 98 %) containing DC or TBC. The sol gel process provides a porous matrix that allows chemical species (in this study cations such as K^+ and Na^+) to diffuse easily and to interact with analyte sensitive material and thus provide for a faster response of the sensor. A typical composition used for coating of the SRG consisted of tetraethyl orthosilicate TEOS (24 mL), ethanol (17.5 mL), deionised water (8mL), 0.04 M nitric acid (3 mL) [19] and 0.1g DC. The amount of DC and TBC varied from 0.05 g to 0.1g. The optimisation involved finding the maximum amount of DC and TBC that can be incorporated in a layer while retaining a good optical quality. The solution was stirred for 24 hours and then spin-coated at 500 rpm on the pre-recorded surface grating. Next the coated samples were left for 24 hours at room temperature before further studies. Then the gratings were exposed to the different molar solutions of K^+ and Na^+ for pre-determined time intervals. The layers were studied under AFM and the change in diffraction efficiency was measured at different stages.

5.3. Results and Discussion

5.3.1. Characterisation of holographic Surface Relief Structures and sensing layer material

5.3.1.2. AFM

AFM was used for characterizing the surface topography. The surface relief profiles are presented in Figure 5.3. The amplitude observed in the structures of SRG is approximately 350-400 nm with line spacing 3.54µm ±3% was observed by AFM.
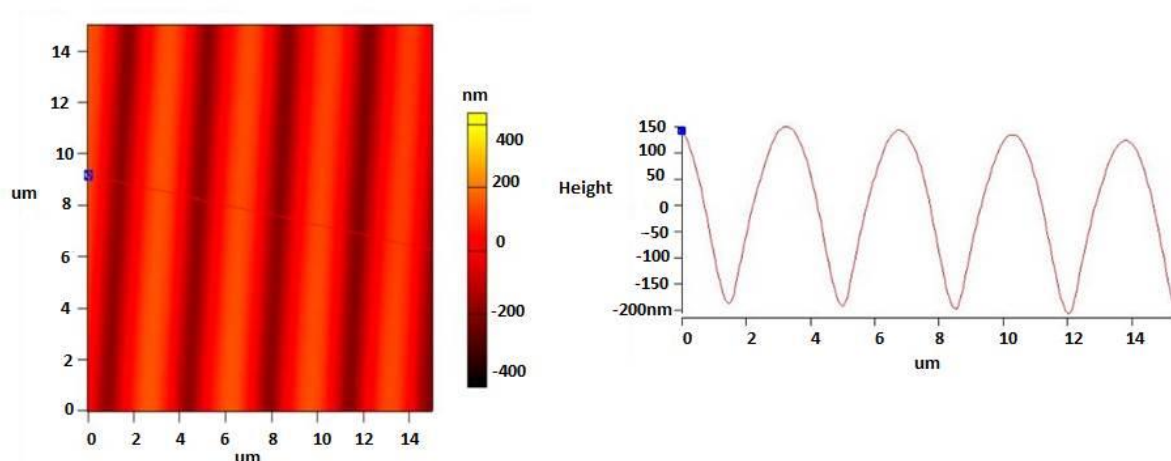
Figure 5. 3. 2-dimensional AFM scans of the SRG after thermal treatment

The diffraction efficiency of the structure was measured simultaneously with the surface relief amplitude at each stage of preparation of the sensor and after its exposure to the analyte. The results are presented in Table 5.2. The gratings were characterized before and after coating the sensing layer. The sensing layer contains chelating agent DC or TBC in PVC.

Table 5.2. Change in DE (%) and surface modulation of SRG

Diffraction Efficiency (DE %)	Surface modulation(nm)
Photopolymer 60% ±5%	<1
After thermal treatment 35% ±3%	400
dibenzo-18-crown-6 (DC) 20% ±3% in PVC matrix	20
Tetraethyl p-tert-butylcalix [4]arene Ionophore (TBC) in PVC matrix 20% ±3%	10
dibenzo-18-crown-6 (DC) 20% ±3% in sol gel matrix	20
Tetraethyl p-tert-butylcalix [4]arene Ionophore (TBC) in sol gel matrix 20% ±3%	18

After the surface structure was coated with DC the amplitude decreased from 350-400 nm to 20 nm approximately which clearly indicated that the troughs were filled with the sensing material. A separate set of samples were coated with TBC. These samples were studied by AFM and it was observed that their SRG amplitude decreased from 350-400nm to 10nm approximately as it can be seen in Figure 5.4.
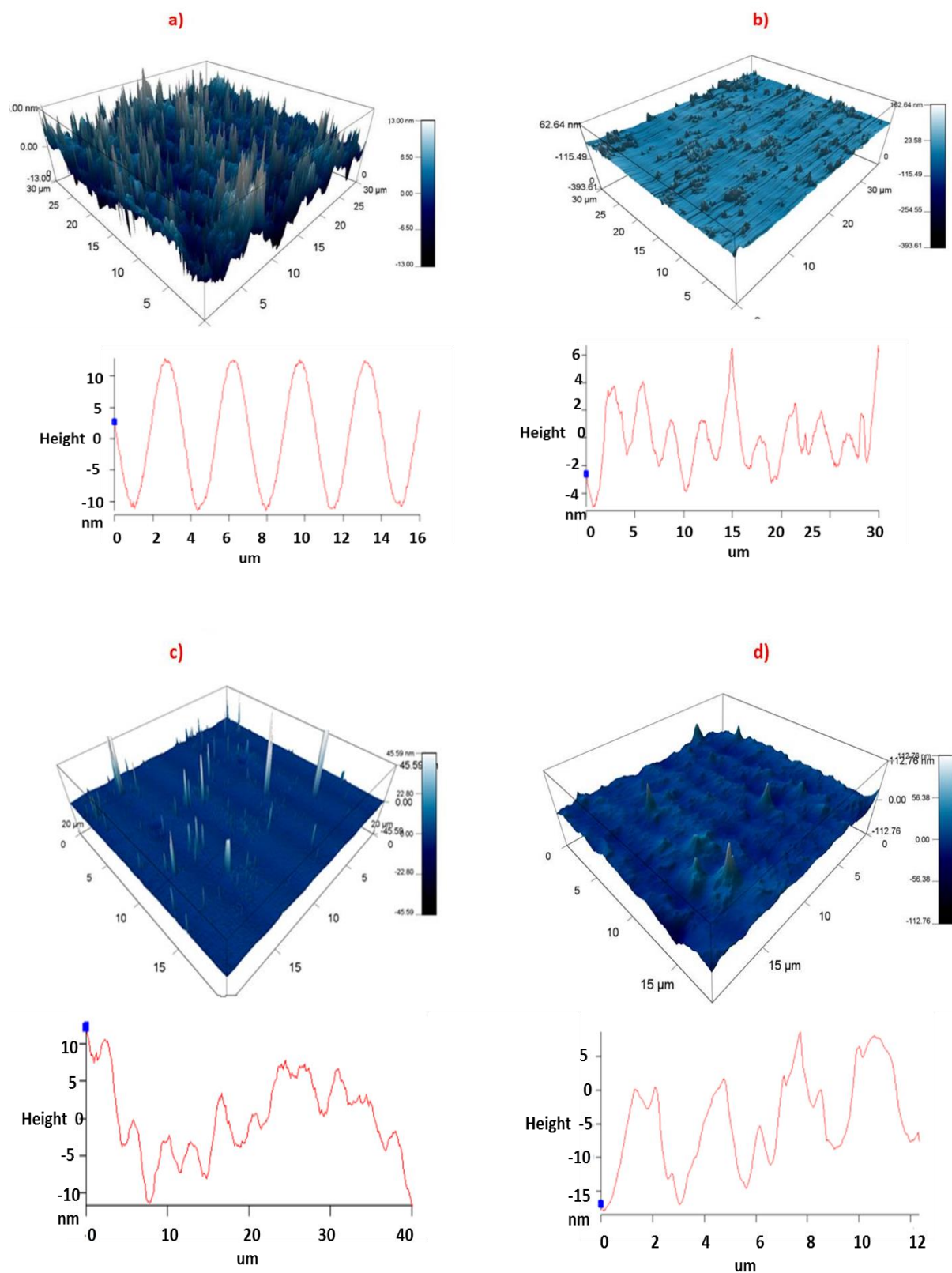
Figure 5. 4. (a). 3-dimensional AFM scans of the SRG coated with DC in PVC and (b) coated with TBC in PVC (c) coated with DC in sol gel matrix (d) with TBC in sol gel matrix

154

5.3.1.3. Diffraction efficiency and angular selectivity studies

The peak diffraction efficiency of 60% achieved for a photopolymer after holographic recording and as listed in table 5.2. The high value of diffraction efficiency is a result of volume diffraction grating as the SRG has negligible amplitude before a thermal treatment and the diffraction efficiency reduced to~ 35% and a shift of the Bragg angle was observed. The shift is observed in the photopolymer layer after thermal treatment possibly due to an increase in the effective refractive index and the density of the layer is clearly increased after thermal treatment. Other possible causes are shrinkage of the layer most probably after being thermally treatment and a possible change of the spatial frequency of the structure. The Bragg angle selectivity curve was then measured for layers functionalised with analyte sensitive materials. Diffraction efficiency further decreased after coating due to substitution of the air in the troughs with material with higher refractive index. Figure 5.5 shows example set of experimental curves for the diffraction efficiency as a function of incident angle for the holographic gratings at different stages of the experiment i.e. before thermal treatment, after thermal treatment, after coating with the DC sensing material, and after exposure to the analytes. The change in the peak value of the diffraction efficiency was followed as indication of the presence of the analyte. The DC and TBC in PVC fully cover the surface relief structure as was observed in AFM images in Figure 5.4. In order to evaluate the response of the structure to the analyte, measurements of the peak diffraction efficiency were taken at different times.
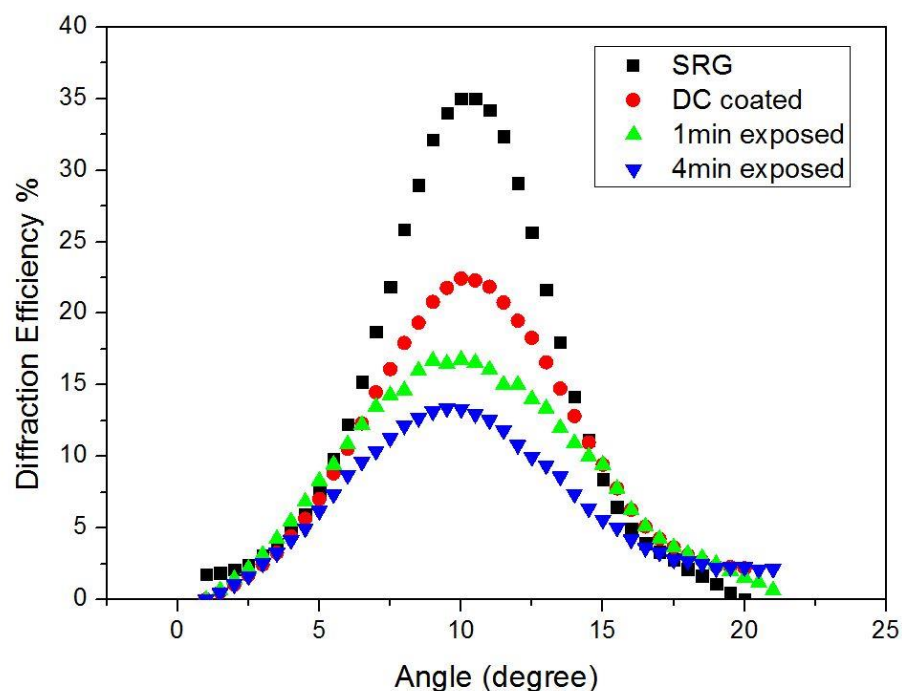
Figure 5. 5. Bragg curves SRG, after spin coating with (DC) PVC layer material and after exposure to analyte K^+ (50mM) at different times

5.4. Evaluation of the selectivity and sensitivity response of the sensor achieved by coating with DC or TBC in Polyvinyl chloride matrix (PVC) matrix

5.4.1. Evaluation of the selectivity in PVC matrix

In order to determine the selectivity of the proposed holographic biosensor for detection of the target analytes K^+ and Na^+, solutions with different concentrations (C) of KCl and $NaNO_3$ were prepared. The higher molar concentrations were chosen in order to compare the signal response in terms of specificity. Their association to become a close fit for the cation to crown cavity and the potential to form stable complexes is a known property of crown ethers. Inspection of Figure 5.6 (a) shows that the dibenzo-18-crown-6 give a dominant response for K^+ ion concentration, while the hologram showed little response to Na^+ and the reference water sample [7]. The diffraction efficiency drops for

K^+ from 1 to 0.6, whereas for Na^+ it drops down only from 1 to 0.9 although the Na^+ concentration was five time higher than the K^+ concentration.
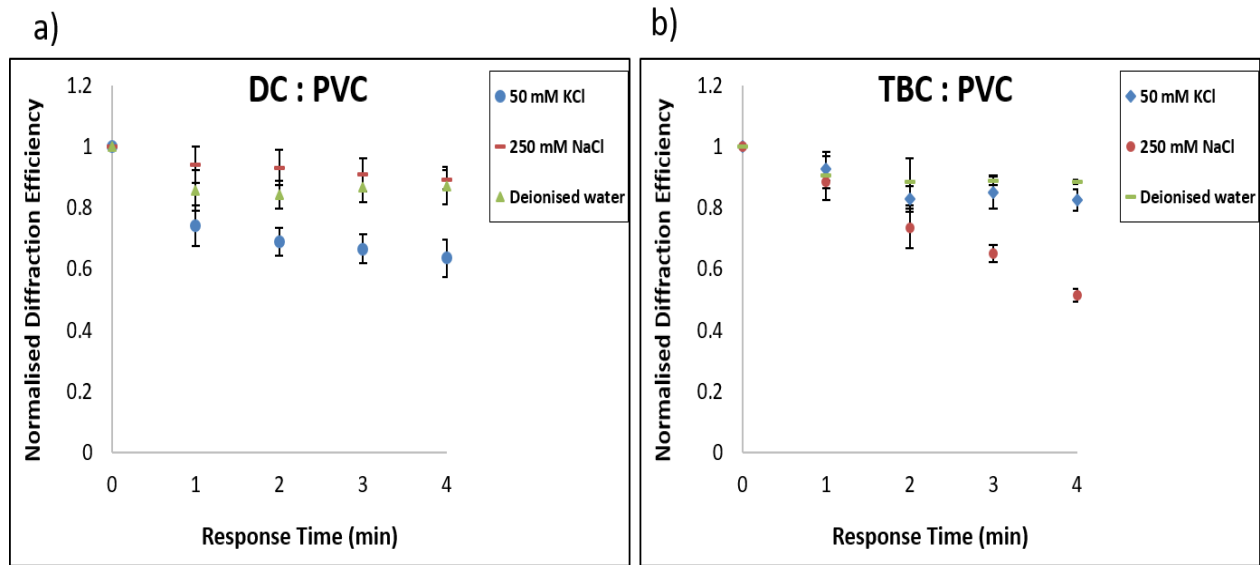
Figure 5. 6. Comparison of relative response in terms of normalised DE change of (a) DC with 250 mM NaCl, 50 mM KCl and deionised water and (b) TBC structures with 50mM KCl, 250 mM NaNO₃, and deionised water (n=3)

The results presented in Figure 5.6 (b) show that the TBC on exposure to Na^+ ions yield a dominant response over K^+ ion concentration, irrespective of the anion, while the hologram showed little response to deionised water (which is control in the current experiment) and K^+. The diffraction efficiency drops for Na^+ from 1 to 0.52, whereas for K^+ it drops down only from 1 to 0.8 but Na^+ concentration is 5 times higher than K^+ because Na^+ physiological ranges are higher than K^+. The aim of these studies is to detect physiological ranges [20] of blood serum which is 3.5 to 5.0 mM for K^+ [21]. The results indicated that with PVC matrix the lowest detected molar concentration is 10mM K^+ and needs further improvement, which is addressed in section 5.5.

5.4.2. Evaluation of the sensitivity in PVC matrix containing DC

The aim of this study is to detect physiological ranges of potassium and in sodium serum [4]. Different molar concentrations solutions were prepared for KCl. The results in Figure 5.7 (a) are from testing the layers when exposed to the prepared molar solutions 10mM-50mM of K^+ and deionised water (DI). As can be seen the normalised diffraction efficiency changes as the exposure time increases and molar concentration increases as it is indicated in Figure 5.7(a). There is dominant response for 50 mM K^+ as the normalised diffraction efficiency drops down from 1 to 0.6. In water it drops down only from 1 to 0.9.
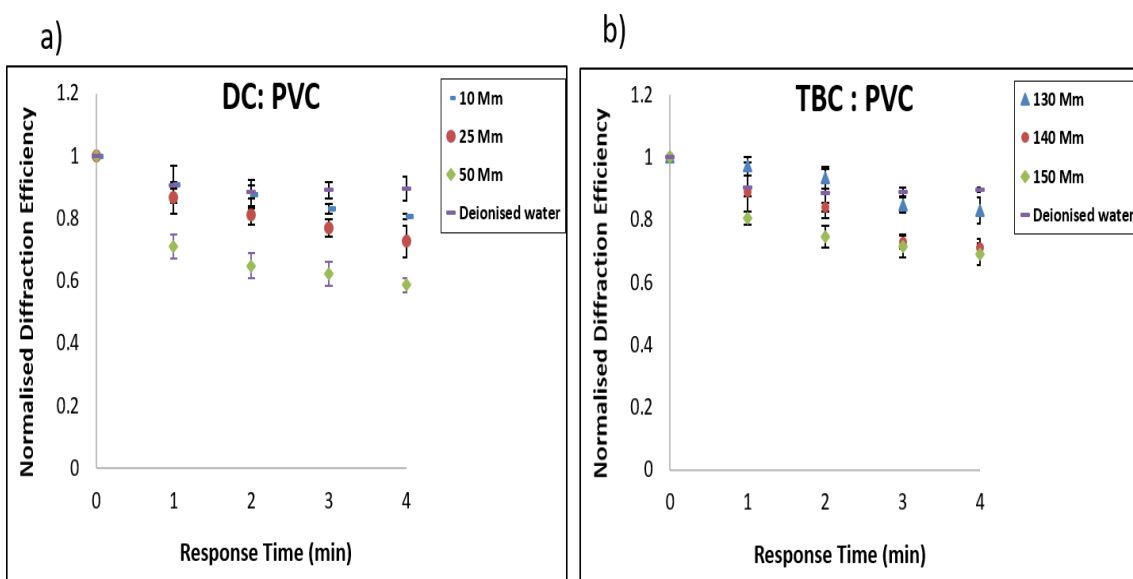
Figure 5. 7. Normalised diffraction efficiency change response DC and TBC in plasticised PVC photonic structures (a) KCl exposure to (10-50 mM) (b) NaNO₃ exposure to physiological levels (130mM-150mM) (n=3)

The normal levels of Na^+ serum in human are in the range 135-148mM [21]. Solutions of NaNO₃ were prepared with three different molar concentrations 130, 140 and 150mM. The sensor based on the TBC ionophore was exposed to concentrations 130-150mM and deionised water. As can be seen the normalised diffraction efficiency

change as the exposure time increases and molar concentration increases as shown in Figure 5.7(b). There is dominant response for higher molar concentration which is 150 mM as the normalised diffraction efficiency drops down from 1 to 0.7. In deionised water it drops down only from 1 to 0.9 whereas in lowest detected molar concentration (130mM) the normalised diffraction efficiency drops down only from 1 to 0.86. The result implies that there is a need to improve the sensitivity toward Na^+ in order to distinguish better the signal at 130mM concentration from the background change in deionised water.

5.5. Improvement of the sensitivity by changing the porosity of the matrix

5.5.1 SEM characterisation of the two matrices

The aim here is to change the matrix and increase the porosity of the matrix for achieving physiological ranges of potassium which was not possible in PVC membrane and improve the differentiation between background signal and response of the sensor to 130 mM Na^+. SEM images were obtained of the thin films coated on glass surface of PVC+DOPT and Sol- gel images are shown in Figure 5.8 in order to compare the porosity of the two materials.
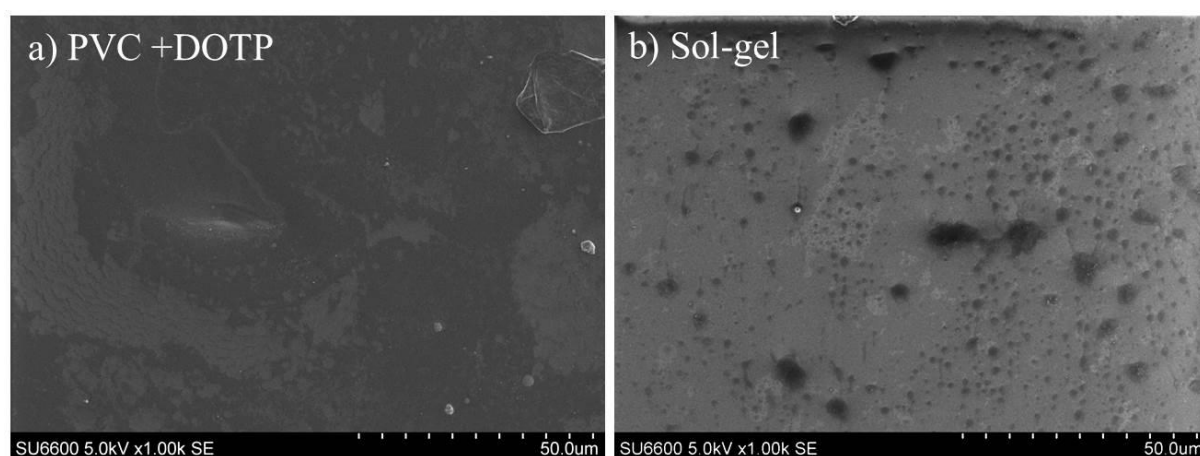
Figure 5. 8. Demonstration of the porosity of the matrix by comparing two matrices (a) SEM image of PVC+DOPT (b) Sol-gel

It is clearly illustrated in the SEM images that the sol-gel matrix has a porous structure. The porous structure of the sol gel will help analytes to easily penetrate into the matrix.

5.5.2. Evaluation of the selective response of the sensor achieved by coating with DC in sol gel matrix

Solutions of KCl were prepared in order to determine the selectivity of the sensor with the sol gel layer. Figure 5.9(a) shows that the dibenzo-18-crown-6 on exposure to K^+ ions give dominant response over Na^+ ion concentration, while the hologram showed little response to DI. Three different molar concentrations of KCl were prepared and exposed to the sensors along with the PVC membrane coated sample. The results in Figure 5.9(a) are from testing the structures when exposed to 3mM-5mM KCl and deionised water. As it can be seen the normalised diffraction efficiency change as the exposure time increases as it is indicated in Figure 5.9 (a). There is a dominant response for 5 mM K^+ as the normalised diffraction efficiency drops down from 1 to 0.244. In DI it drops down only from 1 to 0.78 and from 1 to 0.76 for NaCl. The sensor was coated with DC-PVC or DC-Sol gel and the sensitivity of the sensor was evaluated. The gratings were exposed to the analyte for different time intervals. The sensitivity for PVC matrix at 4 min exposure to the analyte (DE/ mM) is 0.5 % / mM which were observed for 10-50 mM concentrations Figure 5.9(c). The sensitivity at 4 min exposure to the K^+ analyte (DE/mM) is 24.7 % / mM which were observed for 3-5 mM in sol gel matrix Figure 5.9(d). Sensitivities plots are from Figure 5.7 (a) and 5.9 (a)
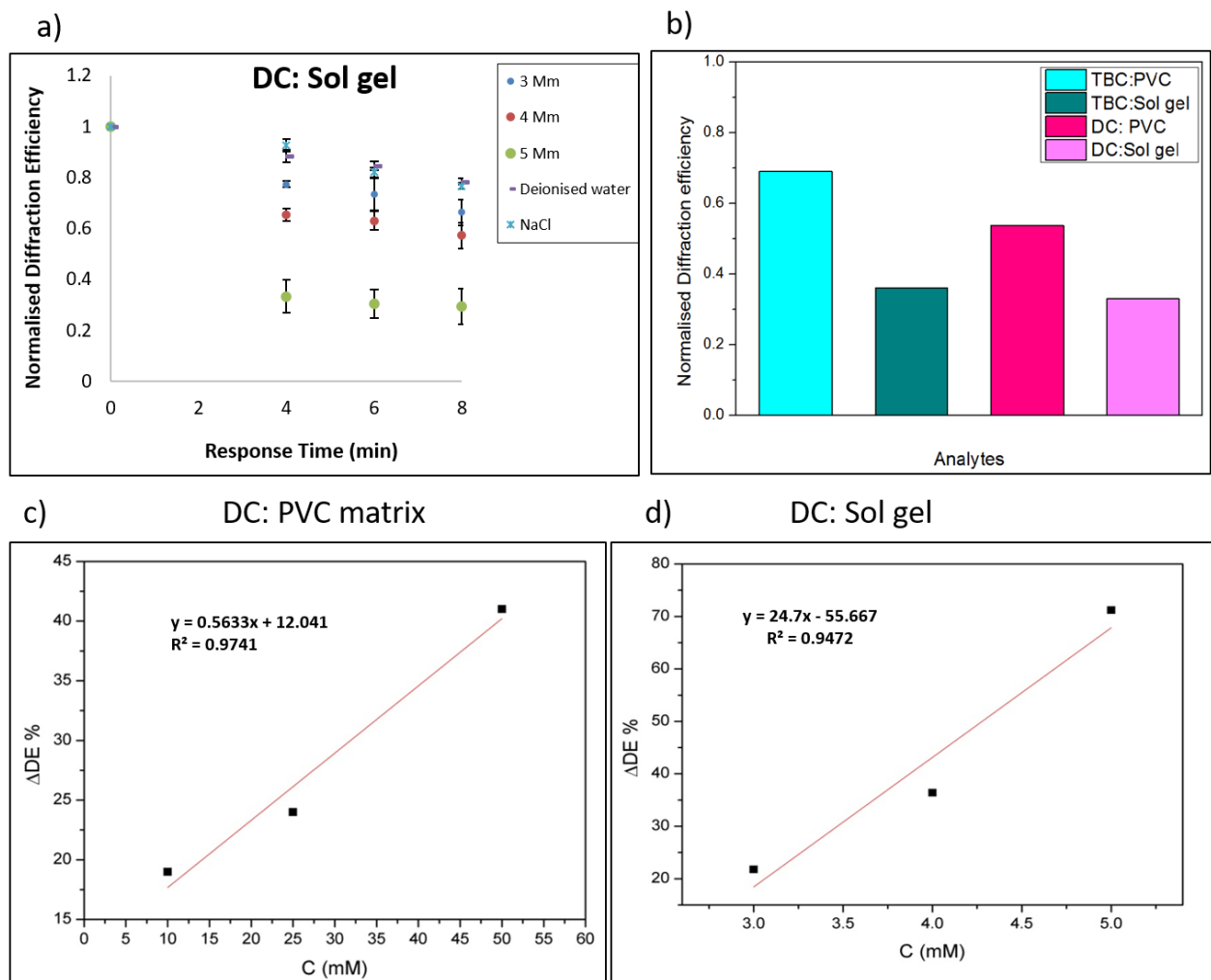
Figure 5. 9. (a) Normalised diffraction efficiency change response DC photonic structures in Sol gel matrix exposure to physiological levels (3-5 mM) KCl, DI and 130mM NaCl (n=3), Sensitivity of the response at 4min for DC (b) comparison of the change in normalised diffraction efficiency in PVC and Sol gel matrix at 4 min data points (c) plasticised PVC (10-50 mM)and (d) sol gel (3-5 mM)

5.5.3. Evaluation of the selective response of the sensor achieved by coating with TBC in sol gel matrix

Next the samples were functionalised with TBC in a sol gel matrix. The sensor based on the TBC ionophore was exposed to concentrations of 130mM-150mM $NaNO_3$. In Figure 5.10(a) it can be clearly seen in the normalised diffraction efficiency change as the exposure time increases. In Figure 5.10(b) data is plotted at 4 min on exposure to analyte for both layers. There is dominant response for Sol gel layer as compared to PVC layer. Next the sensitivity at 4 min exposure to the analyte (DE/ mM) is 0.8 % /

mM which were observed for 130-150 mM physiological concentrations Figure 5.10(c)

for PVC matrix. The sensitivity at 4 min exposure to the Na$^+$ analyte (DE/mM) is 2.0 %

/ mM which were observed for 130-150 mM in sol gel matrix Figure 5.10(d).

Sensitivities plots are from Figure 5.7 (b) and 5.10 (a) However the sol gel sensor still

does not sense lower levels of Na$^+$ and needs to be addressed.
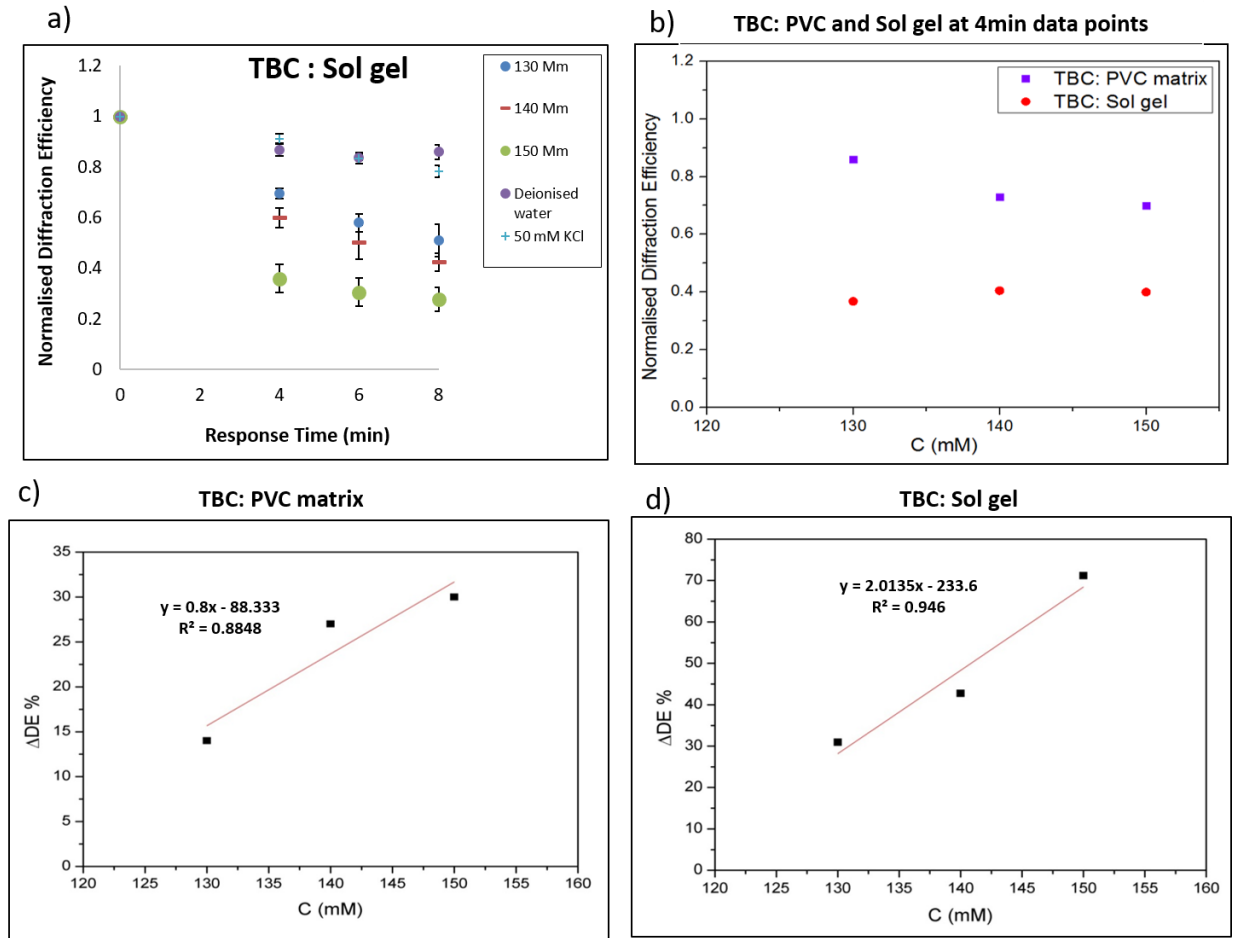
Figure 5. 10. (a) Normalised diffraction efficiency change response TBC photonic structures in Sol gel layers exposure to (130mM-150) Na$^+$ (n=3) (b) comparison PVC and Sol gel at 4min data points (c) Sensitivity of the response at 4min for TBC in PVC and (d) Sol gel

5.6. Conclusions

Holographic sensors for the detection of metal ions were prepared by sensing layer over

surface relief structures with dibenzo-18-crown-6 or 4-tert-butylcalix[4]arene. Dibenzo-

18-crown-6 provides a selective response of the devices to K$^+$ over Na$^+$, whereas for

tetraethyl 4-tert-butylcalix[4]arene there is a dominant response for Na^+ over K^+. The sensor responds to Na^+ within the physiological ranges. Normal levels of Na^+ in human serum lie in the range 135-148 mM and the normal K^+ level is 3.5-5.0 mmol/L [22]. The novelty of the present work is usage of TBC ionophores in holographic sensors. While the results demonstrate that the modified SRG can sense K^+ and Na^+, alternative sensing layers can be used. These layers could comprise the array of ionophores, traditionally used in potentiometry or molecularly imprinted polymers. The advantage of such photonic structures has the ability to modify the surface for different interest of analytes by changing the functionalising material. The proposed sensor has ability for use as a biosensor. The present research work demonstrated the feasibility of the sensor, rather than rigorously validate it as an analytical technique. The results indicate that the DE changes with ion concentration. This novel transduction device gives quick response and its low cost disposable sensor also can be integrated with portable devices

References

[1]   J. Melorose, R. Perroy, and S. Careas, *Biomedical Sensors*, vol. 1. New York: Momentum press, 2015.

[2]   J. Ponmozhi, C. Frias, T. Marques, and O. Frazao, "Smart sensors/actuators for biomedical applications: Review," *Measurement: Journal of the International Measurement Confederation*, vol. 45, no. 7, pp. 1675–1688, 2012.

[3]   J. Bujes-Garrido and M. J. Arcos-Martinez, "Disposable sensor for electrochemical determination of chloride ions," *Talanta*, vol. 155, pp. 153–157, 2016.

[4]   A. K. Balcı, O. Koksal, A. Kose, E. Armagan, F. Ozdemir, T. Inal, and N. Oner, "General characteristics of patients with electrolyte imbalance admitted to emergency department," *World J Emerg Med*, vol. 4, no. 2, pp. 113–116, 2013.

[5]   I. M. Kolthoff and M. K. Chantooni, "Transfer Activity Coefficients in Various Solvents of Several Univalent Cations Complexed with Dibenzo-18-Crown-6," *Analytical Chemistry*, vol. 52, no. 7, pp. 1039–1044, 1980.

[6]   A. G. Mayes, J. Blyth, R. B. Millington, and C. R. Lowe, "Metal ion sensitive holographic sensors," *Anal. Chem.*, vol. 74, no. 15, pp. 3649–3657, 2002.

[7]   B. Madrigal González, G. Christie, C. A. B. Davidson, J. Blyth, and C. R. Lowe, "Divalent metal ion-sensitive holographic sensors," *Analytica Chimica Acta*, vol. 528, no. 2, pp. 219–228, 2005.

[8]   C. J. Pedersen, "Cyclic Polyethers and Their Complexes with Metal Salts,"

Journal of the American Chemical Society, vol. 89, no. 26, pp. 7017–7036, 1967.

[9] A. Elbasyouny, H. J. Brugge, K. von Deuten, M. Dickel, A. Knóchel, K. U. Koch, J. Kopf, D. Melzer, and G. Rudolph, "Host-Guest Complexes of 18-Crown-6 with Neutral Molecules Possessing the Structure Element XH2 (X = O, N, C)," *Journal of the American Chemical Society*, vol. 105, no. 22, pp. 6568–6577, 1983.

[10] C. J. Pedersen, *The Pedersen Memorial Issue Advances in Inclusion Science*, 12th ed. 1992.

[11] G. Olsen, J. Ulstrup, and Q. Chi, "Crown-Ether Derived Graphene Hybrid Composite for Membrane-Free Potentiometric Sensing of Alkali Metal Ions," *ACS Applied Materials and Interfaces*, vol. 8, no. 1, pp. 37–41, 2016.

[12] M. Telting-Diaz, D. Diamond, and M. R. Smyth, "Flow-injection analysis with tetrameric calixarene-based potentiometric detection," *Analytica Chimica Acta*, vol. 251, no. 1–2, pp. 149–155, 1991.

[13] P. Bühlmann, E. Pretsch, and E. Bakker, "Carrier-based ion-selective electrodes and bulk optodes. 2. Ionophores for potentiometric and optical sensors," *Chemical Reviews*, vol. 98, no. 4, pp. 1593–1688, 1998.

[14] R. M. El Nashar, H. A. A. Wagdy, and H. Y. Aboul-Enein, "Applications of calixarenes as potential ionophores for electrochemical sensors," *Current Analytical Chemistry*, vol. 5, no. 3, pp. 249–270, 2009.

[15] P. Bühlmann, E. Pretsch, and E. Bakker, "Carrier-based ion-selective electrodes and bulk optodes. 2. Ionophores for potentiometric and optical sensors," *Chemical Reviews*, vol. 98, no. 4, pp. 1593–1688, 1998.

[16] E. Malinowska, L. Gawart, P. X. Parzuchowski, G. Rokicki, and Z. Brzozka, "Novel approach of immobilization of calix[4]arene type ionophore in 'self-plasticized' polymeric membrane," *Analytica Chimica Acta*, vol. 421, no. 1, pp. 93–101, 2000.

[17] W. Hiller, S. Frey, J. Strahle, G. Bocheb, W. Zargesb, K. Harms, M. Marsch, R. Wollertb, and K.Dehnicke, "Die Kristallstrukturen von (Li3(12-Krone-4)2[HC(CN)2]3}, [HC(CN)2]) und (Na[N(nBu)4,][HC(CN)2,]2. THF}," *Chem. Ber.*, vol. 3, pp. 87–92, 1992.

[18] S. Katsuta, H. Tachibana, and Y. Takeda, "Stabilities in Water of Alkali Metal Ion Complexes with Dibenzo-24-crown-8 and Dibenzo-18-crown-6 and Their Transfer Activity Coefficients from Water to Nonaqueous Solvents," *journal of solution Chemistry*, vol. 31, no. 6, pp. 499–510, 2002.

[19] S. Jaiswal, P. Mchale, and B. Duffy, "Colloids and Surfaces B : Biointerfaces Preparation and rapid analysis of antibacterial silver , copper and zinc doped sol – gel surfaces," *Colloids and Surfaces B: Biointerfaces*, vol. 94, pp. 170–176, 2012.

[20] M. Zacchia, M. L. Abategiovanni, S. Stratigis, and G. Capasso, "Potassium: From Physiology to Clinical Implications," *Kidney Diseases*, vol. 2, no. 2, pp. 72–79, 2016.

[21] Andrew G. Mayes, Jeff Blyth, and Roger B. Millington, and C. R. Lowe, "Divalent metal ion-sensitive holographic sensors," *Analytica Chimica Acta*, vol. 74, pp. 3649–3657, 2002.

[22] C. Burtis, A, R. Edward, and D. Bruns, E, *Fundamentals of Clinical*

Chemistry :6th Ed, no. August. Philadelphia USA: SAUNDERS Elsevier, 2001.

Chapter 6– Development of novel cellulose acetate based volume photonic structures

6.1. Introduction

In this chapter the research aim is to develop a new photopolymer composition, capable of recording volume holograms which can operate in a water environment and remain stable after exposure to water. Volume transmission gratings were recorded in a cellulose acetate (CA) and polyethylene glycol (PEG) based photopolymer containing N-phenyl glycine (NPG) as a photo initiator. Triethanolamine (TEA) was substituted with NPG because it is compatible with the current formulation. It was recently observed that the diffraction efficiency of transmission gratings recorded in a photopolymer composition utilising NPG as an initiator appeared to be unaffected after exposure to 80% humidity [1]. This property of NPG based photopolymers is a key to achieving our aim. The use of the cellulose as a binder is appealing because it is a natural plastic, stable in water and has already has been used to fabricate microfiltration membrane technology used to obtain safe drinking water [2]. Cellulose is an inexpensive and renewable biopolymer and readily available, which makes it a cheap raw material for various applications. Cellulose acetate (CA) has a great potential for applications in the pharmaceutical and medicinal industries [3]. Thermal processability and the ability to interact with other polymers at the molecular level have been cited as useful properties of CA. Research has focused on the development of CA membranes, which contain analytically active microparticles [4]. CA has been studied extensively in the past two decades for possible application in mopping up toxic heavy metals from water [5]. Nowadays, high-performance biosensors are also being developed; they are usually made of bio-functional CA membranes. For instance readily available

antimicrobial agents like silver oxide (Ag$_2$O), zinc oxide (ZnO), titanium dioxide (TiO2) and fullerenes have been incorporated in the membranes to prevent microbial attack [6]. These biosensors can be applied for environmental and clinical purposes. The CA matrix also has good potential for fabricating sensors and biosensors [7] and because of that, the present research work aimed to develop a holographic sensor by using a CA- PEG blended composite.

Furthermore, the membrane can be modified by adding a pore former such as Polyethylene glycol (PEG) in order to get a porous structure or a dense surface [8]. PEG is hydrophilic in nature can be a colorless liquid or waxy solid and is soluble in water. The higher amount of PEG can introduce more porosity to the membrane but at the same time the layers can lose their robustness and can easily start wrinkling after exposure to water. Therefore, an optimum balance is needed in order to achieve control over the porosity while retaining resistance to water. The structure of PEG is commonly expressed as H$-$ (O$-$CH$_2$$-CH_2$) $_n$$-$OH [9]. Here in this research, the choice of CA-PEG is to replace the polyvinyl alcohol (PVA) binder which is used in previous chapters to develop surface sensors. PVA is a water soluble synthetic polymer which in combination with the other photopolymer components cannot withstand in the water environment for long exposure times as observed in studies utilising surface sensors (Chapter 4 and 5). The approach in this chapter is to develop a volume holographic grating (VHG) in order work in a water environment for longer exposure time. The chemical structures of CA, PEG and NPG are presented in Figure 6.1.
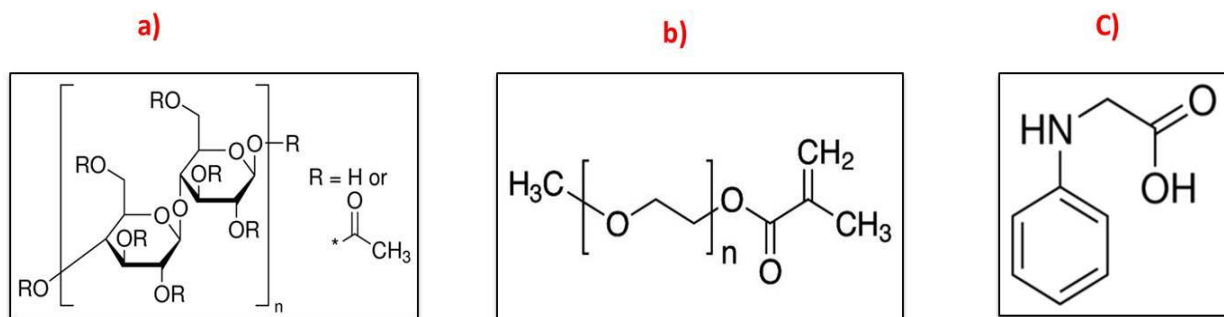
Figure 6. 1. (a) Cellulose acetate (b) Polyethylene glycol and (c) N-Phenylglycine

Birabassov et al. fabricated azo-dye-doped CA films for holographic applications, where both intensity and the state of polorization of the light were recorded. The results proved the significant differences between the CA matrix and polymers such as PVA, PMMA, etc, that are traditionally used for polarization holography. It was observed that the CA matrix provides better support of the dye molecules and has a better memory effect [10].

Wang et al. presented a study of a new photosensitive material comprising Dichromated cellulose triacetate (DCCTA). The DCCTA matrix is good medium of the dye molecules and has been used as a film to record gratings. The material has some special properties, such as good environmental stability, strong relief modulation, light weight and is flexible [11].

In the present research work the photosensitive layer is composed of a CA- PEG blended composite. To our knowledge, this composition is reported for the first time. The recording ability of the photopolymer was investigated in volume transmission mode of recording for a range of different recording parameters, including exposure energy and recording intensity. Results of these studies are presented in this chapter. The layers prepared with the present formulation have an improved resistance to water and are promising as a platform for sensors or biosensors working in a water

environment. The layers can easily be peeled off from the substrate and this is useful because in some applications self-standing layers are required. The initial results reveal that the current photopolymer can be functionalised with 4-tert-butylcalix[4]arene (TBC) ionophores and have good potential to work as a biosensor. Biosensors can be used for a detection of the broad spectrum of biological analytes and are useful in medical laboratories. Levels of blood serum can be easily monitored with high accuracy using biosensors.

6.2. Experimental

6.2.1. Materials and Methods

A number of acrylamide based photopolymer compositions were prepared as described in Table 6.1. Cellulose acetate (Mw 30,000 and acetyl content 39.8%), polyethylene glycol (Mw 950-1050) were dissolved in acetone. All the materials used in this research work were of analytical grade purchased from Sigma Aldrich without further purification.

Components	(A) Amount (g)	(B) Amount (g)	(C) Amount (g)	(D) Amount (g)
Cellulose acetate (CA) (g)	8.0	5.0	9.0	8.0
Polyethylene glycol (PEG) (g)	2.0	5.0	1.0	2.0
Acrylamide (AA) (g)	0.6	0.6	0.6	0.6
N,N'Methylenbisacrylamide (BAA) (g)	0.2	0.2	0.2	0.2
N-phenyl glycine (NPG) (g)	-	0.05	0.05	0.09
Erthrosine B dye (EB) (g)	0.0044	0. 0044	0.0044	0. 0044
Triethanolamine (TEA)	1.12	-	-	-
Total weight	11.924	10.854	10.854	10.894

Table 6.1 shows the chemical composition of photopolymers A, B, C and D in order to develop a new formulation for the fabrication of a volume hologram. In order to facilitate the comparison of the photopolymers used in this study, pie charts of the four compositions are shown in Figure. 6.2. As it can be seen from the pie charts, composition A contains the TEA initiator. The other three compositions contain NPG initiator. For compositions B, C and D the amount of CA-PEG was varied to obtain good optical quality layers which are less sensitive to water and had higher diffraction efficiency. The highest percentage of NPG was in composition D when compared with the other two compositions B and C. The amount of initiator was increased to in order to achieve better diffraction efficiency.
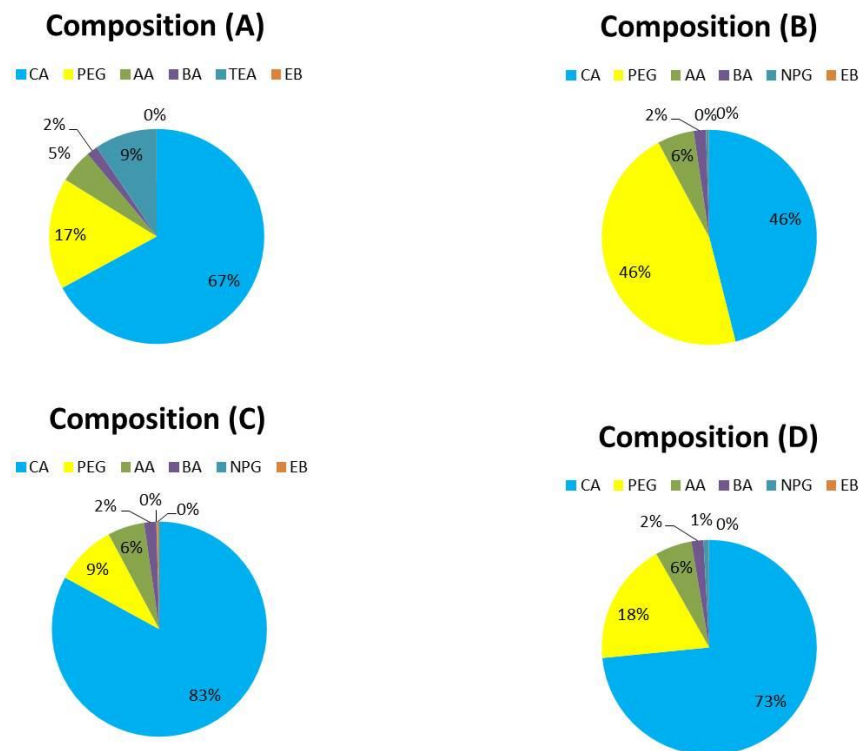
Figure 6. 2. Chemical composition of the dry photopolymer layers (% w/w)

Initially experiments were carried out with composition (A) containing Triethanolamine (TEA) initiator. The layers were exposed to 532nm wavelength laser light but the recording was unsuccessful in this composition. Although a slight bleaching was observed in exposed area the measured diffraction efficiency was 0 (Figure 6.3). The general composition of this material is listed in table 6.1 composition (A).
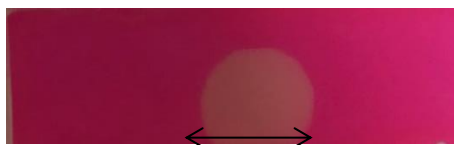
Figure 6. 3. Imaged Layer containing TEA initiator composition 'A' exposed to laser 532nm wavelength

Next layers were prepared containing NPG as initiator along with a CA-PEG blended composite. Composition (B) was successfully recorded but the problem found in this

composition was that the layers were very sensitive to water (Figure 6.4 (a)) and they wrinkled after exposure to water. To avoid this problem it is important to have good balance of CA-PEG in the layers. Thus the amount of CA was increased and the PEG reduced in composition (C) in order to get less sensitivity to water and obtain a robust hologram (Figure 6.4(b)). Results of this composition showed that the layers were very rigid and also the holograms recorded were not bright enough and the diffraction efficiency was less than 1% (C). Then composition (D) was found to be optimum with good optical quality layers (Figure 6.4 (c)) and better diffraction efficiency up to 52%.
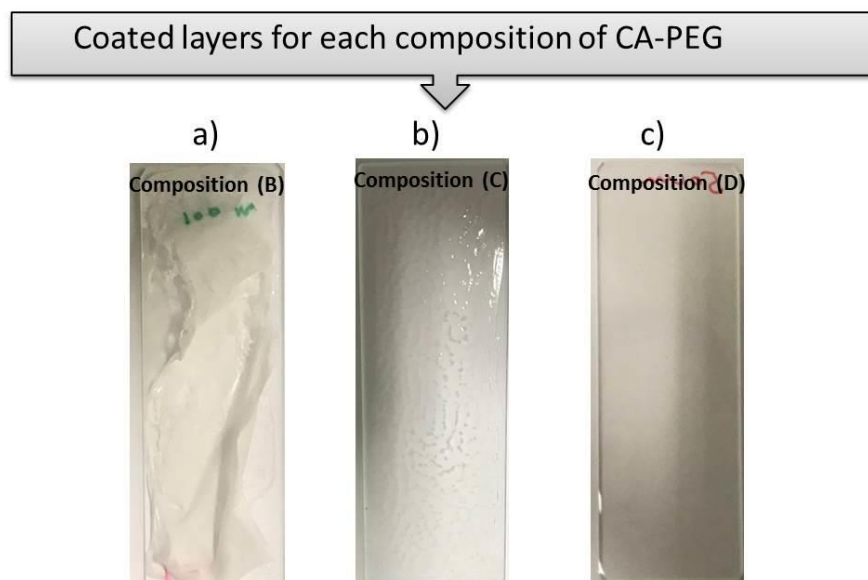
Figure 6. 4. CA-PEG coated layers and images were taken after exposure to water

6.2.3. Steps required obtaining good optical quality layers

In summary the following steps were identified as providing good optical quality layers:

➤ A CA and PEG blended solution was prepared in acetone as solvent.

➤ Layers of CA-PEG were initially coated by depositing 50 µl on a microscope glass slide. As shown in Figure 6.5 (a) the quality of CA-PEG layer was not very

good in the first instance, as acetone is very volatile solvent. It was observed that such thin layers dry very quickly.

➢ The next step was to improve the layer quality. When layers were covered with a glass petri dish as shown in Figure 6.5 (b), the rate of evaporation of solvent decreased and a better quality of layer was obtained, Figure 6.5(c) shows improved layers quality after drying.
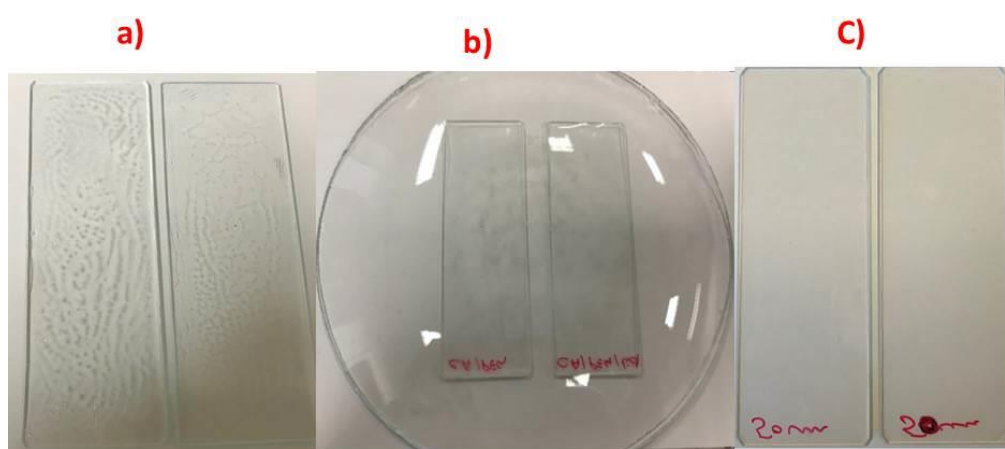
Figure 6. 5. Coated layers typically 50 µm layer thickness (a) Cellulose acetate, (b) Cellulose acetate under glass petri dish for controlled evaporation of solvent and (c) dried layers

6.2.2. Preparation of the optimum composition (D) Photopolymer film

In order to obtain CA-PEG blended solution stock solution of 8 % w/w, cellulose acetate (CA) was dissolved in 100 ml of acetone with constant stirring at 80° C for 3 hours in a fume hood. To obtain a homogenous CA-PEG solution, 2 g of PEG was added with regular stirring at 80 °C for another 3 hours. A viscous and clear solution was obtained which was termed as a blended solution, CA-PEG (Figure 6.6).

Figure 6. 6.Cellulose acetate and polyethylene (CA/PEG) blended solution

The solution was allowed to cool down to room temperature (20 °C). Next acrylamide (AA) and N,N'Methylenebisacrylamide (BAA) were added as the two monomers. Then N-phenyl glycine (NPG) initiator [12] was added into the CA-PEG solution. Erythrosine B (EB) was directly added as dye powder into the solution at the end. Finally, all the components were mixed for 2 hour at room temperature. 700µl volume of photopolymer solution was spread evenly on a glass substrate. The time flow of the chemical procedure and recording are shown in Figure 6.7.
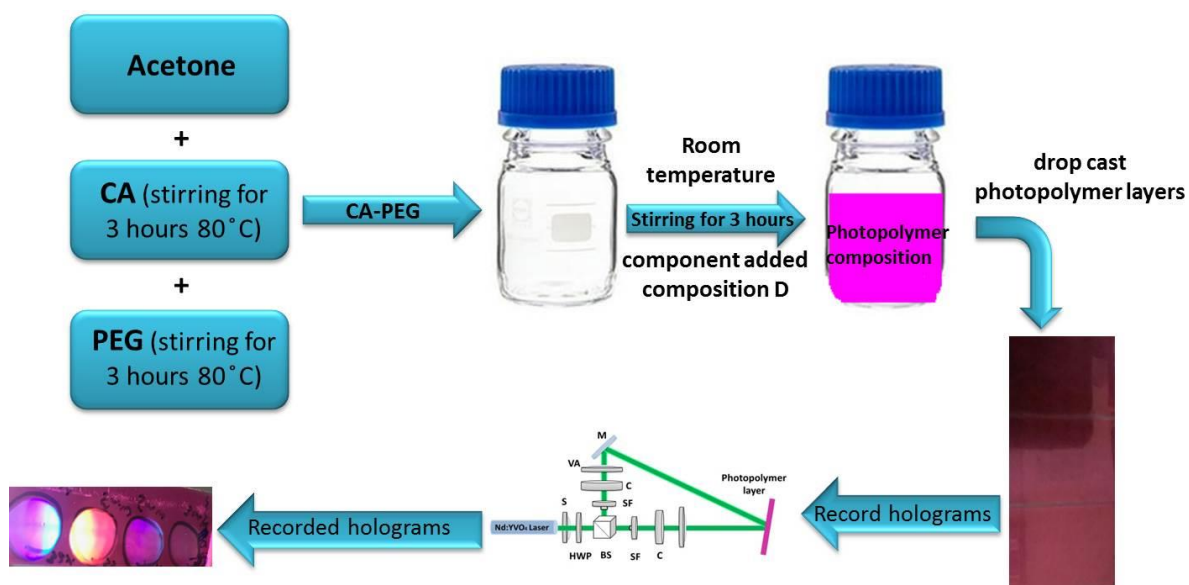
Figure 6. 7. Schematics of the chemical procedure and recording of volume holograms

The coated glass substrate was placed on a levelled surface and allowed to dry in dark under a petri dish for typically 5-6 hours. The thickness of the dry sample was 70 ± 10µm.

6.2.3. Recording and testing the VHG

Holograms were recorded in layers containing NPG composition (B) listed in table 6.1. This composition successfully recorded and the maximum diffraction efficiency at that stage was 20 ± 3 % Figure 6.8(a). The recorded grating was exposed to UV to bleach the dye but the gratings can be easily bleached if they were exposed to normal light as well. Also the results provided the information there is negligible shrinkage observed after UV bleach, Previously it was observed in an acrylamide based photopolymer compositions that after the UV bleaching normally due to shrinkage, diffraction efficiency drops down [13]. In the current composition this is the advantage that after UV bleaching the diffraction efficiency was observed to be stable.
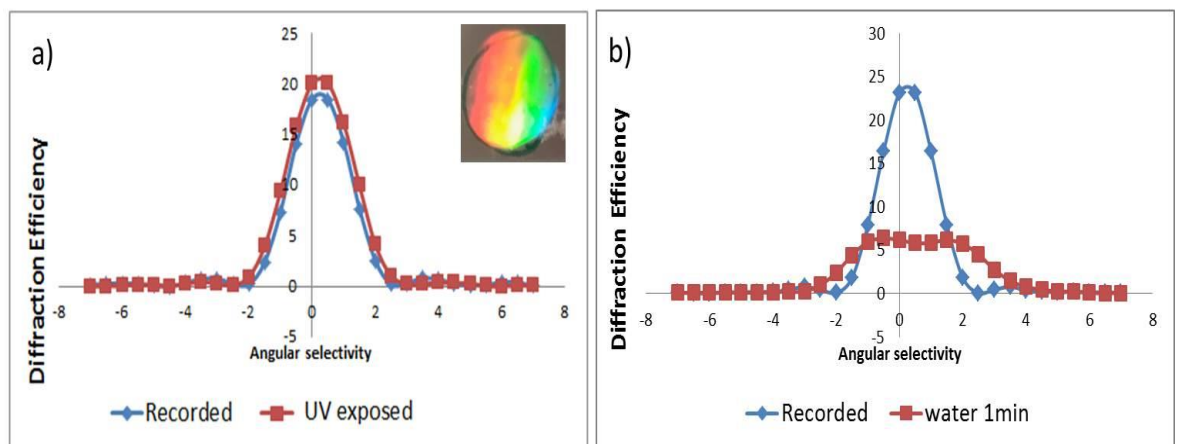
Figure 6. 8. (a). Bragg curves composition (B) with spatial frequency at 800 l/mm recorded in layers with thickness of 100 µm (± 10 µm)on a glass slide taken for the photopolymer before UV exposed and after UV exposed and (b) Bragg curve recorded after exposure to water

The shortcoming of this composition is that the layers were very sensitive to water as mentioned previously. Even on short exposure to water the diffraction efficiency drops down quickly as can be seen in Figure 6.8(b). The amount of NPG was increased for further studies in order to improve the diffraction efficiency. Composition (D) was found to be optimum and further studies were conducted on layers with the same composition. Preliminary studies showed that cellulose acetate materials have the ability to be used as a photopolymer binder in a photopolymer composition because of its excellent optical properties also the composition found to be unaffected after water exposure results are presented in section 6.4.1.

6.3. Recording of the volume phase gratings

The holographic recording setup for recording transmission volume phase gratings is shown in Fig. 6.9. The recording was carried out on an optical table (Newport RS 4000), which was floated in order to minimise vibrations. The photopolymer layers were exposed to two coherent beams of Nd:YVO4 laser operating at a wavelength of 532nm used to record unslanted transmission volume gratings. The angle of the recording beams was adjusted to record the diffraction gratings with the spatial frequency of 800 l/mm. A low intensity helium–neon (He–Ne) laser beam operating at a wavelength of 633nm was employed as a readout beam to monitor the buildup dynamics of the grating since the photoinitiator in the present system is insensitive in the red. The intensity of the diffracted beam was monitored by means of an optical power meter (Newport 1830-C), and the acquired data were transferred to a computer. The diffraction efficiency η of the transmission gratings was calculated as the ratio of the intensity of the 1st order diffracted beam and the intensity of the incident beam.
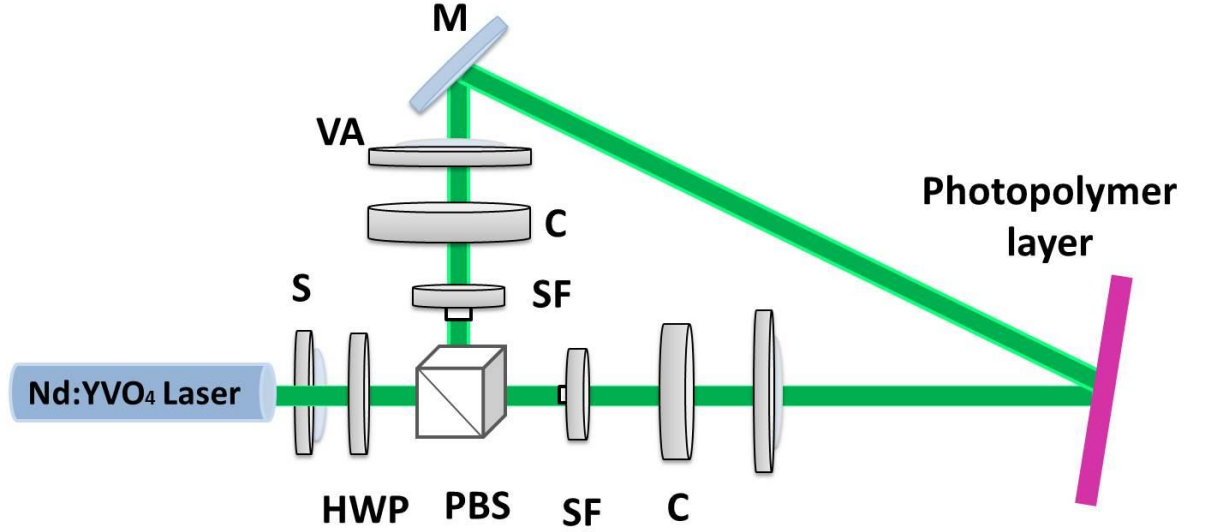
Figure 6. 9. Experimental set up for recording transmission grating (S. shutter; HWP half wave plate; PBS polarising beam splitter; SF spatial filter; C collimator; VA variable aperture and M mirror)

The thickness was estimated from a $\Delta\theta_{FWHM} = \Lambda/d$ fit to the Bragg-angle data with Kogelnik's formula for an unslanted transmission hologram. [14]. To evaluate the applicability of the coupled wave theory in a particular case, Q factor was calculated [15] using Equation (6.1) [16]. In the present research, unslanted volume phase transmission gratings with a spatial frequency of 800 l/mm (1.25 μm) were recorded in the photopolymer layers with thickness of 70 ± 3 μm. According to Equation (6.1), these parameters correspond to Q factor of about 118.78 and, thus, the coupled wave theory for the calculation of the diffraction efficiency/refractive index modulation can be applied. According to the coupled wave theory, refractive index modulation is determined by equation 6.2:

$$Q = \frac{2\pi\lambda_r d}{n_0 \Lambda^2} \qquad (6.1)$$

where n_0 is the recording medium refractive index and λ_r is the reconstruction wavelength, Λ is the period and d is the thickness

$$\Delta n = \frac{\lambda_r cos\,\theta_B\,sin^{-1}(\sqrt{\eta})}{\pi d} \qquad (6.2)$$

where λ_r is the wavelength of the reconstructing beam, θ_B is the Bragg angle inside the photopolymer layer at this wavelength, η is diffraction efficiency of the recorded volume transmission grating. Also the refractive index modulation (Δn) can be extracted from η with the a help of equation 6.2.

6.4. Results and Discussions

6.4.1. Dependence of diffraction efficiency on recording exposure energy at spatial frequency of 800 l/mm

In order to determine the optimum recording exposure time at 800 l/mm spatial frequency, the diffraction efficiency of layers of different thickness were compared. The results presented in Figure 6.10-6.12 show the relationship between first order diffraction efficiency vs. exposure energy of the transmission gratings at same exposure time and varying recording intensities, for a spatial frequency of 800 l/mm, in layers of thicknesses with the range between 50μm -100μm. From the results, it can be observed that the maximum diffraction efficiency is achieved at 300mJ/cm^2 exposure energy (Intensity = 10 mW/cm^2). A clear dependence of diffraction efficiency on exposure energy was observed in layers of 50, 70 and 100μm thickness. Recording at higher exposure typically leads to a higher diffraction efficiency.
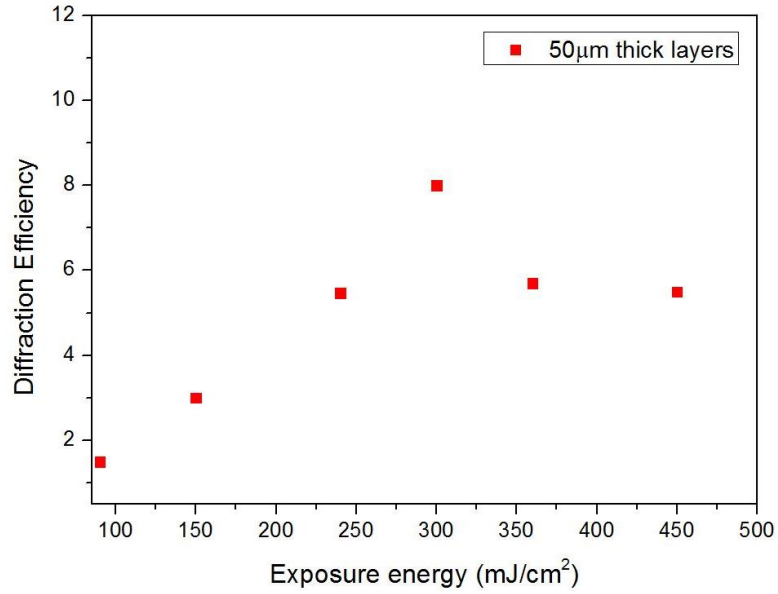
Figure 6. 10. Measured diffraction efficiency vs. exposure energy for the volume transmission gratings with varying recording intensities 3-10 mW/cm^2 at fixed time 30 seconds and spatial frequency of 800 l/mm was investigated for sample thickness of 50µm ± 10 µm
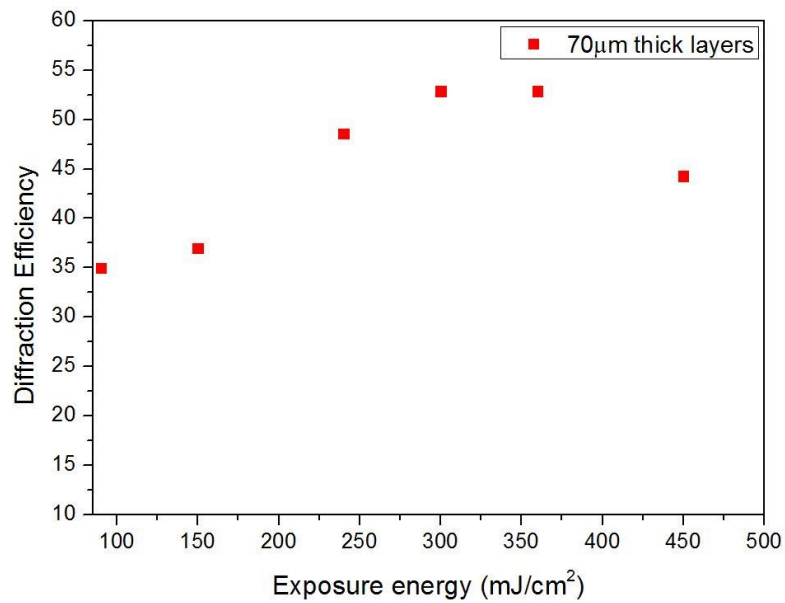
Figure 6. 11. Measured diffraction efficiency vs. exposure energy for the volume transmission gratings with varying recording intensities 3-10 mW/cm^2 at fixed time 30 seconds and spatial frequency of 800 l/mm was investigated for sample thickness of 70µm ± 10 µm
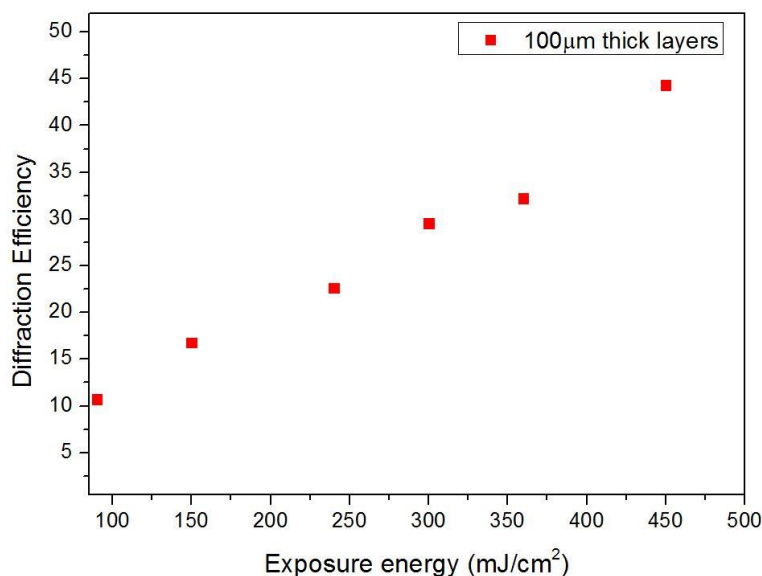
Figure 6. 12. Measured diffraction efficiency vs. exposure energy for the volume transmission gratings with varying recording intensities 3-10 mW/cm^2 at fixed time 30 seconds and spatial frequency of 800 l/mm was investigated for sample thickness of 100µm ± 10 µm

The maximum diffraction efficiency obtained was 52% at 800 l/mm spatial frequency, with the thickness of 70µm ± *10* µm approximately at 300mJ/cm^2. The rate of initiation depends on the recording intensity or exposure time, absorption of the layer, and the production of radicals [17]. At higher spatial frequency the smaller fringe spacing allows easy diffusion of monomer into the bright fringe regions from the dark fringe regions. Also 40% diffraction efficiency was obtained in samples with thickness of 100 µm but a limitation of this thickness is that the layers were found to be opaque after bleaching with normal light.

Water exposure studies

In Figure.6.13 the CA-PEG recorded hologram was exposed to deionised water (DI) in order to investigate the behaviour of the CA-PEG recorded holograms in a water environment and also to get reference readings. The recorded grating was exposed to water for 60 minutes and Bragg curves were recorded before and after exposure to water. It can be seen in Figure 6.13(a) that the layer is stable in water for at least 60

minutes. Future studies will measure the response for longer periods of time, since in some bio applications the exposure to water could continue for days. As it can be seen that normalised η is quite stable even after extended contact with deionised water shown in Figure.6.13 (b). It shows that the sensor is able to work in a water environment which was a challenge in gratings recorded in photopolymer compositions utilising a PVA binder.
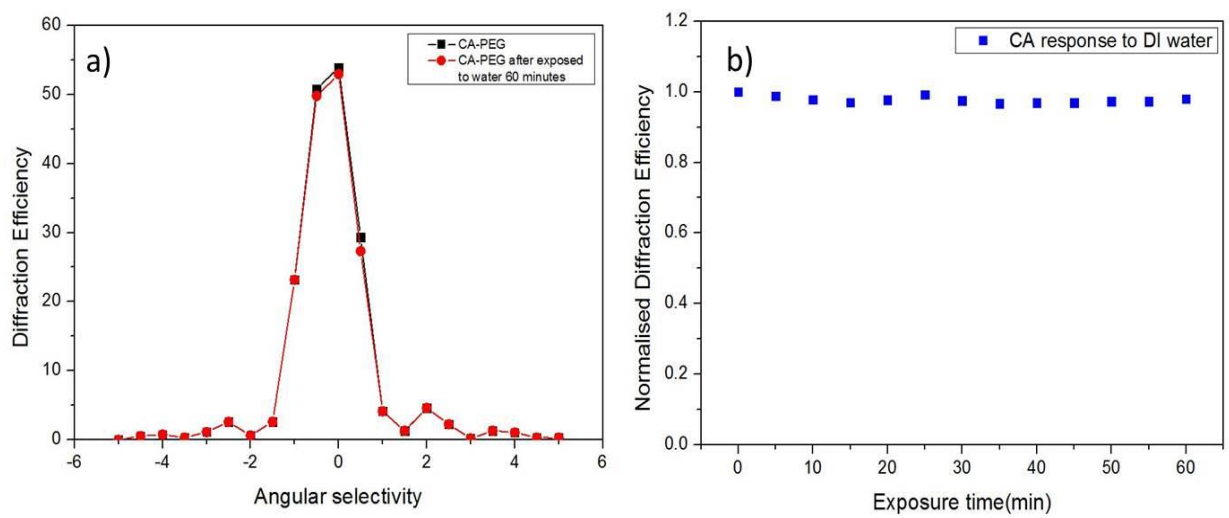
Figure 6. 13. (a) Bragg selectivity curve composition (D) with spatial frequency at 800 l/mm recorded in layers with thickness of 70 µm ± 10 µm before water exposure ─■─ after exposure to water ─●─ and (b) normalised diffraction efficiency vs. DI water exposure response was investigated at different time of intervals for sample thickness of 70µm ± 10 µm

6.4.2. Investigation of the dependence of Δn on CA-PEG photopolymers thickness

Volume phase gratings were recorded with a spatial variation of the refractive index. Depending on the permeability of the polymer matrix which greatly affects the diffusion rate, the main contributor to the refractive index modulation can be either density change or molecular polarisability change [17]. When a photosensitive layer is exposed to an interfering laser beam of appropriate wavelength and intensity, the dye molecules (EB) enter into an excited singlet state. From this state, they undergo intersystem

crossing, to an excited triplet state. The dye molecule in this state will react with an electron donor (NPG) to produce free radicals. These free radicals react with monomer molecules to start a polymerization reaction. When a photosensitive medium is exposed to interfering beams, monomer (AA-BAA) molecules in the light exposed areas are polymerized and the unexposed regions are not polymerized. This creates a monomer concentration gradient, which results in the diffusion of monomer molecules from dark fringe regions into the bright fringe regions. This results in a spatial density distribution of refractive index between exposed and unexposed regions of the interference pattern. The diffusion time depends on fringe spacing. At low spatial frequencies, where fringe spacing is large the diffusion time is long. Whereas in higher spatial frequencies, fringe spacing decreases, the diffusion time becomes shorter. Holographic patterning of the photopolymer leads to the spatial variation of the refractive index of the material due to photopolymerization and diffusion of photopolymer components [18]. The ratio of the polymerisation rate to the rate of diffusion is an important factor. The dependence of Δn on sample layer thicknesses ranging from 50-100µm was determined by recording volume transmission gratings at total exposure energy $300mJ/cm^2$ for a spatial frequency 800 l/mm as can be seen in Figure 6.14. Δn was calculated for each sample by using equation 6.2. 70µm thick layers for 800l/mm was found to be an optimum and achieved a maximum Δn of 2.2×10^{-3}, Δn 1.0×10^{-3} for 50 µm and Δn 1.1×10^{-3} for 100 µm layers were determined using diffraction efficiency measurements η.
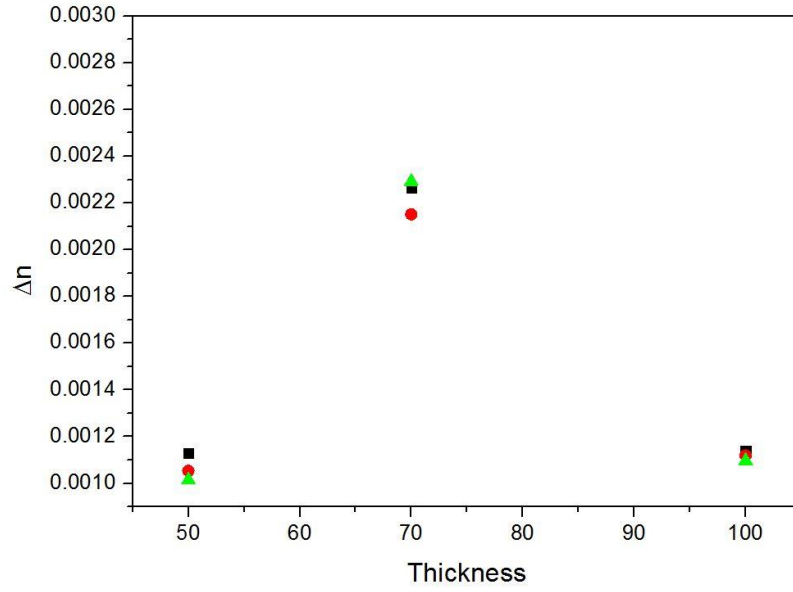
Figure 6. 14. Δn vs sample thickness 50-100μm ± 10 μm for CA-PEG photopolymer composition.

6.4.3. Investigation of the dependence of Δn and intensity for CA-PEG photopolymers

The intensity and exposure energy dependence of the CA-PEG photopolymers was investigated by recording 3 replicate transmission gratings in 70 ± 10 μm thick layers using the holographic setup outlined in section 6.3.1 at a spatial frequency of 800 l/mm. The total recording intensity was varied from 3-15 mW/cm^2, and the exposure energy was kept constant at 300 mJ/cm^2 to study the recording dynamics in real time. The results for the Δn of gratings recorded at each recording intensity in the CA-PEG photopolymer layers, real time diffraction growth curves of transmission gratings recorded in the 70 ± 10μm thick CA-PEG layers and Bragg curves shown in Figures. 6.15-6.18.
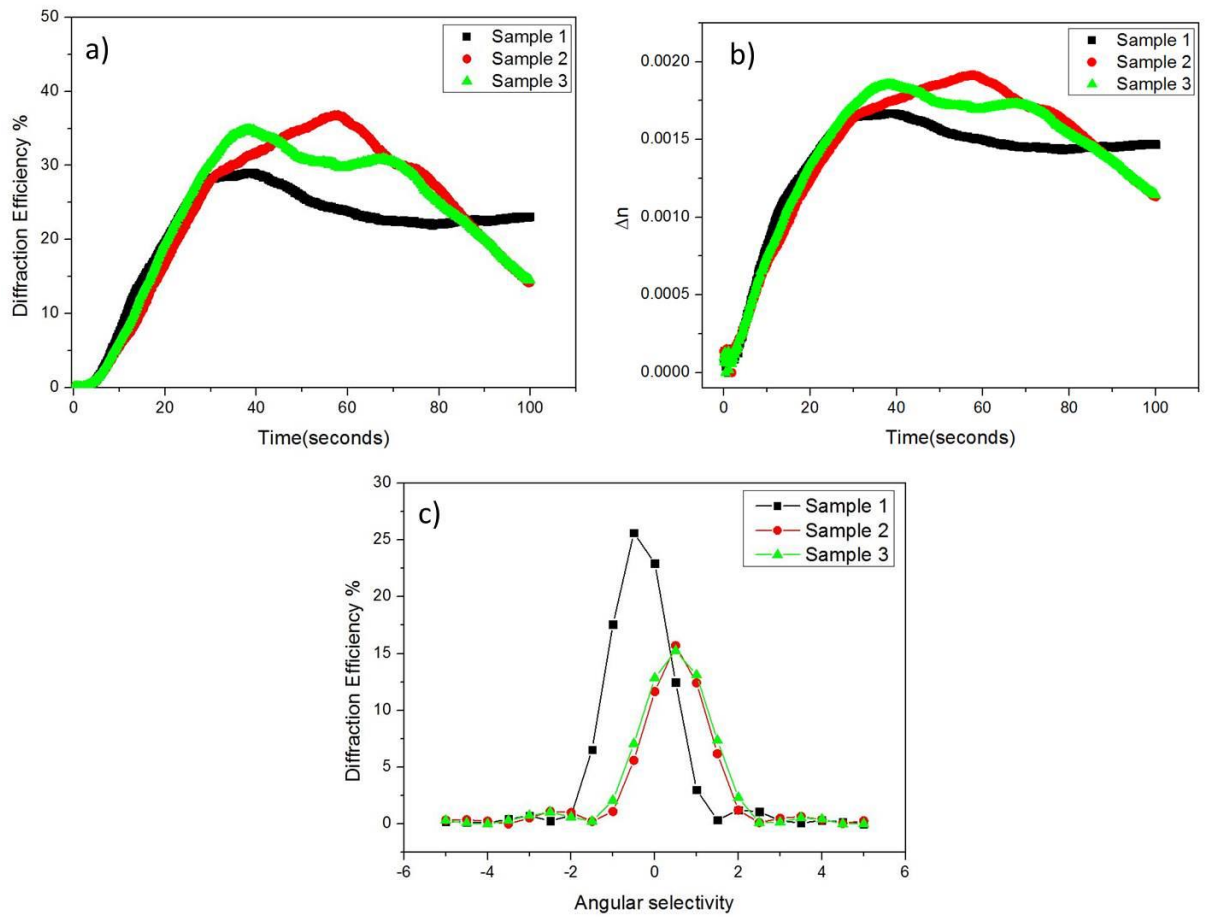
Figure 6. 15. (a). Real time measurements of the diffraction efficiency of gratings recorded in CA-PEG layers of 70µm ± 10 µm thickness; recording intensity 3mW/cm² and the spatial frequency is 800 l/mm (b) refractive index calculated and (c) Bragg selectivity curves of recorded holograms
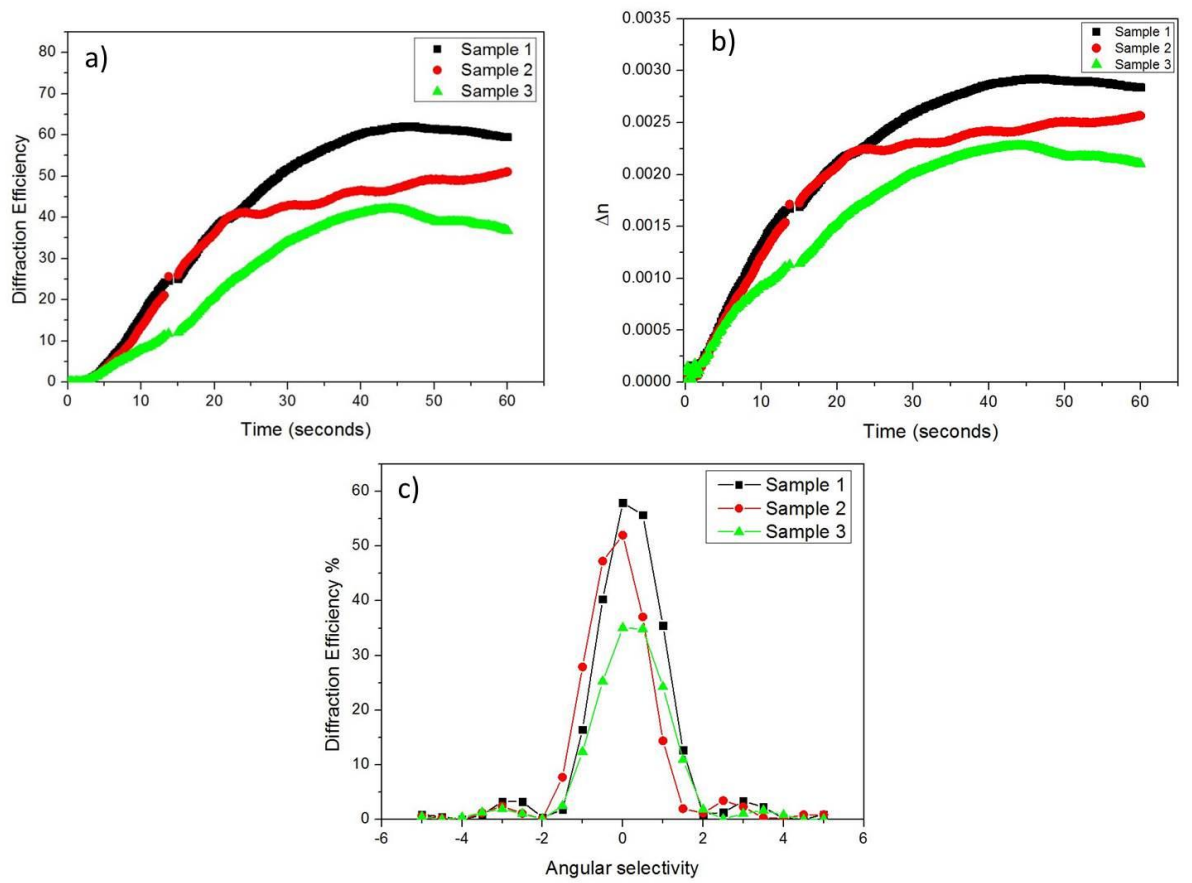
Figure 6. 16. (a). Real time measurements of the diffraction efficiency of gratings recorded in CA-PEG layers of 70µm ± 10 µm thickness; recording intensity 5mW/cm² and the spatial frequency is 800 l/mm (b) refractive index calculated and (c) Bragg selectivity curves of recorded holograms
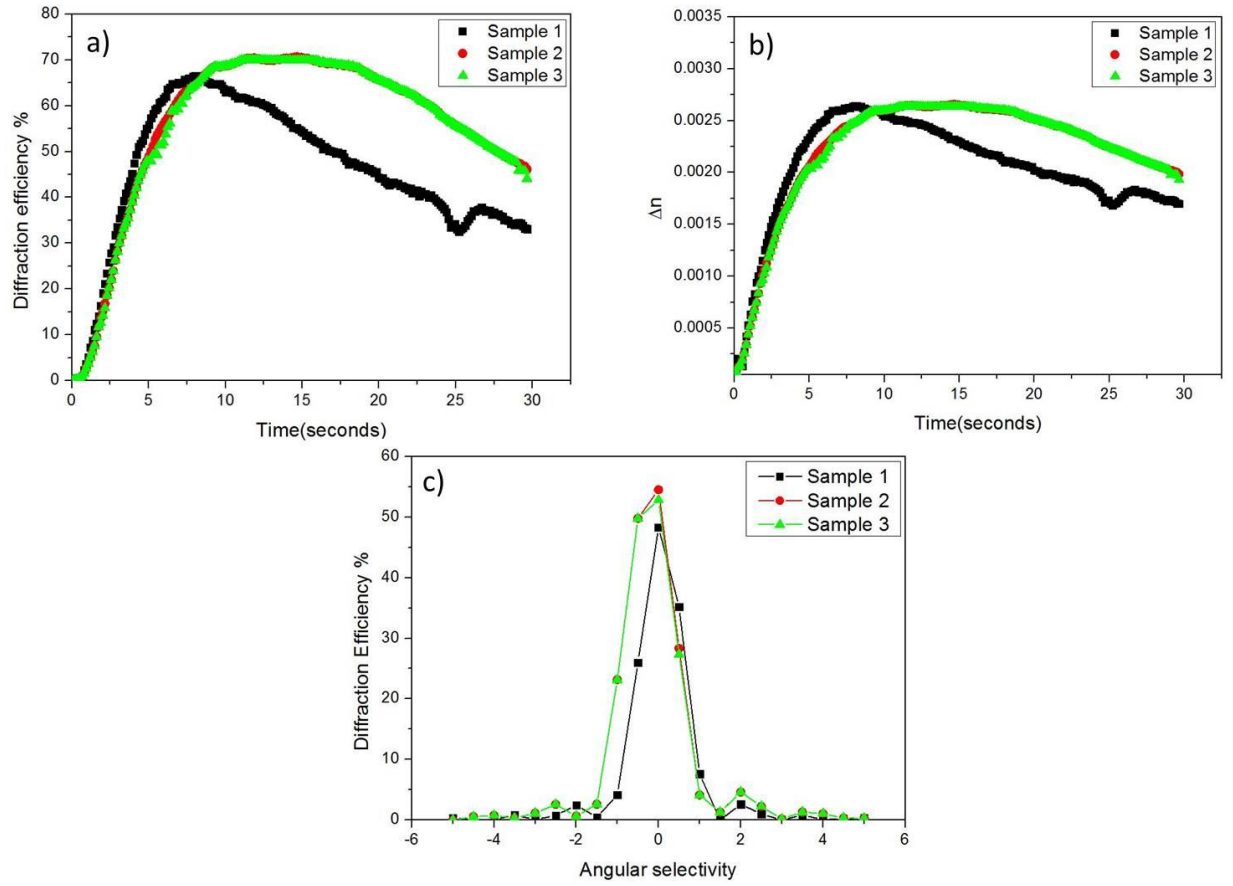
Figure 6. 17. (a). Real time measurements of the diffraction efficiency of gratings recorded in CA-PEG layers of 70µm ± 10 µm thickness; recording intensity 10mW/cm² and the spatial frequency is 800 l/mm (b) refractive index calculated and (c) Bragg selectivity curves of recorded holograms
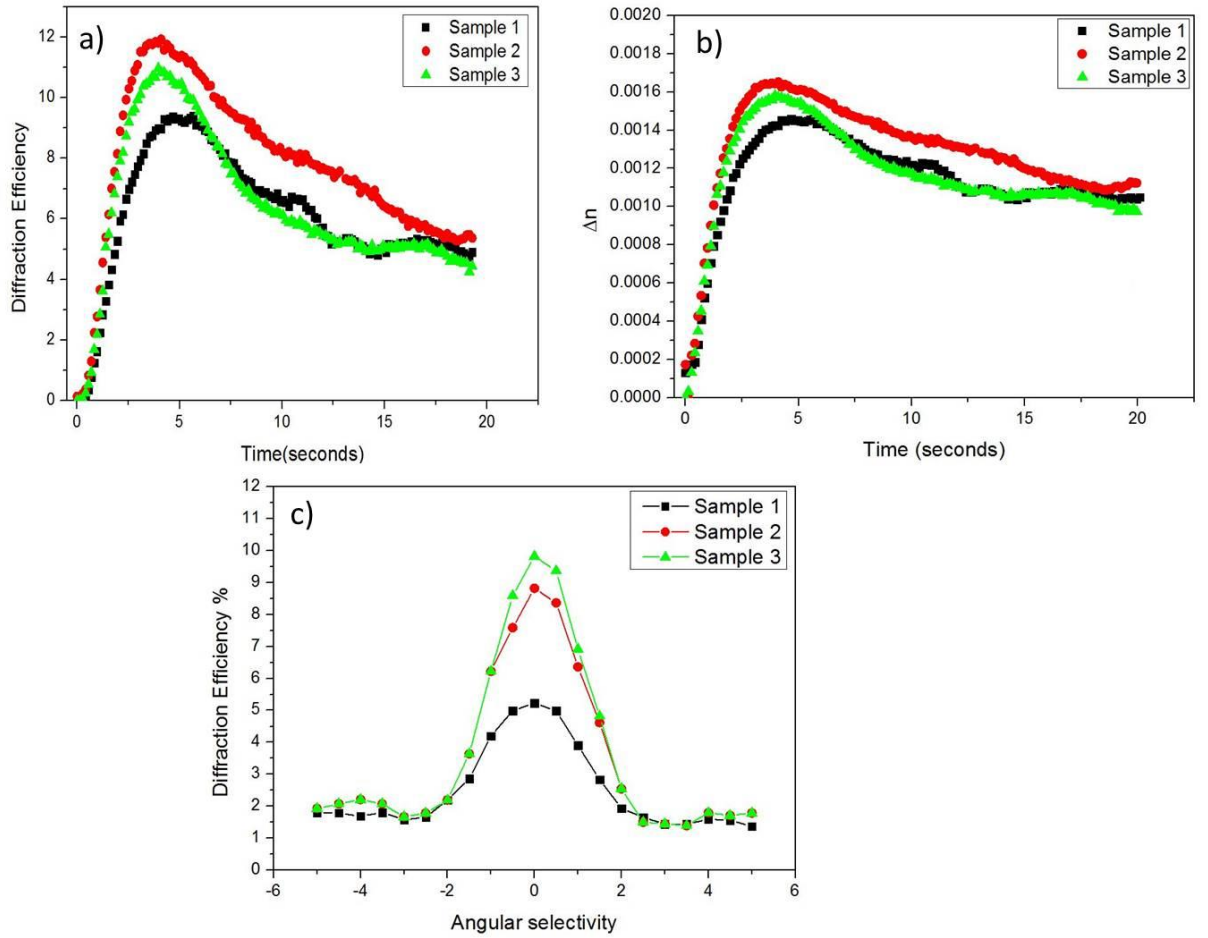
Figure 6. 18. (a). Real time measurements of the diffraction efficiency of gratings recorded in CA-PEG layers of 70μm ± 10 μm thickness; recording intensity 15mW/cm² and the spatial frequency is 800 l/mm (b) refractive index calculated and (c) Bragg selectivity curves of recorded holograms

Diffusion of polymer chains from illuminated to non illuminated regions during holographic recording results in deterioration of grating quality, and significantly η decreases if the exposure is long enough. Therefore, the optimum intensity studies were investigated in above graphs. It was concluded for CA-PEG holographic recordings that 10mW/cm² intensity recorded diffraction gratings (Figure 6.17) had the highest value of 70% for η in real time curves. This condition also achieved a maximum Δn of 2.6×10^{-3} and 52% η was recorded after total exposure time obtained for Bragg curves. However this feature is suitable for production on a large scale in industry, at high intensities short recording times are needed in order to optimise fabrication efficiencies. Also one more desirable feature observed in the CA-PEG material that it is not sensitive to small

changes in intensity, taking into account the results obtained with 5mW/cm^2 intensity recorded diffraction gratings (Figure 6.16). The highest value of 60% for η was obtained in real time curves; it also achieved a maximum Δn of 2.2×10^{-3} and 52% for η was recorded after total exposure time obtained Bragg curves. In Figure 6.19 the mean value of three recorded gratings Δn vs. recording intensities were plotted. It was observed that in all intensities maximum Δn values were obtained after 100 seconds exposure time. At 3mW/cm^2 maximum Δn 1.2×10^{-3} recorded after 120 seconds, 5mW/cm^2 maximum Δn 2.1×10^{-3} recorded after 100 seconds, 10mW/cm^2 maximum Δn 2.5×10^{-3} recorded after 100 seconds and 15mW/cm^2 maximum Δn 1.4×10^{-3} recorded after 105 seconds.
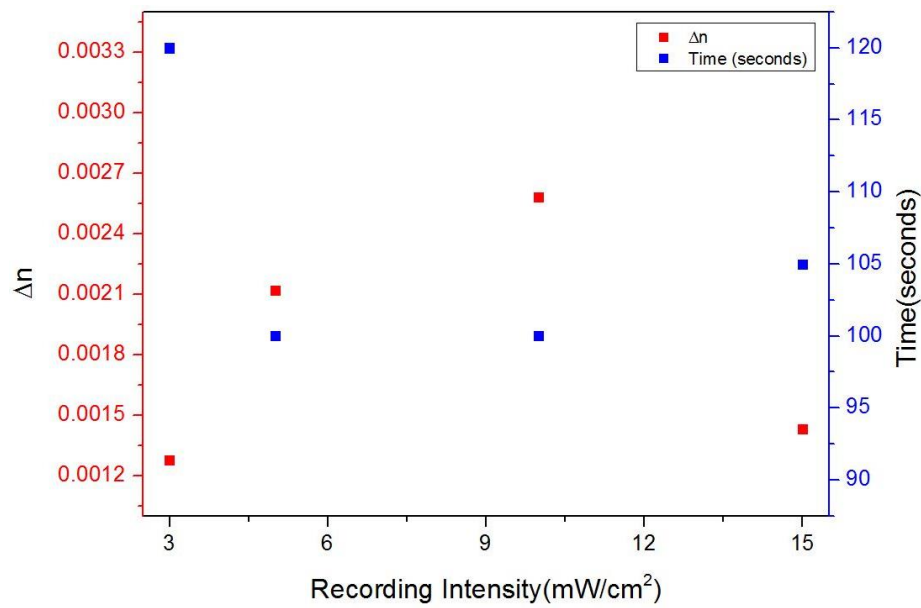
Figure 6. 19. Δn and exposure time vs. recording intensity (mW/cm^2) for the CA-PEG photopolymer at 800l/mm.

The rate of polymerisation is proportional to the recording intensity used, as this controls the number of photons available to produce free radicals which initiate the polymerisation reaction. If the polymerisation rate is very fast, as is the case at higher recording intensities in the results presented in above graphs, the diffusion rate must be

fast also in order to facilitate the movement of the monomer molecules within the illuminated regions, so that they can react with a free radical and be polymerised. (This also results in an increase in the rate of termination due to the increased concentration of free radicals available for recombination. This most likely explains the observed drop in Δn as the recording intensity is increased to 15 mW/cm^2). The difference in refractive index, Δn, typically increases with the intensity of irradiation. However it was found that at the highest radiation intensity there was a decrease in Δn. At lower intensities, there was time for monomer to diffuse from the non irradiated region to the irradiated region. But at the highest intensity, the polymerisation rate was so fast that the monomer did not have enough time to diffuse to the irradiated region and this resulted in a smaller difference between the refractive indices of the irradiated and non irradiated regions.

6.4.5. AFM analysis

The surface roughness parameters were calculated from the AFM images using an AFM software program. Figure 6.20(a) shows 3- dimensional surface view of CA-PEG recorded hologram. In all recorded holograms views, nodule formation was a prominent feature (a nodule is a mass of polymer molecule agglomerates that are entangled with each other). ''Nodules are defined as spherical cells that are compacted irregularly at the membrane surface''[19]. Each nodule contains several tens of thousands of macromolecules. Schultz and Asunmaa were the first to report the observation of nodules on the surface of an ultrathin cellulose acetate membrane by electron microscope. AFM images in Figure 6.20 (b) represents 3-dimensional views recorded CA-PEG hologram exposed to deionised water.
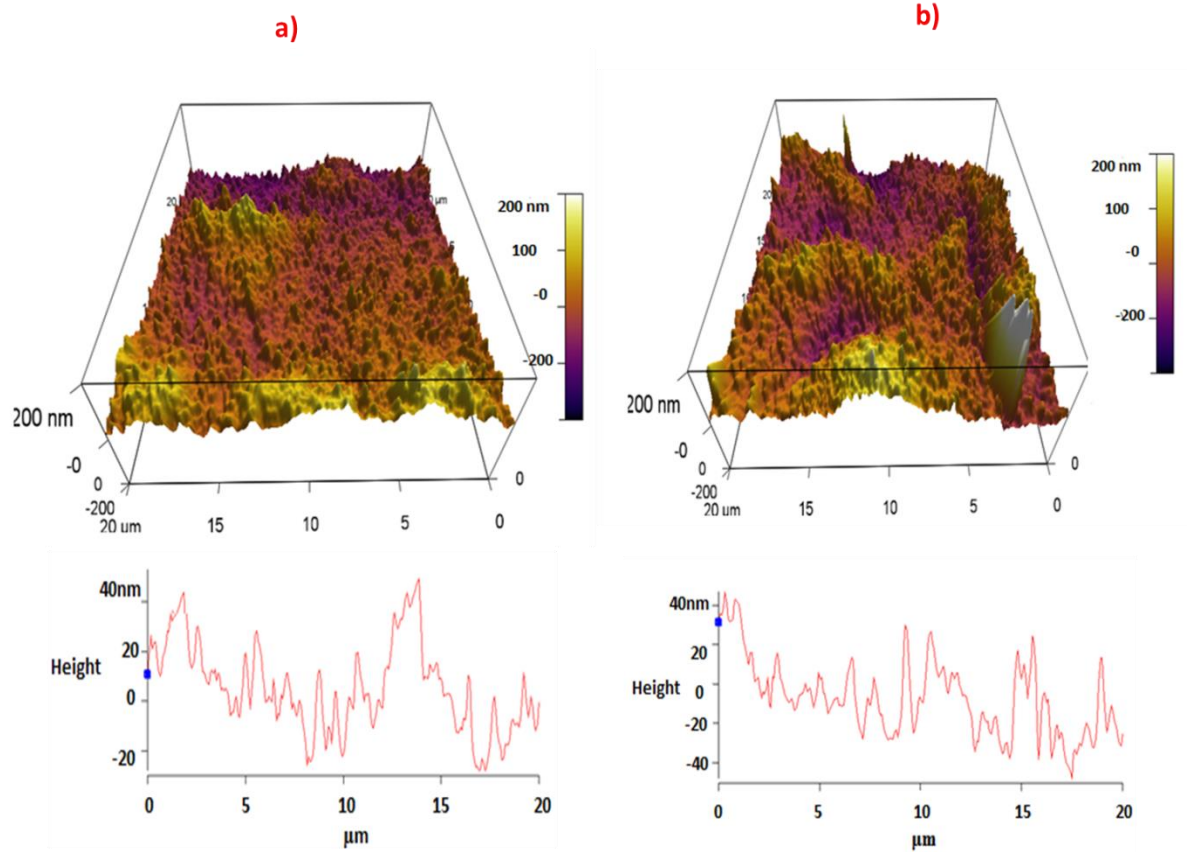
Figure 6. 20. AFM images 3 dimensional view of (a) CA-PEG recorded volume hologram (b) CA-PEG recorded volume hologram exposed to water (spatial frequency 800 lines/mm)

Table 6.2 represents the average roughness (Ra), root mean square average (RMS) values of all peaks to valley distances and height. These parameters were calculated by using AFM software. Ra is the average values of the measured height deviations from the mean surface taken within the evaluation area, Rms is the root mean square average of the measured height deviations from the mean surface taken within the evaluation area [20]. Atomic force microscopy images indicated that on exposure to water possibly leads to an increase in surface roughness (Rms) and decrease in pore size. There is no drastic change observed in average roughness (Ra) parameters of the layer.

Table 6. 2. Average roughness (Ra), root mean square average (Rms)and height

Hologram type	Ra (nm)	Rms (nm)	Height (nm)
CA-PEG	20 ± 5	35 ± 13	50
CA-PEG exposed to water	22 ± 9	43 ± 10	80

6.4.6. Characterisation of materials hardness

Pendulum hardness apparatus was used for coating hardness evaluation. The test consists of measuring the damping time of a pendulum oscillating on a test surface. The hardness is function of the oscillation amplitude, detected by electronic optical cells from 2 specified pendulum deflection positions Figure 6.21.
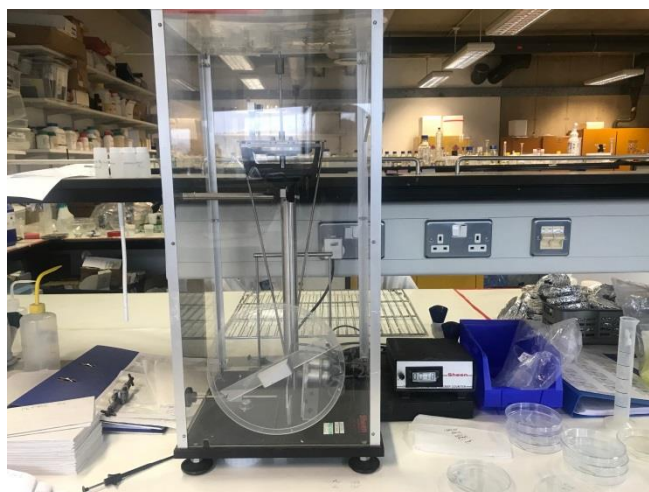
Figure 6. 21. Pendulum Hardness Tester

The lower the value of oscillations indicated the softer the material, higher value indicated hard material. Below graphs shows the number of oscillations results recorded

of coated layers of CA, CA-PEG, SRG, photopolymer and glass substrate. All the readings were repeated thrice in order to confirm the results and mean values are reported in the graph. The results clearly showed that the CA-PEG are harder than IEO photopolymer; 76 oscillations were recorded for CA-PEG layers and 4 oscillations were recorded for acrylamide based photopolymer. 120 oscillations were recorded for pure cellulose and 83 oscillations were recorded for SRG platform as can be seen in Figure 6.22 The SRG platform was used in CH 5 and 6 in order to modify the sensors.
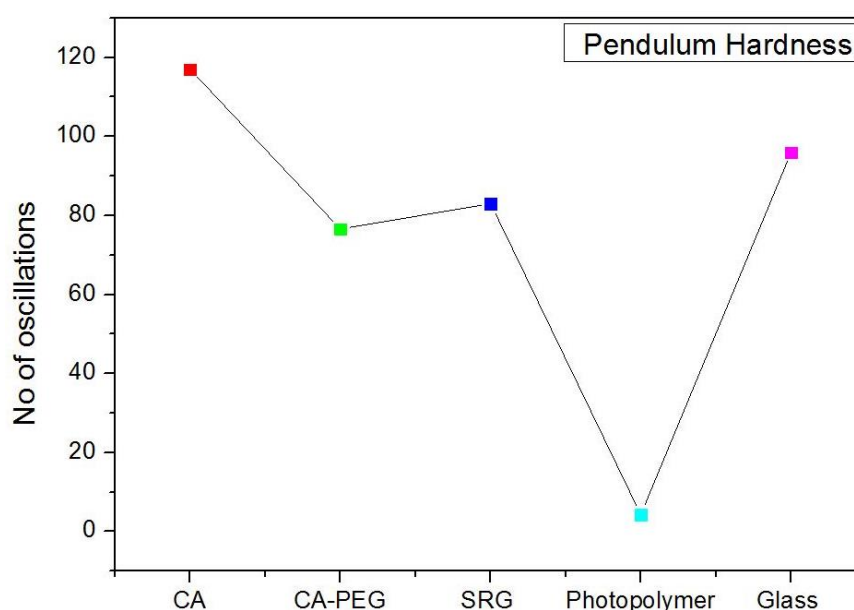
Figure 6. 22. Pendulum hardness studies of CA, CA-PEG, SRG, Photopolymer and glass substrate

6.4.7. Preliminary test of the VHG as a sensor

6.4.7.1. Preparation of sensing layer with TBC

The volume holograms were further modified with Calixarenes ionophores (TBC) in CA-PEG membrane. Previously TBC was used for the detection of sodium in order to modify SRG and results were presented in CH 6. Here after obtaining homogenous viscous solution of CA-PEG. TBC and sodium tetraphenylborate were added to a solution and stirred at 80 °C for another 3 hours until all the chemicals completely dissolved. The composition of chemicals that were used during this experiment is

presented in table 6.3. The viscous and clear solution was obtained which was termed as a blended solution, CA-PEG-TBC. The same procedure which is mentioned in section 6.22 was followed.

Table 6. 3. Composition of the sensing layer

Components	Amounts (g)	Amount in dry layer(%w/w)
Tetraethyl 4-tert-butylcalix[4]arene (TBC)	0.1	0.90
Sodium tetraphenylborate	0.05	0.45

The preliminary results are shown in Figure 6.23. The functionalised sensor was exposed to deionised water and 150mM $NaNO_3$. Maximum diffraction efficiency achieved in this functionalised composition was 25% at 300 mJ/cm^2 exposure (Figure 6.8) and after exposure to Na^+ 150mM the diffraction efficiency dropped down to 19%.
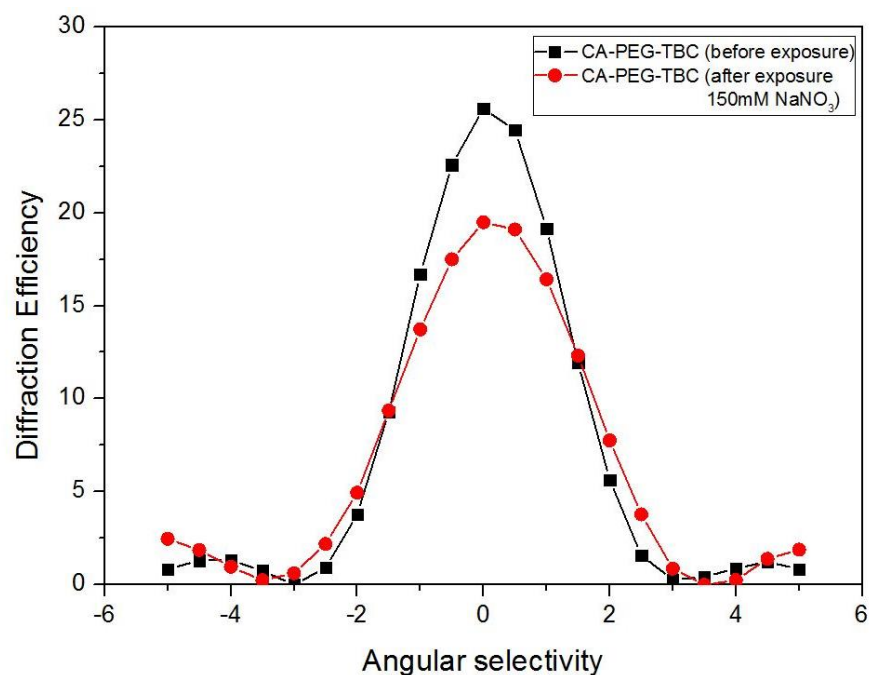
Figure 6. 23. Bragg selectivity curve CA-PEG-TBC (Before and after 8 min exposure to analyte 150mM NaNO₃) with spatial frequency at 800 l/mm recorded in layers with thickness of 70 µm ± 10 µm

The present results yield a response to Na^+ as can be seen in Figure 6.24. The increase in normalised diffraction efficiency was observed during exposure to water this is probably when it exposed to water swelling of the surface leads to change in the refractive index in the layer and after 4 minutes it came back to its original position normalised diffraction efficiency drops down 1.0 to 0.94. Whereas on exposure to sodium solution normalised diffraction efficiency drops down from 1.0 to 0.77 after 6mins.
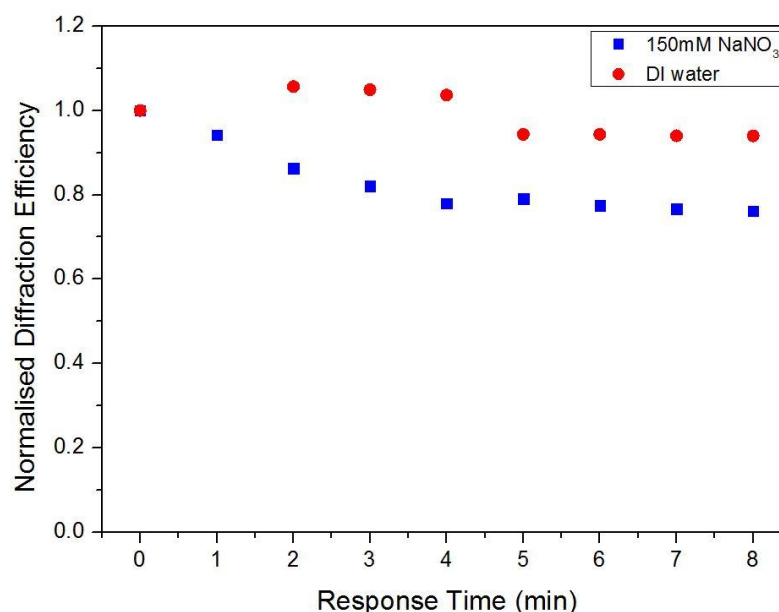
Figure 6. 24. Normalised diffraction efficiency change response CA-PEG blended with TBC on exposure to deionised water (DI) and 150mM Na$^+$

In Figure 6.25 three different matrices results were compared on exposure to 150mM NaNO$_3$. It is clearly seen that the sol gel (SRG) is more responsive as compared to PVC (SRG) and CA-PEG (VHG). This is obvious because the analyte materials can easily diffuse into the matrix and also response time is fast. However in volume gratings the analyte has to diffuse in through the volume of the membrane layer but the preparation of VHG are less complex as compared to SRG. Both methods have their own pros and cons but both methods can be used to fabricate sensors. Also the amount of ionophores is 10 times higher in SRG modified layers but in current composition of volume holograms cannot accommodate the greater amount of TBC in the layers because layers became scattering and opaque with the higher amount of ionophore. In order to achieve higher diffraction efficiency good optical quality layers is a prerequisite.
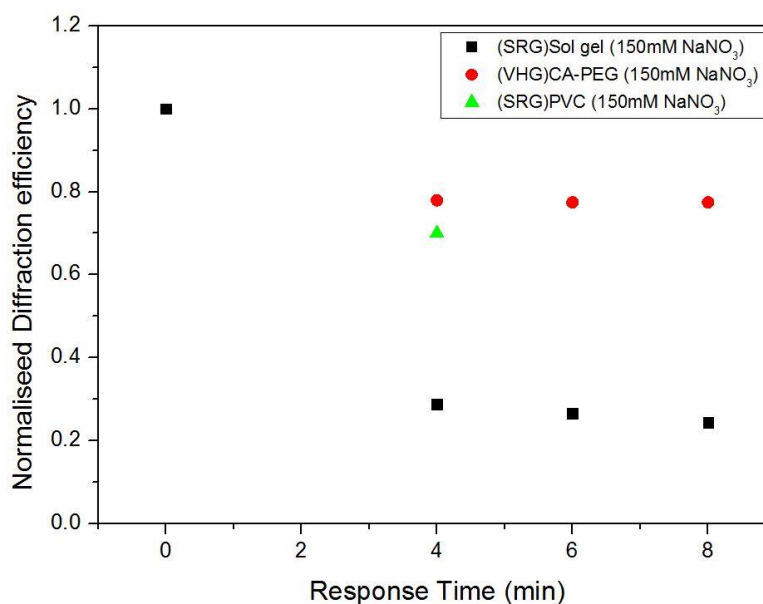
Figure 6. 25. Comparison of normalised diffraction efficiency change response SRG Sol gel, Volume CA-PEG blended with TBC and SRG PVC+DOPT on exposure to 150mM NaNO$_3$

Overall it can be stated that:

- SRG modified with sol gel has greater signal and fast response because of the porous nature of the matrix

- SRG modified with PVC has also fast response time in comparison to VHG CA-PEG

- VHG CA-PEG matrix has smaller signal in comparison to other two matrices possibly because the diffusion of analyte is slow in volume holograms whereas diffusion is much faster in surface holograms.

6.5. Conclusions

A new photopolymer formulation based on CA-PEG blend was developed; volume holograms were recorded successfully with this formulation. The recording conditions and thickness were optimised at 800l/mm. The novel formulation was found stable in water environment. A maximum η 70% was found in growth curves, 52% was obtained

Bragg curves and maximum Δn 2.6×10^{-3} was extracted in preliminary studies. Moreover, CA-PEG polymers used in this study contain a biopolymer, which is promising and leads to sustainable chemistry. Response to DI water was also investigated and the results are very promising as the diffraction efficiency does not drop down after exposure to water for 60min. Intensity dependence characterisation studies show that the material has a good response to a large range of intensities. It allows for exposure times to be significantly reduced via the use of high recording intensities, which is desirable feature for industry applications that would reduce production times. AFM measurements provided information at surface level. One of the key advantages of cellulose based holograms that they can easily be peeled off and thus they can be used in the applications where self-standing holograms are needed. Recorded holograms were found to be stable, robust and reproducible. The method can easily modified by adding different modifiers according to the interest. This new holographic formulation has a potential to work as a sensor with appropriate additives.

References

[1]   T. Mikulchyk, J. Walshe, D. Cody, S. Martin, and I. Naydenova, "Humidity and temperature induced changes in the diffraction efficiency and the Bragg angle of slanted photopolymer-based holographic gratings," *Sensors and Actuators, B: Chemical*, vol. 239, pp. 776–785, 2017.

[2]   A. Kaiser, W. J. Stark, and R. N. Grass, "Rapid Production of a Porous Cellulose Acetate Membrane for Water Filtration using Readily Available Chemicals," *Journal of Chemical Education*, vol. 94, no. 4, pp. 483–487, 2017.

[3]   A. K. Yetisen, I. Naydenova, F. Da Cruz Vasconcellos, J. Blyth, and C. R. Lowe, "Holographic sensors: Three-dimensional analyte-sensitive nanostructures and their applications," *Chemical Reviews*, vol. 114, no. 20, pp. 10654–10696, 2014.

[4]   S. Milovanovic, T. Adamovic, K. Aksentijevic, D. Misic, J. Ivanovic, and I. Zizovic, "Cellulose Acetate Based Material with Antibacterial Properties Created by Supercritical Solvent Impregnation," *International Journal of Polymer Science*, vol. 2017, 2017.

[5]   S. Waheed, A. Ahmad, S. M. Khan, M. Hussain, T. Jamil, and M. Zuber, "Synthesis, characterization and permeation performance of cellulose acetate/polyethylene glycol-600 membranes loaded with silver particles for ultra low pressure reverse osmosis," *Journal of the Taiwan Institute of Chemical Engineers*, vol. 57, pp. 129–138, 2015.

[6]   S. Waheed, A. Ahmad, S. Maqsood, S.- Gul, and T. Jamil, "Synthesis , characterization , permeation and antibacterial properties of cellulose acetate / polyethylene glycol membranes modi fi ed with chitosan," *DES*, vol. 351, pp.

59–69, 2014.

[7]   A. Rezaei, A. Nasirpour, and M. Fathi, "Application of cellulosic nanofibers in food science using electrospinning and its potential risk," *Comprehensive Reviews in Food Science and Food Safety*, vol. 14, no. 3, pp. 269–284, 2015.

[8]   S.- Gul, S. Waheed, A. Ahmad, S. Maqsood, M. Hussain, T. Jamil, and M. Zuber, "Journal of the Taiwan Institute of Chemical Engineers Synthesis , characterization and permeation performance of cellulose acetate / polyethylene glycol-600 membranes loaded with silver particles for ultra low pressure reverse osmosis," *Journal of the Taiwan Institute of Chemical Engineers*, vol. 57, pp. 129–138, 2015.

[9]   http://www.assignmentpoint.com/science/chemistry/polyethylene-glycol.html website {accessed on 14-11-2018].

[10]   Birabassov, T. V Galstian, F. Dechamplain, and a M. R. Ritcey, "Azo-dye-doped cellulose acetate for optical data storage and processing," *Proceedings of SPIE*, no. 418, pp. 704–709, 1998.

[11]   K. Wang, L. Guo, L. Zhou, and J. Zhu, "Imaging mechanism of the holographic recording material dichromated cellulose triacetate.," *Applied optics*, vol. 35, no. 32, pp. 6369–74, 1996.

[12]   T. Mikulchyk, S. Martin, and I. Naydenova, "N-isopropylacrylamide-based photopolymer for holographic recording of thermosensitive transmission and reflection gratings," *Applied Optics*, vol. 56, no. 22, p. 6348, 2017.

[13]   M. Moothanchery, I. Naydenova, and V. Toal, "Study of the shrinkage caused by holographic grating formation in acrylamide based photopolymer film," *Optics*

Express, vol. 19, no. 14, p. 13386, 2011.

[14]   H. Kogelnik, "Coupled Wave Theory for Thick Hologram Gratings," *Bell System Technical Journal*, vol. 48, no. 9, pp. 2909–2947, 1969.

[15]   P.Hariharan, *Context-aware user-driven news recommendation*, vol. 1542, no. 9. University of Sydney, Australia: Cambridge University Press, 2015.

[16]   W. R. Klein and B. D. Cook, "Unified Approach to Ultrasonic Light Diffraction," *IEEE Transactions on Sonics and Ultrasonics*, vol. 14, no. 3, pp. 123–134, 1967.

[17]   M. S. Mahmud, I. Naydenova, T. Babeva, R. Jallapuram, S. Martin, and V. Toal, "Determination of threshold exposure and intensity for recording holograms in thick green-sensitive acrylamide-based photopolymer.," *Applied optics*, vol. 49, no. 28, pp. 5276–5283, 2010.

[18]   I. Naydenova, R. Jallapuram, R. Howard, S. Martin, and V. Toal, "Investigation of the diffusion processes in a self-processing acrylamide-based photopolymer system.," *Applied optics*, vol. 43, no. 14, pp. 2900–2905, 2004.

[19]   I. M. Wienk, T. van den Boomgaard, and C. A. Smolders, "The formation of nodular structures in the top layer of ultrafiltration membranes," *Journal of Applied Polymer Science*, vol. 53, no. 8, pp. 1011–1023, 1994.

[20]   N. Gizli, "Morphological Characterization of Cellulose Acetate Based Reverse Osmosis Membranes By Atomic Force," *Chemistry & Chemical Technology*, vol. 5, no. 3, 2011.

Chapter 7 – Conclusions and Future work

7.1. Main conclusions from PhD research

In this thesis, the development and characterisation of novel holographic chemical sensors has been described. The aim of the current project was to develop holographic chemical sensors based on transmission holograms. The main focus was on surface relief holograms modified by coating the structured photopolymer surface with different analyte sensitive materials and in view of their application in environmental monitoring and biomedical sensing. The response to different analytes in liquid phase was investigated. A change in diffraction efficiency was observed with time and as molar concentration of the analytes increased. Two separate approaches were adopted. First for the development of the holographic sensors SRG photonic structures were utilised as a platform for the sensor fabrication. The proposed technology platform for preparation of sensors is flexible, because the selectivity can be readily tuned by modification of the chemical structure of the functionalising layer. The second approach use of volume holographic gratings required development a new photopolymer formulation which is stable in liquid environment. During the PhD research a new photopolymer formulation to author's knowledge was developed based on cellulose acetate and polyethylene glycol binder. The proposed photopolymer formulation was found to be stable in liquid environment. The main conclusions from this research are as follows:

1. A method for fabrication of SRG with pre-defined properties has been developed and repeatable used to fabricate the photonic structured used as a platform for the sensor. Initially unslanted volume diffraction grating with spatial frequency of 300lines/mm and diffraction efficiency of $60 \pm 5\%$ in $30 \pm$

3μm thick layers after exposure to the total recording intensity of 10 mW/cm^2 for 100 sec. After exposure to elevated temperatures for 100 minutes the volume grating was almost completely erased. Surface properties were studied under WLI and AFM the amplitude of the recorded grating was < 10nm and after thermal treatment it increased up to 350-400 nm and the diffraction efficiency of the photonic structure was 35%. The SRG were utilised as a sensor platform by coating their surface with different layers. The primary advantage of surface relief grating structures for sensing application is that the target analyte is not required to permeate fully into the structure. SRG platform are promising for sensors applications.

2. Surface relief structures (SRG) photonic structures were investigated by the incorporation of zeolite nanoparticles in the fabrication of chemical sensor for view of their application in environmental sensing. The response of the sensor was investigated with copper, lead, calcium, potassium and sodium analytes. This sensor was found more selective for divalent cations than monocations present in water.

3. Photonic structures were sucessfully modified for biosensor fabrication by using Dibenzo18-crown-6 chelating [1] agents and calixarenes ionophores on surface relief structures. These sensors were found to detect physiological ranges of potassium and sodium in model serum samples.

4. A new formulation based on cellulose acetate and polyethylene glycol (CA-PEG) binder was developed which can operate in water enviroment.

5. Voulme holograms were recorded and characterised sucessfully in CA-PEG photopolymer. The material and recording conditions for 800l/mm CA-PEG based holograms were optimised.

The work presented in this thesis it can be divided in five main groups (Figure 7.1):

1. Fabrication of reproducible sensing platforms based on SRG

2. Modification of the sensing platform with different analyte sensitive materials (environmental and biosensor)

3. Characterisation of sensing platform before and after modification

4. Test the sensor device response in the presence of analytes

5. Development of CA-PEG volume holograms
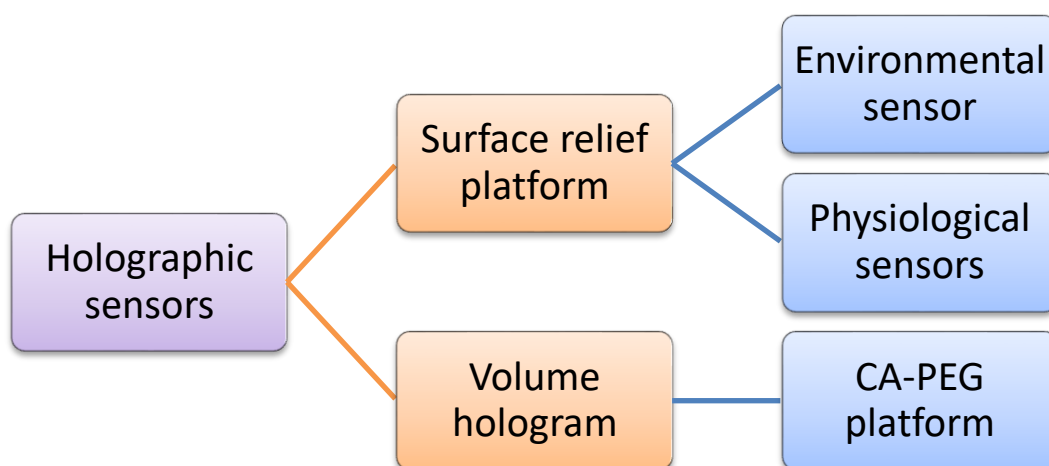
Figure 7. 1. Holographic sensors developed during the research

7.2. Development of the novel SRG environmental sensor for divalent cations detection

The novel sensors are created by holographic recording of surface relief structures in a self-processing photopolymer material and modified by spin coating LTL-zeolites in a sol- gel. To the best of author's knowledge, this is the first use of such type of SRG coated with a sensing layer for analytes detection. The fabrication of sensor is

repeatable, reproducible and characterised by good linearity limit for Pb^{2+} and Cu^{+2} up to 1-4mM and the sensor is also able to detect hardness of water. The loadings of LTL-zeolites were tailored in order to determine Cu^{2+}, Pb^{2+} and Ca^{2+} in model samples. Linear responses were obtained of the proposed sensors with the limit of detection Cu^{2+} 1.15 mM, Ca^{2+} 0.82 mM and for Pb^{2+} 0.73 mM, respectively. It was observed that they were more responsive to +2 oxidation state as compared to the mono oxidation sates. The advantage of disposable holographic sensor also has a relatively quick response time, is low cost, and allows for real time monitoring of environmental water quality.

7.3. Development of the novel SRG biosensor s for metal ion detection in model blood serums

Holographic sensors for the detection of metal ions were prepared by casting a sensing layer over surface relief structures with dibenzo-18-crown-6 or 4-tert-butylcalix[4]arene. Dibenzo-18-crown-6 provides a selective response of the devices to K^+ over Na^+, whereas for tetraethyl 4-tert-butylcalix[4]arene there is a dominant response for Na^+ over K^+ [2]. It was found that the sensor which was functionalised with dibenzo-18-crown-6 was less responsive towards Na^+ ions and more responsive for K^+ ions. Whereas, tetraethyl 4-tert-butylcalix[4]arene was more responsive to Na^+ compared to the results for K^+ ions. Evaluation of the sensitivity in PVC matrix containing DC or TBC was demonstrated. The aim of this study was to detect physiological ranges of potassium and sodium in serum [3]. The porosity of the matrix improved by utilising TEOS (sol gel) coated layers. Selective response of the sensor was achieved by coating with DC or TBC in sol gel matrix. Novelty of this sensor is the usage of TBC ionophores in holographic sensors. To the best of author's knowledge; this is the first use of TBC in holographic sensors. The proposed sensor has ability to be used as a biosensor. The preliminary results indicate that the DE changes

with ion concentration. This novel transduction device gives response in 4 mins and its low cost disposable senor also can be integrated with portable devices.

7.4. Development of the novel photopolymer formulation based on cellulose acetate

A new photopolymer formulation based on CA-PEG blend was developed and volume holograms recorded successfully in this formulation. The recording conditions and thickness was optimised at spatial frequency of 800l/mm. A maximum diffraction efficiency of 50% was achieved. Moreover, CA-PEG polymers used in this study are based on a biopolymer, which is promising and leads to sustainable chemistry. Response to DI water was also investigated; and it was found that the diffraction efficiency did not drop down even after exposure to water for 60 minutes. One of the key advantages of cellulose based holograms can be easily peeled off thus they can be used as self-standing holograms. The recorded holograms were found to be robust as 74 oscillations values indicated by hardness test and reproducible maximum diffraction efficiency 70% was found in growth curves, 52% was obtained Bragg curves and maximum Δn 2.6×10^{-3}. The novel photopolymer is stable in liquid response because the recorded hologram was immersed in water for 60 minutes diffraction efficiency remains unchanged to 52%. To the best of author's knowledge, this is the first report of cellulose acetate - Polyethylene glycol based volume holograms with acrylamide, bisacrylamide, N-phenyl glycine.

7.5. Key contributions:

1. Successful development of new SRG chemical sensor platform sensitive to divalent cations

2. Successful development of new SRG biochemical sensor platform sensitive to metal cations

3. The current research work is a proof of concept rather than an actual analytical device. Further work is required in order to develop an actual device. Suggestions are made in future work section below.

4. Development of new holographic formulation based on cellulose acetate and polyethylene glycol blended membrane. Optimisation and characterisation of new water resistant photopolymer. Initial results showed that the material is capable of working in a liquid environment. Further work is required in order to investigate the properties of the material in detail in order to best avail of it in sensing.

7.6. Future plan

From the research that has been carried out to date, it is clear that there are many areas in which further work would be beneficial

- Further modifications of SRG photonic structures should be carried out in order to develop variety of sensors including gas sensors and humidity sensors. The advantage of these structures they can easily modify according to the application.

- New photopolymer composition based on cellulose acetate is an interesting outcome of this research. The advantage of this composition is that the porosity of the matrix can be controlled. One can have dense structure or have a porous

structure of the blended membrane. If amount of PEG increase the porosity of the membrane increase and it can help analyte materials easily to diffuse in.

- In the present research CA-PEG holograms were recorded only at 800l/mm. Optimisation at different spatial frequencies should be carried out in this material in order to investigate the response of the new photopolymer material on different spatial frequencies.

- It would be useful to record reflection holograms in the cellulose based photopolymer. Reflection holograms are useful for a number of different applications such as holographic optical components, sensors and security holograms.

- New photopolymer have ability to work as a sensor device. This should be further investigated.

- Further work needd to be done in order to develop a device which can work in real time at low cost. One device examples have showed in chapter 4 by combining the SRG with microfluidics chamber. One of the other possible ideas is to fabricate reflection volume hologram. These holograms have an advantage to reconstruct the image with a white light. The interaction with the analyte causes shrinkage or swelling of the sensitive medium. This leads to the variation in fringe spacing and, hence, the wavelength of the reflected light alters. In order to have a portable device colour change algorithms are required where the colour coordinates of the background objects which is similar to the operational colour range of the sensor [4]. Changes in the diffracted light wavelength can easily be captured by an image with mobile camera. The University of Cambridge is working to develop a pH sensitive sensor based on reflection holograms [4]. Multidisciplinary knowledge is required in order to image processing for

holographic sensors. The development of specific algorithms for colour quantification in which the camera characterisation process will be incorporated. In Figure 7.2 simple portable device is proposed which uses a holographic reflection grating. The sensor operates via changes in the wave- length (colour) of the diffracted light with exposure to an analyte. These sensors can be used as visual indicators which can be easily interpreted by non-specialist.

a). Holographic reflection grating
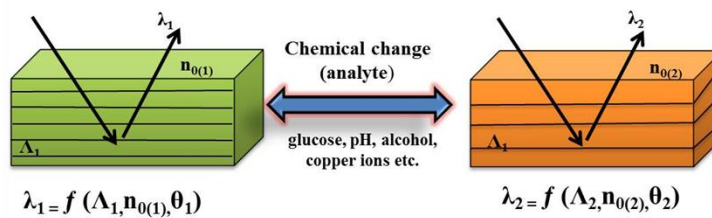
b). Camera colour sensitive profile before exposure to analyte

c). Camera colour sensitive profile after exposure to analyte
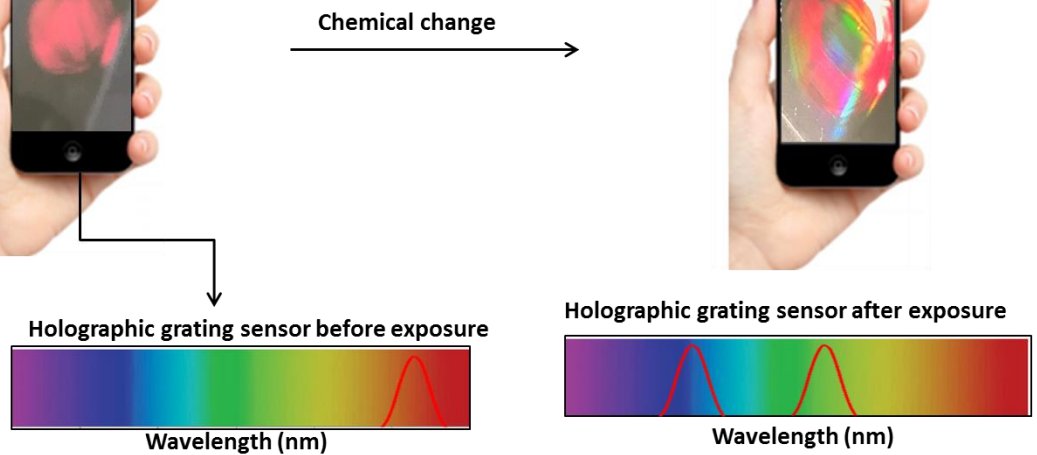
Figure 7. 2. (a) Holographic reflection gratings and (b) capturing of image of hologram before exposure to analyte (c) after exposure to analyte and analysing the colour change

IEO has been focused on holography and its applications using, low cost photopolymers which are water soluble and require no chemical or other form of further post recording

processing. IEO is capable of making acrylamide photopolymer reflection holograms that can be viewed in ordinary light, like the holograms on credit cards [5]. To allow cheap mass production holograms can be copied by optical means similar to holographic recording, or in the case of surface relief holograms they can be copied by stamping. Such stamped holograms can be used as security features on credit cards. The Royal Canadian Mint even produces holographic gold and silver coinage through a stamping process. The stamping process can be carried out with a simple heated press. The bottom layer of the duplicating film is heated above its softening point and pressed against the stamper so that it takes up its shape. This shape is retained when the film is cooled and removed from the press [6]. The SRGs recorded (master copy) in the current research work can easily be copied on Polydimethylsiloxane layer. However more work is required in order modify the copied structure in order to work as a sensing platform.

7.7. Dissemination of the PhD research

7.7.1. Journal Publications

- ❖ **S. Gul**, D. Coddy, A. Kharchenko, S. Martin, S. Mintova, J. Cassidy, I. Naydenov, Functionalised diffractive surface structures for application in development of environmental sensors, Microporous and Mesoporous Materials, 2018 [I.F 3.649]

- ❖ D. Coddy, **S. Gul**, T. Mikulchyk, M. Irfan, A. Kharchenko, K. Goldyn, S. Martin, S.Mintova, J. Cassidy, I. Naydenova, Self-processing photopolymer materials for versatile design and fabrication of holographic sensors and interactive holograms, Applied Optics, 2018[I.F 1.791]

7.7.2. Paper submitted

- ❖ **S.Gul**, J.Cassidy, I.Naydenova, Modified Surface Relief layer created by holographic lithography: Application to Sodium and Potassium Sensing (under review ''Sensors'')

7.7.3. Conference Proceedings

- ❖ **S.Gul**, Martin, J. Cassidy, I. Naydenova, Development of sensitive holographic devices for physiological metal ion detection, Proc. of SPIE Vol. 10354 103540C-1, 2017, doi: 10.1117/12.2275734.

7.7.4. Publications in process

- ❖ S. Gul, A. Kharchenko, S. Mintova, J. Cassidy, I. Naydenova, Development of modified surface relief photonic structures for detection of copper and calcium ions in water embedded with microfluidics chamber.

Publication on the new recording material

- ❖ S.Gul, J.Cassidy, I.Naydenova, A novel volume hologram based on cellulose acetate and polyethylene glycol composite material for holographic recording.

7.7.5. Oral presentations

- ❖ S. Gul, D. Cody, A. Kharchenko, V. Madjarova, T. Babeva, C. Barrett, S. Martin, S. Mintova, J. Cassidy, I. Naydenova, Modified photonic structures created by holography: Application to metal ions sensing, 30th International conference on Materials Chemistry and Science 27-28 August 2018, Toronto, Canada (oral presentation).

- ❖ T. Mikulchyk, S. Gul, P.Gilligan, J. Browne, I. Naydenova D. Cody, A colour-changing holographic sensor for calibration of the pressure output of therapeutic ultrasound, 3rd International Caparica conference on ultrasonic-based applications: from analysis to synthesis, 11-14 June 2018, Caparica Portugal.

- ❖ S. Gul, S. Martin, J. Cassidy, I. Naydenova, Development of sensitive holographic devices for physiological metal ion detection, SPIE Optics and photonics 6-7 August, 2017, San Diego, CA, United States (oral presentation).

- ❖ S. Gul, A. Kharchenko, S. Martin, S. Mintova, J. Cassidy, I. Naydenova, Holographic Sensors for the detection of liquid phase analytes, 7th Annual Graduate Research Symposium 16 February 2017, DIT, Ireland (oral presentation)

- ❖ M. Zawadzkaa, T. Mikulchyk, S. Gul, A. Khartchenko, S. Mintova, J. Casidy, S. Martin, I. Naydenova, Development of Functionalized Materials for Holographic Sensor Applications, EUROPT(R)ODE XIII, March 20-23, 2016, Graz, Austria (oral presentation).

- ❖ S. Gul, A. Kharchenko, L. Oneill, M. Zawadzkaa, S. Martin, S. Mintova, J. Cassidy, I. Naydenova, Fabrication of photonic microscopic surfaces for copper+2 ions detection in fresh water by incorporation of LTL-zeolites nanoparticles, MSI 2016, DIT, Ireland (oral presentation)

- ❖ S. Gul, A. Kharchenko, M. Zawadzkaa, S. Martin S. Mintova, J. Cassidy, I. Naydenova, Development of Holographic Sensors for Copper+2 Ions Detection in Fresh Water by Incorporation of LTL-Zeolites nanoparticles, ICEST 2016 Barcelona. (oral presentation: Won excellent presentation award)

7.7.5. Poster presentations

- ❖ T. Mikulchyk, J. Browne, S. Gul, I. Naydenova, D. Cody, A novel calibration device for quality assurance of therapeutic ultrasound, Irish Association of Medical Physicists Annual Meeting, 17 February 2018, Derry, Ireland (Poster presentation).

- ❖ S. Gul, A. Kharchenko, S. Martin, S. Mintova, J. Cassidy, I. Naydenova, A platform technology for flexible fabrication of functionalized photonic surfaces for application in sensing The international conference on Optics and Surfaces and interfaces'' 25-30 June 2017, Trinity College Dublin. (Poster presentation)

- ❖ S. Gul, A. Kharchenko, S. Martin, S. Mintova, J. Cassidy, I. Naydenova, Development of surface relief holographic sensors by incorporation of LTL-zeolite nanoparticles for detection of copper ions in fresh water, 7th FEZA Conference "The ZEOLITES: Materials with Engineered Properties" July 3-7, 2017, Sofia, Bulgaria (Poster presentation)

- ❖ S. Gul, A. Kharchenko, M. Zawadzkaa, S. Martin, J. Cassidy, S. Mintova, I. Naydenova, Zeolites Based Sensors for Water Quality Monitoring, 6th

International Symposium Advanced Micro- and Mesoporous Materials, 2015, Burgas, Bulgaria. (Poster presentation)

- ❖ S. Gul, M. Zawadzkaa, S. Martin, J. Cassidy, I. Naydenova, Optical Sensors for Water Quality Monitoring, Environ 2015, IT Sligo, Ireland. (Poster presentation

References

[1]   K. Trainer, K. Wearen, D. Nazarova, I. Naydenova, and V. Toal, "Optimization of an acrylamide-based photopolymer system for holographic inscription of surface patterns with sub-micron resolution," *Journal of Optics*, vol. 124012, pp. 1–7, 2010.

[2]   C. Burtis, A, R. Edward, and D. Bruns, E, *Fundamentals of Clinical Chemistry :6th Ed*, no. August. Philadelphia USA: SAUNDERS Elsevier, 2001.

[3]   A. K. Balcı, O. Koksal, A. Kose, E. Armagan, F. Ozdemir, T. Inal, and N. Oner, "General characteristics of patients with electrolyte imbalance admitted to emergency department," *World J Emerg Med*, vol. 4, no. 2, pp. 113–116, 2013.

[4]   G. K. Moghaddam and C. R. Lowe, "Smartphone-based quantitative measurements on holographic sensors," *PLoS ONE*, vol. 12(11), pp. 1–21, 2017.

[5]   E. Mihaylova, D. Cody, I. Naydenova, S. Martin, and V. Toal, "Research on Holographic Sensors and Novel Photopolymers at the Centre for Industrial and Egnineering Optics," 2013.

[6]   http://www.newworldencyclopedia.org/entry/Holography [accessed 13/2/2019].

Appendix

Appendix A: Basel function Appendix A: Calculation solution of

$$\eta = J_m^2(\Delta\varphi)$$

$$\Delta\varphi = \frac{2\pi}{\lambda_r}\,\Delta n.\,d$$

One can calculate refractive index change whereas,

$\lambda = 633$nm,

m = 1 and

d = 0.4um

n = $1.5_{polymer}$ - 1_{air} = 0.5

n_{S+R} surface and receptor

$$\Delta\varphi = \frac{2\pi}{0.633}\,0.4 \times 0.5$$

$$\Delta\varphi = 1.98 \text{ rad}$$

$$\eta = J_m^2(\Delta\varphi)$$

$$\eta = J_m^2(1.98)$$

$$\eta = 0.3340$$

Diffraction efficiency 33.4%

Diffraction efficiency change after LTL-zeolites coating

$$\eta = 0.20$$

$$\eta = J_m^2(\Delta\varphi)$$

$$J_m^2(\Delta\varphi) = \sqrt{\eta}$$

$$\Delta\varphi = J_m^{2\,-1}(\sqrt{\eta})$$

$$\Delta\varphi = J_m^{2\,-1}(\sqrt{0.20})$$

$$\Delta\varphi = 1.023$$

$$\Delta\varphi = \frac{2\pi}{\lambda_r}\,\Delta n.\,d$$

$$\frac{2\pi}{\lambda_r}\Delta n.\,d = 1.023$$

$$\Delta n = \frac{1.023 \times 0.633}{2 \times 3.14 \times 0.4}$$

$$\Delta n = 0.257$$

$$\Delta n = n_p - n_{S+R}$$

$$0.257 = 1.5 - n_{S+R}$$

$$n_{S+R} = 1.5 - 0.26$$

$$\Delta n = 1.24$$

Diffraction efficiency change after LTL-zeolites coating and exposure to target analyte

$$\eta = 0.03$$

$$J_m^2 (\Delta\varphi) = \sqrt{0.03}$$

$$\Delta\varphi = J_m^{2\ -1} (\sqrt{\eta})$$

$$\Delta\varphi = 0.3518$$

$$\Delta\varphi = \frac{2\pi}{\lambda_r} \Delta n.\,d$$

$$\frac{2\pi}{\lambda_r} \Delta n.\,d = 0.3518$$

$$\Delta n = \frac{0.3518 \times 0.633}{2 \times 3.14 \times 0.4}$$

$$\Delta n = 0.0.886$$

$$\Delta n = n_p - n_{S+R+T}$$

$$0.0.8865 = 1.5 - n_{S+R+T}$$

$$n_{S+R+T} = 1.411$$

$$\Delta n = 1.411 - 1.24$$

$$\Delta n = 0.173$$

Appendix B: LTL zeolites synthesis and Characterisation

LTL nanoparticles synthesis

Zeolite nanocrystals with LTL-type structure were prepared from clear precursor solutions, free of organic template, with the following molar composition: 5 K_2O: 10 SiO_2: 0.5 Al_2O_3: 200 H_2O. The as prepared precursor solutions were aged at room temperature for 24 h prior to hydrothermal treatment at 170 °C for 18 h. After crystallization, the nanosized crystals were recovered by multistep centrifugation (20000 rpm, 40 min) and washed with doubly distilled water. The LTL nanocrystals were stabilized in water at pH = 8 and with concentration of solid particles of about 1.5 wt% [4].

Characterization of LTL- Zeolites nanoparticles
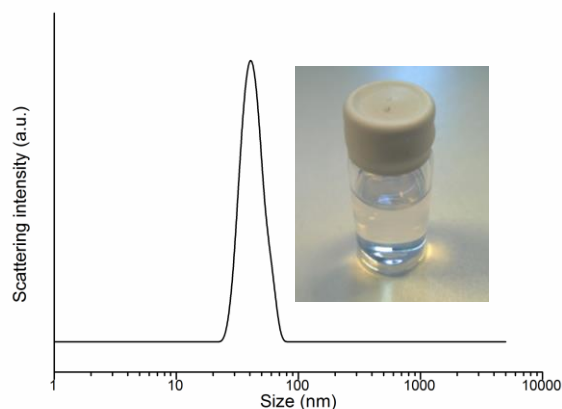
Figure 1. DLS studies of LTL nanoparticles

The particle size distribution of LTL zeolites was investigated by DLS. The standard the cumulant method for the characterization of the samples was applied. The mean particle diameter is centered at 40 nm. It is worth noticing, that the width of the particle size

distribution curve for the LTL sample is relatively narrow, starting from 20 to 80 nm (Figure. 1). However, it is known that the colloidal particles tend to agglomerate depending on the suspensions concentration, nature of solvent, and degree of polydispersity of the particles.[5]
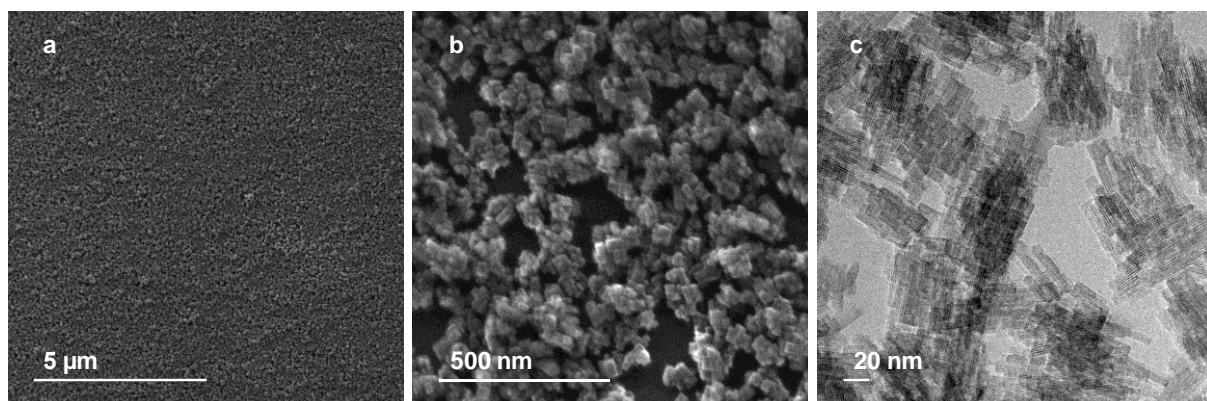
Figure 2. SEM (a and b) and TEM (c) images of LTL nanocrystals

The SEM and TEM results are in line with the XRD and DLS observations (Figure 2). The fully crystalline LTL sample consists of many aggregates combined of single rectangular crystalline domains with well-defined edges and crystalline fringes with the size of 10 – 25 nm. No entities with amorphous appearance are observed in the sample.

Table 1 Elemental ratios for LTL zeolite measured by ICP-OES and EDX

Sample	Si/Al		K/Al	
	ICP	EDX	ICP	EDX
LTL	2.85	2.37	2.05	0.88

The Si/Al ratios in crystalline particles, measured by ICP-OES and EDX, are in good agreement (Table 1). However, the results show significant difference in K/Al ratio obtained by ICP-OES and EDX. This excess of potassium can be explained with the K^+

cations occluded in cancrinite cadges, which cannot be removed or exchanged by other cations,[6] or with the systematic mistake of the ICP-OES measurements.
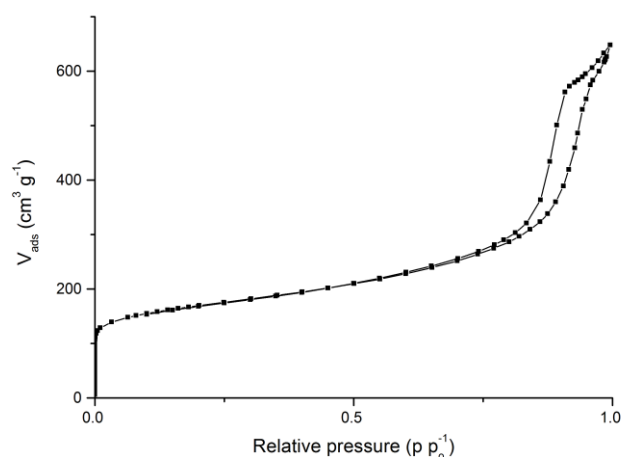
Figure 3. Nitrogen sorption/desorption isotherm of LTL zeolite

Table 2 Textural properties of LTL zeolite obtained from N_2 sorption

Sample	BET surface area, m^2/g	V_{mic}, cm^3/g	V_{mes}, cm^3/g	V_{tot}, cm^3/g
LTL	571	0.13	0.72	0.85

The porosity and specific surface area of the LTL sample were characterized by nitrogen adsorption measurements. Samples exhibits a mixture of Type I and IV isotherms with a large H1-type hysteresis (Figure. 4). This result is associated with formation of mesopores pores by the close packing of monodispersed and well-shaped nanosized crystallites.[7]

The results (Table 1) emphasize the high crystallinity of the LTL crystals; that is in good agreement with the data listed above.

References

[1]   K. Trainer, K. Wearen, D. Nazarova, I. Naydenova, and V. Toal, "Optimization of an acrylamide-based photopolymer system for holographic inscription of surface patterns with sub-micron resolution," *Journal of Optics*, vol. 124012, pp. 1–7, 2010.

[2]   C. Burtis, A, R. Edward, and D. Bruns, E, *Fundamentals of Clinical Chemistry :6th Ed*, no. August. Philadelphia USA: SAUNDERS Elsevier, 2001.

[3]   A. K. Balcı, O. Koksal, A. Kose, E. Armagan, F. Ozdemir, T. Inal, and N. Oner, "General characteristics of patients with electrolyte imbalance admitted to emergency department," *World J Emerg Med*, vol. 4, no. 2, pp. 113–116, 2013.

[4]   A. Kharchenko, O. I. Lebedev, V. Zholobenko, V. de Waele, and S. Mintova, "Formation of Copper Nanoparticles in LTL Nanosized Zeolite: Kinetics Study," *The Journal of Physical Chemistry C*, vol. 120, p. 26300−26308, 2016.

[5]   M. Hölzl, S. Mintova, and T. Bein, "Colloidal LTL zeolite synthesized under microwave irradiation," *Studies in Surface Science and Catalysis*, vol. 158, pp. 11–18, 2005.

[6]   S. M. Auerbach, K. A. Carrado, and P. K. Dutta, *Handbook of zeolite science and technology*, vol. 2004. CRC Press, 2004.

[7]   H. Awala, J.-P. Gilson, R. Retoux, P. Boullay, J.-M. Goupil, V. Valtchev, and S. Mintova, "Template-free nanosized faujasite-type zeolites," *Nature Materials*, vol. 14, no. 4, pp. 447–451, 2015.

Appendix C: Ellipsometry data information about Refractive index change due to exposure to analyte

Ellipsometry is an optical technique used to investigate the dielectric properties, such as refractive index, of thin films.
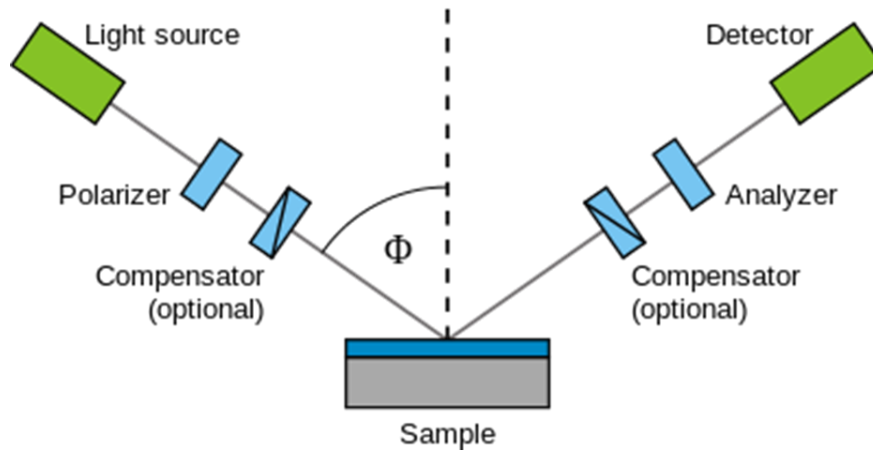

Figure. 1: Schematic setup of an ellipsometry experiment

1. Two different ellipsometry studies were carried out to quantify the change in the refractive index, n_z, of the zeolite-TEOS films due to exposure to Cu^{2+} metal ions in solutions 0, 2 and 4 mM concentration.

2. The influence of curing the samples at two different temperatures, 170 and 320°C, for 3 hours prior to Cu^{2+} exposure was also investigated.

3. Variables measured: Two ellipsometric angles Δ and Ψ. These angles are related to the ellipsometric ratio:

$$\rho = \frac{r_p}{r_s} = \tan \psi . e^{i\Delta}$$

r_p, r_s = reflection coefficients as derived by Fresnel of the parallel and normal components of the electric field (with respect to the plane of incidence).[2]

Single Wavelength Ellipsometry studies: Dynamics

1. A 633 nm single wavelength Multiskop (OptrelGbR) ellipsometer was used for this real-time measurement of the change in optical refractive index, n, of the layer due to Cu^{2+} adsorption.

2. Tests were carried out using TEOS layers spin-coated onto silicon substrate both with and without LTL.

3. The samples were cured at 170°C for 3 hours prior to testing.

4. The samples were initially placed in water at time t=0. Concentrated Cu^{2+} solution was added at t=150 seconds to yield an overall concentration of 0, 2 and 4 mM Cu^{2+}

5. The refractive index is observed to decrease with increasing exposure time, and with increasing concentration of Cu^{2}
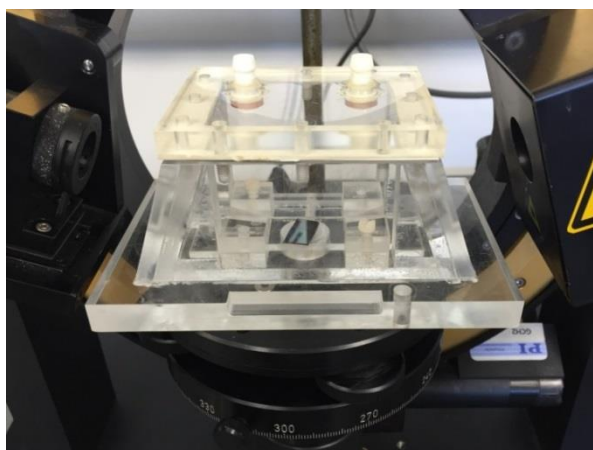
Figure 2. Custom real-time ellipsometry cell with quartz windows (designed and manufactured by the Barrett Research Group, McGill University).
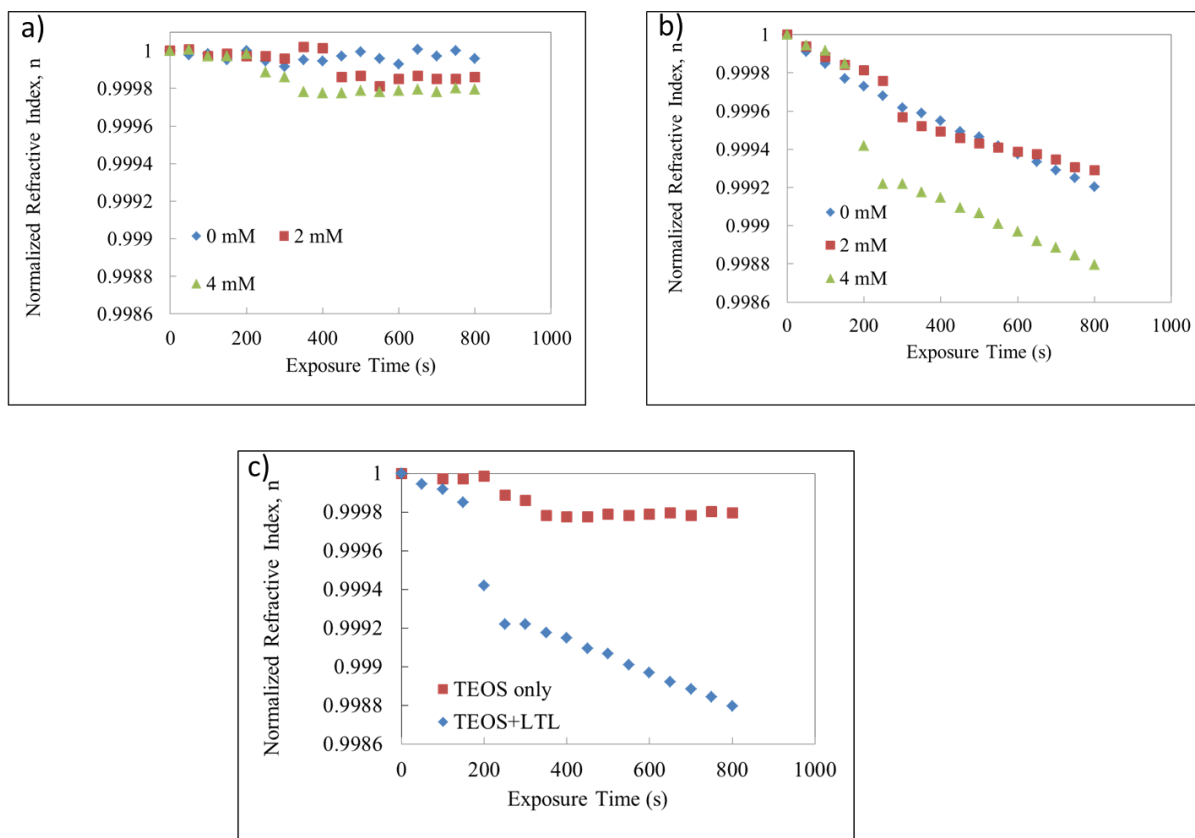
Figure 3. (a) Normalised n vs exposure time for TEOS only films (no zeolites) exposed to 0, 2 and 4 mM Cu²⁺ solution, (b) Normalised n vs exposure time for TEOS+LTL films exposed to 0, 2 and 4 mM Cu²⁺ solution and (c) Normalised n vs exposure time for TEOS only and TEOS+LTL films exposed to 4 mM Cu²⁺ solution.

The samples were initially placed in water at time t=0. Concentrated Cu^{2+} solution was added at t=150 seconds to yield an overall concentration of 0, 2 and 4 mM Cu^{2+}. The refractive index is observed to decrease with increasing exposure time, and with increasing concentration of Cu^{2+}.

Appendix D: Calculation solution of Δn

$$n = Sin^2 \left(\frac{\pi \, \Delta nd}{\lambda \, Cos \, \theta_B} \right)$$

$$\sqrt{\eta} = Sin \left(\frac{\pi \, \Delta nd}{\lambda \, Cos \, \theta_B} \right)$$

$$\Delta n = \frac{\lambda_r cos \, \theta_B \, sin^{-1}\left(\sqrt{\eta}\right)}{\pi d}$$

One can calculate the Δ*n* by putting the values of η for each sample whereas,

λ =633nm,

θ =12.4,

η = 52

d = 70

$$\Delta n = \frac{633 \times 10^{-9} \, (12.4) sin^{-1}\left(\sqrt{0.52}\right)}{3.14 \times 70 \times 10^{-6}}$$

$$\Delta n = 0.0022642$$

$$\Delta n = 2.2 \times 10^{-3}$$